DIPARTIMENTO DI SCIENZE
DELL'AMBIENTE E DEL TERRITORIO
E DI SCIENZE DELLA TERRA
Università degli Studi di Milano-Bicocca

"Fr.lli Confalonieri"
fellowship

Volcanism versus Tectonics in the Sedimentary Record

PhD Thesis

Andrea Di Capua
Matricola 702625

Tutor:	*Academic Years:*	*Co-Tutors:*
Dott. Gianluca Groppelli	**2014** **(XXVII Cycle)**	**Dott. Giovanni Vezzoli** **Prof. Roberto A. Scasso**

Index

Introduction page 1

First case history page 3
Volcanism versus tectonics in the Oligocene Northern Apennines Foredeep: the Val d'Aveto Formation (Northern Apennines Foredeep Basin, Emilia-Romagna, Italy)

- Tectonism, volcanism and climate signal in an ancient foredeep basin: the Val d'Aveto Formation (Northern Italian Apennines)
- Emplacemenet of welded pyroclastic density currents (PDCs) in a deep-marine environment: the Val d'Aveto Formation body (Northern Apennines, Italy)

Second case history page 40
Syn-volcanic versus post-volcanic sedimentation: application of actualistic models to unravel primary volcanic control on source-to-sink (Taveyanne Sandstones, Oligocene Northalpine Foreland Basin, France and Switzerland)

- Taveyanne Sandstones: syn- or post-volcanic sedimentation?
- Magnetic fabric from incipient to multistage deformed turbidite sequences: the Oligocene Taveyanne Sandstones (Northern Alpine Molasse)

Third case history page 70
Volcanism versus tectonics in a Jurassic continental basin: from the Las Leoneras Formation to the Lonco Trapial Formation (Cañadon Asfalto Basin, Chubut Province, Argentina)

Four case history page 93
Post-volcanic sedimentation: from tectonically controlled melting to tectonically driven erosion (Late Oligocene Southalpine Foredeep, Northern Italy – published paper)

Conclusion and final remarks page 109

References

Introduction

The idea of this work was born at the conclusion of my Masters degree dissertation when the study of the Val d'Aveto Formation stratigraphy stroke me with a question: “what is the meaning of volcanoclastic sequences in the stratigraphic records?”. Around the Alps different volcanoclastic sequences are known to have been supplied by the Periadriatic Magmatism volcanism (40-28 Ma, Bergomi et al., 2014), during short phases of tecto-climatically driven erosion (Sinclair, 1992; Ruffini et al., 1997). However, in modern settings, sedimentologists have highlighted that volcanoes are geological features whose life, even if too short in terms of geological persistence in time, can dramatically influence the stratigraphic record, thanks to their high capability to inject energy in the sedimentary systems, as well as to cannibalize the sediment production (explosive events e.g. pyroclastic density currents). Thus, this PhD thesis contains 6 different works (six different papers in press or in preparation) that try to dig into the problem through different techniques (fieldwork analyses, clast-counts, image analyses, optical analyses, classical sandstone point-counts X-ray diffraction, X-ray fluorescence, minero-chemical SEM-EDS analyses, rock paleomagnetism) with the aim of finding clues that allow to distinguish syn-volcanism sedimentation, i.e. controlled by primary volcanic activity, versus post-volcanic sedimentation, i.e. controlled by tectonically-driven erosion (e.g. Dal Piaz and Venturelli, 1984; Ruffini et al., 1997).

I decided to order these works starting from the one that has been carried out on Val d'Aveto Formation where the discovery of pyroclastic density current (PDC) deposits preserved in a foredeep volcanoclastic turbidite system attests the activation of syn-sedimentary explosive volcanism in the source-to-sink. It also gives the possibility to discuss on different temporal impact of volcanism, tectonics and climate on the sedimentary records, and transport mechanisms of PDCs moving below the sea level. The second case history considered is the most complicated, as no PDC deposits have been surely recognized in the stratigraphic sequences. In this case history, combination between facies analyses in the field, compositional analyses (point-counts and X-ray diffraction analyses), and application of modern sedimentation models of volcanic-related source-to-synk systems (e.g. Manville et al., 2009; Sisavath et al., 2011, 2012) result fundamental to unravel the temporal relationship between volcanism and sedimentary deposition, and to reconstruct the source-to-sink system. Paleomagnetic analyses have been used to detect the tectonic deformation suffered by the studied sections. As third case boundary between Las Leoneras Formation and Lonco Trapial Formation in the Cañadón Asfalto basin (Chubut Province, Argentina) has been inserted. Here, syn-sedimentary volcanic centers are still preserved in the region and volcanic supply has been already documented by previous authors (e.g. Cunéo et al., 2013). The Formations considered represent a natural laboratory to study both the effect of volcanism activation versus active tectonics on sedimentation in a transtensional basin, and how volcanic events are preserved in the stratigraphic records. The last case is about the tectonic signature of the Villa Olmo Conglomerate (27.3 – 26.5 Ma, Tremolada et al., 2010), lower member of the Como Conglomerate into the Gonfolite Lombarda Group (31.2 – 13.5 Ma, Tremolada et al., 2010), where andesite clasts are considered to have been liberated from the tectonic erosion of Oligocene volcanic centers (Malusà et al., 2011).

Volcanism versus tectonics in the Oligocene Northern Apennines Foredeep: the Val d'Aveto Formation (Northern Apennines Foredeep Basin, Emilia-Romagna, Italy)

Tectonics, volcanism and climate signal in an ancient foredeep basin: the Val d'Aveto Formation (Northern Italian Apennines)

Abstract

Tectonics, volcanism and climate are the main factor controlling sediment supply across source-to-sink systems. Ancient foreland/foredeep basins are considered to preserve long-terms information that, integrated to actualistic models of sedimentation, can give us a better resolution on the interconnection between these processes and sedimentation. In this work, we focused on the Val d'Aveto Formation (Northern Apennines-Italy), an Oligocene (32 – 29 Ma) foredeep Formation where tectonic, climate and volcanic events are amalgamated together in a complex stratigraphic sequence, post-deformed by the growth of the Apennines Belt. Through facies analyses and logs correlation, we have reconstructed and correlated the stratigraphic architecture of the submarine fan to classical models present in literature. Clast counts in the field, grain size image analyses, optical and minero-chemical (XRD and SEM-EDS) investigations on more than 50 layers between sandstones, conglomerates and pyroclastic density current deposits have been carried to get information on sediment compositions and depositional mechanisms controlling the sedimentation in the Apennines Oligocene foredeep. Further optical and minero-chemical analyses on pebbles and rock fragments unraveled detritus provenance from SE France-Corsica system. All the results document the high but rapid impact of volcanism on the environment, the strong climatic control on the evolution (progradation and retrogradation) of the submarine fan and types of deposits, and the tectonics control on shifting of sediment supply, due to the progressive activation of different deformational fronts.

1. Introduction

In 2003, professor Ricci Lucchi wrote that “historically, the turbidite bodies of northern Apennines represent an unique data base, which was utilized, at first for the definition of the flysch concept, then for the definition of the turbidity current concept and, more recently, for the recognition and characterization of facies schemes and the modeling of deep-water depositional systems” (Ricci Lucchi, 2003). In this sense, Val d'Aveto Formation (32 – 29 Ma, Northern Apennines, SW of Piacenza, Italy, Fig.1A - Elter et al., 1999a,b; Catanzariti et al., 2009) constitutes a singular example where interactions among tectonism, volcanism and climate have been recorded (Elter et al., 1999a; Di Capua et al., 2014). In a preliminary work, Di Capua et al. (2014) inferred that the singular

4

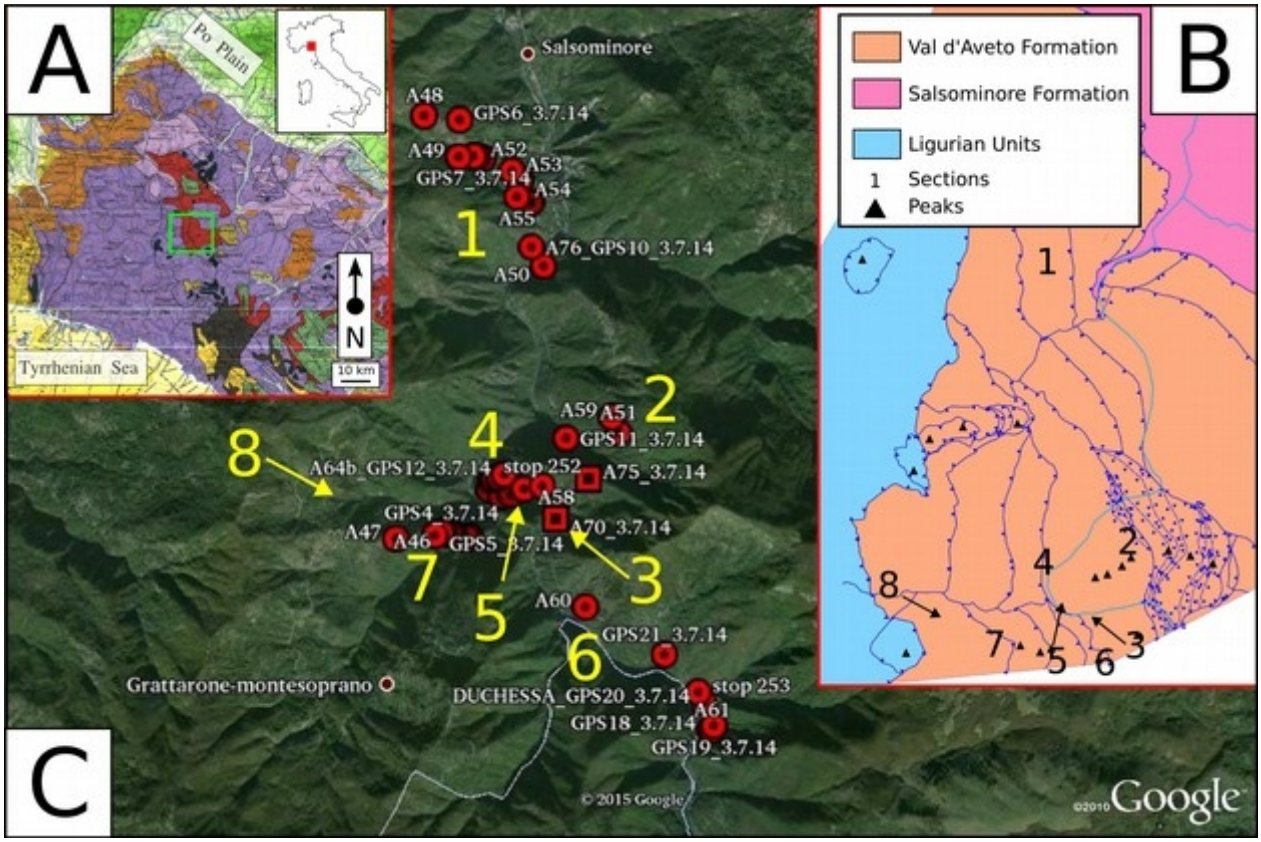

Figure 1: fieldwork map; a) tectonic map of the Northern Apennines; b) tectonic sketch of Val d'Aveto area; c) ubication of logs measured in the field.

sedimentary record of the Val d'Aveto Formation is the result of two main events: the forced regressive stage owing to the Oligocene global cooling, and the activation of an important volcanism in the source area. The occurrence of primary pyroclastic events (referred in this work as preserved PDC deposits) intercalated in the sedimentary record (Di Capua & Groppelli, 2014) confirmed the syn-sedimentary activation of volcanic centers in the source-to-sin system. In this work, we present new field and laboratory data we collected on the Val d'Aveto Formation, with the aims of 1) geometrically reconstructing the sedimentary architecture of the turbidite system, 2) reconstructing the source-to-sink system from where the detritus was discharged, and 3) discussing the role of tectonics, climate and volcanism on foredeep sedimentation.

2. Geological setting

Val d'Aveto Formation crops out in the Bobbio tectonic window (Northern Apennines, Italy - Fig.1A) (Elter et al., 1999a), and forms the Canetolo Unit with Petrignacola Formation (Vescovi, 1998; Elter et al., 1999a; Cibin et al., 2001; Catanzariti et al., 2009; Mattioli et al., 2012). This unit was deposited in the sub-Ligurian basin, originally located between the Ligurian oceanic domain

5

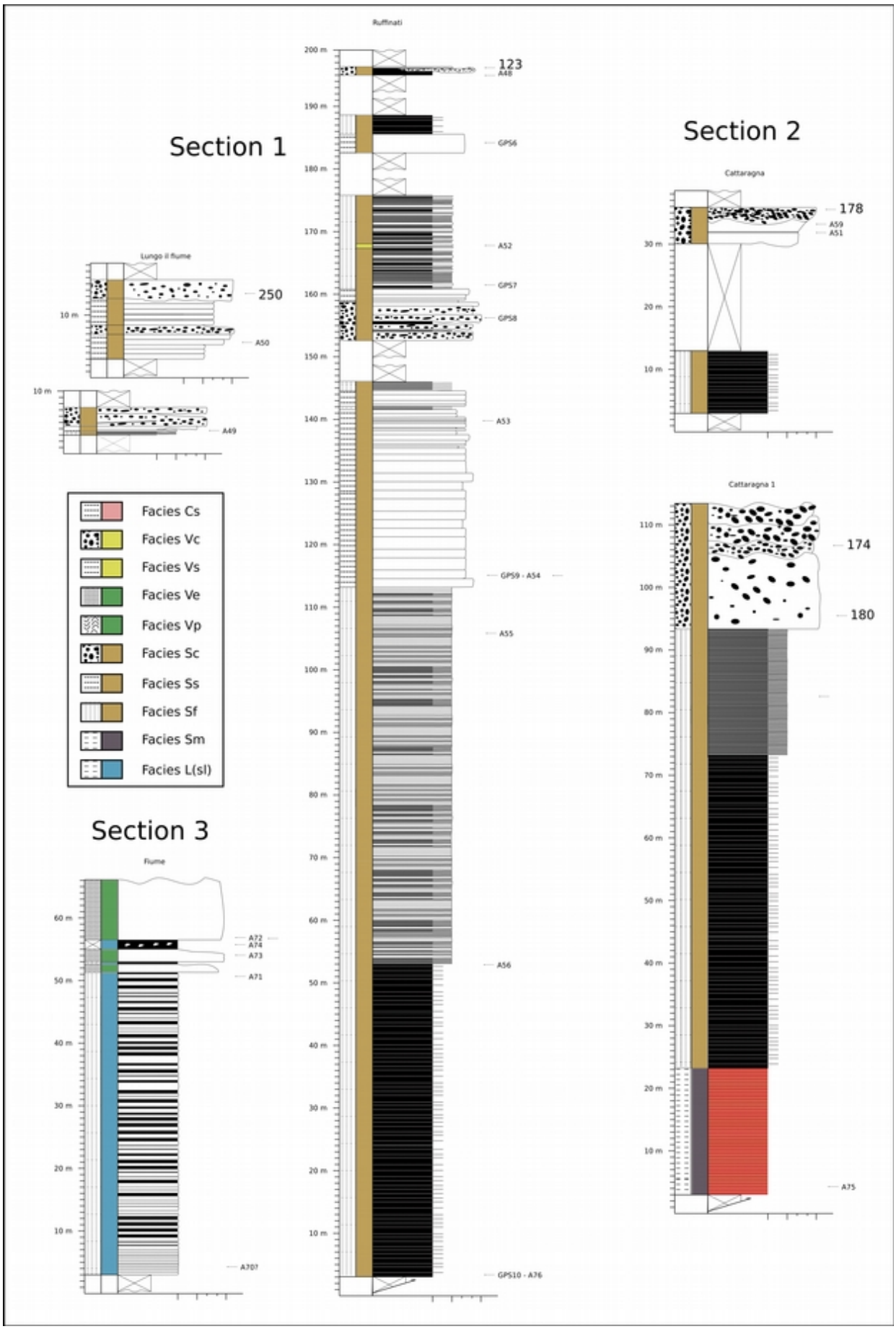

Figure 2: stratigraphic logs measured in the field (lower Val d'Aveto Formation). Ubication in Figure 1b-c.

6

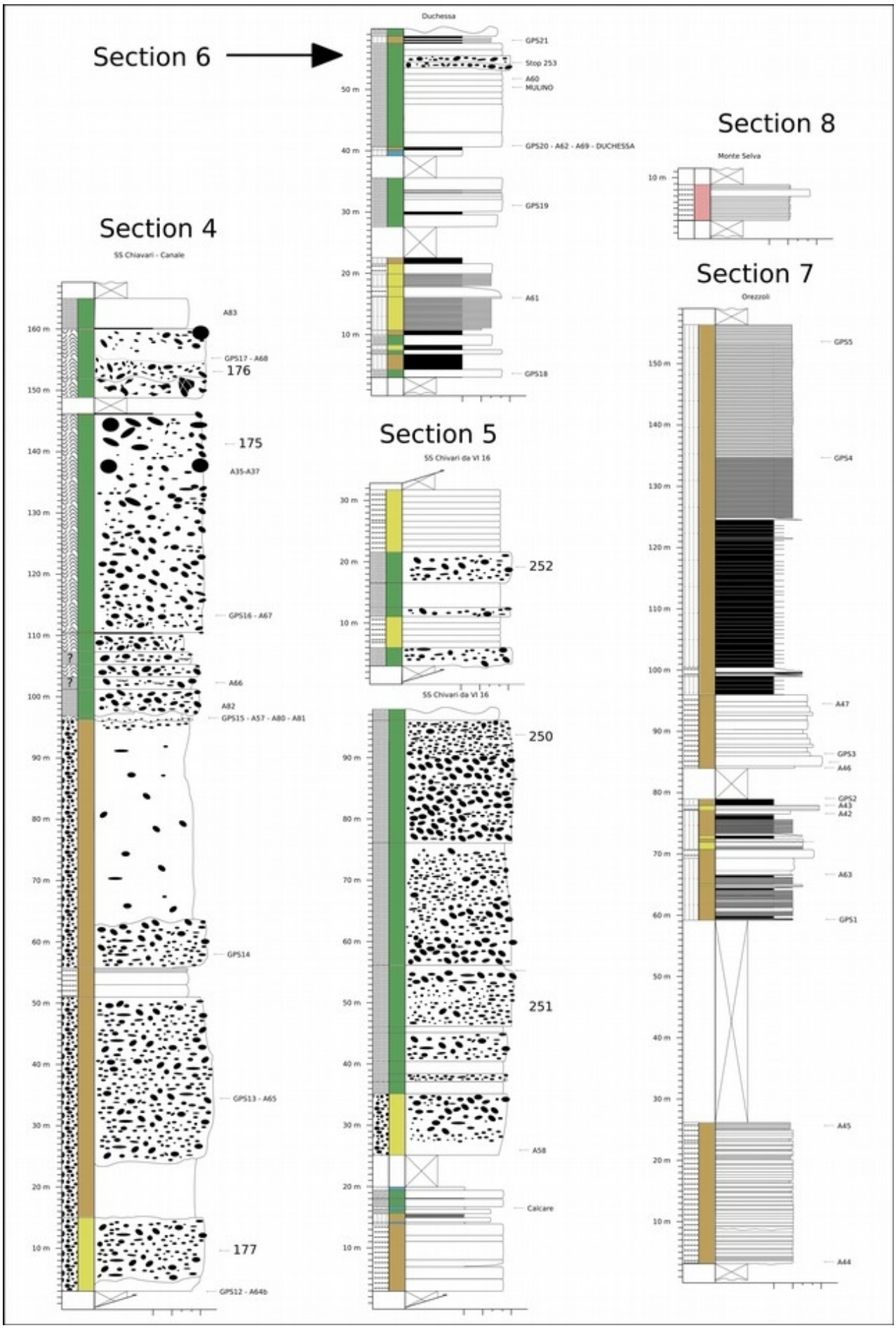

Figure 3: stratigraphic logs measured in the field (lower Val d'Aveto Formation). Ubication in Figure 1b-c.

7

and the Tuscany continental margin (Mutti et al., 1995; Elter et al., 1999a), and represents the first clastic input of the Oligo-Miocene Northern Apennines foredeep (32 – 29 Ma-Catanzariti et al., 2009). Post-depositional deformation developed high-angle thrust faults that altered the real sequence of the Val d'Aveto Formation (Elter et al., 1999a). Reconstructed stratigraphy was proposed by Elter et al. (1999a) and comprises three members: 1) a lower siliciclastic pelitic-arenaceous member, closed on top by metric conglomerate bodies, including the ones of Mutti and Ricci Lucchi (1972); 2) a middle volcaniclastic arenaceous-conglomeratic member; 3) an upper volcaniclastic to siliciclastic arenaceous member. In the same work, sandstone petrography analyses allowed to identify two sandstone petrofacies, one composed of metamorphic, plutonic and sedimentary rock fragments and single minerals, and the other one characterized by an andesite debris-rich assemblages. Polygenic conglomerates, instead, do not show any change in clast association lithologies, but an increase in clast dimensions from siliciclastic to volcaniclastic matrix supported bodies (Elter et al., 1999a; Di Capua et al., 2014). 40Ar/39Ar radiometric data on amphiboles separated from three volcanic clasts constrain at 29±0.2 Ma the main volcanic event (Mattioli et al. 2002), which was fed by a local Apennines volcanic source, as inferred only through the volcanic geochemical signal by Mattioli et al. (2012). Di Capua et al. (2012) recognized other two minor members: one at the bottom, composed of calcareous turbidites intercalated by thinner pelitic layers, and one at the top of the Formation, composed of carbonate sandstones and microconglomerates. Heavy mineral composition of an upper microconglomerate layer pointed to a sediment supply from a medium to low metamorphic basement (Di Capua et al., 2012). Correlation between the depositional ages of the Val d'Aveto Formation and the global eustatic curve (Haq et al., 1987; Zachos et al., 2001; Kuhlemann et al., 2002; Wade and Pälike, 2004; Jovine et al., 2009; Miller et al., 2011) allowed Di Capua et al. (2014) to infer a climate control on the siliciclastic sedimentation trends.

3. Methods

We carried on a fieldwork-based study on the Val d'Aveto Formation in order to reconstruct its stratigraphic architecture (Fig.1B-C). Fieldwork-based study comprises: 1) measurement of 12 logs all along the Aveto valley (Fig. 2-3); 2) facies analyses, with particular attention to small scale depositional structures; 3) conglomerate clast counts. Granulometry analyses on conglomerate bodies have been performed using the shaper analysis tool of an open-source software named JMicroVision (Roduit, 2007), simply re-drawing pebble boundaries of scaled pictures on transparent paper. Equivalent circular diameter (ECD) values have been extract and insert in a

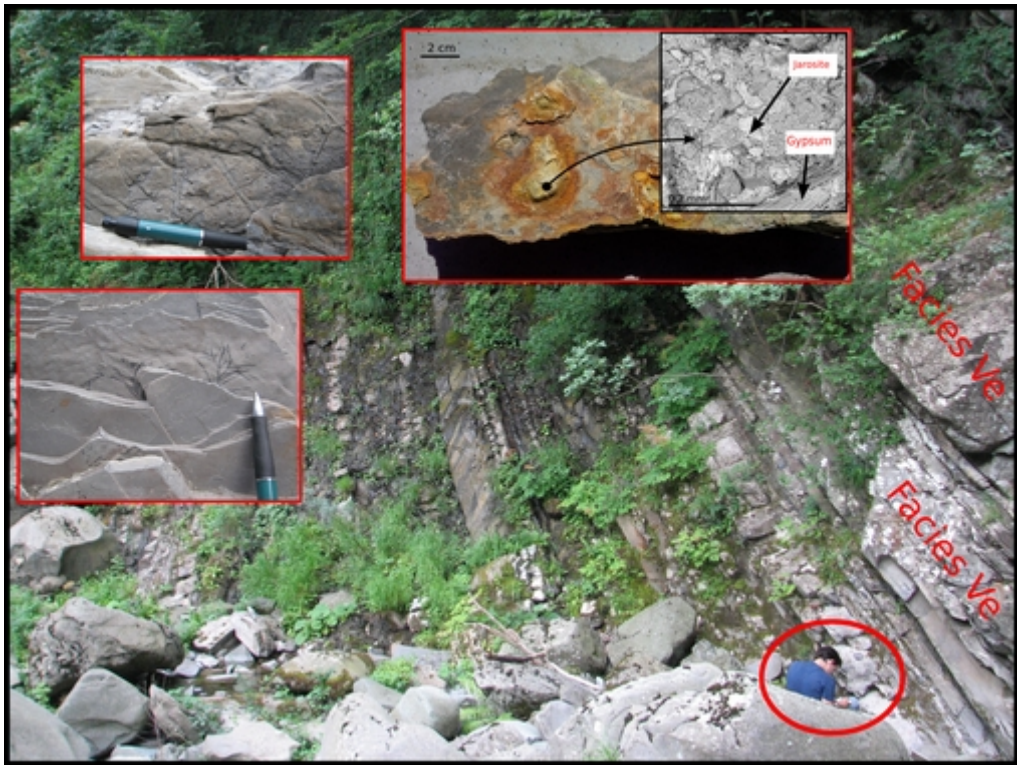

Figure 4: facies L(sl), with bioturbation structures (left) and gypsum nodular concretions (right). Doctor G. Coletti as scale.

Figure 5: facies Sm

spreadsheet for calculations. More than 50 samples have been collected and cut into standard thin section and analyzed under a polarized microscope. Sandstone composition of 10 samples has been

9

obtain through the classical Folk methods (Folk, 1980) and has been compared with the one of Elter et al. (1999a) after ricalculation. On a total of 15 fine-grained samples we performed X-ray powder diffraction (XRPD, PANalytical X'Pert PRO PW3040/60 diffractometer in θ-θ Bragg-Brentano

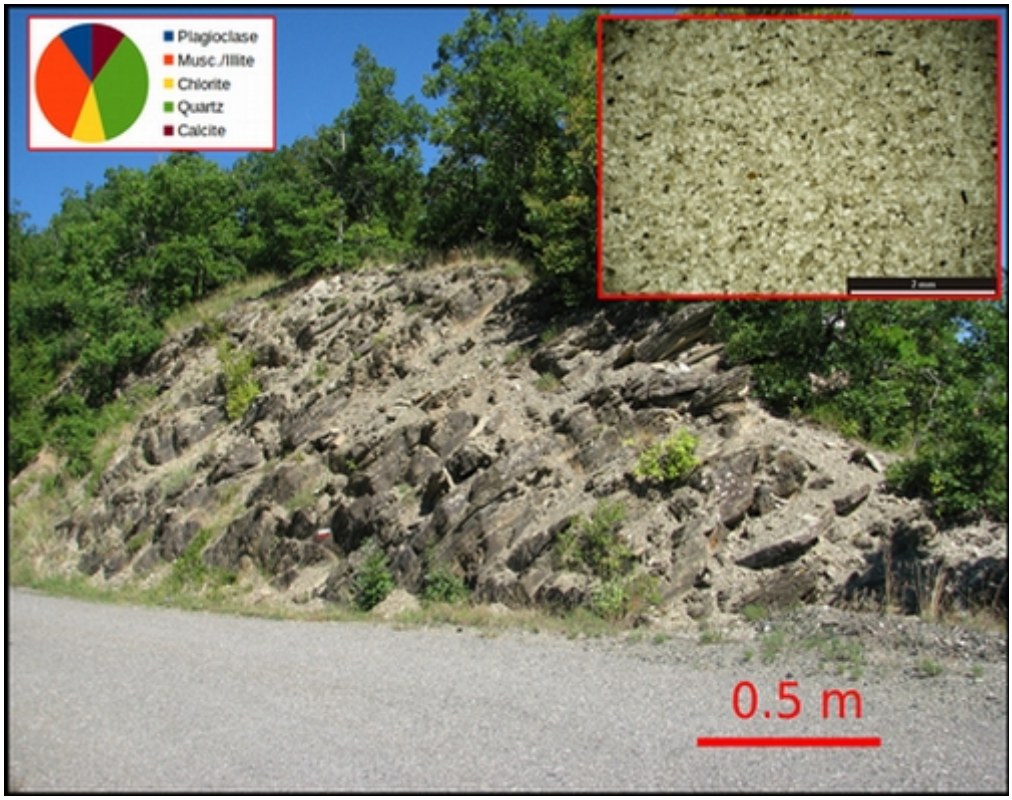

Figure 6: facies Sf with relative composition (XRD)

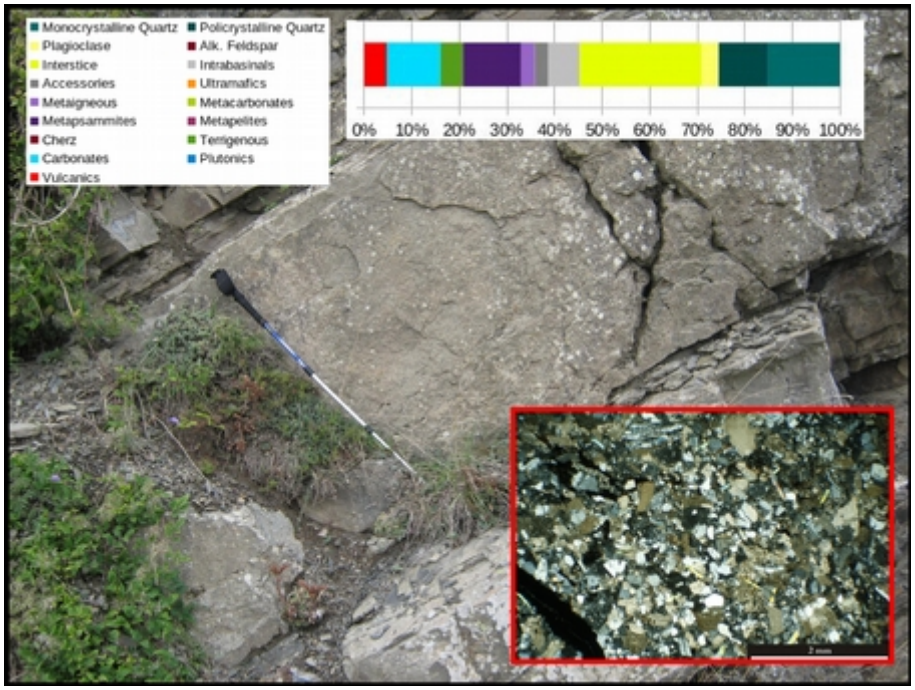

Figure 7: facies Ss with relative composition (point-count)

parafocusing geometry with Ni-filtered Cu Kα radiation at 40 kV and 40 mA, in the 4-80° 2θ

10

range), and compositional results have been analyzed running the PANalytical X'Pert High-Score software, with the ICSD PDF2 database. Optical and minero-chemical (SEM-EDS) analyses have been also performed on single pebbles and/or rock fragments of metamorphic detritus, both in the siliciclastic and volcanogenic/volcanoclastic detritus.

4. Results

4.1 Facies analyses

Several different facies have been recognized in the Val d'Aveto Formation and resumed in Table 1. We grouped all the facies in four groups on the base of their sedimentary features, microtextures and matrix compositions: calcareous (1 facies), siliciclastic (4 facies), volcanogenic/volcanoclastic (4 facies), carbonatic (1 facies).

Calcareous facies, named facies L *s.l.* (Fig.4), crops out at the bottom of the Aveto River, as well as intercalated in the silico-volcanoclastic deposits (also according to Boni et al. (1969) and Elter et al. (1999a)). It is constituted of an association of bioturbated calcareous turbidite layers and dark gray pelitic layers, usually packaged in pluricentimetric to plurimetric sequences, interpreted as low density turbidite events (Shanmugam and Moiola, 1988; Shanmugam, 2000; Haugton et al., 2009).

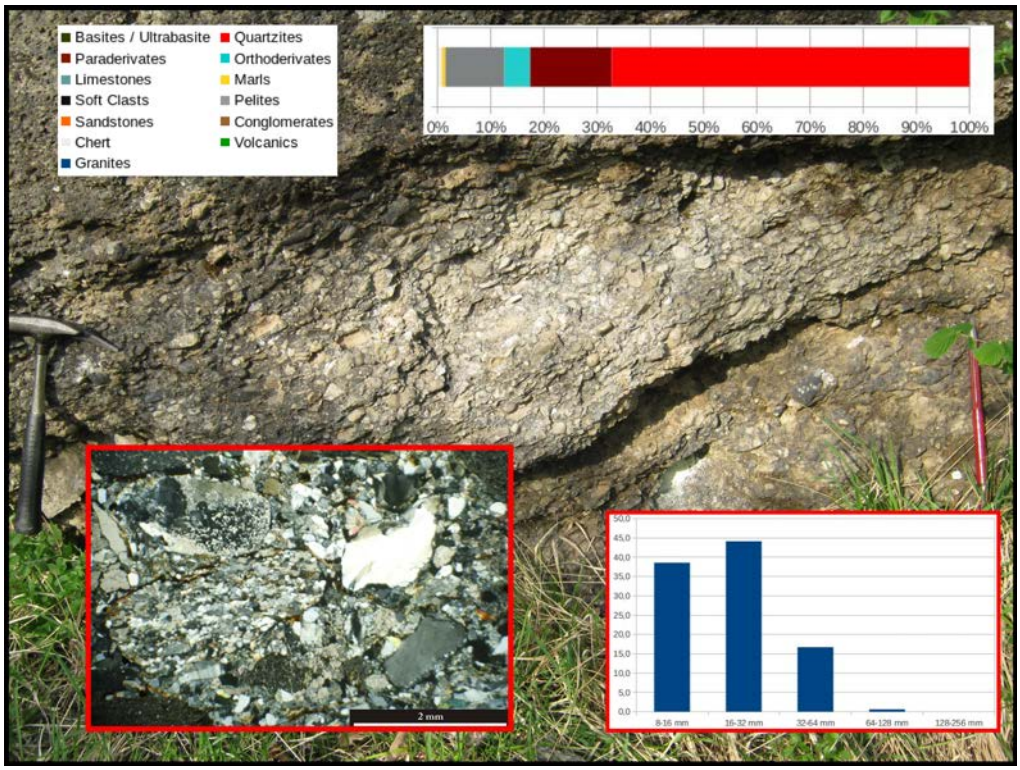

Figure 8: facies Sc, with composition and granulometry of gravel-sized detritus

11

Siliciclastic facies are widely exposed in the Aveto Valley and comprises a wide spectrum of deposits, from varicolored shales to pluri-metric conglomerate bodies (Sm, Sf, Ss, Sc – Fig.5-8). They constitute the thickest part of the Aveto sequence, in which the volcanic signal is interbedded. Compositional analyses shows a preponderance continental fingerprint of the detritus, according to Elter et al. (1999a,b) and Marroni et al. (1999), and sedimentation mechanisms were controlled by hemipelagic sedimentation (Shanmugam et al., 1988), low density turbidites (Shanmugam, 2000; Talling et al., 2013), and hyper-concentrated flows (Mulder and Alexander, 2001; Mulder et al., 2003; Haugton et al., 2009), the latter dominating the thicker part of the sequence.

Volcanogenic/volcanoclastic facies association groups together syn- and post-volcanic facies of the stratigraphic sequence. With “volcanogenic” we here refer to all those deposits directly supplied by volcanic activity. They are alternatively 1) pyroclastic density currents (PDCs) deposits, characterized by felty porphyritic to eutaxitic textures (Fig.9); or 2) epiclastic deposits, characterized by pyroclastic fragments forming a dark green pseudomatrix (Fig.10). In both cases, we assume that detritus was discharged during catastrophic events or soon after them, i.e. when free, unconsolidated volcanic material was still mantelling part of the source-to-sink system and classical fluvial-dominated mechanisms of sedimentations were not yet reestabilished (Smith, 1991; Mandville et al., 2009). With “volcanoclastic” we define deposits composed for more than 50% of volcanic material ascribable to principal PDC events, but supplied by classical fluvial-dominated sedimentation (Fig.11-12). Discrimination has been made 1) through sandstone point-counts (following Folks, 1961), or 2) through XRD analyses. For the latter, we compared XRD analysis spectrum of sandstones and pelites with that of the primary PDC event.

Finally, only one carbonatic facies (Cs, Fig.13) has been observed in the Val d'Aveto Formation sequence in the Monte Serra section (Fig.1c, 3). It is constituted of dark gray, silty to fine sandy-carbonate layers, with microconglomerate intercalations, rich in basement-derived detritus (association “epidote+light mineral”, “garnet+epidote”, loose crystals of epidote, apatite, rare zircon, rutile and horneblende - Di Capua et al., 2012). They are interpreted alternatively as low density turbidites (Shanmugam, 2000) or massive sandy flows (Shanmugam, 2002; Mutti et al., 2003). They maybe represent the transition between the Val d'Aveto Formation and the Salsominore Formation (Sanguineto Unit - Elter et al., 1999b; Elter et al., 2005), but no biostratigraphic data can support this suggestion.

4.2 Metamorphic clast petrography

Results of clast counts performed in the field (Fig.14) highlighted the homogeneous lithological

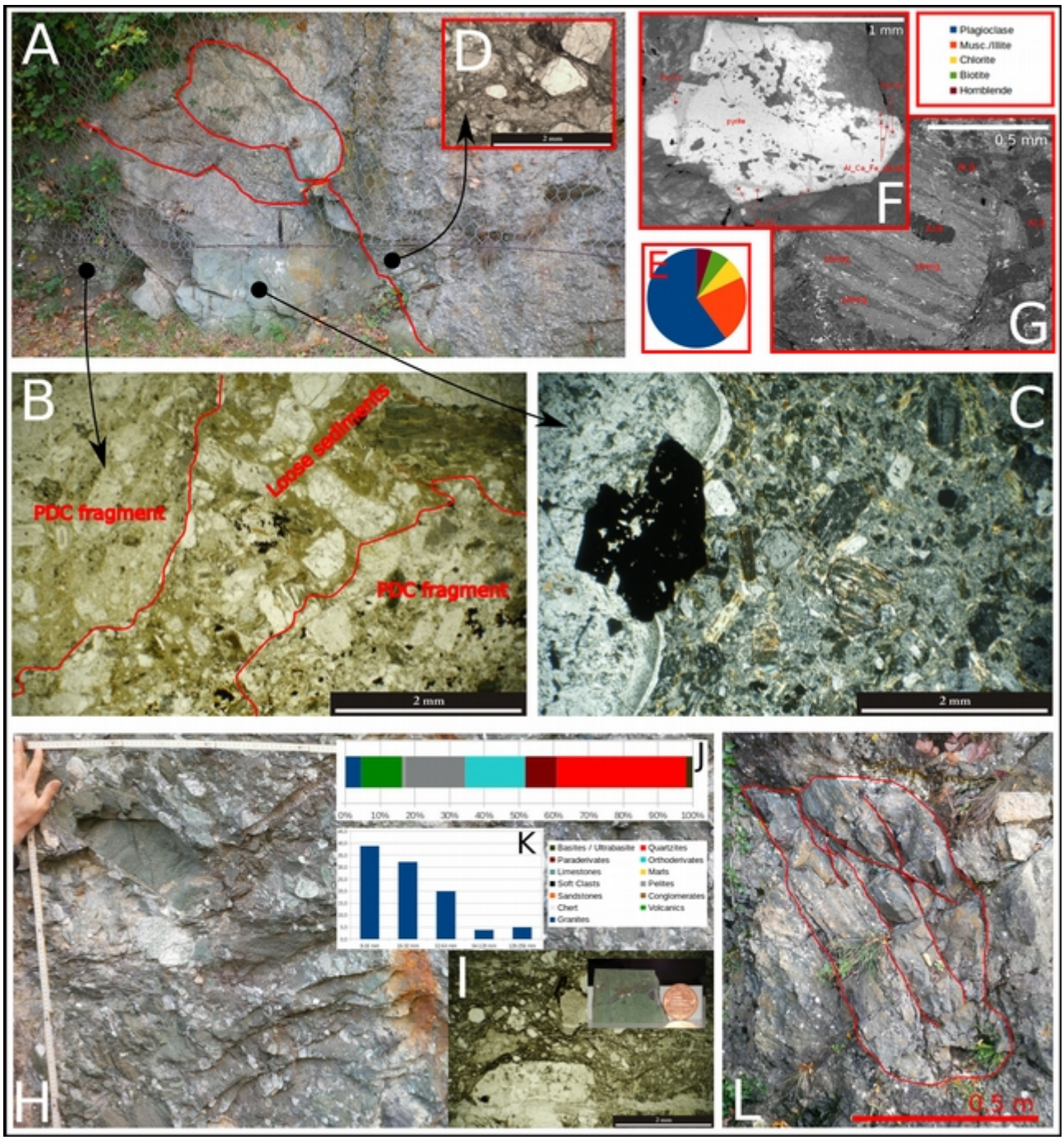

Figure 9: facies Vp; a) first PDC event (see Fig. 3 for complete PDC sequence, sector 4); b) thin section of the boundary between the PDC and the underlain siliciclastic deposit; c) thin section of the main body of PDC1; d) thin section of the epiclastic event overlain PDC1; e) results of X-ray diffraction analysis on the main body of PDC1; f) pyrite crystal in SEM-EDS g) phengite-schist in SEM-EDS; h) blocky-sized part of PDC4 with i) groundmass thin setion (note the eutaxitic texture), results of j) pebble count and k) granulometry analysis; l) jig-saw structure on a metric boulder (PDC5).

associations characterizing the gravel-sized detritus of entire the Val d'Aveto Formation, according to Elter et al. (1999) and Di Capua et al. (2014). Metamorphic lithotypes result the most abundant, and are generally represented by orthoderivates and paradericates, with metagabbros in minor

13

Figure 10: facies Ve

amounts. Orthoderivates characterized by quartz, feldspars and biotite, or biotite and muscovite associations. Biotite may be altered in chlorite. Textures show generally low grade of deformation, but proto-milonitic samples have been also observed. Mineralogical associations observed in paraderivate pebbles document different grades of metamorphic deformation suffered by them (Fig.15A). They are usually composed of muscovite, biotite, chlorite, and quartz, with secondary kyanite and garnet (Fig.15B). Metagabbroic pebbles are characterized by plagioclase, epidote, chlorite, pyroxene and hornblende (often chloritized) as main mineralogical assemblages, with textures that range between undeformed to mylonitic (Fig.15C-D). Plagioclase, when preserved, is usually albitized, chlorite is chamosite (a Fe-Mg member with rare Ti), pyroxene is augite and preserved hornblende is Mg-rich member.

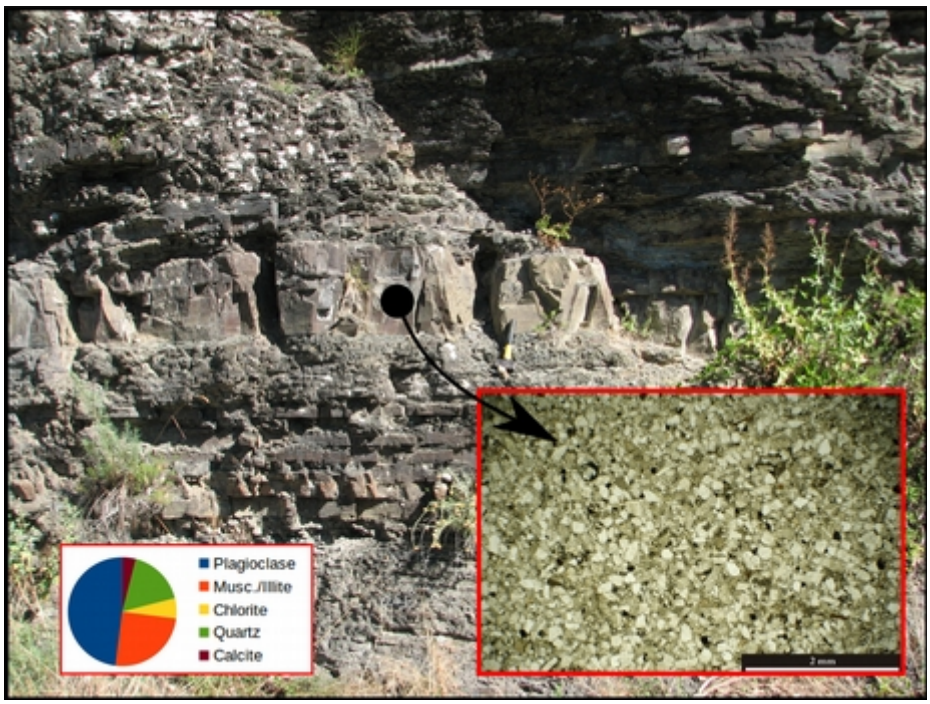

Figure 12: facies Vs and relative composition (XRD)

14

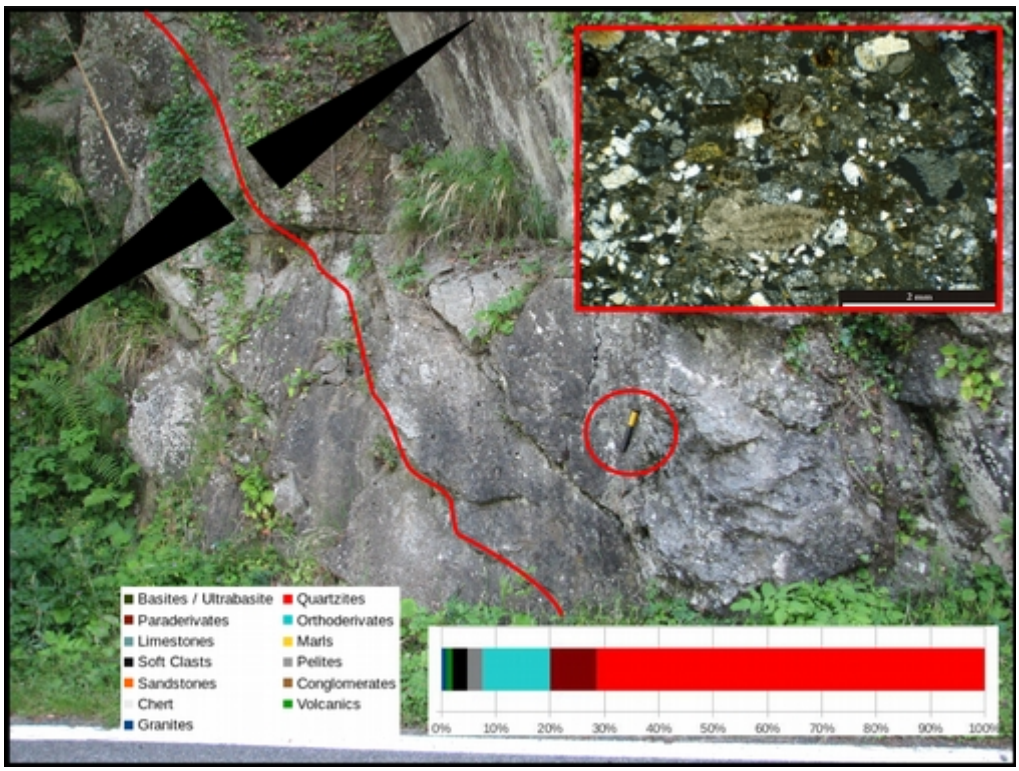

Figure 11: facies Vc and lithological association of gravel-sized detritus

Chamosite also shows different concentration of Fe and Mg, probably due to the original concentration of Fe-Mg in the substituted mineral. Secondary minerals are ilmenite, apatite and barite. Accessory minerals are zircon and pyrite, partially hydroxidized.

5. Discussions and final remarks

Figure 13: facies Cs.

15

Facies	Description	Petrography	Interpretation
L (*s.l.*)	Pluricentimetric to metric (up to 1.5 m thick) calcilutite layers, often packages with pluricentimetric (up to 50 cm thick) black pelite layers. Calcilutite layers are characterized by parallel lamination (Tb of Bouma, 1962), normal grading, basal flute casts, and bioturbation structures, which range between *chondrites targionii*, *phycosiphon* and *granularia* (these last two have been observed at the bottom of the Aveto River). At the bottom of the Aveto River, also fossil leaves (?) and yellow to orange concretions of gypsum and jarosite (SEM-EDS analyses) have been observed.	Massive mudstones (after Duhnam, 1962) containing rare loose crystals of quartz and ghosts of foraminifera planktonica (<10%). XRD analyses still ongoing	Facies D of Shanmugam et al. (1985), deposited by suspension fall-out dominated turbidity currents (Shanmugam et al., 1985; Mulder and Cochonat, 1996; Mulder and Alexander, 2001).
Sm	Varicolored (green and red) shales, weakly laminated, and shows *chondrite* trace fossils, up to 2 mm long. In thin section, trace fossils widely perturb the muddy detritus, composed of quartz and mica (probably muscovite).	In thin section, clay mineral aggregated and quartz loose crystals have been recognized. XRD analyses still ongoing.	Facies G (pelagic and hemipelagic sediments) of Shanmugam and Moiola (1988). According to Bromley and Ekdale (1984), Ekdale and Mason (1998), Miller (2007) and Seilacher (2007), the only presence of *Chondrite* trace fossils indicate low-oxigen conditions of sedimentation in a deep basin.
Sf	Dark gray pelite layers, up to 50 cm-thick, grouped in single packages up to 20 m-thick, or in single layers intercalated in more energetic events (like facies Ss or Vp). It is characterized by fine silty detritus, rarely passing to mud through normal grading, good sorting, convolute laminations (Tc of Bouma, 1962), asymmetric ripples (Tc of Bouma, 1962) to parallel laminations (Td of Bouma, 1962).	Micas are the most representative mineral, followed by quartz, while small leaves and dark clay rip-up clasts are quite common. Calcite is common. In thin sections, alignment of loose crystals of muscovite, quartz and subordinate biotite, and by rip-up clasts of mud are common. Intrabacinal fragments (calcilutite mudstones - after Dunham, 1962 - and fossil fragments - foraminifera) have been documented. Calcite cement has been commonly observed.	Low density turbity currents of Lowe (1982), facies D (turbidity currents – low energy) of Shanmugam and Moiola (1988), facies F9 (dilute tail of turbidite currents) of Mutti et al., 2003. Principal flow driven mechanisms are represented by traction and suspension (Lowe, 1982; Mulder and Alexander, 2001). Sedimentary petrography “a” described by Elter et al., (1999a,b).
Ss	Very coarse (microconglomerate) to fine brownish sandstones, up to 1.5 m-thick, characterized by massive layers and/or normal graded layers, with structureless to convolute structure (Ta to Tc of Bouma, 1962), rip-up clasts, flute casts, bioturbation structures (*Chondrites targionii* (?)).	Loose crystals of quartz and micas (muscovite and subordinate biotite), with subordinate dark gray rock fragments. Rare carbonate cement.	Facies B and C of Shanmugam et al. (1985), facies F5 (massive sandy flow), and F8 (structureless Bouma “a” division) and F9 (Bouma “b” through “e” divisions) of Mutti et al. (2003). Massive sandy debris flows were deposited by hyperconcentrated density flows (Mulder and Alexander, 2001, Mulder et al., 2003) or high density turbites of Talling et al. (2012). Normal graded

Facies	Description	Petrography	Interpretation
			strata are “banded” sandstones of Haughton et al. (2009) deposited by hybrid events, or low-density turbites (Lowe, 1982; Mulder and Alexander, 2001; Haughton et al., 2009). Sedimentary petrography “a” described by Elter et al., (1999a,b).
Sc	Metrix to plurimetric matrix- and clast-supported conglomerates, up to 21 m-thick, massive, normal graded or reverse to normal graded, characterized by rounded to subordinate sub-angular gravel-sized detritus in a brownish matrix. Matrix-supported conglomerates are generally massive, whilst clast-supported bodies show a weak imbrication, and overlay the lower facies Ss through erosional contact.	Gravel-sized detritus: abundant crystalline rocks, with subordinate limestones, rare sandstones and volcanics (andesites). Matrix: siliciclastic matrix with abundant rock fragments of metapsammites, carbonates, metaigneous, plutonics, terrigenous and metacarbonates, and loose crystals of K-feldspar, plagioclase, monocrystalline quartz, biotite, muscovite, and rare chlorite.	Facies A of Mutti and Ricci Lucchi (1978), facies F2 (structureless, poorly sorted conglomerates) and F3 (clast-supported conglomerates) of Mutti et al. (2003), facies A and F of Shanmugam et al. (1985). Normal graded events comparable to hyperconcentrated flow deposit overlain by a base cut-out hyperpycnite of Mulder et al. (2003). Sedimentary petrography “a” described by Elter et al., (1999a,b).
Vp	Metric massive sandy-sized deposit and plurimetric (up to 30 m thick) blocky-rich deposits, characterized by good grade of welding, weak imbrication (conglomerate deposits), dark green matrix, chilled margins around accidental clasts. Jigsaw structures have been also recognized in one deposit.	Gravel-sized detritus: abundant accidental lithics (up to 70 cm) of orthoderivates, limestones, volcanics, paraderivates, metagabbroes and rare plutonics. Matrix: felty porphyritic to eutaxitic, rich in euhedral zoned plagioclase, amphibole pyrite, subordinate relicts of pyroxene, loose crystals of quartz, phlengite-schist fragments. XRD analyses have identified plagioclase (59.6%), muscovite/illite (22.2%), clinochlore (7.1%), biotite (6.1%) and horneblende (5.1%) as major mineralogical fractions.	Lava-likeTl(nl) PDC deposit (massive lapilli-sized deposit) and five EmLTlCo PDC deposits (clast-supported conglomerate deposits), according to the no-genetic classification of Branney and Kookelar (2002). They represent ignimbrite and debris avalanche deposits preserved below the sea level (Branney et al., 1992; Branney and Kookelar, 1992; Branney and Kookelar, 2002). Never described by Elter et al. (1999a,b).
Ve	Massive coarse sandstones and conglomerates, up to 20 m-thick, alternatively packaged in sequences up to ca. 60 m-thick, characterized by green matrix (similar to that facies Vp), basal groove casts, flute casts, aligned rip-up clasts of marl, mud and Vp facies, and bioturbation structures (*Chondrites*). Conglomerate deposits can be alternatively massive or revers to normal graded.	Monogenic volcanic fragments tend to form a dark green pseudomatrix, with accidental lithics, fossil fragments (*Nummulites*) and crystals dispersed. Accidental particles can be both angular or rounded.	Facies F3 (clast-supported conglomerates) and F5 facies (massive sandy flows) of Mutti et al. (2003), sandy debrite facies of Talling et al. (2012). Monogenic pyroclastic composition and reverse to normal grading are ascribable to rapid discharge of

Facies	Description	Petrography	Interpretation
			reworked unconsolidate PDC deposits into the basin as lahar (e.g. Calder et al., 2000; Mulder et al., 2003; Lube et al., 2012). Sedimentary petrography “b” described by Elter et al., (1999a,b).
Vf	Thin green pelite layers, up to 5 cm thick, characterized by parallel lamination (Tb of Bouma, 1962), rarely observed.	Not observed	F6 (horizontally- and cross-stratified megaripple-shaped beds) of Mutti et al. (2003), representing reworked unconsolidated tuff events (e.g. Cuitino and Scasso, 2013), underwater deposited by tractional turbidite currents (Lowe, 1982). Sedimentary petrography “b” described by Elter et al., (1999a,b).
Vs	Greenish, very coarse to fine sandstone layers, up to 2 m-thick, usually in packages up to 10 m-thick, characterized by massive or normal grading, showing massive to laminar sequences (Ta to Te of Bouma, 1962) and flute casts.	Almost volcaniclastic, with andesite rock fragments angular to sub-angular, metamorphic (ortho- and paragneiss rock fragments), sedimentary fragments, loose crystals of quartz, plagioclase, k-feldpars and white mica between sub-angular and rounded shaped.	Quite similar to facies Ss in terms of depositional mechanisms. Facies B and C of Shanmugam et al. (1985), facies F5 (massive sandy flow), and F8 (structureless Bouma “a” division) and F9 (Bouma “b” through “e” divisions) of Mutti et al. (2003). Massive sandy debris flows were deposited by hyperconcentrated density flows (Mulder and Alexander, 2001, Mulder et al., 2003) or high density turbites of Talling et al. (2012). Normal graded strata are “banded” sandstones of Haughton et al. (2009) deposited by hybrid events, or low-density turbites (Lowe, 1982; Mulder and Alexander, 2001; Haughton et al., 2009). Sedimentary petrography “a” described by Elter et al., (1999a,b). Sedimentary petrography “b” described by Elter et al., (1999a,b).
Vc	Massive greenish conglomerates, up to ca. 11 m-thick, reverse to normal graded, characterized by coarse-sandy base (up to ca. 2 m-thick), which is sharpy overlain by the main matrix-, locally clast-supported conglomerate unit.	Gravel-sized detritus: abundant orthoderivates and paraderivates, with rare sandstones. Matrix: volcanic and orthoderivate fragments constitute alternatively the most abundant detritus components, with loose	Facies F2 (structureless, poorly sorted conglomerates), locally passing to F3 (clast-supported conglomerates) facies, of Mutti et al. (2003). They are ascribable to debrite facies of Mulder et al. (2003), or “linked” debrite of Haughton et al. (2009).

Facies	Description	Petrography	Interpretation
		crystals of quartz, feldspar, muscovite and fossil fragments.	Sedimentary petrography “a” described by Elter et al., (1999a,b).
Cs	Dark gray, parallel laminated (Tb of Bouma, 1962), silty to fine sandy-carbonate layers, up to 30 cm thick, with a massive, matrix-supported micro-conglomerate event intercalated (1,5 m thick)	Associations of “epidote+light mineral” (usually quartz) and “garnet+epidote”, single crystals of epidote, apatite, zircon, rutile and horneblende (Di Capua et al., 2012).	Facies F9 (Bouma “b” through “e” divisions) and locally F5 (massive sandy flows) of Mutti et al. (2003). Mixing between carbonatic and siliciclastic detritus is ascribable to climate-driven floods of Brandano and Ronca (2014).

Table 1: facies constituting the Val d'Aveto Formation

5.1 Stratigraphic architecture of the Val d'Aveto Formation

The reconstruction of the Val d'Aveto Formation architecture appears a puzzle, due to the intense brittle deformation that deleted most of the original geometries and stratigraphic relations of the deposits. Our logs have been correlated to the general stratigraphic log of Elter et al. (1999a), which has been defined through biostratigraphic data and modified after Di Capua et al. (2014).

As recognized on the western side of the Aveto River, the bottom of the Val d'Aveto Formation is alternatively represented by facies L *s.l.* and Sf, but no stratigraphic relationship has been observed between them in the field. Facies L *s.l.* is directly overlain by facies Ve (Fig.4), whereas facies Sf is overlain by facies Ss and Sc in a thickening upward sequence (Fig.2). As Elter et al. (1999a) documented a couple of calcareous events, we consider facies L *s.l.* as the base of the sequence on the western side of the Aveto River. On the eastern side, instead, the bottom of the Formation is only represented by facies Sm, overlain by facies Sf and Sc (facies Ss is missed). Thus, facies L *s.l.* and facies Sm are the lower facies of the Val d'Aveto Formation, once in heteropic contact, and represent, respectively, the outer foredeep sequence and the deepening-upward ramp succession of Mutti et al. (2003), or the basin plain association of Shanmugam et al., (1988). They formed an underfilled depositional system comparable to that documented in the Eocene Perialpine basins, where facies L *s.l.* is the turbidite unit, and facies Sm the middle

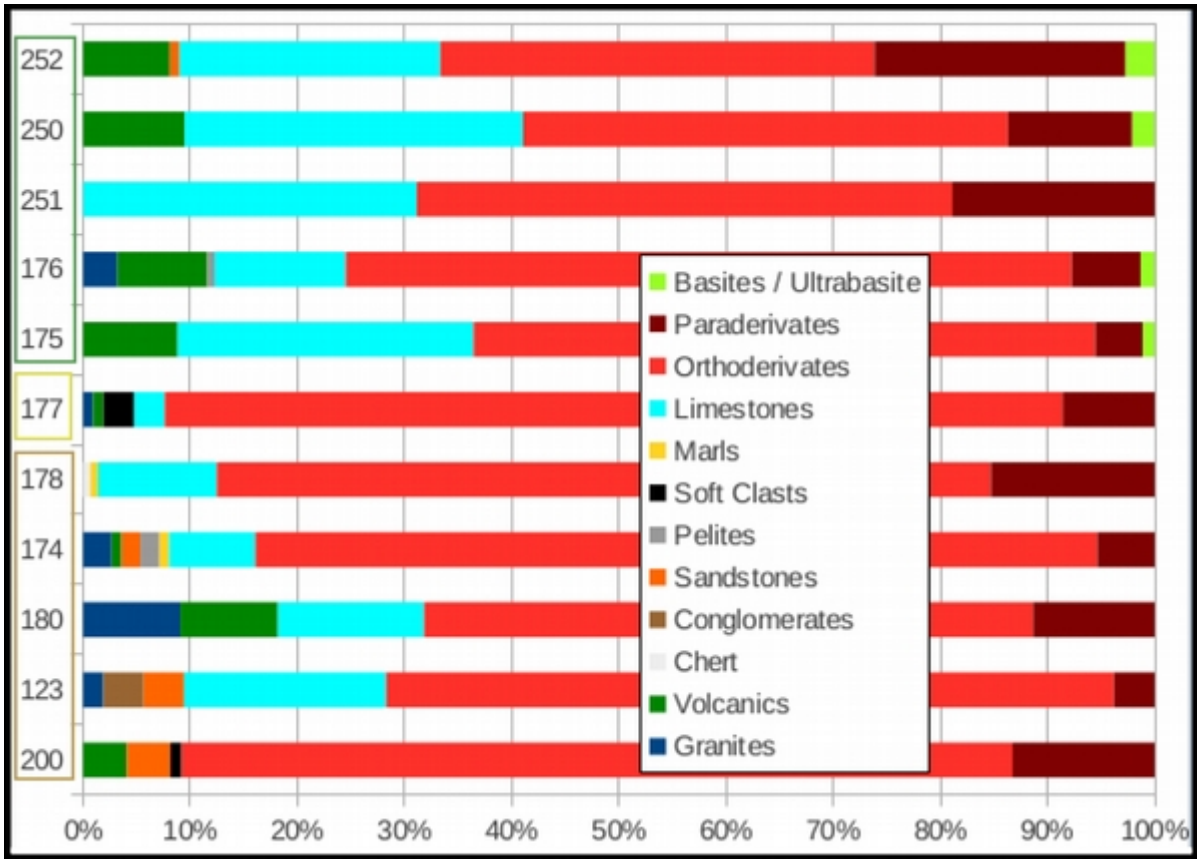

Figure 14: clast-count results. Brown squared numbers referred to facies Sc, light green to Vc and green to Vp/Ve. See Fig.2 and 3 for stratigraphic ubications.

hemipelagic unit (Sinclair, 1997; Allen et al., 2001). Facies L *s.l.* may be also ascribable to the distal part of the calcareous turbidites of the Canetolo Unit, but furher biostratigrapic constrains are needed to confirm this hypothesis.

As the siliciclastic inputs increase, carbonate signal is rapidly diluted by the terrigenous one, and a basinal turbidite system begins to prograde seaward above the basinal plain, according to the general model of Mutti et al. (2003). On the western side of the Aveto River facies Sf deposition onset and passage to facies Ss deposition in a thickening-upward sequence document the development of a fan fridge zone deep into a lobe area (Shanmugam et al., 1985; Shanmugam and Moiola, 1988; Catuneau, 2002), as shown in Figure 16. Incoming of gravel-sized detritus (facies Sc) and subsequent fining-upward identify two channel-fill sequences (or slope sequences) and the seaward fan progradation (Shanmugam and Moiola, 1988). This progradation appears to be better exposed on the eastern side of the Aveto River, where channel-fill deposits (facies Sc) have been encountered thicker than lobe sequences (facies Sf and Ss), and where volcanogenic detritus (facies Vc, Vp and Ve) start to be first mixed and than superimposed on the siliciclastic sedimentation.

As huge amounts of volcanogenic detritus start to supply the basin in relatively short times, submarine fan becomes wider, channels migrate and overbank deposition is promoted, as observed

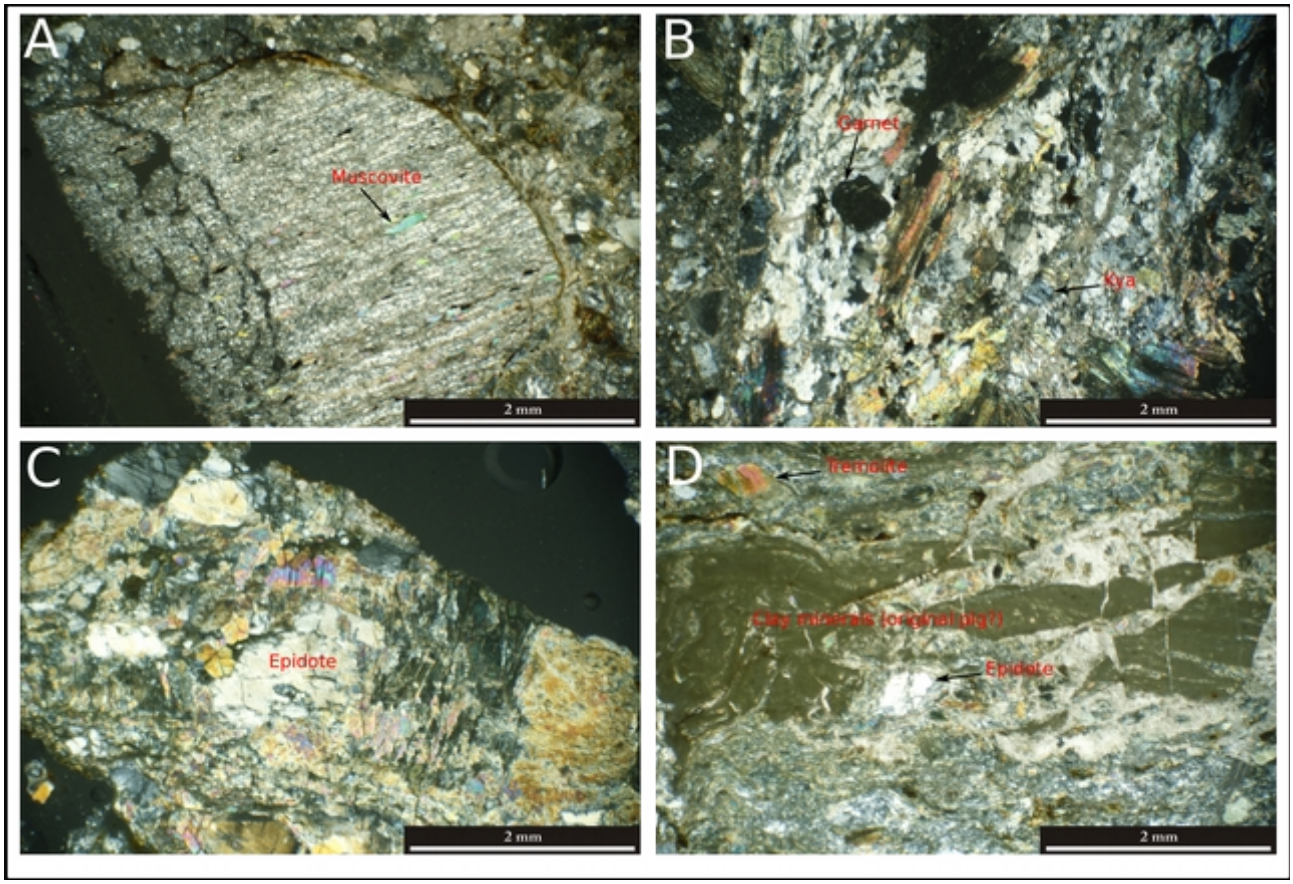

Figure 15: mineralogical association in metamorphic pebbles. A-b) micaschists; c) metagabbro with low deformed texture; d) gabbro with mylonitic texture.

17

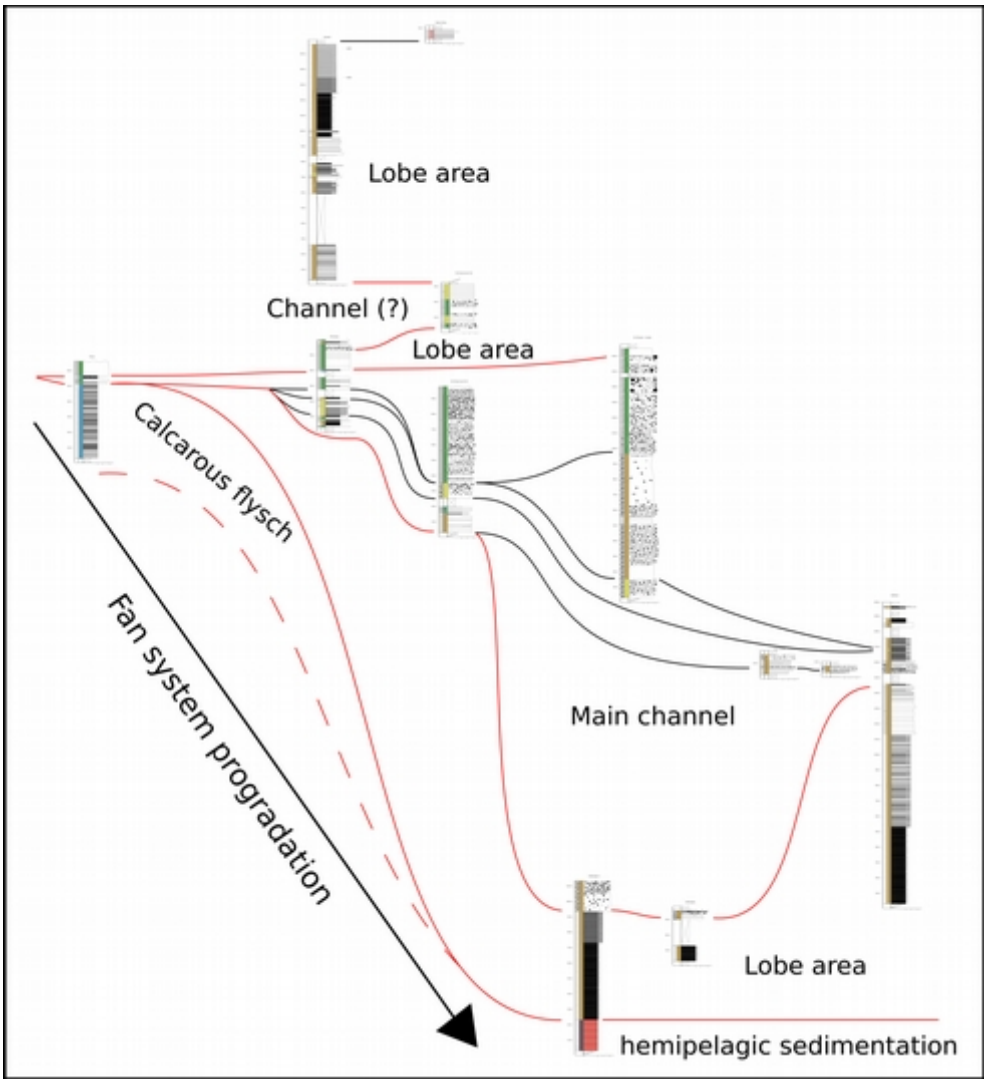

Figure 16: log correlations and reconstruction of the stratigrafic architecture of the Val d'Aveto Formation

at the bottom of the Aveto River, where facies Ve directly overlays facies L *s.l.* The coarser facies (Vp, Ve clast-rich and Vc) remain channelized in the fan system, also according with geometries recognized in the field by Elter et al. (1999a,b), pinching out to NW. These deposits can be also interpreted as slope deposits, according to Shanmugam and Moiola (1988). Large volumes of pyroclastic detritus rapidly enter the water and deposit thick primary and secondary sequences, often rich in accidental fragments and clasts scraped off the drainage system and/or the submarine slope (Calder et al., 2000; Trofimovs et al., 2006). Minor or rare siliciclastic (facies SS and Sf) and calcareous (facies L *s.l.*) are interbedded in this phase.

In the upper part of the Formation, volcanogenic sedimentation (facies Vp and Ve) tends to disappear, or to be constrained in few, fine and thin events (facies Vs and Vf), according to Mattioli et al. (2012). Here, siliciclastic sedimentation is dominated by facies Ss and Sf, forming a middle to lower submarine fan association (Shanmugam et al., 1985) or a lobe-fringe facies association

(Shanmugan and Moiola, 1988), together with facies Cs. Facies associations here exposed reflect architectures of immature passive margin models (Shanmugam et al., 1988) or sandy-rich system of Stow and Mayall (2000). Further discussions on detritus provenance and role of tectonics versus climate in sediment supply are provided in paragraph 5.3.

5.2 Reconstruction of the source-to-sink system

The reconstruction of the Val d'Aveto Formation source-to-sink system is still debated. Sandstone petrography seems to reflect an Alpine provenance (e.g. Cibin et al., 2001), partially rejected by Mattioli et al. (2012), who however do not consider the large amount of continental detritus in the Val d'Aveto Formation. In both cases, sedimentary and volcanogenic information have been considered separately, or one has been considered much more suitable for provenance reconstructions rather than the other. Preserved PDC deposits (facies Vp, Fig.9) represent a temporal-constrained snapshot on syn-sedimentary magmatism and source-to-sink system, as they are instantaneously discharged into the basin after having flown across it. As the huge amount of many volcanic sequences along the Alps, different in ages (e.g. Permian and Triassic), makes geochemical correlations particularly weak and potentially mistakable, as suggested by Di Capua et al. (2015) for the Tertiary Southalpine Foredeep sequences of the Villa Olmo Conglomerate, the andesite nature of the PDCs need to be firstly considered in the identification of the magmatic source. It agrees with the Oligocene age of Mattioli et al. (2002) inferred on an andesite lava clast (29.5 Ma), and together with other two dacite ignimbrite clasts aged by the same authors (32.1 Ma and 29.7 – 29 Ma), represents the syn-sedimentary magmatic suite discharged into the foredeep basin. All the other volcanic products considered by Mattioli et al. (2012), overall resulting to have been experienced by different metamorphic conditions (basic/ultrabasic - this work - and rhyolite detritus - Elter et al., 1999a), testify that other older volcanic suites were contemporary drained into the basin, and the Oligocene age cannot be extended to all of them. So, as three different volcanic suites were active during the same Oligocene time (Biella Volcanic suite - Beger et al., 2010 - Tertiary SE France Volcanism - Montenat et al., 1999 - and Sardinia/Corsica volcanism - Réhault et al., 2012), provenance needs to be traced considering the continental detritus signal.

As documented by different authors (e.g. Pirkenseer et al., 2011; Coletti and Basso, 2014; Di Capua et al., 2015), fossil associations in calcareous pebbles can represent a strong provenance constrain, as are features identifying specific depositional basins through times. In the Val d'Aveto Formation, the large amount of Cretaceous to Tertiary carbonate flyschoid pebbles (Elter et al., 1999b) results fundamental on at least spatially confining the source-to-sink system. In fact, as no Cretaceous to Tertiary carbonate flyschoid units are exposed in the internal part of the western Alps,

nor in the volcanoclastic deposits of the Biella Volcanic Suite (Kapfener et al., 2010), this part of the Alps and magmatic suite can be excluded from the potential source area. More suitable as sourcing sequences, instead, appear to be the Cretaceous helmintoid flysch, named Antola Unit and already discharged in the Tertiary Piedmontese Basin during the Oligocene times (*cf.* Savignona Conglomerate and Molare Conglomerate - Elter et al., 2006; Capponi et al., 2008, 2009; Marroni et al., in press), and the Oligocene, upper flyschoid External Ligurian units (Elter et al., 2005), exposed from the Ligurian Alps far to Western Corsica during the Rupelian times (Carmignani et al., 2004). This implicates that the already exhumed and structured Ligurian Units were constituting an orogenic boundary dividing the Tertiary Piedmontese Basin and the Apennines Foredeep Basin. Thus, the Val d'Aveto Formation would represent an “embryo” of the Apennines Foredeep, if compared with the younger Macigno and Marnoso-Arenacea Formations (upper Oligocene to Miocene - Mutti et al., 2002), as the Alps are not considerable as sedimentary source. We are

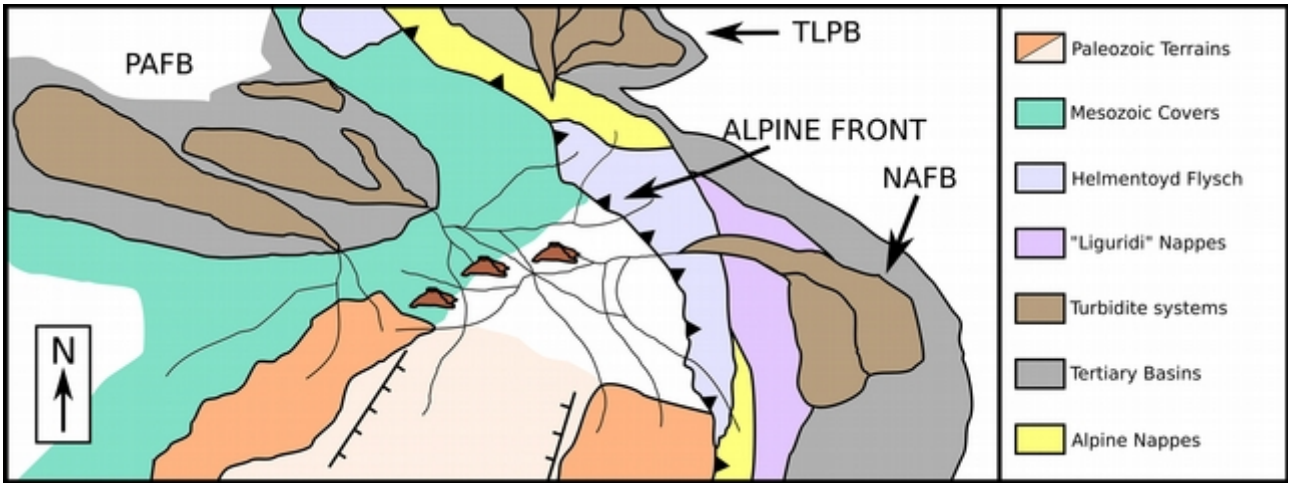

Figure 17: paleogeographic reconstruction of the source-to-sink. TLPB: Tertiry Ligurian Piedmont Basin, NAFB: Northern Apennines Foredeep Basin; PAFB: Peripheral Alpine Foreland Basin

probably looking at a confined basin, far away from the developed basins in which Macigno and Marnoso-Arenacea detritus were deposited (Cibin et al., 2001, 2003; Catanzariti et al. 2009; Dall'Olio et al., 2013; Di Giulio et al., 2013; Talling et al., 2013).

As northward confined by the exhumed Antola Unit, detritus pathways result more suitable with the general directions of sediment discharge from the Sardinia-Corsica-SE France area up to the western peripheral foreland basins around the Western Alps (Annòt Sandstones, St. Antonine Conglomerate, Bârreme Sandstones - e.g. Stanley, 1980; Evan and Mange-Rajetzky, 1991; Sinclair, 2000; Joseph and Lomas, 2004; Amy et al., 2007; Etienne et al., 2012; Grosjean et al., 2012; Simicek and Bàbek, 2015). Rhyolite ignimbrite clasts described by Mattioli et al. (2012) and partially metamorphosed, according to Elter et al. (1999a), are ascribable to the Permian rhyolitic province which extends from the Estérel Massif (SE France), offshore to the Tyrrenean sea and the

northern part of Corsica (Poitrasson and Pin, 1998; Cortesogno et al., 1998; Sinclair, 2000; Rollet et al., 2002). This provenance is also consistent with 1) the preponderant amount of orthoderivate and paraderivate pebbles and 2) the minor amount of crystalline pebbles, which are all ascribable to the Varisican Belt of SE France and Corsica (Cortesogno et al., 1998; Sinclair, 2000; Corsini and Rolland, 2009). Metamorphic conditions and mineralogical associations we documented in the Val d'Aveto Formation clasts are similar to those suffered by the Varisican terrains (from initial HP-HT conditions, to MP-MT and late LP-HT conditions defined by Corsini and Rolland, 2009), and crystalline clast associations to the calc-alkaline Carboniferous granitoids (granodiorites, tonalites and granites - Cortesogno et al., 1998; Onézime et al., 1999; Rollet et al., 2002). Also the limited amounts of underfomed to mylonitic basic/ultrabasic clasts (corresponding to picro-gabbroes of Mattioli et al., 2012) are here ascribed to the basic/ultrabasic lenses (amphibolite, gneiss and serpentine) now exposed in the Varisican Belt of SE France (Western Maures - Bellot et al., 2000), as well as to the ophiolites exposed in Northern Corsica (Rollet et al., 2002). Anyway, the limited amounts of such material suggests that was liberated from limited terrains. The ophiolite-rich detritus (ultrabasites, basites, radiolarites and Cretaceous-Tertiary limestones), constituting further

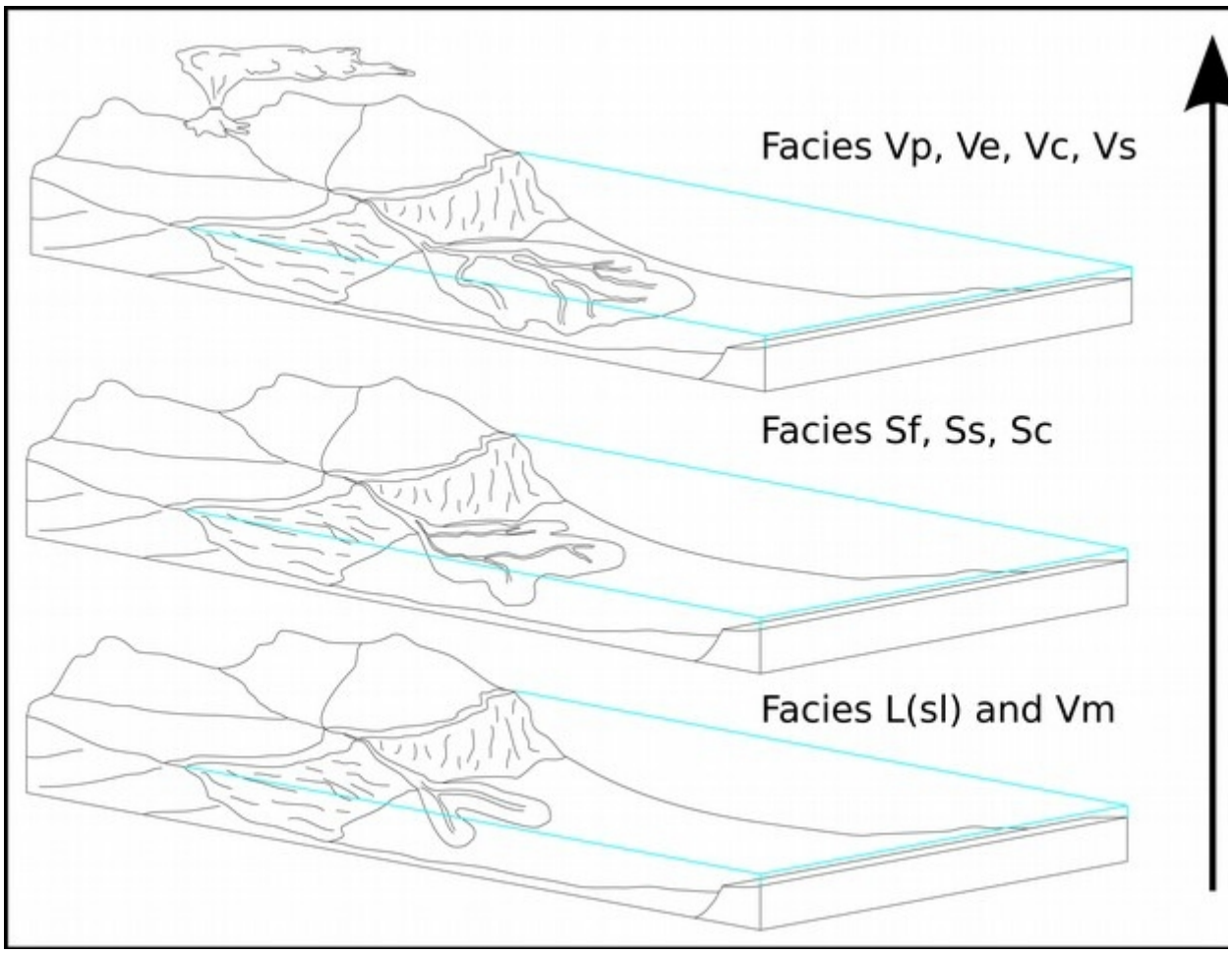

Figure 18: response of the source-to-sink to the tectono-climatic (first and second stage from the bottom) and volcanism (third stage).

to NW the upper member of the Val d'Aveto (Marroni et al., 1999), might be derived from the activation of the Sestri-Voltaggio zone, according to Federico et al. (2004) and Capponi et al. (2009). A similar provenance may be also traced through heavy mineral associations, characterizing the upper facies Cs and provided by Di Capua et al. (2012), comparable with the mineralogical associations documented by Evan and Mange-Rajetzky (1991) in the Bârrem basin. Phengite-schist accidental lithics recognized in the first PDC event are related to the erosion of “Schistes lustrés” sequences and find a correlation with phengite-schist fragments of the “Schistes lustrés” documented in a lava block, characterized by fluidal texture, plagioclase phenocrysts up to 2 mm, ghosts of ferromagnesian minerals in a crypto-crystalline matrix in the Tristanite Ridge (43±2.3 Ma - Rénault et al., 2012).

The last constrain in source-to-sink reconstruction is represented by the Ar-Ar ages of Mattioli et al. (2002) on andesite to dacite products of the Val d'Aveto Formation, more consistent with the general ages of the SE France volcanism (36.1±2.2 – 29.0±0.5 Ma) rather than that of Corsica (from 19.6±1.3 Ma in NW Corsica – except for the 43±2.3 Ma age inferred on a lava block) (Montenat et al., 1999; Rollet et al., 2002; Réhault et al., 2012), implying a direct control on the volcanogenic sedimentation by the SE France volcanic centers. These inferences may be verified taking in account provenance traced by Stanley (1980 and ref. therein) for the andesite-rich (33 Ma-Rollet et al., 2002, and ref. therein) Saint-Antonin Conglomerate (Upper Eocene – Lower Oligocene), where lithological associations, comparable to that of the Val d'Aveto Formation, have been recognized as fed by the SE France volcanism and SE France-Corsica Varisican Belt detritus (e.g. Stanley, 1980; Montenat et al., 1999; Joseph and Lomas, 2004). This suggest a brotherhood between the Early Oligocene Northern Apenines Foredeep basin (Val d'Aveto Formation) and the Early Oligocene peripheral Western Alpine Foreland basin (SE France sedimentary formations) (Fig.17), enhancing a continental location of the volcanic source (Elter et al., 1999a; Di Capua et al., 2014), rather than a local one (Mattioli et al., 2012).

5.3 Volcanism, tectonics and climate in clastic sediment supply

In general, clastic sedimentation depends on erosion and transportation of detritus, as accumulation rates are controlled by detritus liberation from source rocks and transportation along the system (e.g. Allen, 2008). Climate, tectonics and volcanism act on these surfacial processes at different spatial and temporal scale in a single source-to-sink system. Climate produces sediments by rock weathering and mechanical erosion, and transport them by water and wind along the source-to-sink system (e.g. Howard et al., 1994; Fielding et al., 2009). In terms of processes, climate signal results particularly relevant at short temporal scales (e.g. Peizner et al., 2001), when violent episodic events

are recognizable (e.g. Mulder et al., 2003), but tends to be diluted during long periods in the tectonic signal (e.g. Mutti et al., 2003). Tectonics has a strong control on sediment production, as able to mechanically deform rocks, rapidly raise slopes and modify fluvial systems (e.g. Stewart et al., 2008), resulting in the liberation and supply of large amounts of detritus in the environment (e.g. Burbank et al., 1988), and is persistence at long temporal scale (e.g. Garzanti and Malusà, 2008). However, tectonics cannot transport material and water is needed to discharge detritus into the basin (e.g. Milliman and Syvitski, 1992). Volcanism can: 1) produce huge amounts of sediments independently from rock weathering (Smith, 1991), as pyroclasts are generated during violent explosive manifestations and form thick, unconsolidated deposits whelming topography, and 2) transport detritus far away from the source, as volcanogenic material can either be ejected in the air (e.g. Zanchetta et al., 2011) or flow downslope from the volcanic flank along the surrounding environment during PDC events (e.g. Sulpizio et al., 2014). As in the Val d'Aveto Formation these three signature are recognized (Elter et al., 1999a; Mattioli et al., 2012; Di Capua et al., 2014, this work) further discussion are needed to define how climate, tectonics and volcanism have influence this stratigraphic record (Fig.18).

As in all the peripheral Alpine basins, also in the Val d'Aveto Formation the first, calcareous, flyschoid inputs reflect a period of low sediment supply (Mancin et al., 2001; Ford and Lickorish, 2004; Garzanti and Malusà, 2008; Di Capua et al., 2015). Supply of fine calcareous detritus (facies L *s.l.*), resedimented below the shelf, is consequence of the subaerial exposure and karsification of the Nummulitic Limestones carbonate ramp (Sinclair, 2000), at the beginning of sea level fall (Merino-Tomé et al., 2007; Reijmer and Andresen, 2007), rather than as driven by slope instability (Drzewiecki and Simò, 2002). Minor siliciclastic turbidites were discharged by flood dominated river and fan deltas draining the continent (Merino-Tomé et al., 2007).

At the beginning of the siliciclastic sedimentation (32 Ma – Elter et al., 1999a), the SE France-Corsica system started to be affected by reactivation of Alpine thrust, feeding the SE France basins since the Early Priabonian times (e.g. Evan and Mange-Rajetzky, 1991; Joseph and Lomas, 2004), as normal faults owing to the incipient Ligurian rifting (Jolivet et al., 1999; Rollet et al., 2002; Dumont et al., 2011). In contrast with the geodynamic evolution of the source area, Aveto fan is characterized by sedimentological trends of active margin fans (Shanmugam and Moiola, 1988; Shanmugam et al., 1988; Mutti et al., 2003), as though controlled by thrust progradation toward the outer margin of the Apennine basin. Therefore, a rapid respond to sea level fall during the Early Oligocene (Wade and Pälike, 2004; Jovine et al., 2009), is more suitable to explain the seaward fan progradation, according to the model proposed by Catuneau et al. (2011) for mixed carbonate-clastic mi-Carboniferous Yoredale cycles of northern England. Increase of hyper-concentrated flow

events, discharged by rivers in the small shelf canyon heads during sea level drops (Mulder et al., 2003) and persistence in liberation of calcareous clasts by the still exposed Creta-Oligocene sequences, as documented in similar climatic conditions by Merino-Tomé et al. (2007), support these inferences.

When volcanism begins, volcanogenic events rapidly discharge into the basin large volumes of detritus, cannibalizing the source-to-sink system, and almost hiding at all the siliciclastic/calcareous sedimentation. Moreover, even though field clast counts resulted in an ephemeral increase (up to 10%) of volcanic gravel-sized detritus, granulometric analyses performed on siliciclastic and volcanogenic deposits show an increase in mean and maximum size of sediments discharged when volcanism begins, according to Elter et al. (1999a) and Di Capua et al. (2014). This is due to multiple impact of volcanism on the environment.

First, during syn-eruptive periods, environment is overloaded by large amounts of unconsolidated, volcanic, sandy-sized detritus that tends to destabilize fluvial systems, even at regional scale (Mandville et al., 2009). This increases sediment yield and alteration of pre-eruptive drainages, whose modification can persist over thousands years (Smith, 1991). Eruptions and consequently acid rains can also damage vegetation, resulting in exposition of terrains to rapid erosion and promotion of flash flood events (Alexander et al., 2010). As documented in the Val d'Aveto Formation, PDC events (facies Vp) are all followed by epiclastic episodes (facies Ve), detecting periods during which the drainage patterns of the source-to-sink system were continuously modified by flash floods and lahars fed by the on-shore unconsolited deposits. Instead, facies Vc and Vs, together with minor or rare siliciclastic (facies SS and Sf) and calcareous (facies L *s.l.* inputs, are interpreted as marking quiescence periods in the volcanic activity and consequently reestablishment of normal, fluvial-driven supply (Smith, 1991).

Second, as PDCs are triggered and often sustained by explosive events, they result as high energetic events that can move for tens kilometers from the source (Branney and Kokelaar, 2002). If channelized, PDC erosional behavior and flow capacity are enhanced (Calder et al., 2000; Sulpizio et al., 2007; Doronzo, 2012; Brand et al., 2014). Flow capacity can also be favored by water injection under particular conditions (Branney and Kokelaar, 2002). Thus, PDCs constitute the most rapid way to transfer detritus across the source-to-sink system and/or discharge it into the basin. When such flows enter the water, if sustained by volcanic events like fountaining in a Plinian column (Branney and Kokelaar, 2002) or triggered by volcanic sector collapse (Ui et al., 2001), they have a higher kinematic energy, rather than that of fluvial-induced turbidites, which increases when added to kinematic energy of flows moving downslope into the basin, typical of classical turbite currents liberated from the delta fronts. This energy allows subareal to submarine PDCs to

run further than all the other turbides and trasport larger volumes of material deeper into the basin.

When volcanism switched off, siliciclastic and carbonaceous sedimentation again began to reach the basin. As already discussed in paragraph 5.1, facies associations documented in the upper part of the Formation results more consistent with facies of immature passive fan of Shanmugam et al. (1988), rather than an active fan (Shanmugam and Moiola, 1988; Mutti et al., 2003). This submarine fan retrogradation is the result of: 1) the progressive NW shifting of sediment supply, as testified by an upper ophiolite-rich member of the Val d'Aveto Formation documented by Marroni et al. (1999), tectonically-driven by the activation of the Sestri-Voltaggio Zone (Capponi et al., 2009); and 2) the sea level rise (Wade and Pälike, 2004; Jovine et al., 2009), which promoted sediment accumulation along the fluvial system (Allen, 2008) and limited detritus discharge into the basin.

5.4 Final remarks on sedimentary signals

Unraveling the sedimentary signals preserved in the Val d'Aveto Formation took us to the following conclusion:

1) Volcanism has a high but rapid impact on the environment, as its effects panted soon after the brief life of the volcanic source. In syn-eruptive periods, sediment production and transportation owing to explosive episodes net increased both sediment supplied to the basin, and energy of the events, as documented by the granulometric trends of gravel detritus.

2) Climate controlled the evolution (progradation and retrogradation) of the submarine fan, as respond to cyclical sea level, and types of deposits (increase of hyperconcentrated events from flash floods, according to Mulder et al., 2003).

3) Tectonics promoted shifting in sediment supply, due to the progressive activation of different deformational fronts.

Emplacemenet of welded pyroclastic density currents (PDCs) in a deep-marine environment: the Val d'Aveto Formation body (Northern Apennines, Italy)

In this section, we wider discuss mechanisms of transportation and emplacement of the pyroclastic density currents discovered in the Val d'Aveto Formation (Fig. 1). They represent facies Vp described in the previous chapter.

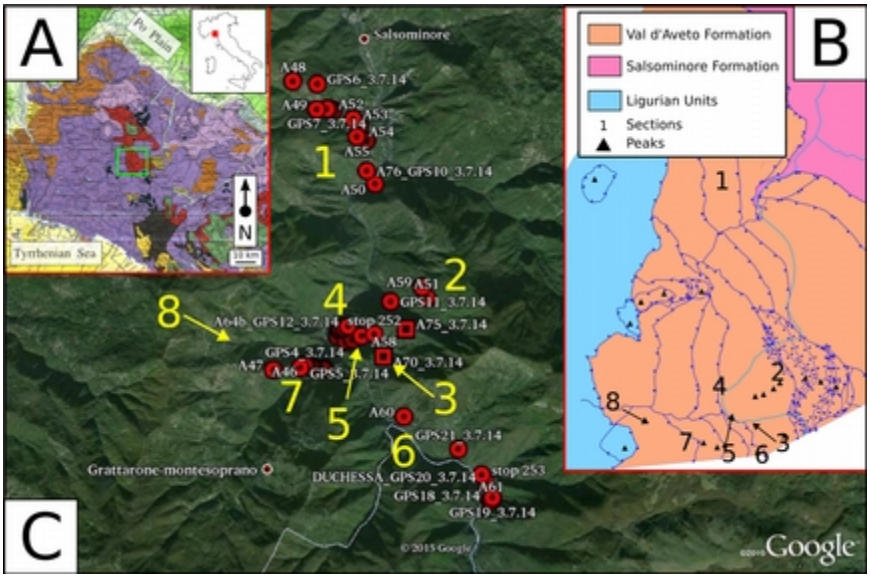

Figure 1:fieldwork map; a) tectonic map of the Northern Apennines; b) tectonic sketch of Val d'Aveto area; c) ubication of logs measured in the field.

1. Stratigraphic and textural features of the bodies

PDC n°1

The first PDC deposit (Fig.2-3a) is composed of a basal blocky-sized unit, 30 cm thick, with rounded, granule-sized accidental lithics of quarzoderives metamorphic rocks and shales in a green, sandy-sized matrix (Fig.3b), overlain by a massive, sandy-sized, strongly welded unit, 70 cm thick, with loose, euhedral crystals of plagioclase, cubic (most common), octahedral and pyritohedral pyrite, and dark fragments of schists (Fig.3c), sharply eroded by a post-eruptive event (Fig.2-3d). No gas pipe has been observed. Microscopically, blocky-sized unit shows a felty, porphiritic groundmass, characterized by euhedral primary volcanic zoned plagioclase (albite), amphibole and angular accidental schist fragments, with subordinated relicts of pyroxene, k-feldspar (accidental?), and quartz. Felty groundmass results brecciated, and quarzo-feldspatic sandy-sized accidental detritus, calcite and brown material (clay minerals from devitrified glass) fill fractures (Fig.3b).

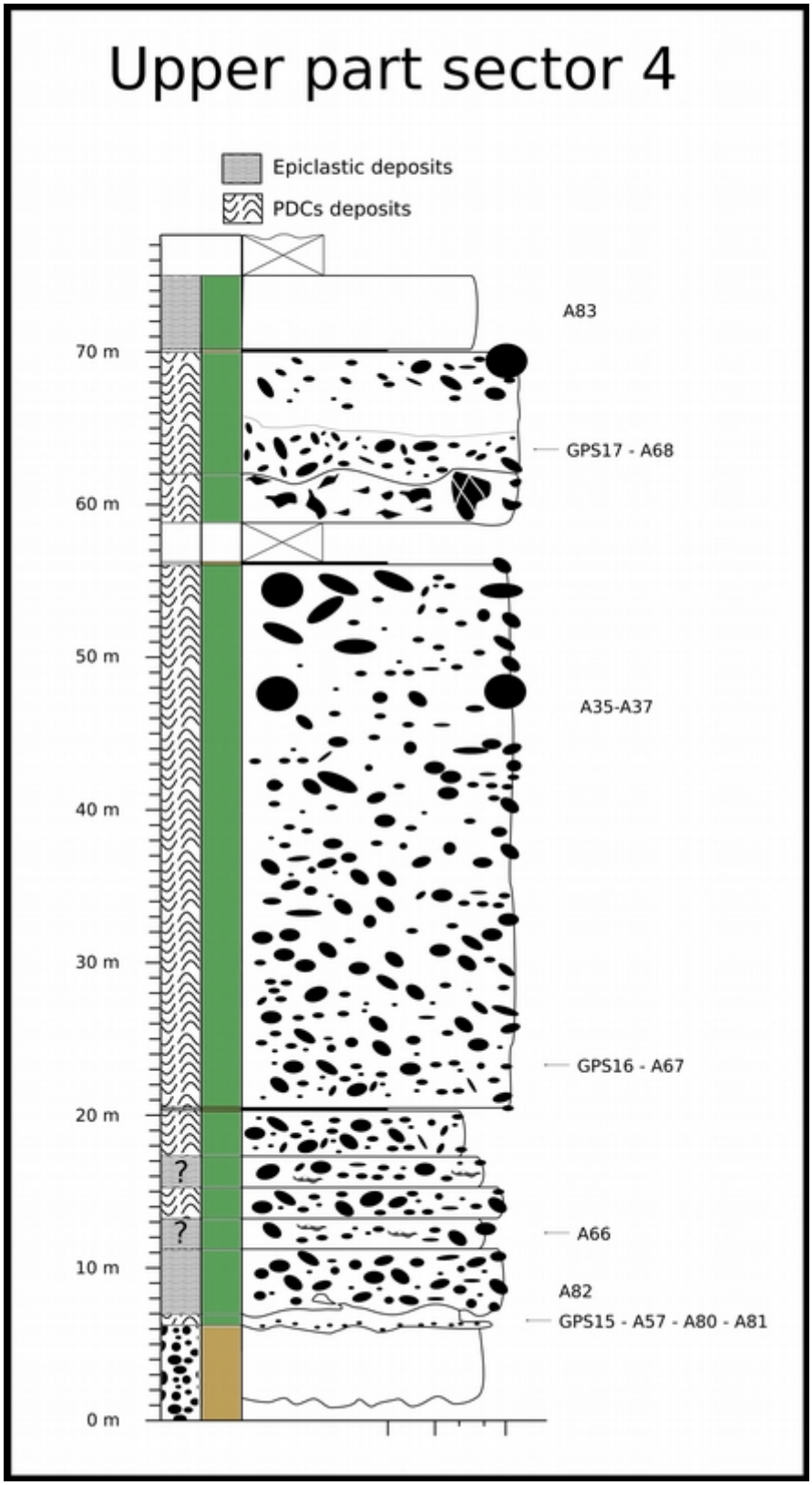

Figure 2: Stratigraphic log of the volcanogenic events in the Val d'Aveto Formation. Ubication in Fig.1b-c.

Pervasive secondary calcite is also present both on volcanic and siliciclastic components. The upper, massive unit has a felty, porphyritic volcanic texture, with euhedral primary volcanic zoned

plagioclase, amphibole, pyrite, and angular accidental phengite schist fragments (qualitatively up to 15% of the whole sample). Secondary illite and clorite pervasively altered the groundmass (Fig.3c). On the base of its features, this PDC deposit has been defined as a lava-likeTl lithofacies (Branney and Kookelar, 2002). XRD analyses identified plagioclase (59.6%), muscovite/illite (22.2%), clinochlore (7.1%), biotite (6.1%) and horneblende (5.1%) as major mineralogical fractions (Fig.3e). SEM-EDS analyses revealed that pyrite grains have oxidized rims and are spotted by silicate of Al, Ca and Fe (Fig.3f), and plagioclase is generally albite (secondary?), and schist fragments are rich in phengite (Fig.3g). On top, an erosional contact divides the PDC sequence from a 4 m-thick epiclastic conglomerate, composed of rounded quarzite-type rocks and shales, in a volcanoclastic matrix.

PDC n°2 and 3

These two bodies have been observed in a tectonically disturbed zone. Nevertheless, some features were still observable. Both results massive welded blocky-sized deposits, ca. 2 m-thick, with green sandy-sized matrix. Gravel-sized detritus is sub-rounded to rounded, and aligned outsize soft clasts (up to 50 cm long) are quite common. They are marls, unconsolidate tuffites (as observed in thin section) and green pelites. No gas pipe has been observed. The features preserved may indicate that these deposits can be defined as emLTlCo lithofacies (Branney and Kookelar, 2002). PDC n°4 is overlain by a thin layer of dark pelite, which has been squeezed into the upper PDC event n°5.

PDC n°4

PDC n°4 is composed of a poorly sorted, massive, welded, blocky-sized deposit, 35 m-thick, with a dark green, sandy matrix, with local, crudely clast alignment (Fig.3h-i). Clasts, up to 25 cm long, are weakly reverse graded and their shape ranges between sub-rounded and rounded (Fig.3k). Lithological association is mainly composed of substrate-derived material, in particular metamorphic rocks (ortogneiss, paragneiss, quarzite and amphibolite), with minor dark calcilutite (Fig.3j). Pyroclastic green rounded clasts generally represent a minor component, but locally can increase up to 45% of a 1 m^2 area. Rare rounded andesite lava blocks have been also observed. No gas pipe has been observed. In thin section, matrix appears eutaxitic, characterized by loose crystals of plagioclase and accidental rock fragments (pyroclastic, terrigenous and metamorphic), or glassy welded, characterized by glassy particles (with plagioclase composition) embedding loose crystals (metamorphic and plutonic loose crystals of quartz, and pyrite) and accidental rock fragments (terrigenous and metamorphic rocks), when distance between accidental lithics is very low (Fig.3i). On the base of its features, this deposit has been define as a emLTlCo lithofacies (Branney and

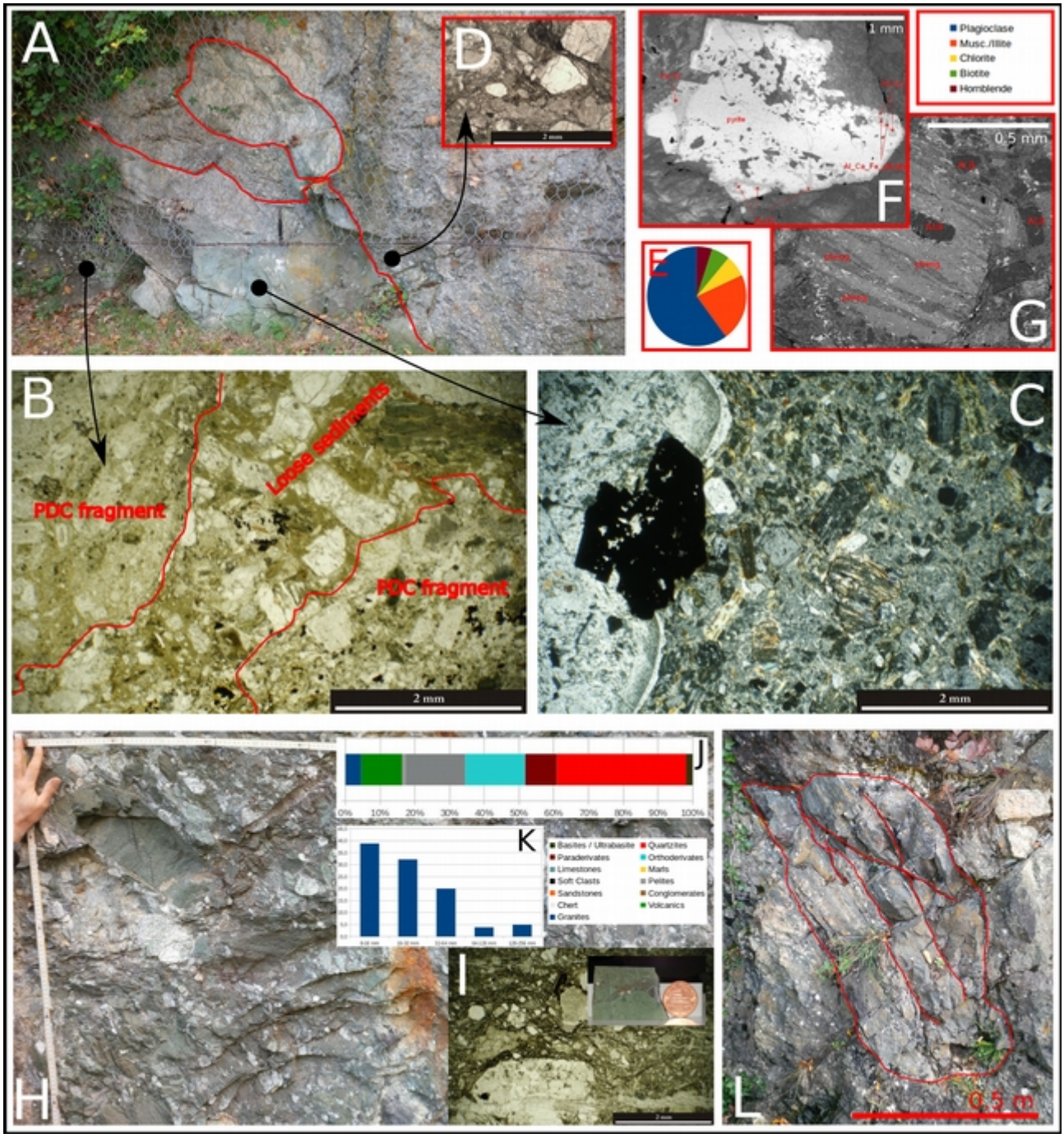

Figure 3: facies Vp; a) first PDC event; b) thin section of the boundary between the PDC and the underlain siliciclastic deposit; c) thin section of the main body of PDC1; d) thin section of the epiclastic event overlain PDC1; e) results of X-ray diffraction analysis on the main body of PDC1; f) pyrite crystal in SEM-EDS g) phengite-schist in SEM-EDS; h) blocky-sized part of PDC4 with i) groundmass thin setion (note the eutaxitic texture), results of j) pebble count and k) granulometry analysis; l) jig-saw structure on a metric boulder (PDC5).

Kookelar, 2002). It is overlain by a thin dark pelite layer.

PDC n°5

Unfortunately, PDC n°5 has been only observed from a bridge, because it appears in a narrow

valley. It appears again as a blocky-sized deposit, 3 m-thick, rich in angular, strongly heterometric accidental lithics, quite similar to PDC n°4, but without pyroclastic soft clasts. On the other hand, two boulders with jigsaw structures have been recognized (Fig.3l). No gas pipe has been observed. On the base of its features, this deposit has been define as a emLTlCo lithofacies (Branney and Kookelar, 2002). It is overlain by PDC n°6 through an erosional contact.

PDC n°6

The uppermost PDC event results quite similar to the fourth one. It is a massive, welded blocky-sized deposit, 8 m-thick, with metamorphic accidental lithics that dominate on the other blocky-sized components, usually dark limestones. Chilled margin around accidental lithics are observed. Green pyroclastic soft clasts (up to 35 cm ca.) are rare. Locally, erosional, not continuous surfaces with granule-sized accidental clasts and loose minerals (usually angular quartz) are preserved. No gas pipe has been observed. Microscopically, matrix shows an eutaxitic texture, in which loose crystals of plagioclase and accidental rock fragments (pyroclastics, terrigenous and metamorphics) are observed. On the base of its features, also this deposit has been define as a emLTlCo lithofacies (Branney and Kookelar, 2002).

2. Discussions

The studied deposits have a primary volcanic origin, as detected by matrix textures, jigsaw structures and chilled margins around accidental lithics, and they are intercalated in a deep-marine sequence. They have also a strong continental fingerprint, as documented by lithological associations of the detritus. Features described allow us to reconstruct flow mechanisms and type of PDCs, and to speculate the reason why the volcanic structure has been preserved entering the water.

5.1 Flow mechanisms and types of PDCs

5.1.1 Lava-likeTl$_{(nl)}$ lithofacies

Lava-likeTl$_{(nl)}$ lithofacies (PDC n°1) preserves information on flow behavior occurred both above (subaerial phase) and below the sea level (subaqueous phase). The upper lapilli-sized unit reflects features of the original volcanogenic process. It represents the plug zone of Branney and Kookelar (2002), and its general massive aspect indicates that granular interactions dominated the flow (Lowe, 1982; Mulder and Alexander, 2001; Branney and Kookelar, 2002; Sulpizio et al., 2014). Lava-like texture and low concentration of fragmented crystals are ascribable to a quasi-steady, hot current from a low fountaning event (Branney et al., 1992; Branney and Kookelar, 1992; Branney and Kookelar, 2002), and mineral assemblage reflects chemical composition of the syn-sedimentary

volcanic source (Elter et al., 1999; Mattioli et al., 2002). Immature shapes of phengite fragments indicate that PDC erosion involved portions of basement proximal to the eruptive center (Sparks et al., 1997). Instead, brittle brecciation and more rounded, metamorphic accidental granules characterizing the basal conglomerate unit reflect distal interaction between PDC and wet, loose sea floor sediments.

5.1.2 EmLTlCo lithofacies

EmLTlCo lithofacies sedimentary characteristics point out that flow was characterized by a granular flow-dominated flow-boundary zone (Branney and Kookelar, 2002), in which clast interactions and collisions sustain the flow and promote kinetic sieving and kinematic squeezing mechanisms (Sulpizio et al., 2007, 2010, 2014). These interactions have influenced the matrix texture variabilities that we above described. Glassy welded structures suggest increasing pressure and shear along clast boundaries, when clasts become closer. This behavior favors the flow to maintain sufficient expansion, allowing its movement, and segregation of large blocks, as inferred for the lithic rich pyroclastic flow of the Pollena eruption of Somma-Vesuvius by Sulpizio et al. (2007). Processes of channelization, which laterally confine the flow, prevent too rapid expansion that causes flow density leak and mechanical energy dissipation (e.g. Bursik and Woods, 1996; Calder et al., 1999; Branney and Kookelar, 2002; Doronzo, 2012), and enhances current erosional behavior (Sparks et al., 1997; Calder et al., 2000; Sulpizio et al., 2007; Brand et al., 2014). Erosional surfaces observed in PDC n°6 may confirm a self-channelization behavior (Brand et al., 2014), even though no emphasis will be put on their interpretation, because it has been impossible to clearly observe and follow them in the outcrops. Poor sorting and absence of gas pipes indicate that fludization and elutriation processes probably have not been promoted during flow (Roche et al., 2001; Branney and Kookelar, 2002; Trofimovs et al., 2008). Continental fingerprint and clast roundness observed in the Val d'Aveto event, directly comparable to typical clast lithological associations and shapes of the lower turbidite deposits (Di Capua et al., 2014) and continental alluvial deposits (Lindsey et al., 2005, 2007), reflect these topographic effects. Subaerial processes of channelization and enrichment in accidental lithics, combined with deposit thickness and mineralogical association comparable with what has been documented by Sparks et al. (1980a) for the dacite ignimbrite flow of the Grande Savanne submarine apron, indicate that the Val d'Aveto Formation body has been deposited directly from a primary thick, dense and forced convection-dominated PDC (Sparks et al., 1980a,b; Branney and Kookelar, 1992; Doronzo, 2012). At least one of them (PDC n°5) can be classified as a debris avalanche deposit, by jigsaw structures and clast shape. This implies that flow support mechanism was controlled by particle collisions and matrix strength (Talling et al., 2013).

5.2 Emplacement mechanisms below the sea water

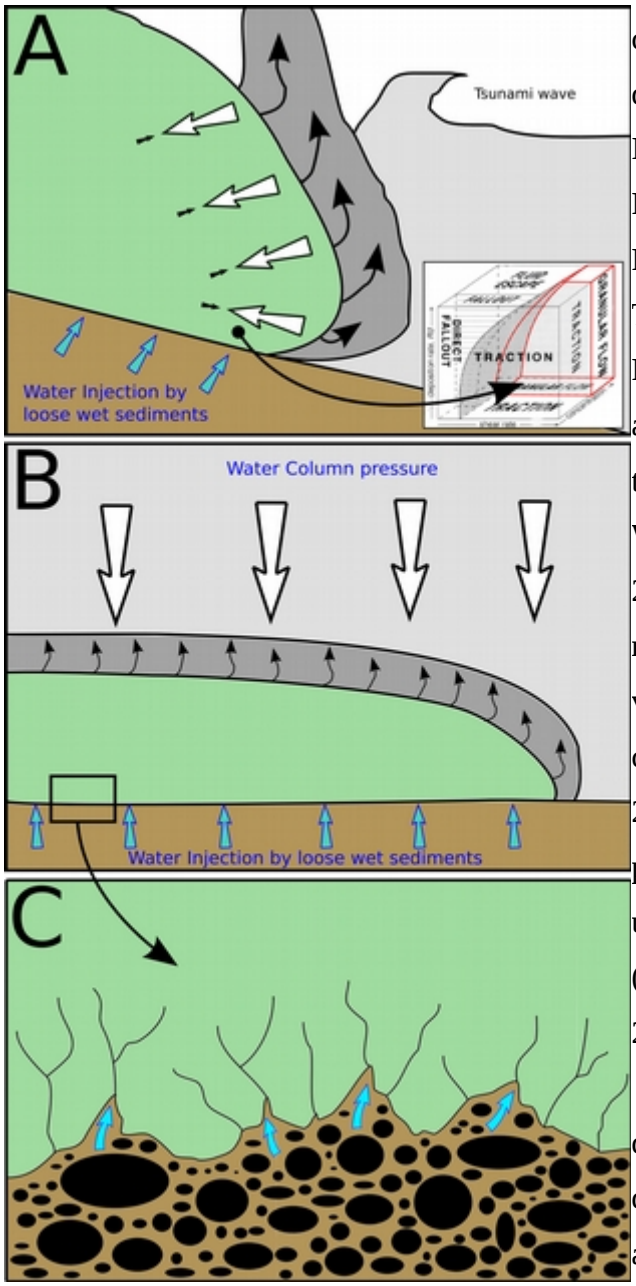

Figure 4:emplacement of PDCs below the water; a) granular flow inhibits vapor gas to push particles apart; b) PDC is settled below the sea level, sourronded by gas carapace; lithostatic load promote injection of loose material in the welded PDC deposit.

In subaqueos flows, injection of water primary control on bulk physical properties, as velocity, density and preservation of the flow itself (e.g. Inverson et al., 1989; Inverson, 1997; Rickenmann, 1999; Mulder and Alexander, 2001; Roche et al., 2001; Branney and Kookelar, 2002; Trofimovs et al., 2006; Breien et al., 2010). In PDC, differences in temperatures between flow and water constitute a further variance, probably the most limiting one (Cas and Wright, 1991; White and McPhie, 1997; Branney and Kookelar, 2002; Cassidy et al., 2013). PDC/water contact rapidly generates steam through rapid vaporization of water due to water/hot particles contacts (Sparks et al., 1980b; Legros and Druitt, 2000; Freundt, 2003), and promote violent phreatomagmatic explosions, from the shoreline up to hundreds meters below the sea level (Whitman, 1989; Freundt, 2003; Trofimovs et al., 2006).

In Val d'Aveto Formation, different PDC deposits have been recognized preserved in a deep-water turbidite succession. Microscopical analysis have shown that at least one of them, the lowest one, suffered a certain grade of water/flow interaction. Its basal brittle deformation (Fig.3b), together with the complete absence of syn-volcanic material in fractures, indicate that hydrofracturation process took place after PDC welding (Roche et al., 2001). Nevertheless, clay minerals from devitrified glass and euhedral pyrite grains seems to support the idea that water interacted with a still hot PDC (Fig.3c). Euedral pyrite grains (Fig.3f), in particular, develop from hydrothermal reactions that involved sulfur-rich vapors

(Sawlowicz, 1993; Shikazono and Utada, 1997; Wilkin and Barnes 1997; Sánchez-España et al., 2000). As inferred by Graham and Ohmoto (1994), pyrite crystal habit growth is function of the hydrothermal reaction temperature: 1) cubic crystals grow at temperatures between 90° and 280°C (according also to Wu et al., 2004); 2) octahedral crystals between 250° and 350°C; 3) pyritohedral crystals between 300° and 350° C. FeO rims can develop during acqueos oxidation at high temperatures (250° – 350°C), according to Graham and Ohmoto (1994) and Chandra and Gerson (2010).

As calculated by Sparks et al. (1980) and documented by Mandeville et al. (1994), heat loss during subaqueous motion is less than what it is expected, so flows can be emplaced at high temperatures, and hydrothermal reactions may occur either during or after the deposit emplacement. Branney and Kookelar (2002) affirm that a PDC can trap and resorb quantities of soluble gases, lowering its viscosity, favoring its rheomorphism and enhancing its welding. So, water vapor resorption alone does not prevent the preservation of primary volcanogenic texture of subaqueous deposits. What really influences the possibility of PDC preservation are the flow-boundary zone dominant conditions, because directly controls capacity of gases resorption and PDC permeability (as permeability is function of sorting - Branney and Kookelar, 2002). Gas resorption is inhibited when gas can escape (Branney and Kookelar, 2002), so when PDC is characterized by a strong fluidization process (Lowe, 1976). Fluidization promotes fine elutriation, which increases current sorting and permeability (Mulder and Alexander, 2001; Breien et al., 2010). It is likely to be an auto-fed circular process, in which the more fines are depleted, the better sorting characterizes the flow (and its deposit), the more gas can enter the flow. This agrees with what has been documented by Whitman (1989), White and McPhie (1997) and Trofimovs et al. (2008), who note that subaqueous PDC deposits are usually characterized by very good sorting, much better than the subaerial equivalents. All of these authors invoke rapid vaporization and phreatomagmatic explosions to explain elutriation strengthening from subaerial to subaqueos conditions. We envisage that rapid vaporization takes place not or not only at the water/PDC boundary, but fluidization ensures the water to be injected into the flow and vaporize between PDC hot particles. As high pore pressures support fluidized flow motion and extremely reduce particle-particle shear interactions (Roche et al., 2010), intraclast water vaporization abrupt increases pore pressures, resulting in flow rapid expansion that causes density leak and mechanical energy dissipation (Freundt, 2003; Roche et al., 2010; Doronzo, 2012). According also to Roche et al. (2006), depletion of fines also contrasts flow motion, so subaqueous motion is only driven by gravity and supported by water (Trovimovs et al., 2006).

In contrast, granular flow-dominated flow-boundary zones of PDCs are supposed to be

supported by clast interactions and collisions, and interstitial fluid phase is considered to be represented by dusty gas, i.e. a mixture of small particles and gas in thermo-mechanical equilibrium (Branney and Kookelar, 2002; Sulpizio et al., 2014). Increasing pore pressures due to intraclast rapid water vaporization are here contrasted by particle-particle shear (Doronzo et al., 2012), so pore expansion is inhibited and gases can be easier resorbed into the flow. In this case, PDC mass appears as an unique body, so steam upward motion seems to affect only the external part of the flow. When PDC enters the water and flows downslope, steam upward liberation starts to be contrasted by water column pressure, becoming an involving film which isolates PDC and reduces heat transfer between PDC and water (gas carapace concept of Sparks et al., 1980b) (Fig.4a-b). Motion might also be favored by this film that creates a “gas planing” effect at the PDC bottom, similar in behavior to the hydroplaning effect described by De Blasio et al. (2004) for submarine debris flow. This effect decreases the flow/surface friction, drastically reducing the erosional capacity of the flow in absence of important topographic effects. This effect might has driven the Val d'Aveto PDCs down to the bottom without interacting with sea floor, as suggested by the secondary hydrofracturation and sediment intrusion (Fig.4c).

Direct fallout-dominated flow-boundary zone and traction-dominated flow-boundary zone PDCs are too dilute (due to low clast concentrations), so grain interactions are negligible (Branney and Kookelar, 2002) and they are supposed to behave like low-density turbite current (Lowe, 1976, Mulder and Alexander, 2001).

Syn-volcanic versus post-volcanic sedimentation: application of actualistic models to unravel primary volcanic control on source-to-sink (Taveyanne Sandstones, Oligocene Northalpine Foreland Basin, France and Switzerland)

Taveyanne Sandstones: syn- or post-volcanic sedimentation?

1. Introduction

Volcanogenic sedimentation has widely accepted to have a high impact on the environments (Smith, 1991; Sohn et al., 2005; Manville et al., 2009). Fluvial response to volcanism has been followed deep into submarine basins (e.g. Alexander et al., 2010; Sisavath et al., 2011, 2012), providing accurate examples of volcanoclastic turbidite system records. In spite of them, volcanogenic signature in the ancient foreland basin bordering the Alps is still a controversial topic of the Alpine geology. In this work, we focused on the volcanoclastic turbidite system of the Taveyanne Sandstones, deposited between SE France and Central Switzerland in the Oligocene times (32 – 29 Ma - Sinclair, 1992, 1997; Ruffini, 1995; Ruffini et al., 1997; Boyet et al., 2001), investigating the temporal and spatial relationship between sedimentation and volcanism. Through new fieldwork (stratigraphic logs and facies analyses) and minero-chemical data (sandstone point-counts and X-ray diffraction analyses), we re-discuss the reconstruction of the Oligocene source-to-sink system which fed the Taveyanne Sandstone basin, considering 1) potential preservation of PDCs below the sea level and relative deposits, and 2) impact of volcanism on the modern environments.

2. Geological settings

The lithostratigraphy of the Eocene – Oligocene Molassa Basin exposed between SE France and Central Switzerland (Fig.1a) is characterized by the so called Priabonian Trilogy Group, consisting of Nummulitic Limestones (*Calcaires Nummulitiques*) and Globigerina Marls (*Marnes à Globigerines*), overlain by turbiditic sequences of various composition (e.g. *Grès de St. Antoin, Grès d'Annot, Grès de Champseur, Grès de Taveyanne*) (Sinclair, 1997; Ford & Lickorish, 2004). The most enigmatic of turbidites, the Taveyanne (or Taveyannaz) Sandstones, is widely but not continuously exposed between the Savoie region of France, where it was described in the Bornè-Aravis and Platè Massifs (Doudoux et al., 1987, Ruffini et al., 1995), and in Western and Central Switzerland (Sinclair, 1992). Along this outcrop area, the Taveyanne Sandstones have been involved in post-Oligocene deformation at various scales (Rivaro Garcia, 1978; Doudoux et al., 1987) ranging from non-metamorphic conditions to metamorphism of pumpellyte-actinolite grade (Schimdt et al., 1997, 1999). The Taveyanne Sandstones consist of turbiditic volcanoclastic sequences, rich in andesitic pebbles and clasts, and isolated amphibole, clinopyroxene and plagioclase crystals, plus a low but constant presence of plutonic, sedimentary, and metamorphic rock fragments (Sinclair, 1992; Ruffini et al., 1995; Boyet et al., 2001). Chemical analysis performed on the volcanic rock fragments show their calc-alcaline nature and their strong affinity with the magmatic suite of the Adamello and Bergell plutonic complexes (Boyet et al., 2001). Ar/Ar

radiometric dates on amphiboles constrained at 32.5 Ma and 30.5 Ma the main magmatic events in the source area of Taveyanne volcanoclastics (Fèraud et al., 1995; Ruffini et al., 1995), while calcareous nannofossils constrained to Zone NP23 between 32 and 29 Ma the sedimentation of Taveyanne volcanoclastics (Ruffini et al., 1994). Two different schools of thought exist on the provenance region of the Taveyanne Sandstones based on different interpretations of the available sedimentological, petrological, and chronological data: the first school considers the volcanic material as primary in origin and formed by phreatomagmatic explosions occurring in the basin area (Lateltin 1998 and ref. in it), while the second one interprets the volcanic material as resulting from the erosion of an “andesitic nappe” that originated in the inner part of the Alpine Chain and was tectonically transported in the study area during the Oligocene (Dal Piaz e Venturelli, 1983; Vuagnat, 1983).

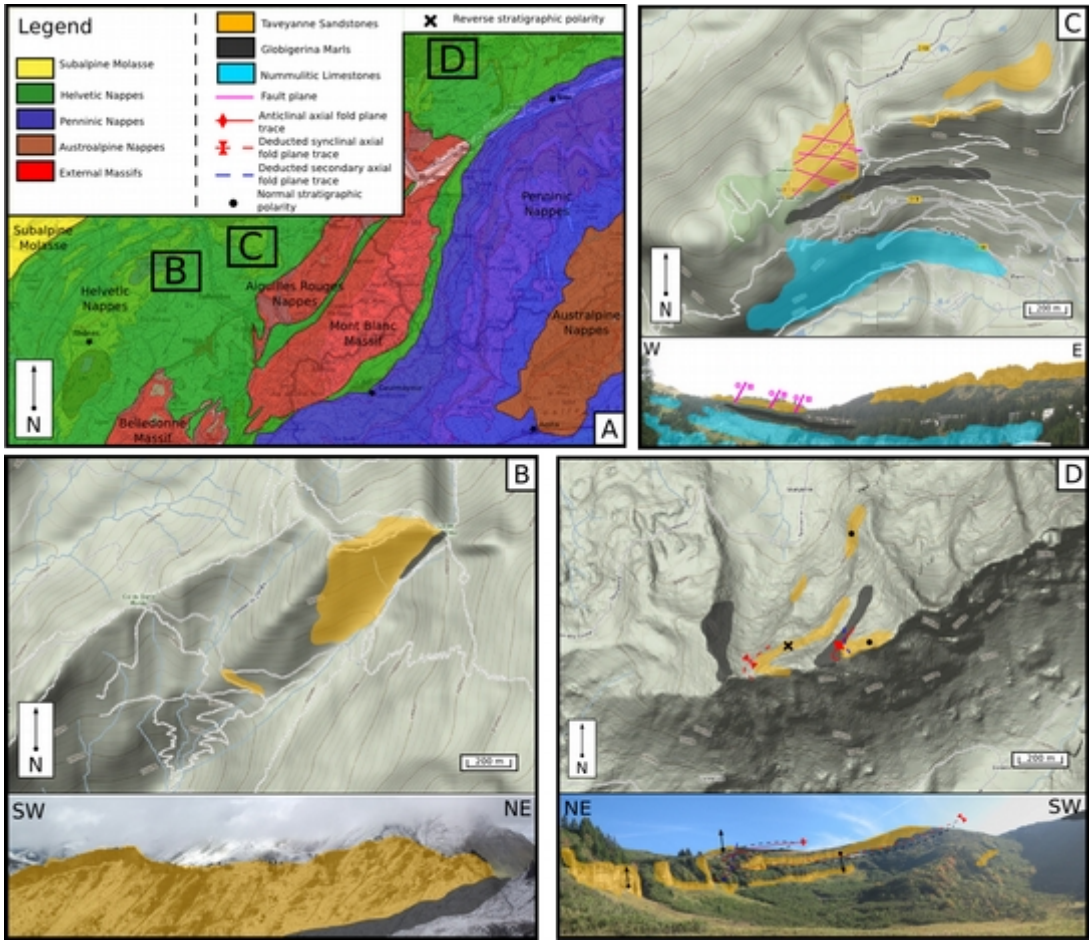

Figure 1: a) Geological sketch map of Alpine domains and fieldowork locations; b) Col de l'Oulette fieldwork map and section; c) Flaine fieldwork map and section; d) Taveyanne fieldwork map and section.

3. Methods

This work is focused on three main sections (Fig.1a) (Col de l'Oulette and Flaine - SE France, Fig.1b-c - and Taveyanne - Western Switzerland, Fig.1d), already studied by other authors (e.g.

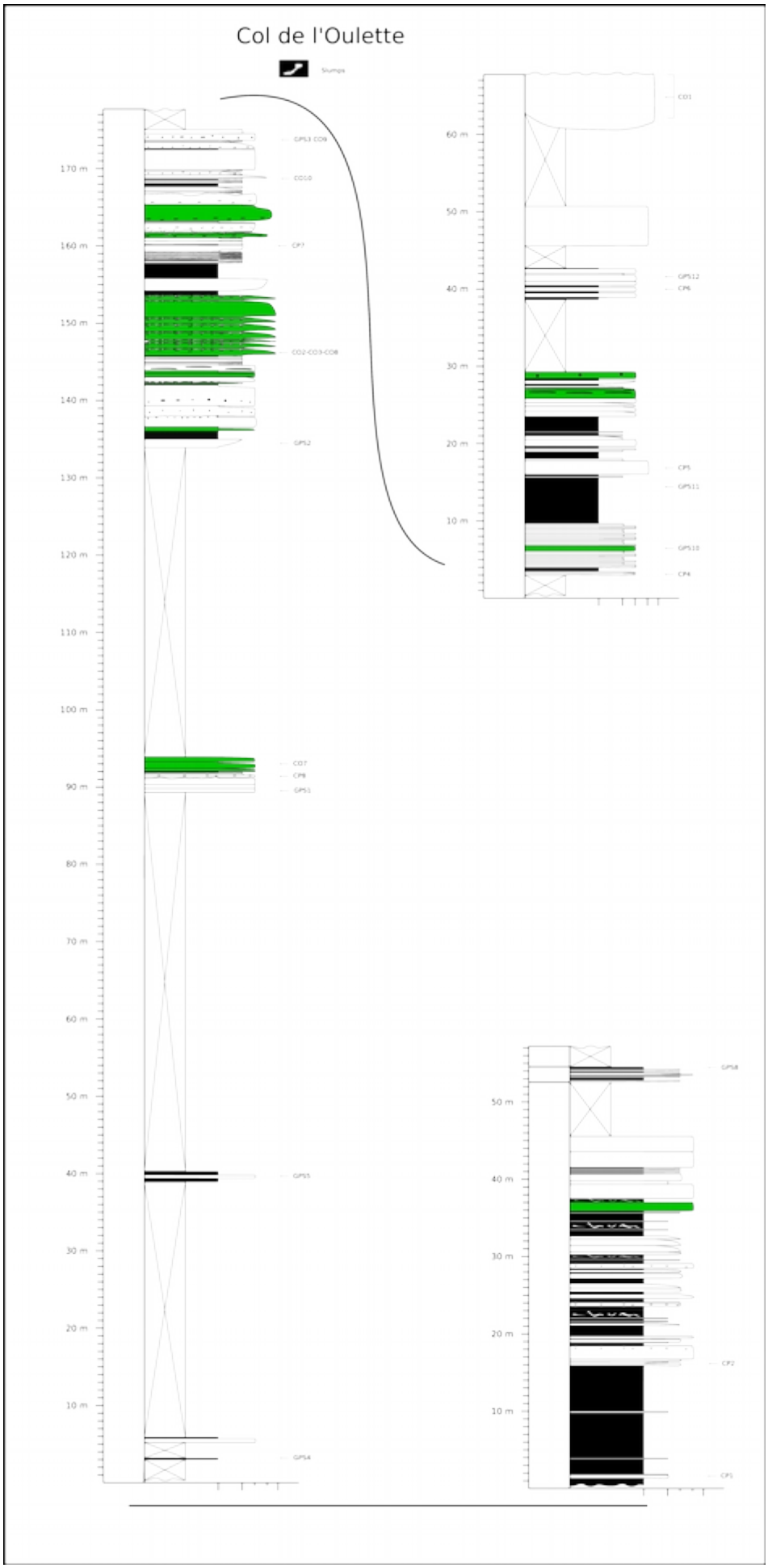

Figure 2: stratigraphic logs measured at Col de l'Oulette. Facies 1: black layers; Facies 2; white layers; Facies 3 green layers.

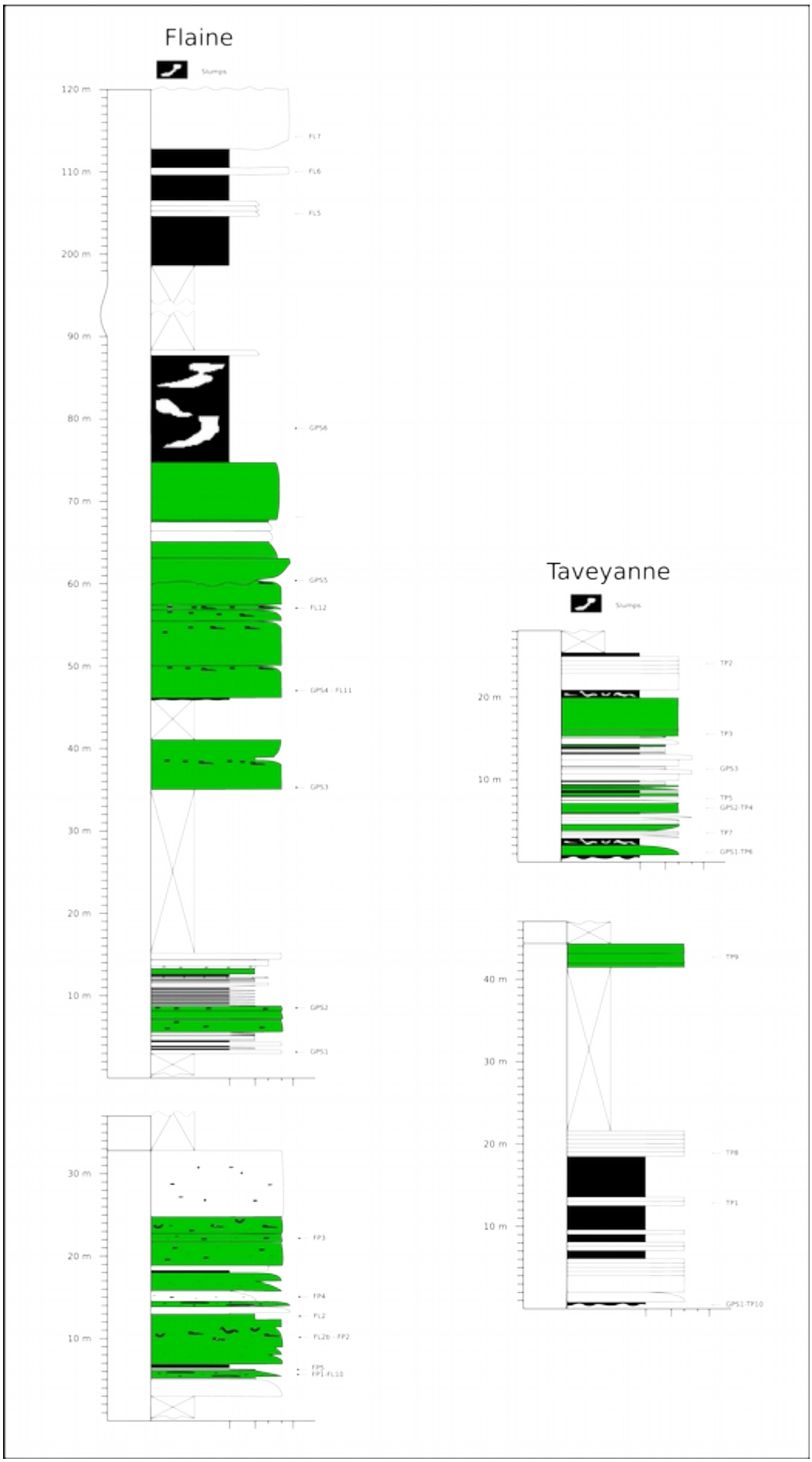

Figure 3: stratigraphic logs measured at Flaine (left) and Taveyanne (right). Facies 1: black layers; Facies 2; white layers; Facies 3 green layers.

Ruffini, 1995; Boyet et al., 2001), in order to join together different analytical techniques (chemical, Ar/Ar, quantitative point-count analyses following the Gazzi-Dickinson methods – Ingersoll et al., 1984) with stratigraphic log measurements (Fig.2-3), facies analyses, texture microscopic observations and quantitative sandstone classified following the methodology of Folk (1980). Folk method has here preferred to Gazzi – Dickinson method in order to obtain compositional results comparable to modern composition of volcaniclastic submarine deposits (e.g. Smith, 1991; Trofimovs et al., 2008; Sisavath et al., 2011). On the finest layers, we performed X-ray powder diffraction (XRPD, PANalytical X'Pert PRO PW3040/60 diffractometer in θ-θ Bragg-Brentano parafocusing geometry with Ni-filtered Cu Kα radiation at 40 kV and 40 mA, in the 4-80° 2θ range), and compositional results have been analyzed running the PANalytical X'Pert High-Score software, with the ICSD PDF2 database. Discrimination of fine detritus volcanogenic nature has been carried on by comparing sediment mineralogical composition with the mean andesite mineralogical association of volcanic clasts recognized by Ruffini (1995), i.e. plagioclase, laumontite (resulting from the hydrothermal alteration of plagioclase - Ruffini, 1995), amphibole and pyroxene.

4. Results and discussions

Three main facies have been recognized. Differences are based on fieldwork evidences, grain size, microtextural characteristics and sediment composition. One of them (facies 3) is discussed to be either discharged by volcanic eruptive events or not.

Facies 1

Description: facies 1 is constituted of dark gray to dark brown pelite and marl layers that can be grouped in packages up to 7 m-thick. They are characterized by parallel to convolute lamination, and rare flute casts (Fig.4). In the Flaine section, dark gray pelites embed green sandstone layers, forming a slumping succession up to 20 m-thick. Optical and mineralogical (XRD) analyses reveal that rocks are constituted of aligned muscovite/illite and quartz, with subordinate calcite and K-feldspar, and rare chlorite and plagioclase.

Interpretation: facies 1 corresponds to sequence Te of Bouma division (1962) and facies D of Shanmugam et al. (1985). It is constituted of low-density currents deposited by suspension fall-out in a basin plain (Shanmugam et al., 1985; Mulder and Cochonat, 1996; Mulder and Alexander, 2001). The slumping succession observed in Flaine corresponds to facies F of Shanmugam et al. (1985), and is constituted of unsteady, non-uniform flows, arrested proximally to the source area (Strachan, 2008). Sediment composition reflects a strong crystalline basement supply, with minor inputs from sedimentary covers and rare from volcanic terrains.

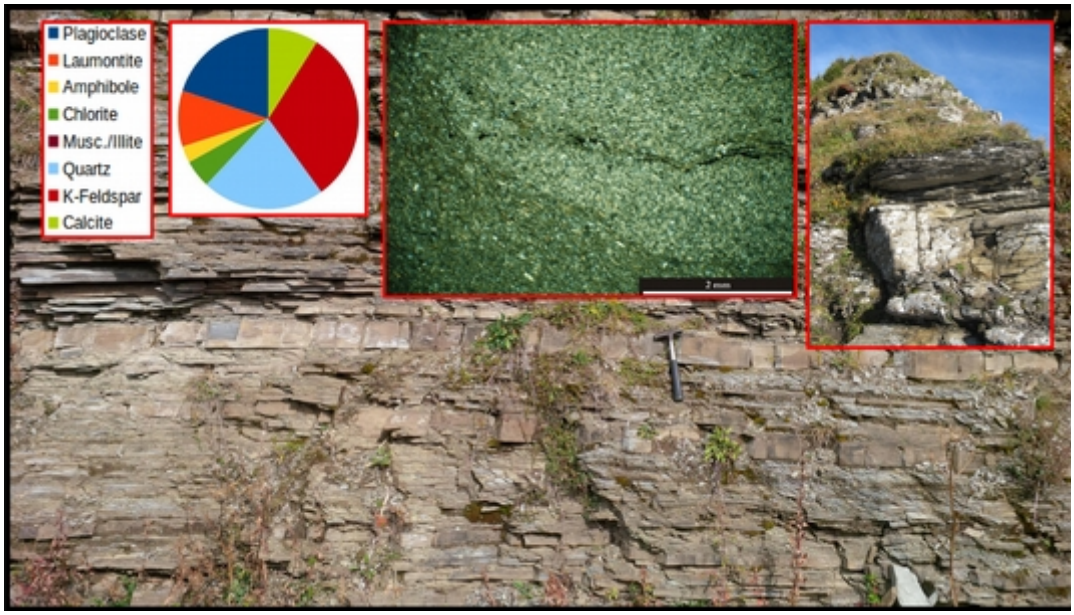

Figure 4: facies 1, with an example of sample in thin section and X-ray diffraction result

Facies 2

Description: Facies 2 groups greenish to light brown, very fine to coarse sandstones (Fig.5a-c), up to 1 m-thick, and microconglomerates, up to 5 m-thick. They are characterized by medium to good sorting, occasionally normal grading up to dark silty-sized detritus, and are alternatively massive, massive to laminated or laminated, sometimes with ripples and/or convolutions. Flute casts and groove casts may be observed at the base. Detritus is composed of dark gray shale and green andesite fragments, and loose crystals of plagioclase and amphibole, with subordinate quartz. Carbonate cement may be present. In thin section, sandy detritus is subangular to subrounded shaped, and volcanoclastic material constitutes more than 50% of the bulk, represented by porphyritic rock fragments (plagioclase or plagioclase + amphibole), plagioclase and flash-

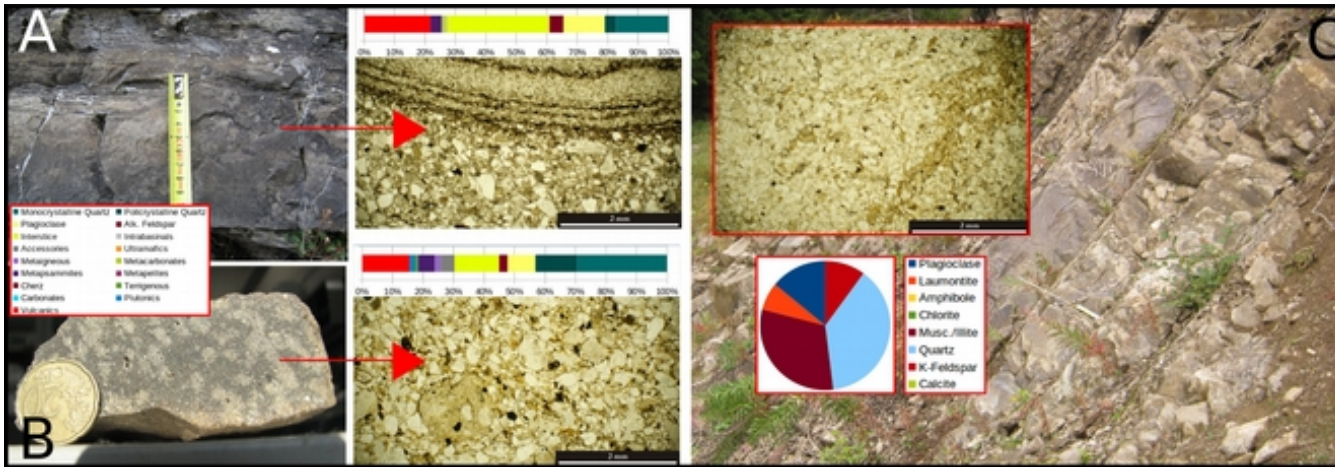

Figure 5: facies 2, a) composition of fine sandstone (point-count); a) composition of coarse sandstone (point-count); c) composition of very fine sandstone (XRD).

extionction quartz in variable percentages, with subordinate amphibole and pyroxene (up to 5% and grouped in “accessory”). The other fractions are represented by plutonic, metaigneous, metapsammite, carbonate and rare terrigenous fragments, polycrystalline quartz and rare k-feldspar (orthoclase). Fossil fragments (e.g. Nummulites) have been observed. Finest layers are characterized by plagioclase, quartz, muscovite/illite, K-feldspar (orthoclase), with minor carbonate and chlorite, and rare laumontite and hornblende. Plagioclase is largely the most abundant component in two of six sample (CP1 and CP4), where it reaches the 51% of the bulk, or the 32% + 14% of laumontite (from hydrothermal alteration of plagioclase - Ruffini, 1995). In sample TP4, amounts of plagioclase, quartz or orthoclase are similar. In samples CP8, TP5 and TP7 quartz and muscovite/illite are the most abundant component (between 29 and 38%), whilst plagioclase + laumontite (when present) are less abundant (between 12 and 21%).

Interpretation: facies 2 groups different submarine events, characterized by incomplete to complete sequence of Bouma (1962), or incomplete to complete sequence of type-A mixed system deposits of Mutti et al. (2003). They are ascribable to facies A, B, C and D of Shanmugam et al. (1985), and facies F5 to F9 of Mutti et al. (2003). Massive deposits (facies B of Shanmugam et al., 1985; F5 of Mutti et al., 2003) are ascribable to grain-to-grain supported flows (hyperconcentrated flows - Mulder and Alexander, 2001; Mulder et al., 2003). Massive to laminated deposits (facies C of Shanmugam et al., 1985; facies F5 to F7 of Mutti et al., 2003) are alternatively intended as turbidity to concentrated density flows, such as high density turbidites (Talling et al., 2012), hybrid events (Haghton et al., 2009) and surge-like turbidity flows (Mulder and Alexander, 2001). Laminated to convolute flows (facies D of Shanmugam et al., 1985; facies F7 to F9 of Mutti et al., 2003) are related to turbulent flows (low-density turbidity currents - Lowe, 1982; Mulder and Alexander, 2001; Haughton, 2009). Microconglomerate layers are ascribable to facies A of Shanmugam et al. (1985), facies F5 of Mutti et al. (2003), and represent channel-fill deposits, according to Ruffini (1995). Their massive aspect reminds to grain-to-grain supported flow (hyperconcentrated flows of Mulder and Alexander, 2001). Sediment compositions reflect supply alternatively from volcanic centers (coarser deposits - point counts) and/or crystalline basement (finest deposits - XRD analyses), with ephemeral sedimentary cover inputs.

Facies 3

Description: Facies 3 is constituted of green, spotted green and beige deposits of fine to very coarse sandstones, bad to good sorted, up to 7 m-thick (Fig.3a-c). They are often characterized by a basal, lithified, dark gray pelite layer, with flute casts or groove casts, sharply divided from the main sandy body. This part can alternatively be massive, reverse to normal graded, or multiply graded, and may preserve pelitic rip up clasts and fine sand- to pelite-wave structures. The latter can evolve

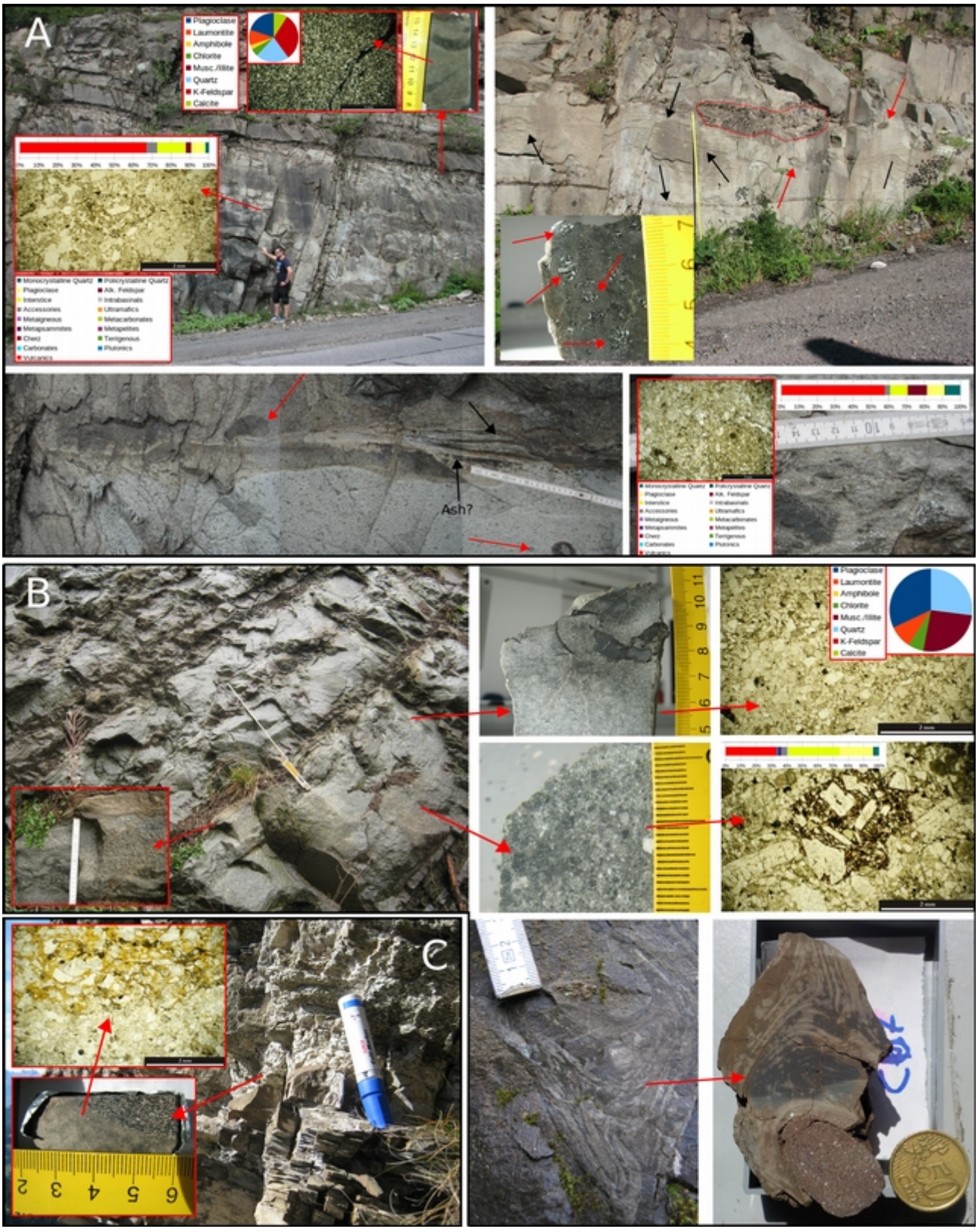

Figure 6: sedimentological features of facies 3; a) double stratified density current in Flaine (up, left) with results of XRD analysis on fine fractions (right) and point-count (left), bedforms (down, left and up, right), with possible ejected clasts (red arrows), sediment plug (red round), very angular andesite fragments, and point-count result of sandstone layer rich in andesite fragments; b) double stratified density current in Col de l'Oulette, with XRD result on fine fraction (right, up) and point-count in coarse fraction (right, down), and soft clast surrounding an andesite pebble; c) andesite pebbles in a sandstone layer (Taveyanne).

in laminae bedsets and sediment plugs (Fig.3a), embedding very angular dark gray pebbles (pelites?). Wave structures are normally deflected by plastically rounded andesites, or andesitic, pelitic and calcareous pebbles (Fig.3a), also characterized by contact aureole. These structures have been alternatively observed on top of clean sand intervals or marking change in particle grading. Small very angular andesites are commonly observed in patches or aligned along the flow. In the Col de l'Oulette section, a plastically deformed rip up clast, surrounding an andestite pebble, has been recognized (Fig.3b). In the central part of Flaine section, sandstone pebbles with dark pelite core embedding andesitic fragments are dispersed in coarse, sandstone deposits (Fig.3a). On their top, such deposits may also preserve angular to subrounded andesite decimetric pebbles (Fig.3c), and pieces of pelite or calcareous stratified layers, up to 50 cm-long, alternatively folded, on top. Sequence may also be closed by convolute silty- to muddy-sized layers defined by dark gray and greenish laminae (Fig.3a,b). In thin section, sediments are immature, with very angular porphyritic volcanic fragments and ideomorphic crystals of volcanic plagioclase and amphibole. Porphyritic volcanic fragments are the most abundant detritus component (up to 67%), followed by plagioclase (up to 26.8%). Flash-extinction quartz, accessory minerals, polycrystalline quartz and rock fragments of metaigneous, metapsammites, carbonate and terrigenous are also present in minor amounts. Interstice is usually constituted of plagioclase fragments and green fragments of andesitic groundmass (Fig. 3b). XRD analyses on fine samples confirm this mineralogical association, with abundant plagioclase + laumontite, quartz, pyroxene, amphibole, muscovite/illite, chlorite, and rare carbonate and K-feldspar. Convolute layers, instead, are characterized by higher concentrations of carbonate and feldspars in dark laminea, and generally by more abundant K-feldspar (31%) rather than the overlain bodies, followed by plagioclase + laumontite association (20+10%) and quartz (22%), with minor carbonate (9%), chlorite (5%) and rare amphibole (3%) (Fig.3a-b).

Interpretation: facies 3 is constituted of subaqueous events ascribable to facies B and C of Shanmugam et al. (1988), or facies F5 to F9 of Mutti et al. (2003), dominated by A1 to A3 facies sequences of type-A mixed system deposits (Mutti et al., 2003). Facies B groups deposits characterized by coarser andesite patches and alignments, clast discrete horizons and grading, and corresponding to hybride events of Haughton et al. (2009) or Dcs (clean sand debrite) flow type of Talling et al. (2012), supported by direct fallout. Facies C groups currents dominated by aggradation of reverse to normal graded pulses, accretion and deflection of wave-structures by pebbles precipitation, sediment plugs and convolute layers, resulting from interaction between direct fallout and tractional flow support mechanisms. This interaction appears to be consistent with double density current deposits from density-stratified currents (Shanmugam, 2002; Gladstone et al., 2004; Amy et al., 2005), or concentrated density flow evolving to quasi-steady concentrated density currents (Mulder and Alexander, 2001), in which fluidization promotes strong elutriation and

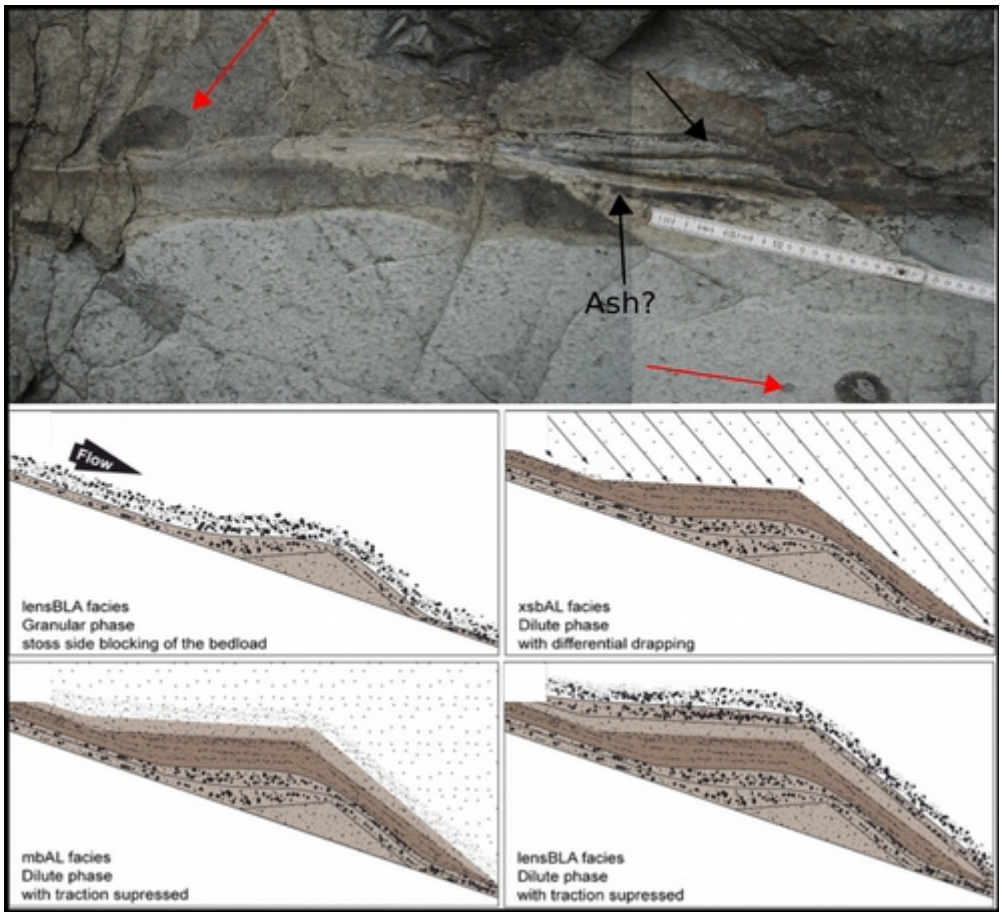

Figure 7: comparison between bedforms at Flaine (black arrows) and mechanisms of bedform depositions in dilute PDCs by Douillet et al. (2013). Red arrows indicate possible ejected clasts

generation of a buoyant plume (Breien et al., 2010).

Sediment composition reflects a strong volcanic supply, with ephemeral inputs from a crystalline basement and relative sedimentary covers. In convolute layers, instead, volcanic supply is diluted by crystalline basement signal.

5.1 Preservation of PDCs and relative deposits below the sea level

Identification of primary volcanogenic deposits (PDCs) is the only undoubted way to distinguish syn-eruptive from inter- or post-eruptive sedimentation in ancient basins (e.g. Schneider et al., 2001; Cassidy et al., 2014). Unfortunately, preservation of primary PDC structures is extremely rare when PDCs enter the water (e.g. Cas and Wright, 1991; White and McPhie, 1997; Cassidy et al., 2013; Jutzeler et al., 2014), as water is injected into the current and rapidly transformed in steam on the hot surface of the particles, steam tends to expand, contrasting intergranular forces and pushing particles apart. In fluidized currents (Lowe, 1967), i.e. in currents where clast support is predominantly a result of upward gas motion, steam rapidly escapes from the current through violent explosions, which enhance fine elutriation (Whitman, 1989). As permeability of PDCs is a function of sorting (Branney and Kokelaar, 2002), the more fine are depleted, the more water will

be injected and vaporized into the current, triggering an auto-feed process until PDC temperatures allow water vaporization. Such behaviors have been observed both in laboratory experiments (Freundt, 2003), and during violent explosive events around Montserrat (West Indies), where different subaerial pyroclastic currents have been observed directly discharged into the sea in the last two decades (Calder et al., 1999; Sparks and Young, 2002; Carn et al., 2004; Trofimovs et al., 2006, 2008; Le Friant et al., 2009, 2010). Shoreline and submarine explosions disaggregate the PDC, which moves downslope as a cold, water-supported turbidite current for tens of kilometers (Edmonds and Herd, 2005; Allen and Freundt, 2006; Trofimovs et al., 2006). Once settled, PDC deposit results in a sandy-sized, extremely elutriated turbidite deposit that can either be or not mantelled by fine plume detritus (Trofimovs et al., 2008, 2012). Compositions may vary as function of the erosional behavior of the current that tends to incorporated fragments of seafloor bedrock and loose seafloor detritus (Cassidy et al., 2014).

Plenty of deposits grouped into facies 3 of Taveyanne Sandstones may appear to have been fed by such eruption-triggered events. Different features documented in this work, in fact, are directly comparable to features characterizing both modern dilute PDC deposits above the water (Doronzo, 2012; Sulpizio et al., 2007; 2014) and volcanogenic deposits below the sea level (Trofimovs et al., 2008; Cassidy et al., 2013; 2014). Sand-wave structures (Fig.3a,7) above described are comparable to sand-wave structures, or “dune bedforms”, so common in “dry” and “wet” dilute PDC deposits (Cole, 1991; Douillet et al. 2013), so rare in siliciclastic turbites (Talling et al., 2012). Immaturity of sandstone components, also compared with major roundness of facies 2, and large amounts of volcanic detritus, interpreted as owing to *in situ* phreatomagmatic explosions by French authors (Giraud and Didier, 1981; Giraud, 1983; La Pierre et al., 1995; Boyet et al., 2001), remind to instantaneous production and remobilization of detritus, rather than generation by weathering and transport by fluvial drainages (Smith, 1991). Sediment compositions and differences obtained in clear sand bodies and convolute cap layers are comparable to those documented by Trofimovs et al. (2008) in the turbidite deposit directly fed by the July 2003 dome collapse of Montserrat Island. Thus, we partially agree with those previous authors who supposed a phreatomagmatic origin of volcanoclastic detritus, in the sense that volcanoclastic detritus was produced by violent explosions due to water/flow mixing, which disaggregated dilute PDCs entering the basin. Flows also eroded and trapped seafloor fine detritus, subsequently elutriated to form the buoyant plume (Trofimovs et al., 2008). Absence of glassy shards may indicate that dilute PDCs were fed by block and ash flow from a lava-dome collapse, similar to those observed around the Montserrat Islands (Trofimovs et al., 2008; Le Friant et al., 2009; Cassidy et al., 2014).

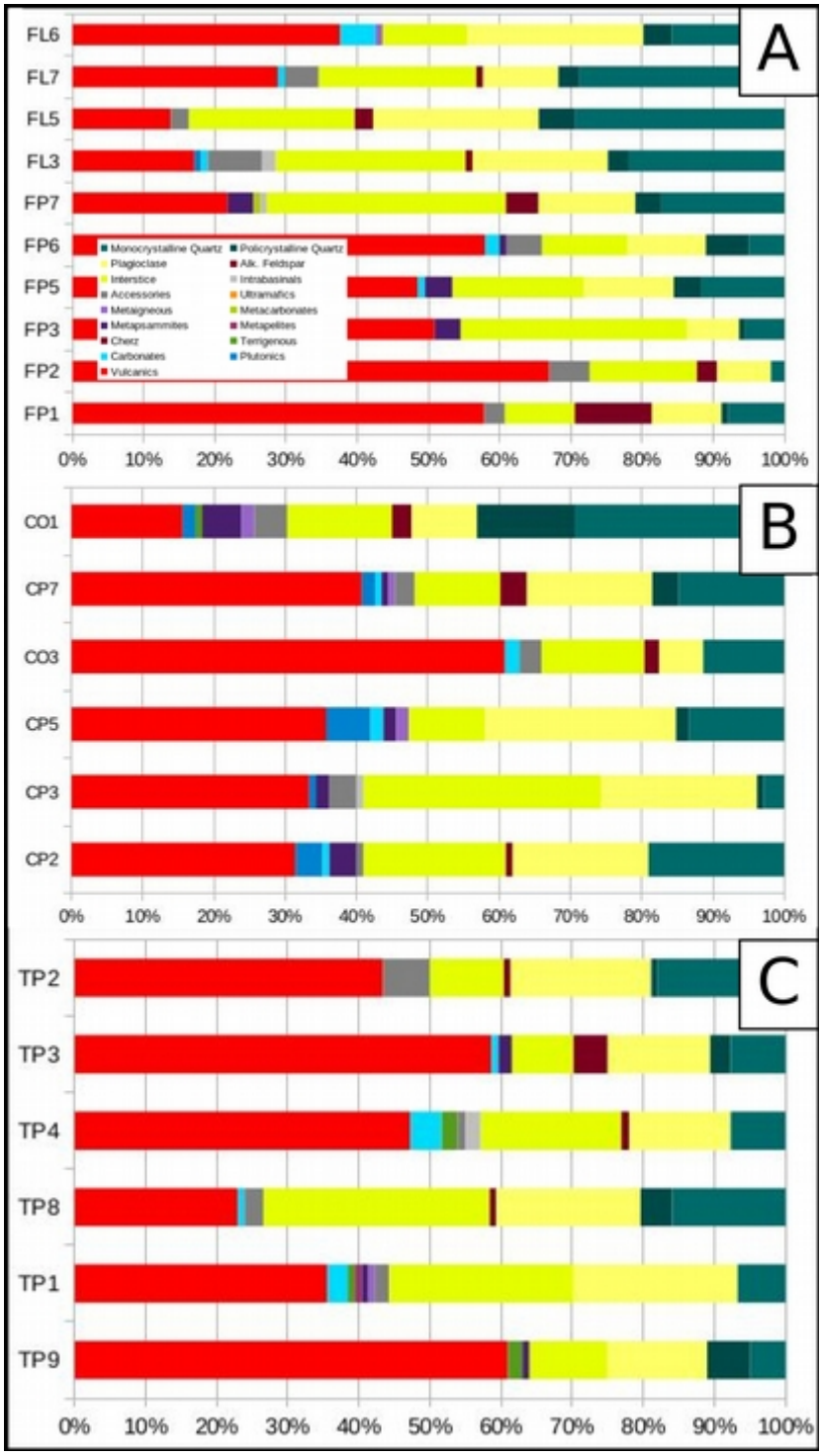

Figure 8: point-count results of a) Flaine; b) Col de l'Oulette and c) Taveyanne.

5.2 Volcanoclastic sedimentation during syn- and inter-eruptive periods

Beyond the possible interpretation of facies 3 deposits as due to eruptive events, the stratigraphic record of Taveyanne Sandstones preserves other information that can lead to unravel the significance of the strong volcanoclastic signature. According to Ruffini (1995), our analytical results document that volcanoclastic inputs are definitively preponderant in coarse detritus (facies 3 and part of facies 2), while tend to be diluted by the orogenic signal in fine sediments (facies 3 -

convolute layers - part of facies 2, facies 1). These trends (Fig.8a-c) reflect two different mechanisms of sediment supply active in the source-to-sink: 1) classical tectono-climatically driven sedimentation, draining detritus from the growing Alpine belt (e.g. Sinclair, 1997; Ospina-Ostios et al., 2013), and 2) syn-volcanic sedimentation, episodically inundating the environment with large amounts of sandy-sized sediments (Smith, 1991). On the background, thrust propagation toward the basin (e.g. Dumont et al., 2011) was liberating metamorphic and sedimentary detritus, transported and discharged into the basin following the classical hydraulic laws of transport in fluvial systems (e.g. Miall, 1996; Allen, 2008). This resulted in packages of thin, orogenic-derived turbidites (facies 1). During episodic eruptive events, pebble to sandy-sized, nearly monolithologic volcanogenic detritus was rapidly produced and instantaneously transported along the environment (facies 3). When not directly discharged into the basin from PDCs, large amounts of unconsolidated volcanoclastic material was aggradated in sheets that are meters to ten meters thick, abrupt increasing the environmental sediment load (Smith, 1991; Manville et al., 2009). Such sediment load, together with widespread vegetation damage, promote strong modifications of the environment that can persist during tens to thousands years, triggering, for example, increase in flash-flood event frequency and delivery of sediments to more distal depositional areas (Manville et al., 2005; Kataoka et al., 2009; Alexander et al., 2010; Cuitiño and Scasso, 2013). Once sediment supply system approaches pre-eruptive conditions, volcanoclastic detritus begins to be progressively diluted by the background signal, as consequence of reestablishment of classical tectono-climatically driven sedimentary dynamics (Smith, 1991). Differences in grain size, amount of rock fragments and compositional signature characterizing facies 2 reflect time of progressive restoration of pre-eruptive conditions. Thus, we infer that sediment aggradation-regradation cycles owing to syn-sedimentary volcanism had the main control on sediment supply and sedimentary architecture of the Oligocene Northern Alpine foreland basin, better explaining the alternation of sand and mud sedimentation, commonly recognized in modern volcanoclastic deep-sea turbidite systems (e.g. Gamberi, 2001; Le Friant et al., 2011; Saint-Ange et al., 2011, 2013; Sisavath et al., 2011, 2012), but previously interpreted as due to the dynamic combination of rapid eustatic variation and thurst wedge accretion by Sinclair (1992, 1997).

5.3 Reconstruction of the source-to-sink system

For the first time, the application of modern models of volcanogenic sedimentation on the Oligocene Alpine foreland basin (Taveyanne Sandstones) allows to break through the previous interpretations, which considered syn-sedimentary magmatism inconsistent with provenance of volcanic material from the Central Alps Plutons (Bergell and Adamello) (e.g. Giraud and Didier, 1981; Giraud, 1983; Dal Piaz and Venturelli, 1983; La Pierre et al., 1995; Ruffini et al., 1997; Boyet

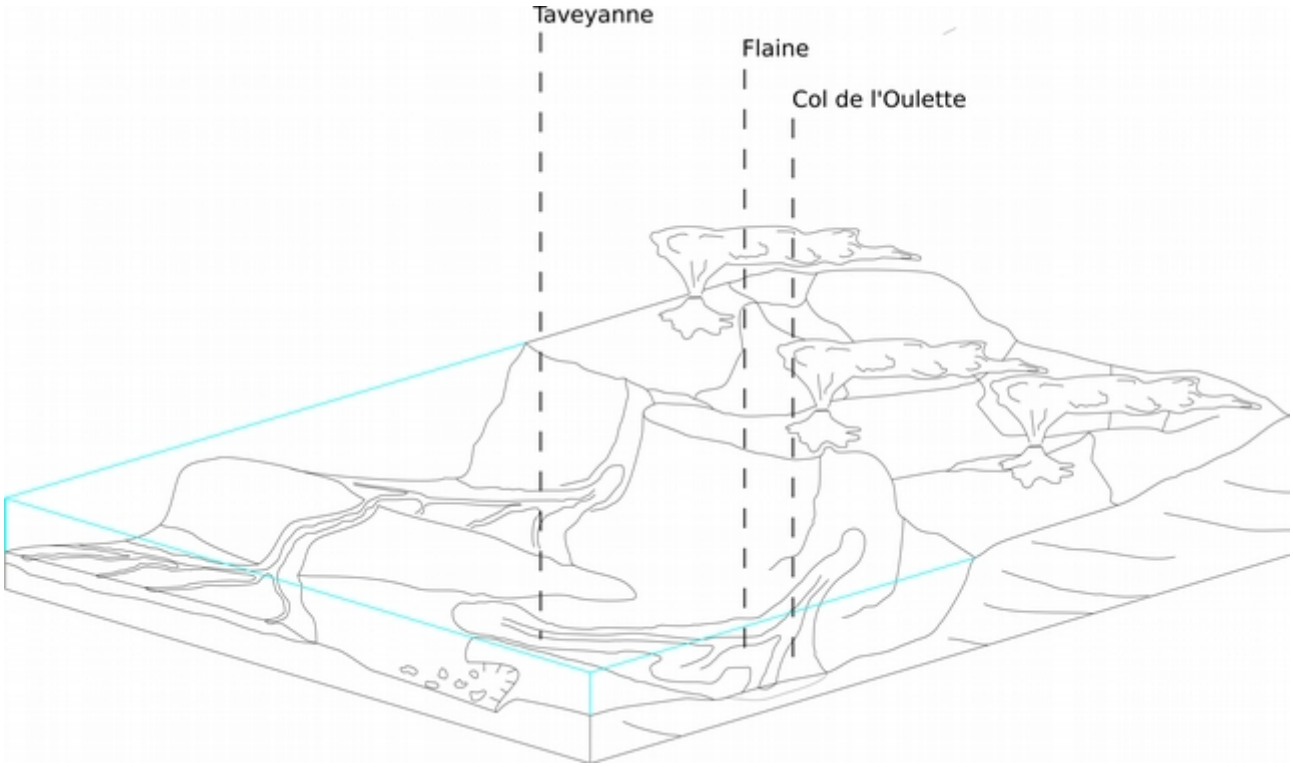

Figure 9: tectonically-controlled model proposed by Sinclair (1992), Sinclair and Tomasso (2002) and Sinclair and Cowie (2003) for foreland basin shape from in Central Switzerland extended to the Haute Savoie area, as the studied sedimentary succession was ponded within the confines of a tectonically shaped basin (by the growing Thone synclinal?) and separated from the outer part of the foreland basin (Chaplet, 1992; Ruffini, 1995 and ref.therein)

et al., 2001). As volcangenic sedimentation can impact subaerial and subaqueous environments tens to hundreds kilometers from the source (Smith, 1988; Manville et al., 2005; Sohn et al., 2005; Trofimovs et al., 2008; Sisavath et al., 2011, 2012; Hunt et al., 2013), sediment transfer from the Central Alps to the foreland basin appears to be a negligible problem. In our opinion, a Central Alps provenance may also be consistent, for example, with the presence of Mesozoic sediment fragments (Ruffini, 1995), ascribable to the Northern Calcareous Alps (Schmid et al., 2004 and ref.therein) that board the southern margin of the basin considered by Sinclair (1992) (Fig.9). However, further work is needed, considering all non-volcanic fraction of the detritus (e.g. Ruffini, 1995), variations in volcanic products (Ruffini et al., 1997), sandstone petrography, minero-chemical analyses and ages on the Central Switzerland part of the Taveyanne Sandstones (Sinclair, 1992) and post-Oligocene volcanoclastic turbidite system displacement from the volcanic sources (amounting to some 100 km ? - Handy et al., 2005 and ref.therein).

5.4 Final remarks

The long-term debate on the significance of Taveyanne Sandstones origin and location of volcanic their source can be solve considering actualistic models of sedimentation raised up in the last two

decades (e.g. Smith, 1988, 1991; Manville et al., 2009; Sisavath et al., 2012). This allows:

- to identify deposits, previously interpreted generally as pheatomagmatic-derived, as deposited by dilute PDCs disaggregated by shoreline explosions owing to water/flow interactions, and moving downslope as cold, water-supported turbidite currents.
- to interpret the sedimentary sequence as reflecting sedimentation during syn- and inter-eruptive periods, just through sediment composition trends.

On the location of the volcanic centers, our model allow to consider the internal part of the Alpine chain as a suitable source of the volcanic detritus (Boyet et al., 2001), without invoking extreme tectonic events as “deus ex machina” (e.g. Ruffini et al., 1997).

Magnetic fabric from incipient to multistage deformed turbidite sequences: the Oligocene Taveyanne Sandstones (Northern Alpine Molasse) (with professor Giovanni Muttoni)

Abstract

In recent years, paleomagnetic investigations have been used as a tool to detect the progressive development of deformation in rocks. In the present work, we focused on the very low grade metamorphic turbidite sequence of the Taveyanne Sandstones (Haute Savoie, SE France - SW Switzerland), through the study of the anisotropy of magnetic susceptibility (AMS) and ferromagnetic fraction signal. Our results allow to extend a previous model applied on brittle deformed mudstone sequences to clastic sedimentary sequences affected by polyphasic folding deformation. Moreover, the additional paleomagnetic analyses performed on the ferromagnetic fraction were useful to unravel ambiguities on the temporal sequence of tectonic events during a multistage deformation, as well as to get information about time and deformation conditions during the magnetization.

1. Introduction

The anisotropy of magnetic susceptibility (AMS) provides an useful tool to detect the progressive development of tectonic fabrics in sediments that mesoscopically show no evidence of deformation, as documented in Eocene mudrocks from the Southern Pyrenean Foreland Basin by Parès et al., 1999. Their study highlighted that the magnetic fabric is a sensitive indicator of progressive deformation, showing characteristic geometries as a function of degree of cleavage development.

In this work, a wider range of lithologies comprised of the Oligocenic turbiditic Taveyanne Sandstones of the Northern Alpine Molasse Basin (e.g. Dal Piaz e Venturelli, 1983; Vuagnat, 1983; Ruffini et al., 1997), has been considered. They have been sampled in three different localities between SE France and SW Switzerland, whose tectonic settings vary from a simple piling of tectonic units to stacks of polyphasic folds (Rivaro Garcia, 1978; Doudoux et al., 1987), and the metamorphic condition from diagenetic to laumontite facies (Ruffini 1995; Schimdt et al., 1997). Our AMS results, supported also by additional paleomagnetic analyses (see below), documented that:

1. the evolution of the anisotropy of the magnetic susceptibility (AMS) proposed by Parès et al. (1999) can be extended through the observation of Borradaile and Jackson (2004) to clastic sedimentary sequences affected by polyphasic folding deformation;
2. differences in orientation between the anisotropy of the magnetic susceptibility (AMS) and the anisotropy of isothermal remanence (AIRM) result an useful tool to reconstruct the deformation history of polyphasic folding events;

3. the match between ferromagnetic mineralogy and remanent magnetization allow to get information about time and deformation conditions during the magnetization.

2. Taveyanne Sandstones: geologic and stratigraphic setting

The lithostratigraphy of the Eocene-Oligocene Molasse Basin exposed between SE France and Central Switzerland is characterized by the so called Priabonian Trilogy Group, consisting of Nummulitic Limestones (*Calcaires Nummulitiques*) and Globigerina Marls (*Marnes à Globigerines*), overlain by turbiditic sequences of various composition (e.g. *Grès de St. Antoin, Grès d'Annot, Grès de Champseur, Grès de Taveyanne*) (Sinclair, 1997a; Ford and Lickorish,

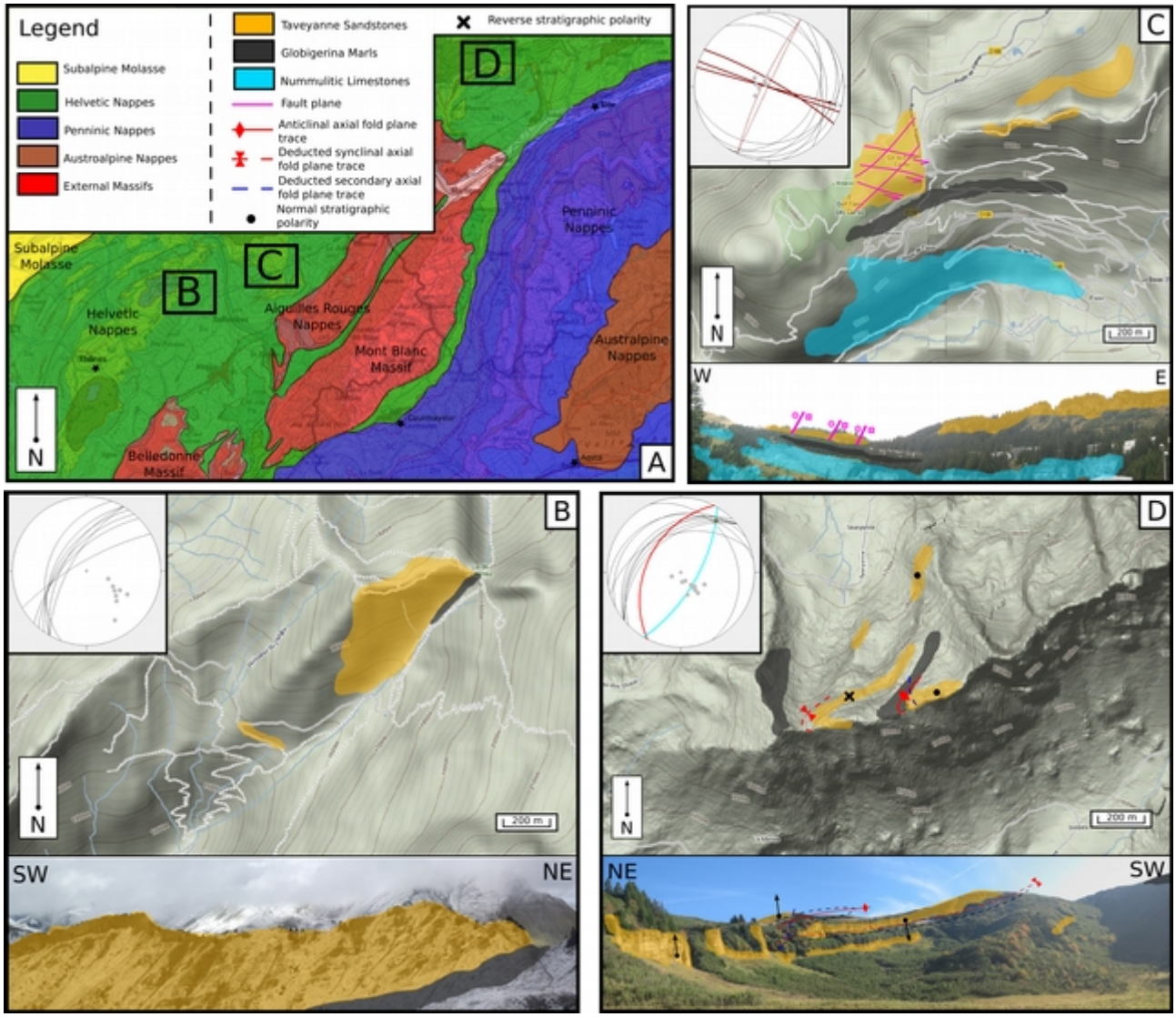

Figure 1: A) Geological sketch map of Alpine domains and fieldowork locations; B) Col de l'Oulette fieldwork map, section and stereogram; C) Flaine fieldwork map, section and stereogram; D) Taveyanne fieldwork map, section and stereogram. In all the stereograms, bedding is represented as black line, pole to bedding as gray dot; in Flaine stereogram fault planes are represented by purple bold line, with an arrow indicating the orientation of calcite slickenfiber lineations, while secondary planes in purple dashed line; in Taveyanne stereogram, red line represents schistosity of isoclinal folding phase, measured on field, light blue line represents secondary axial plane surface, while yellow dot represents its corresponding axis orientation.

2004). The Taveyanne (or Taveyannaz) Sandstones are widely but not continuously exposed between the Haute Savoie region of SE France, where it was described in the Bornè-Aravis and Platè Massifs (Doudoux et al., 1987; Ruffini et al., 1997), and in Eastern Switzerland (Sinclair, 1992). Along this outcrop area, the Taveyanne Sandstones have been involved in post-Oligocene deformation at various scales and intensities (Rivaro Garcia, 1978; Doudoux et al., 1987) ranging from very low grade metamorphic conditions (zeolite facies) to metamorphism of greenschist grade (Schimdt et al., 1997 and 1999). The Taveyanne Sandstones consist of turbiditic volcanoclastic sequences rich in different lithotypes of volcanic clasts (basalts, cpx-opx andesites, amph andesites, dacites, rhyolites and pumice), and amphibole, clinopyroxene and plagioclase crystals, in association with a low but constant presence of plutonic, sedimentary, and metamorphic rock fragments (Sinclair, 1992; Ruffini, 1995; Ruffini et al., 1997; Boyet et al., 2001). Chemical analyses performed on the volcanic rock fragments show their calc-alcaline nature and their strong affinity with the magmatic suite of the Adamello and Bergell plutonic complexes (Boyet et al., 2001). Ar/Ar radiometric dates on amphiboles constrain at 32.5 Ma and 30.5 Ma the main magmatic events in the source area of Taveyanne volcanoclastics (Fèraud et al., 1995; Ruffini et al., 1997), while calcareous nannofossils constrain the sedimentation of Taveyanne volcanoclastics to Zone NP23 between 32 and 29 Ma in the early Oligocene (Ruffini et al., 1997). According to Lateltin, 1988 and ref. therein, the volcanic material as primary in origin and formed by phreatomagmatic explosions occurring in the basin area. (Lateltin, 1988 and ref. therein). Dal Piaz and Venturelli (1983), Vuagnat (1983) and Ruffini et al. (1997), instead, prefer to consider the volcanic material as the result of the erosion of an “andesitic nappe” that originated in the inner part of the Alpine chain and was tectonically transported in the study area during the Oligocene.

We conducted fieldwork in three localities of the Western Alps (Fig. 1a): Col de l'Oulette and Flaine (Haute Savoie, SE France), and Taveyanne (Gryon, Vaud, SW Switzerland). In all of them, the stratigraphic succession starts with ~20 m of 20 cm-thick sandstone layers occasionally interbedded with thin pelitic to marly intervals; ~1 m-thick slumping layers are also observed in this interval. Above follows a ~350 m of 0.5 to 2 m-thick layers of light green to light blue sandstones with occasionally flute casts and groove casts at their base. Fining upward sequences have been documented, particularly in the thickest layers. These sequences are characterized by marly soft clasts and andesitic pebbles aligned along at their basis, and ripples on top of every layer. Moreover, occasional microconglomerate bodies can occur in the upper part of the formation (Fig. 2). In the Col de l'Oulette section (Fig. 1b), the Taveyanne Sandstones consist of a succession of strata outcropping above the Globigerina Marls, generally dipping to the NW. The Flaine section (Fig. 1c) consists of a succession of strata partially covered by the vegetation, gently dipping towards the NE to SE. Subvertical fault planes, dipping to the SSW (195°E / 85°), show sinistral strike-slip

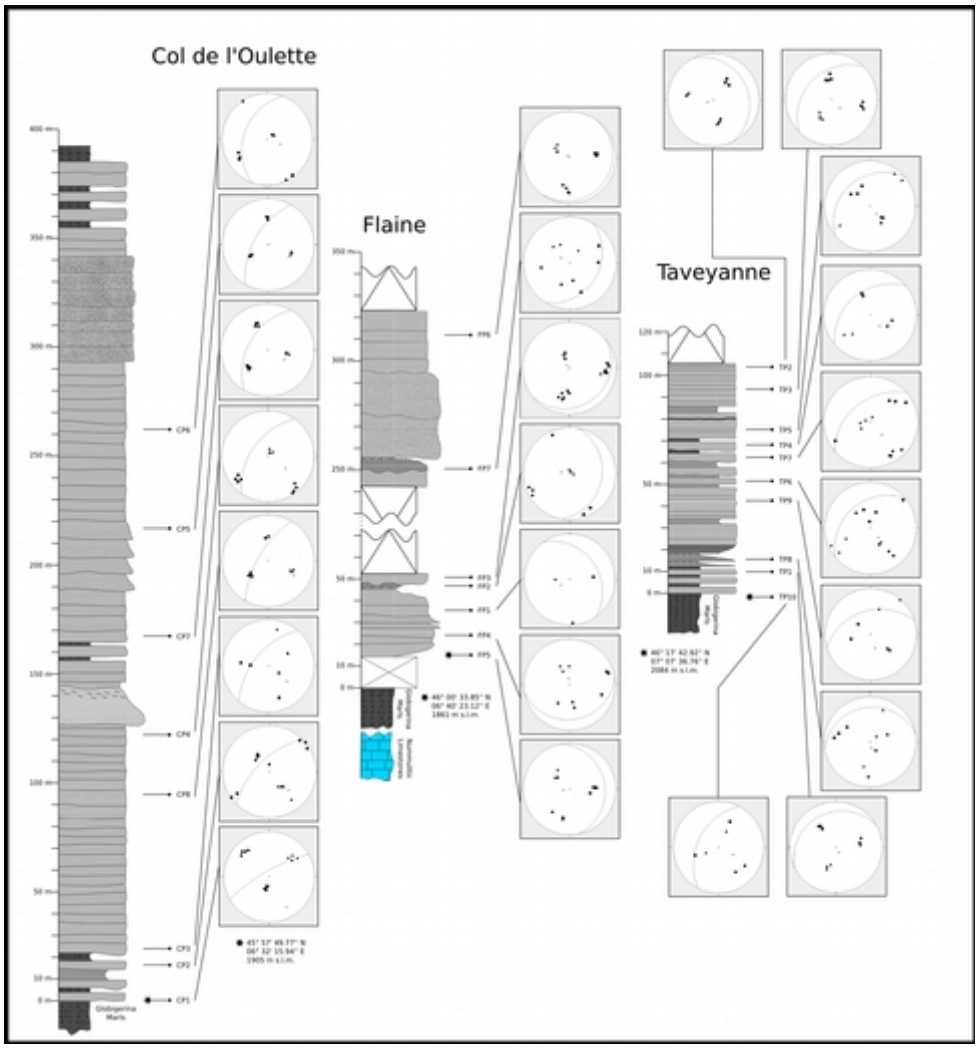

Figure 2: Stratigraphic columns of the sections observed, showing samples position and AMS "in situ" results on stereograms. Bedding is represented as black line, pole to bedding as gray dot, Kmax as black square, Kint as black triangle and Kmin as black dot.

displacement (115°E / 10° on calcite slickenfiber lineations). Secondary planes, highly dipping to the NNE, has been measured (030°E / 80°). The Taveyanne section (Fig. 1.d), outcropping near the Taveyanne village, shows the higher degree of deformation due to its involvement in a regional stack of isoclinal recumbent folds, corresponding to a third type polyphase deformation. The main folding event generated isoclinal recumbent folds, gently dipping to the NW (343°E / 35°). The secondary folding event has axial planes highly dipping to the SE (142°E / 63°).

3. Methods

A total of 25 layers have been hand-sampled in the three studied sections: 8 hand-samples have been taken at Col de l'Oulette, 7 at Flaine, and 10 at Taveyanne. All hand-samples have been subsequently cored in the laboratory, obtaining 85 cylindrical (11,4 cm^3) oriented cores, 30 at Taveyanne, 25 at Flaine, and 30 at Col de l'Oulette. All paleomagnetic analyses have been carried out at the Alpine Laboratory of Paleomagnetism of Peveragno, Italy.

The AMS is a second order tensor with three principal susceptibility axes (Kmax ≥ Kint ≥ Kmin) (Jelinek, 1981; Borradaile and Jackson, 2004). Through them, the AMS tensor can be represented as an ellipsoid oriented in space; its form and elongation are useful parameters to define rock petrofabrics and strain or depositional histories (Borradaile, 1981; Jelinek, 1981; Borradaile and Henry, 1997; Parès et al., 1999; Borradaile and Jackson, 2004; Borradaile and Jackson, 2010).
On each core, a low magnetic field has been applied along 15 axes with a KLY-3 Kappabridge, following the Agico KLY-3 User's Guide (1998). Susceptibility tensors (and associated errors) were calculated for each sample -using SUMA software and were rotated into tilt-corrected coordinates and plotted using Stereo32 software, version 1.0.3.

The anisotropy of isothermal remanent magnetization (AIRM) represents a tool to quantify the contribution of ferromagnetic (s. l.) particles to the AMS petrofabric (Tarling and Hrouda, 1993). Each sample has initially subject to alternating field (AF)-demagnetization in a field of 60 mT, using a Molspin tumbler demagnetizer, and subsequently magnetized along 6 directions, each one along two opposite verses, in a direct field of 20 mT with a PUM-1 Agico Pulse Magnetizer. After every magnetization step, the magnetic remanence has been measured on an Agico JR6 spinner magnetometer.

In order to investigate the nature of the ferromagnetic minerals, the thermal demagnetization of a 3-component IRM imparted in 1 T, 0.3 T, and 0.12 T orthogonal fields (Lowrie, 1990) has been conducted on 5 cores (1 from Taveyanne, 2 from Flaine and 2 from Col de l'Oulette) and measured with a 2G Enterprises 755 DC-SQUID cryogenic magnetometer. In addition, we performed isothermal remanent magnetization (IRM) analyses by subjecting fresh rock fragments (2 from Taveyanne, 1 from Flaine section and 2 from Col de l'Oulette) to progressively increasing magnetizing fields from 4 to 1000 mT imparted with an ASC Scientific Pulse Magnetizer-, and measuring the induced remanence on a Agico JR6 spinner magnometer, and AF-demagnetization has been applied on 12 samples (8 oriented cores, 3 of which of Taveyanne section, 1 of Flaine section and 4 of Col de l'Oulette section; 3 oriented fragments, 2 of Taveyanne section and 1 of Flaine section; 1 non-oriented fragments of Flaine section) throughout an increasing field up to 80 mT, measuring after every magnetizing step on a Agico JR6 spinner magnometer.

The natural remanence magnetization (NRM) has been obtained on a suite of 40 fresh cores (12 of Col de l'Oulette section, 11 of Flaine section and 17 of Taveyanne Sandstones) imparting a thermal demagnetization up to 600° C. At every heating step, the magnetic remanence has been measured with a 2G Enterprises 755 DC-SQUID cryogenic magnetometer.

4. Results

4.1 Col de l'Oulette

Samples of the Col de l'Oulette section are characterized by oblate to partial neutral AMS ellipsoids (Fig. 3a). The Kmax axes lay on the bedding planes in *in situ* coordinates, the Kint axes are grouped around the poles to bedding, and the Kmin axes are grouped along the NW and SE directions (Fig. 3b). After correction for bedding tilt (Fig. 3c), a tectonic control on the AMS fabric is evident: the Kmax are subhorizontal while the Kint and Kmin lie at high angle along a NW-SE plane, which is typical of the development of a weak cleavage (Parès et al., 1999).

The AIRM ellipsoids are oblate with Pj values higher than the AMS ones (Fig. 3a). The pattern observed is characterized by Kmax and Kint axes coinciding with the poles to bedding, and the Kmin axes lying on the bedding planes (Fig. 3d), suggesting a strong tectonic control on the AIRM pattern.

The results of the thermal demagnetization of a 3-component IRM reveal the ferromagnetic mineral content of the Col de l'Oulette section. The hard coercivity fraction identified by the 1 T curve shows high unblocking temperatures of about 600°C (Fig. 4a). The IRM acquisition curve reaches saturation of 600 mT (Fig. 4.b). The AF-demagnetization results show that 80 % of the NRM is demagnetized at 10 mT. This magnetic properties suggest the presence of the maghemite in the Col de l'Oulette samples (de Boer and Dekkers, 1996; de Boer, 1999).

Paleomagnetic component directions of the NRM have been obtained using thermal and AF demagnetization and are defined at least by 5 aligned points on the Zijderveld diagrams over 250°C (Fig. 5). Both their *in situ* (Fig. 6a) and tilt corrected projections (Fig. 6b) highlight the secondary origin of the magnetic signal. In particular, the orientations of paleopoles obtained are comparable to the bedding orientations.

4.2 Flaine

In the Flaine section, AMS ellipsoids result prolate to partial neutral (Fig. 3a). AMS fabric shows the Kmax signal arranged at low angle on E position, corresponding to the direction of movement measured on field, Kint signal on central position, around poles to bedding, and Kmin signal on the S direction (Fig. 3e). After correction for bedding tilt (Fig. 3f), no significant change in the axes orientation has been detected, documenting a strong cleavage fabric (Parès et al., 1999).

The Pj values of the AIRM ellipsoids are higher than the AMS ones (Fig. 3a). As in the Col de l'Oulette section, the Kmax and the Kint correspond to poles to bedding and the Kmin lay on the bedding planes (Fig. 3g).

The results of the thermal demagnetization of a 3-component IRM reveal the ferromagnetic mineral content of the Flaine section, as shown by high unblocking temperatures of about 600°C of the hard coercivity fraction (1 T curve) (Fig. 4a). The IRM acquisition curve reaches saturation of

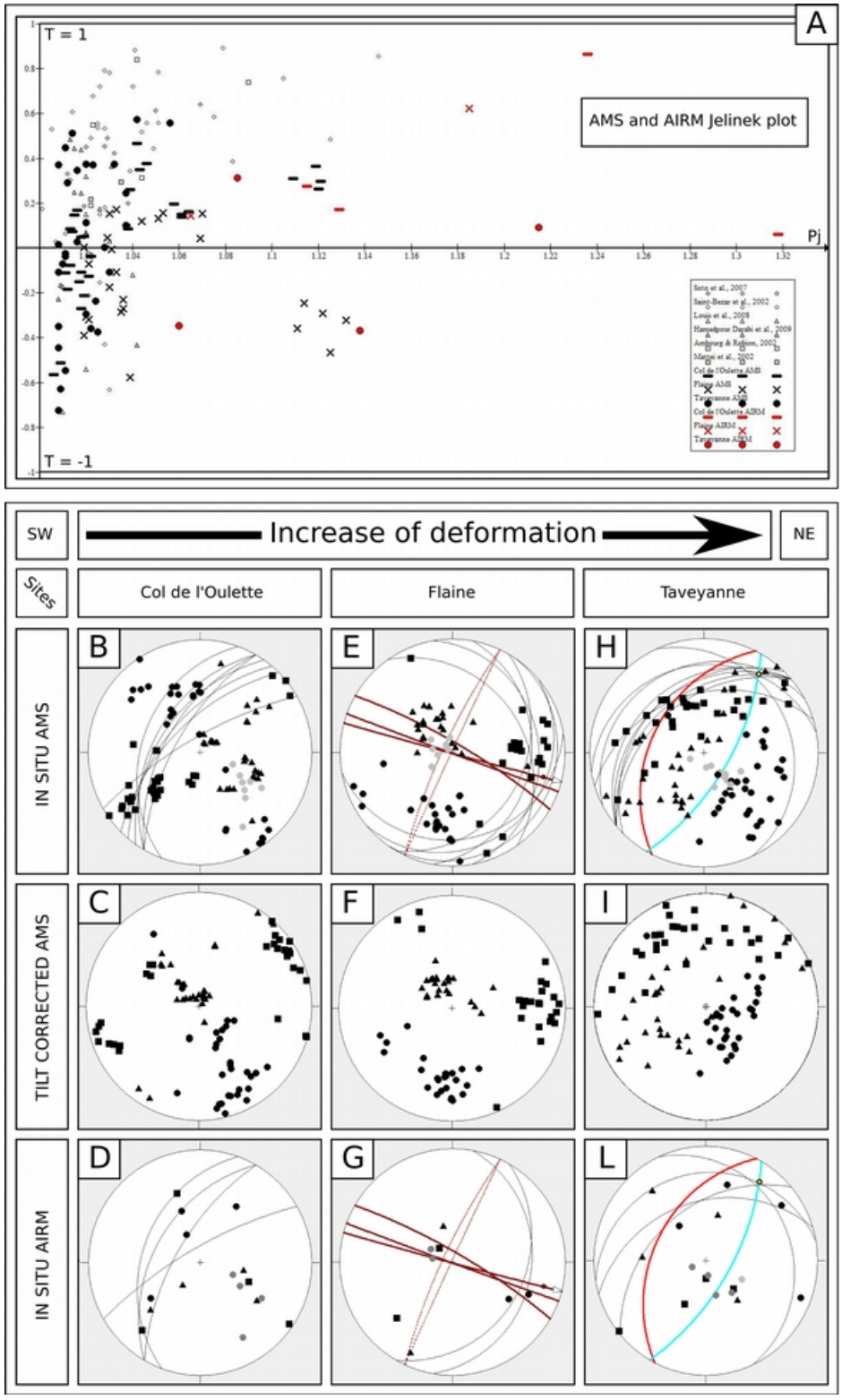

Figure 3:a) AMS and AIRM Jelinek plot. AMS values are represented as black symbols (line-Col de l'Oulette; cross-Flaine; dot-Taveyanne) and AMS literature data are represented as white / gray symbols. AIRM values are represented as red symbols (line-Col de l'Oulette; cross-Flaine; dot-Taveyanne); b-l) AMS in situ and tilt-corrected stereograms, AIRM in situ stereograms. In all the stereograms, bedding is represented as black line, pole to bedding as gray dot, Kmax as black square, Kint as black triangle and Kmin as black dot; moreover, in Flaine AMS and AIRM stereogram fault planes are represented by purple bold line, with an arrow indicating the orientation of calcite slickenfiber lineations, while secondary planes in purple dashed line; in Taveyanne AMS and AIRM stereogram, red line represents schistosity of isoclinal folding phase, measured on field, light blue line represents secondary axial plane surface, while yellow dot represents its corresponding axis orientation; b-c-d) Col de l'Oulette stereograms; e-f-g) Flaine stereograms; h-i-l)

600 mT (Fig. 4.b). The AF-demagnetization results show that 80 % of the NRM is demagnetized between 15 and 20 mT. This magnetic properties are consistent with the presence of the maghemite in the Flaine samples (de Boer and Dekkers, 1996; de Boer, 1999).

Again, paleomagnetic component directions of the NRM have been obtained using thermal and AF demagnetization and are defined at least by 5 aligned points on the Zijderveld diagrams over 250°C (Fig. 5). The NRM and AF-demagnetization paleomagnetic poles again show a secondary origin of the magnetic signal. Perhaps, in Flaine section paleomagnetic orientations are quite similar to the poles to bedding (Fig. 6c), while tilt corrected projections have no paleomagnetic sense (Fig. 6d).

4.3 Taveyanne

The Taveyanne section is characterized by prolate to oblate ellipsoids with low Pj values (Fig. 3a). The *in situ* AMS fabric shows a strong clustering of Kmax values on the intersection between bedding and schistosity planes, and the Kmin values near the poles to bedding (Fig. 3h). A three steps-retrodeformation path has been applied to restore the potential AMS anitropy pattern before the folding events, resulting in Kmax values almost aligned along a NNW gently dipping plane, Kmin almost grouped to the SE direction and Kint values without a preferred orientation (Fig. 3i). Even if a tectonic control can be inferred, we did not find any relationship with the structures highlighted by Parès et al. (1999).

The AIRM ellipsoids show both prolate and oblate shapes, with Pj values higher than the AMS ones (Fig. 3a). Again, the Kmax and Kint axes correspond to poles to bedding and the Kmin axes lay on the bedding planes (Fig. 3l).

In Figure 4a, the results of the thermal demagnetization of a 3-component IRM are shown: high unblocking temperatures of the hard coercivity fraction (1 T curve) is about 600°C. The IRM acquisition curve reaches saturation of 600 mT (Fig. 4b). The AF-demagnetization results show that 70 % of the NRM is demagnetized before 30 mT. This magnetic properties are consistent with the presence of the maghemite in the Taveyanne samples (de Boer and Dekkers, 1996; de Boer, 1999).

The *in situ* projections of NRM and AF-demagnetization paleopoles (Fig. 6e) show a strictly correlation with the folding structure affecting the Taveyanne area, which have completely deleted the primary signal (Fig. 6f).

5. Discussions and conclusion

The evolution of the AMS pattern (Fig. 7a) has been compared with the pattern described by Parès et al. (1999) (Fig. 7b). These authors recognized four main stages of AMS fabric development during early cleavage formation in Eocene mudrocks of the Ebro basin (Pyrenees, Spain): (1)

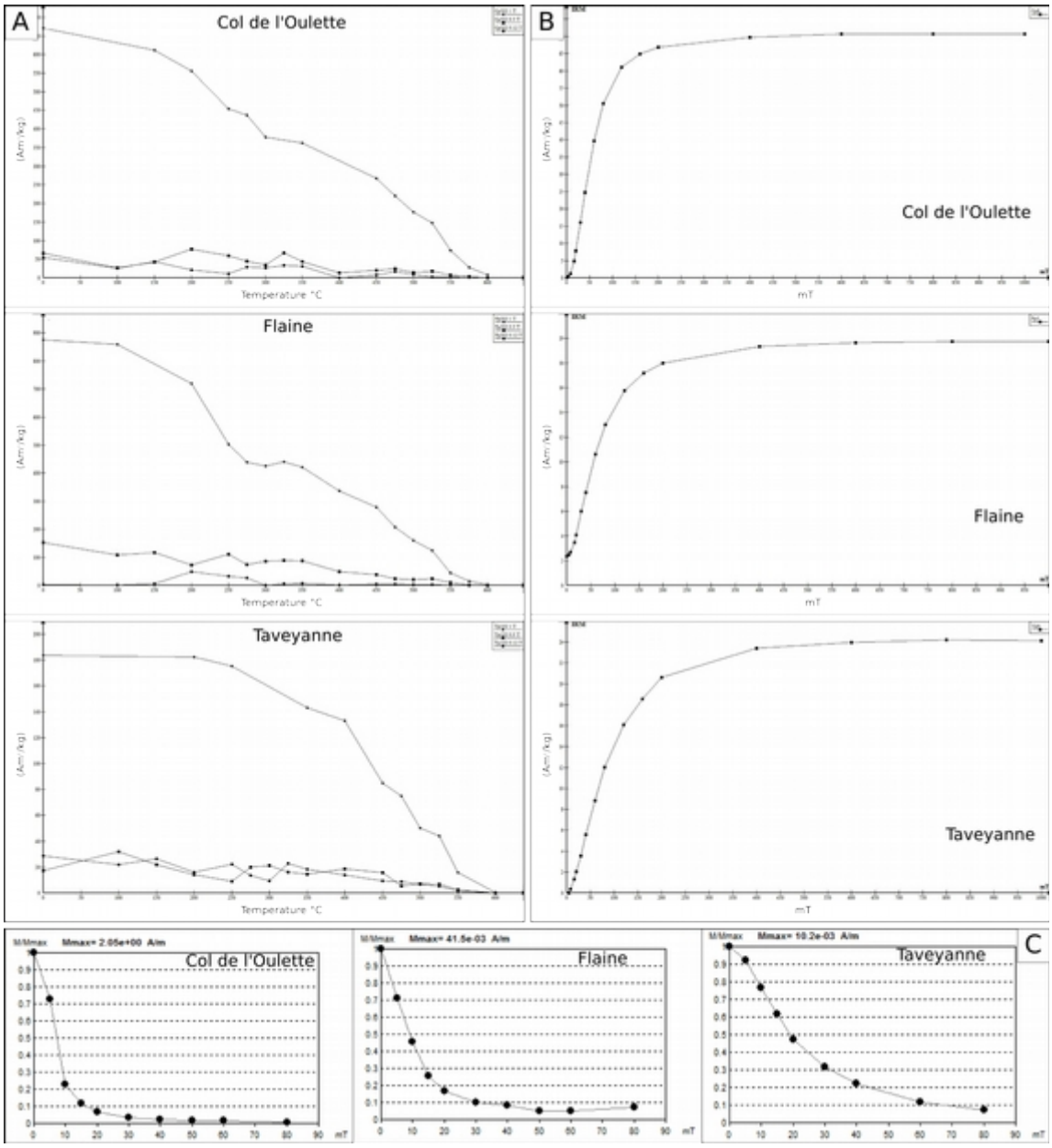

Figure 4: Ferromagnetic mineralogy investigations; a) ThIRM diagrams. In strong fraction of Col de l'Oulette and Flaine samples, a no decay segment, between 250 and 400° C ca, highlights the presence of maghemite, near hematite and magnetite. b) IRM diagrams and c) AF-demagnetization diagrams, the latter showing the low magnetic signal preserve both in Col de l'Oulette and Flaine samples.

earliest deformation stage, (2) pencil structure stage, (3) weak cleavage stage, and (4) strong cleavage stage. In Figure 7b, only stages(3) and (4) are reported. The weak cleavage stage (3) is characterized by maximum susceptibility axes grouped on the bedding plane, whereas the intermediate and minimum axes are distributed on a plane perpendicular to bedding. Our samples from Col de l'Oulette show a similar pattern (Fig. 5a), which is regarded as transitional between primary depositional and secondary tectonic fabrics as described by Borradaile and Jackson (2010). As the cleavage becomes stronger (stage 4), the distribution of the minimum susceptibility axes changes into a cluster that is normal to the cleavage plane (Parès et al., 1999). This distribution has

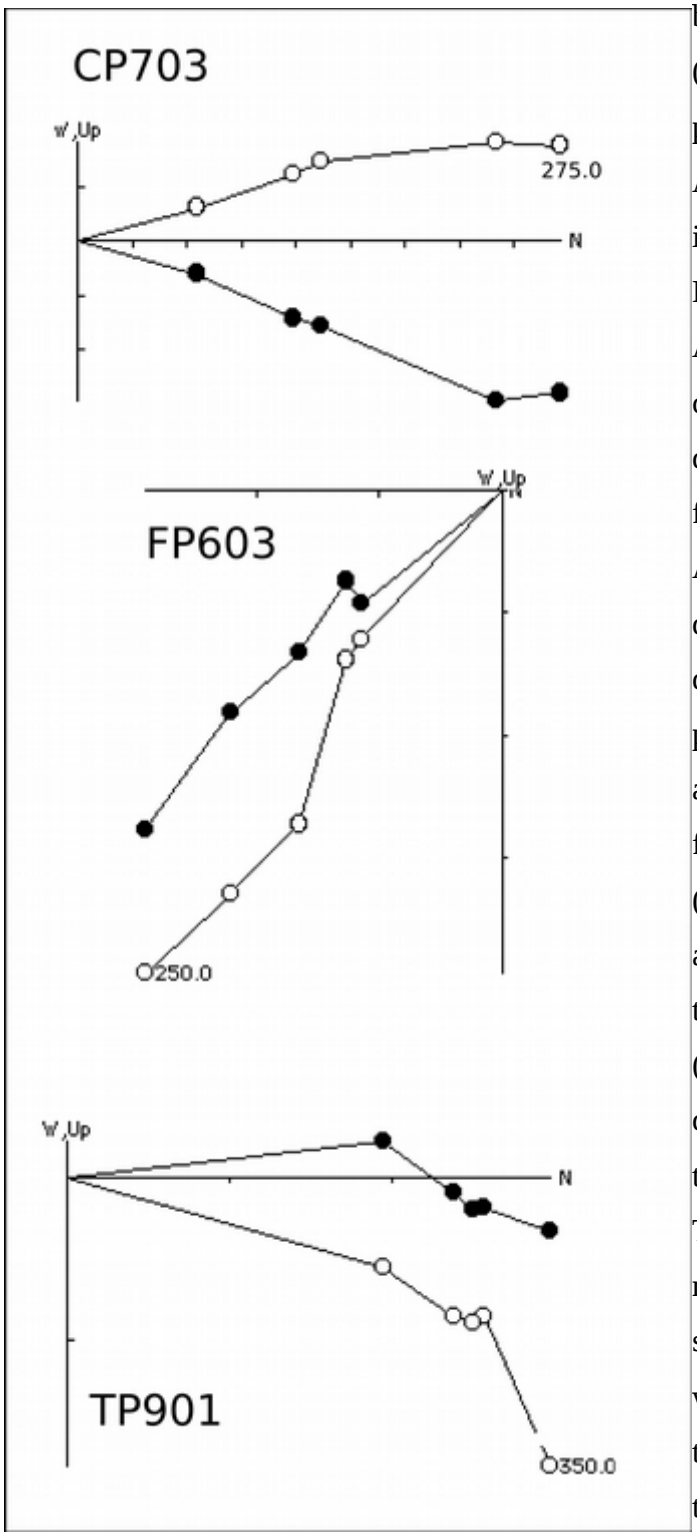

Figure 5: Zijderveld diagrams of three significant sites: CP703 from Col de l'Oulette, FP603 from Flaine and TP901 from Taveyanne.

been documented in samples from Flaine (Fig. 5a-b), where the development of a persistent, strong cleavage, recorded by the AMS pattern, is regarded as the result of initial tectonic compaction (Borradaile and Henry, 1997; Borradaile and Jackson, 2010). At Flaine, this tectonic compaction is controlled by the pervasive, brittle deformation imposed by sinistral strike-slip faults.

As the deformation becomes pervasive, ductile multistage folding can occur, as documented in the Taveyanne area. As previously described, the turbidite sequence at Taveyanne is characterized by double folding deformation, constituted by a first (primary) isoclinal recumbent folding event associated with pervasive schistosity parallel to the axial plane, and a subsequent (secondary) folding phase with higher dipping fold axis oriented perpendicular to the primary recumbent fold axis (Fig 7a). The associated AMS pattern shows maximum susceptibility axes grouped on the schistosity planes measured in the field, while the intermediate susceptibility axes tend to crosscut the schistosity planes, and the minimum axes are normal to them (Fig. 3h). In order to gauge the effects of each deformation phase on the AMS fabric, we first corrected for tilting the limbs of the secondary folding structure, and then rotated the primary isoclinal structure in a vertical position. This correction makes the AMS pattern (Fig. 7a) comparable to the pattern described by Borradaile and Jackson (2004) for a vertical axis fold with pervasive schistosity parallel to the axial plane (Fig. 7c). Both cases show maximum susceptibility axes clustering on the schistosity parallel to the fold

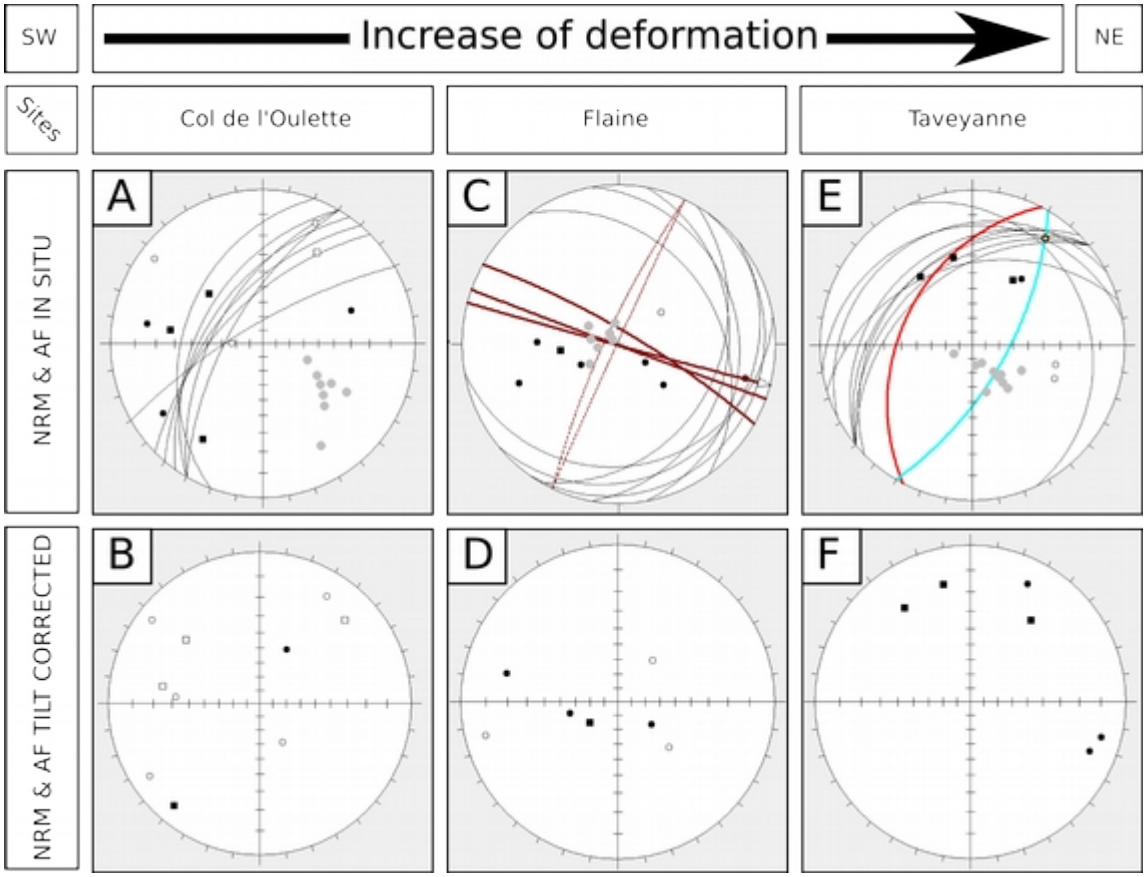

Figure 6: NRM and AF-demagnetization results, both in situ and tilt corrected; a-b) Col de l'Oulette stereograms; c-d) Flaine stereograms; e-f) Taveyanne stereograms. In the in situ stereograms (a-c-e), bedding is represented as black line, pole to bedding as gray dot, normal / reverse NRM polarity as empy / full dot, normal / reverse AF-demagnetization polarity as empy / full square; moreover, in Flaine in situ stereogram (c) fault planes are represented by purple bold line, with an arrow indicating the orientation of calcite slickenfiber lineations, while secondary planes in purple dashed line; in Taveyanne in situ stereogram (e), red line represents schistosity of isoclinal folding phase, measured on field, light blue line represents secondary axial plane surface, while yellow dot represents its corresponding axis orientation.

axial plane, whereas the minimum axes cluster around the poles to bedding. The intermediate susceptibility axes of the restored Taveyanne structure seem to define a sub-vertical plane trending NE (Fig. 3h), while in the diagram of Borradaile and Jackson (2004), they cluster on the horizontal plane (Fig. 7c). This discrepancy can be explained with the development at Taveyanne of an incipient cleavage related to the secondary folding plane. This comparison thus suggests that in the highly deformed mudstones and sandstones at Taveyanne, the maximum and minimum susceptibility axes are controlled by the schistosity associated with the primary isoclinal structure, whereas the intermediate axes are controlled by the incipient cleavage associated with the secondary folding. This complex deformation generated low anisotropy degrees (Fig. 3a), in apparent contradiction with the high deformation and incipient metamorphism that these rocks suffered (Schmidt et al., 1997; 1999). A solution to this contradiction comes from the realization

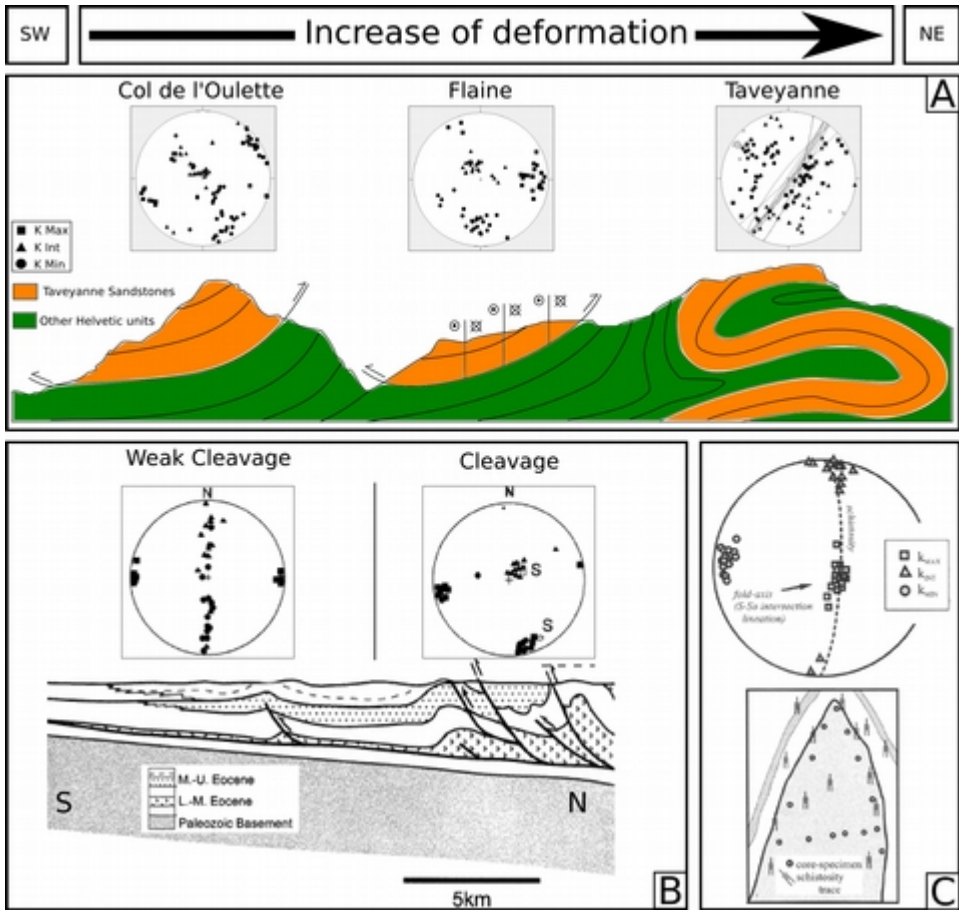

Figure 7: a) Equal-area, lower-hemisphere projection of anisotropy of magnetic susceptibility data a SW–NE section in the Northern Alpine Molassa Basin; b) Equal-area, lower-hemisphere projection of anisotropy of magnetic susceptibility data for representative sites along a N–S sectionin the Ebro Basin, southern Pyrenees (modified from Parès et al., 1999); c) a penetrative schistosity in a vertical isoclinal fault (from Borradaile and Jackson, 2004).

that the two subsequent stages of folding developed along perpendicular directions, resulting in the mutual permutation of maximum extension and maximum compression. Hence, in case of multiple folding, the anisotropy degree does not appear to be a good proxy for deformation intensity.

The AIRM fabric is everywhere either transitional or tectonic, with one axis (Kmax or Kint) grouped on poles to bedding, the other two on the relative bedding planes (Fig. 3D-g-l), and Pj values ranging between 1.06 and 1.32. These results reflect a discrepancy between the AMS and the AIRM fabrics, owing to different deformation responds. Similar discrepancies have been documented in the Archean greenschist metasedimentary rocks of Northern Ontario (Canada) by Borradaile and Dehls (1993). These authors used differences in orientations between schistosity, AMS and AIRM fabrics as temporal indicators of the development of successive sub-fabrics in the rocks, inferring that AIRM fabric only records the latest components of tectonic events. We applied this model to the Taveyanne site, in order to reconstruct the folding phase history. Here, AIRM fabric is characterized by Kmax axes grouped on the axial plane of the secondary fold, and the other

axes aligned along the AMS Kmax plane (Fig. 3l). These orientations underline that only the main folding event acted both on the AMS and AIRM fabric, and only AIRM fabric preserves the signal owing to the second folding event. Thus, we speculated that, in a first stage, the main folding event aligned both the AMS and AIRM fabrics along the principal schistosity measured in the field. In a second stage, instead, the superimposition of a second folding event pervasively reoriented the AIRM fabric, whereas the AMS one recorded only a minor deformation.

Maghemite identified through IRM, 3-component IRM and AF-demagnetization analyses was originated by maghemitization (oxidation) process of the magnetite (Dunlop and Özdemir, 1997; de Boer, 1999) present in the abundant basic to intermediate volcanic rock fragments of Taveyanne Sandstones detritus (Ruffini et al., 1997). In sediments, maghemitization can result both from diagenetic or hydrothermal processes in water-rich ambients, at temperature lower than 250°C (de Boer & Dekkers, 1996; Dunlop and Özdemir, 1997; Lagoeiro, 1998; de Boer, 1999; Goguitchaichvili et al., 2000). At these conditions, the process triggers the obliteration of detrital remanent magnetization (DRM) and the rapid acquisition of a chemical remanent magnetization (CRM), often oriented along the ambient field direction (Kelso et al., 1991; De Boer, 1999; Fuller et al., 2002). At the same P/T and water-rich conditions, metamorphism prevents the maghemitization process (Lagoeiro et al., 1998). So, the occurrence of maghemite in Taveyanne Sandstones detritus is consistent with NRM and AF-demagnetization orientations characterized by the absence of a primary sedimentary signal, as we obtained in this work. The signal measured was acquired during the early stage of deposition, when syn-depositional tectonic (Sinclair, 1992; Ruffini, 1995; Sinclair, 1997a) and diagenetic/hydrothermal processes overprinted the primary DRM.

In conclusion, the paleomagnetic study we carried out on the Taveyanne Sandstones deposits, cropping out in the Haute Savoie region (SE France and SW Switzerland), allowed us to integrated the model proposed by Parrés et al. (1999) with the observations of Borradaile and Jackson (2004). This integration considers areas where polyphasic folding deformation deeply acted on a clastic sedimentary sequence. Moreover, through differences in orientation between the anisotropy of the magnetic susceptibility (AMS) and the anisotropy of isothermal remanence (AIRM), we unraveled the deformation history of this polyphasic folding deformation. Finally, the analyses on the ferromagnetic mineralogy and its remanent magnetization allowed us to document the syn-depositional tectonic (Sinclair, 1992; Ruffini, 1995; Sinclair, 1997a) and diagenetic/hydrothermal conditions affecting the detritus during the early stages of the deposition.

Volcanism versus tectonics in a Jurassic continental basin: from the Las Leoneras Formation to the Lonco Trapial Formation
(Cañadon Asfalto Basin, Chubut Province, Argentina)

1. Introduction

The study of how volcanism can affect continental environments, characterized of fluvial and lacustrine settings, can offer a wide range of topics on how the stratigraphic record responds to the rapid onset of proximal magmatism (e.g. Smith et al., 1988, 1991; Manville et al., 2005, 2009). This includes not only the possibility to document the critical changing in sedimentation rates, in relation to different stages of volcanism, but also to better understand which are the conditions for that primary volcanic/volcanoclastic structures can be preserved, once deposited in a fresch-water basin (Smith, 1991). For this, continental environments constitute perfect laboratories for testing hypothesis on physical parameters controlling these events, as distance to go, depth of basins, thickness of single events, and provides primary information also useful for the comprehension and interpretation of the stratigraphic record of distal volcanoclastic sequences, as the deep-sea one, where a complete “volcanic source - basin” system is not still preserved. We focused on the Jurassic volcano-sedimentary sequences, named Las Leoneras Formation and Lonco Trapial Formation, in the Cañadon Asfalto basin (Chubut Province, Argentina-Fig.1) (Cunéo et al., 2013). Here, the onset of volcanism is subsequent to the onset of sedimentation, primary fed by the erosion of crystalline rocks, and reaches its climax with the rapid deposition of thick volcanoclastic sequences, due to explosive/effusive behavior of volcanism itself (e.g. Cabaleri and Benavente, 2013). This work aims to:

1. describe in detail lithological, optical, petrographical and magnetic anisotropic (where possible) features that characterize sedimentary and volcanic facies;
2. detect primary volcanic/volcanoclastic flows deposited into the water, in the field and/or through optical and petrographical observations;
3. compare sediment composition of lacustrine and fluvial facies during different stages of volcanism, in order to detect the real influence of it on sediments supply, and also in relation to explosive/ effusive events;
4. document the high instability of fluvial systems during syn-volcanism periods rather than periods of volcanic quiescence or erosion.

2. Geological setting

Lower part of the Cañadon Asfalto Basin

The Cañadon Asfalto-Somuncurá basin represents one of the sedimentary basins developed in the Patagonia region through the Triassic-Cenozoic times (Fig.1). In it, Cañadon Asfalto sub-basin constituted a rift basin that evolved to a pull-apart basin, filled with a thick sedimentary sequence

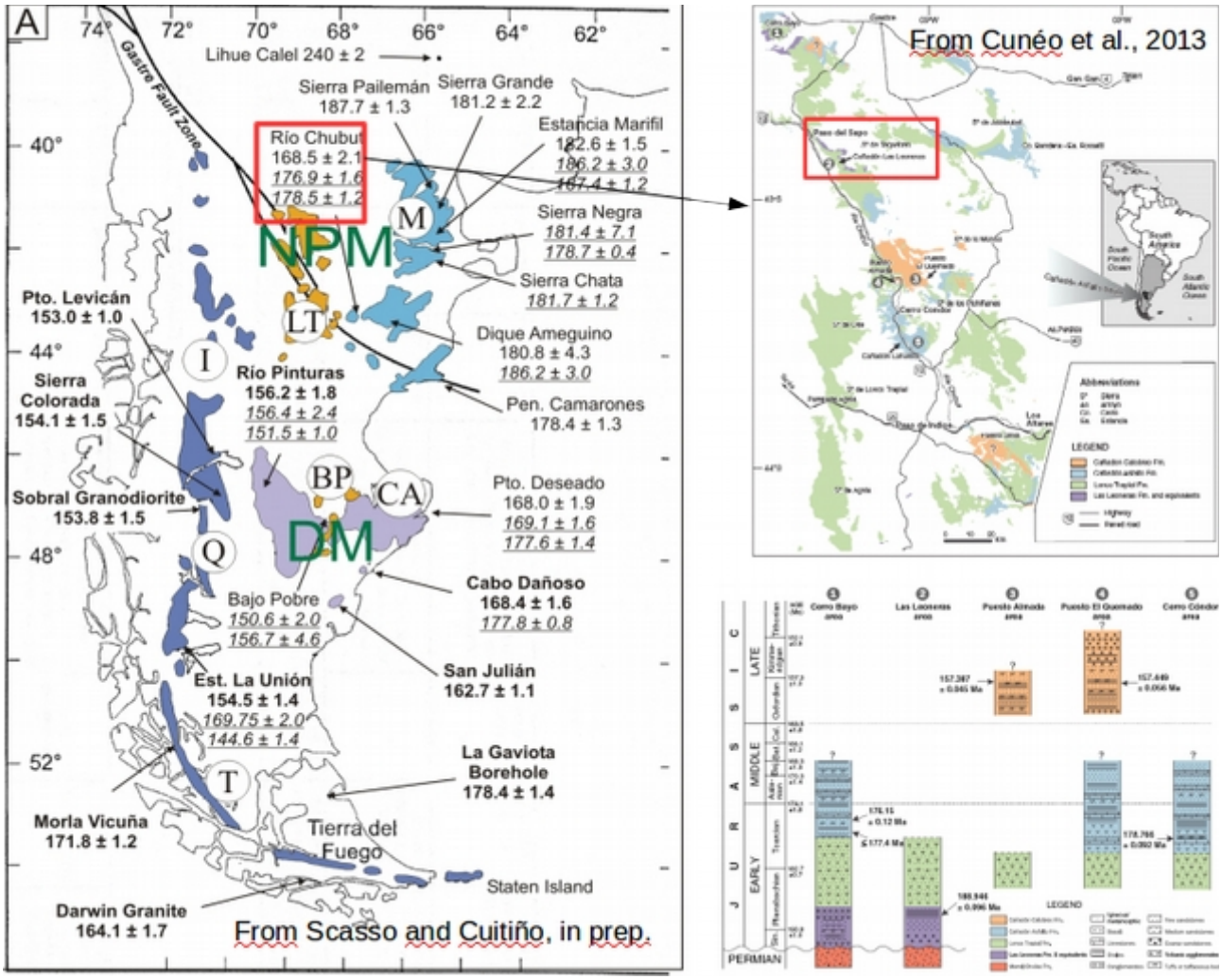

Figure 1: age constrains of Permo-Mesozoic volcanism in Argentina (from Scasso and Cuitiño (in prep.), maps of volcanic sequence in Chubut Province (up, right) and general stratigraphy of Cañadon Asfalto basin (down,right) (from Cunéo et al., 2013).

that represents lacustrine and fluvial systems with several olivine basalt flows and pyroclastic intercalations (Cabaleri and Benavente, 2013). It extends between the latitudes of 40º30` and 44°30` south and the longitudes 66°00` and 70°30`west. The early, continental deposits above the granitic rocks of the Mamil Choique Formation (Lower Ordovician) were first recognized and described as Las Leoneras Formation by Nakayama (1973b) and successively constrained at the Early Jurassic, most probably in the latest Sinemurian, by Cúneo et al. (2013). Pol et al. (2011) divided them into three main members: a lower member of white, medium and coarse-grained, poorly to moderately sorted sandstones (fluvial sedimentation supplied by basement-derived detritus); a second member of purple, massive, sandy mudstone with thin intercalations of white, coarse to medium-grained sandstone (lacustrine and turbiditic sedimentation); a third member of greenish gray, massive to laminated, bioturbated, slightly tuffaceous claystones (lacustrine to fluvial transition during syn-rift volcanic activity). Conformably and transitionally above, the Lonco Trapial Formation marks the massive incoming of volcanism into the fluvial system, and consists of a widespread, volcanic to

volcanoclastic Formation marking the onset of a Early Jurassic, volcanic-dominated paleogeography in the east-central Patagonia (Page and Page, 1993). Rapid and significant lithofacies lateral changes of volcanogenic deposits typically indicate the intense alternation of explosive and effusive events, defining a bimodal magmatic association (Cúneo et al., 2013). Traditionally assigned to the Middle Jurassic *sensu lato* (e.g. Page and Page, 1993), Cúneo et al. (2013) have been recently bracketed Lonco Trapial Formation between 188.95 Ma and 178.77 Ma, entirely within the Early Jurassic (Pliensbachian±Toarcian), in the Cerro Cóndor region. These ages, with all the other ages of the Chon Aike province, indicate possible contemporaneity between the latter and the voluminous basaltic magmatism of Early Jurassic age in South Africa and West Antarctica (e.g. Page and Page, 1993; Pankhurst et al., 2000).

3. Methods

Fieldwork has been carried out on sections exposed in Paso del Sapo area (Fig.2), measuring 11 stratigraphic logs (Fig.3) and analyzing the volcano-sedimentary facies here exposed. When possible, clast counts have been performed on conglomerate deposits. More than 50 samples have been collected and cut in standard thin sections for optical observation and point-count analysis (Folk, 1980). Ten of them have been also drilled at the Earth Sciences Department of Buenos Aires University in standard cylindrical (11,4 cm^3) oriented cores.On each core, a low magnetic field has been applied along 15 axes with a KLY-3 Kappabridge, following the Agico KLY-3 User's Guide (1998). Susceptibility tensors (and associated errors) were calculated for each sample -using SUMA

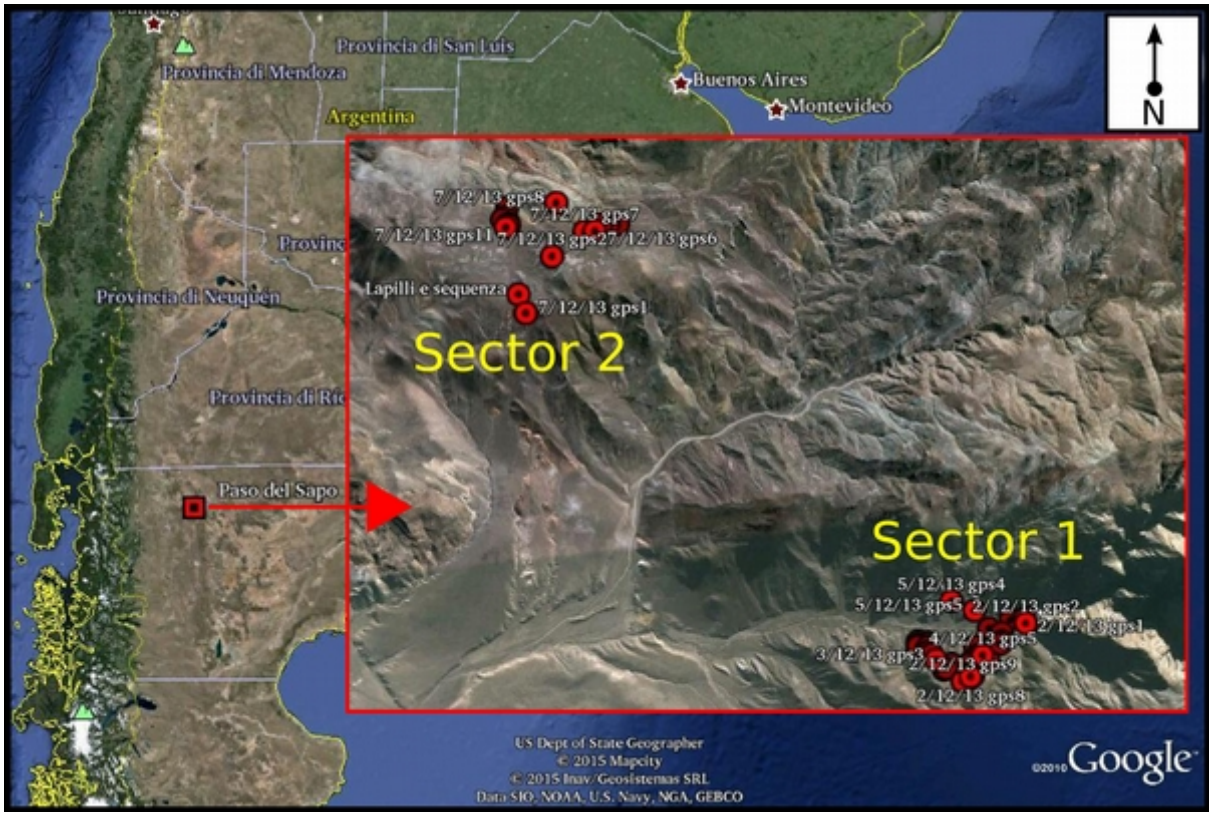

Figure 2: fieldwork area and ubication of studied logs

software and were rotated into tilt-corrected coordinates and plotted using Stereo32 software, version 1.0.3. All the data have been matched together to reconstruct the evolution of the palaeoenvironment from pre-volcanic conditions to syn-volcanic conditions.

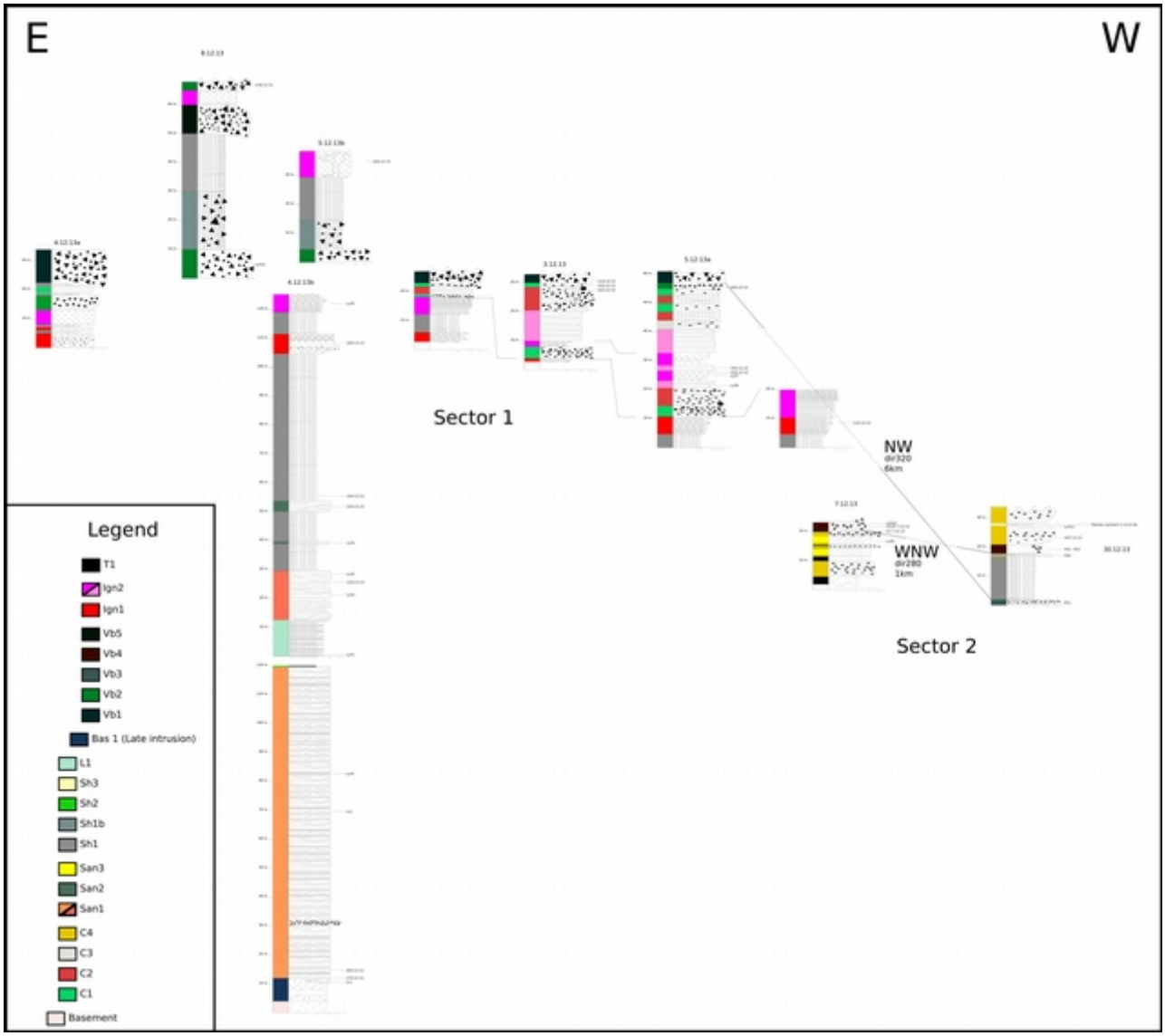

Figure 3: studied logs and correlation between the two sectors (see Figure 2 for geographic ubication).

4. Results and discussions

4.1 Facies

23 facies have been identified through fieldwork and optical analysis, 10 volcanogenic and 13 sedimentary. The volcanogenic facies are breccias, ignimbrites and tuffs that remind to a strong explosive activity (e.g. Jutzeler et al., 2014). The sedimentary facies reflect abrupt changes in sediment supply and/or environments. All the facies have been resumed in Table 1.

4.2 Palaeoenvironment evolution

Facies	Description	Petrography	Interpretation
C1	Clast-supported, polymictic conglomerates, with rounded volcanic clasts up to 30 cm in diameter, and a minor amount of rounded quartz and angular ignimbrite clasts, in a dark-green, coarse matrix. Conglomerate bodies are typically lens-shaped, up to 14 m thick, with common cross-bedding and clast imbrication in meter to few meter thick beds. Intercalations of beds with C2 and C3 facies are common. Thickness and grain-size decrease to the ESE, where sandstone and rare, thin shale intercalations have been observed. Paleocurrents from imbricated clasts point to NW-oriented flow.	Microscope analyses of the matrix reveal high content of porphyritic andesite (up to 6.8 mm in diameter) and tuff fragments, with minor plagioclase and quartz, and rare olivine and metamorphic lithics. Mostly sub-rounded but also sub-angular fragments compose the matrix. Abundant chlorite cement is responsible of the green colour of the matrix, and calcite cement fills the pores.	Facies Gt (gravel through cross beds facies - Miall, 1996), normally associated to Sp facies (sand planar cross beds - Miall, 1996), which is comparable to the sandstone intercalations of facies C1. It represents channel fills of a shallow, gravel-bed, braided river (Miall, 1996). The predominance of fluvial dynamics of transport and deposition are also consistent with the round shape, mainly characterizing both the pebbly and the sandy fractions, and the occurrence of different lithotypes, and a relatively well-organized drainage network. The development of this type of fluvial system reflects braking of the syn-volcanic sediment supply, during inter-eruptive periods (Smith, 1991 and references therein).
C2	Red, massive, polymictic, matrix-supported conglomerates, in which the gravel fraction is almost completely represented by volcanic rocks, with trace of granites (~1%). Mean grain-size is 10 cm and larger clast can reach 40 cm. The uppermost conglomerate bed shows inverse grading and is capped by an erosional surface.	Microscope analyses of the matrix show sub-rounded rock fragments of porphyritic andesites rich in plagioclase phenocrysts, porphyritic andesites with amphibole, tuffs and rare metaquartzites, quartz, plagioclase, spotted Ti-oxides and K-feldspar. This facies comprises lens-shaped conglomerates (up to 8m thick), passing laterally/upwards to parallel-laminated, coarse-grained sandstones.	Facies Gcm (clast-supported massive gravel) lithofacies of Miall (1996), laterally and upward passing to Sh (sand,very fine to coarse, maybe pebbly) lithofacies of Miall (1996) and represents channelized deposits in the upper part of a large paleovalley (see below). It represents channelized lahars dominated by granular flow mechanism of sediment transport. Occasional inverse grading was probably driven by kinetic sieving and kinematic squeezing (Sulpizio et al., 2007). The Sh-equivalent sediments represent the lahar-runout facies (Scott, 1988).
C3	Gray, lens-shaped, granule-conglomerate beds, showing high-angle cross-bedding, interbedded with thinner sandstone and shale layers, forming bodies about 3 m thick. Laterally they pass to fine-grained sandstone beds.	Not observed	Facies Gt lithofacies of Miall (1996). C3 facies represents 3D bars formed in the channels of shallow gravel-bed braided rivers. Sediment source was loose syn-erutive volcanic material (Smith, 1991; Miall, 1996) sourced from reworking of

Facies	Description	Petrography	Interpretation
			Ign2/Ign2r deposits (see below).
C4	Polymictic, dark-yellow to gray, matrix-supported conglomerates. Clast are mainly from volcanic rockas and matrix to clast ratio significantly decreases with the increase of clast dimension (max. 50 cm). Locally, gravel clasts are concentrated in single clast layers with little matrix. This facies is found intercalated in the sub-aqueous lacustrine beds of the Lonco Trapial Formation and thins out to the NW in the lower, lacustrine part of Lonco Trapial Formation.	Microscope analyses revealed an heterogeneous volcaniclastic composition for the matrix, with dominant trachytic andesite fragments, subordinated angular tuff fragments, characterized by quartz phenocrysts in a brown to gray matrix, and microgranular rhyolite fragments. Single-mineral clasts of volcanic quartz, plagioclase and biotite are rare.	Facies F2-F3 lithofacies of Mutti et al. (2003). The single layer beds are interpreted as traction carpets in suspension-to-traction dominated transport regime, reflecting grain to liquefied flow structures (e.g. S1 and R3 facies of Lowe, 1982), common triggering mechanisms for hyper-concentrated density flows (Mulder and Alexander, 2001). This type of flows may result as sub-aqueous propagation of flash flood events, which are pretty common in volcanic settings after widespread ashfall depositions (Lavigne and Suwa, 2004; Alexander et al., 2010).
San1	Coarse to fine, reddish sandstones, locally passing to thin conglomerates, which show frequent parallel to cross-bedding and normal grading. Sediments are composed of sub-angular to rounded fragments of quartz, feldspar, mica and rock fragments. Analogous sandstone beds, packaged in a lens-shape body with centimetric to decimetric silt intercalations, appear just above the limestones (Facies L, see below) of the lacustrine sequence for ca.17m, constituting the sub-facies San1d. Here, cross-bedding trend S60°W and S85°W. On top, matrix color gradually changes from red to green.	Under the microscope they show good sorting and small primary sedimentary structures, like microcross-bedding and parallel bedding, and rare cyclic variations in grain size reflecting different pulses in sedimentary supply. Grain shape ranges from angular to sub-angular, but some sub-rounded and rounded grain are also present. Single-mineral clasts dominate over rock fragments, and comprise plutonic, volcanic and metamorphic quartz, plagioclase, K-feldspar, mica (muscovite and chloritized biotite flakes lying parallel to the stratification) and oxides. Rock fragments are composed of rhyolite, tuff, granite, ortogneiss and rare amphibolite.	Facies San1 is comparable to lithofacies Sl and Sh, and locally Gcm (San1c) of Miall (1985, 1996), and represents the deposition in a shallow perennial sandy-bed, braided system developed close the source area in which basement rocks (plutonic/metamorphic) were exposed. It is the first coarse-grained terrigenous input recorded in Las Leoneras Formation. The occurrence of volcaniclastic material (rhyolite and tuff clasts) can be associated to distal, incipient, explosive syn-sedimentary volcanism, that later became more frequent and voluminous and yielded the ignimbrite deposits exposed in the upper part of the Las Leoneras Formation.
San2	Tabular, metric, fine to medium sandstone beds, rich in feldspars and angular quartz. Sandstone bodies show cross-bedding and/or parallel bedding. It is interbedded with the lacustrine shales of Las Leoneras Formation.	Optical microscope analyses revealed the single-mineral clast fraction dominates over the lithic one, with volcanic, plutonic and minor metamorphic quartz, feldspar, biotite (sometimes chloritized), muscovite and chlorite. Rare crystals of olivine and epidote have also been observed. When	Characterized by Tb and/or Tc sequence of Bouma (1962), it corresponds to lithofacies F7 to F8 of Mutti et al. (2003). They were deposited by low-density turbidity currents dominated by turbulent flow mechanisms (Lowe, 1982; Mutti et al., 2003). These structures and depositional mechanisms,

Facies	Description	Petrography	Interpretation
		present, lithic fraction is represented by plutonic (quartz+plagioclase, quartz+k-feldspar and quartz+muscovite association) fragments. Particles are mainly angular.	together with the tabular geometry observed in the field, make facies San2 beds consistent to sand sheets in a small sand lobe (Shanmugam and Moiola, 1988). In terms of provenance, the proximity of source area, testified by sediment immaturity and the common angular shape of the particles, and the preponderance of a basement supply, with a minor but almost constant input of volcanic minerals, make facies San2 a continuation of facies San1.
San3	Dark yellow to gray massive, medium to fine sandstones, widely interspersed between the the conglomerate bodies. They are usually organized in single, tabular bodies, whose thickness is extremely variable from 40 cm to 2 m. Facies Sans 3 is interbedded with lacustrine shales.	Optical microscope analyses revealed sub-angular to sub-rounded clasts, with the prevalence of volcaniclastic crystals and lithics over the plutonic ones. Zoned plagioclase is abundant, followed by plagioclase strongly affected by sericite alteration, and minor biotite, amphibole and plutonic K-feldspar. The lithic fraction comprises andesite porphyroids (plagioclase+amphibole) and rare rhyolites. A polycrystalline basement fragment, composed of quartz and K-feldspar has been observed. Oxide aggregates are common.	Facies F8 structureless “a” Bouma division of Mutti et al. (2003). The deposition of this type of facies is generally controlled by low-density turbidity currents in lobe regions, dominated by laminar to turbulent regime of flow (Lowe, 1982; Shanmugam et Moiola, 1988; Mulder and Cochonat, 1996).
Sh1	Brown to dark gray massive shales, with variable thickness, interbedded with pluricentimetric tuffaceous layers and isolated layers of rounded/elongated soft intraclasts (up to 5mm in size). Facies Sh 1 is the most common shale facies.	The tuffaceous layers are constituted of fine ash, mostly composed of devitrified shards, with broken points, and minor quartz, biotite, plagioclase and zircon, in a very fine devitrified matrix, often altered to sericite and chlorite.	Distal to proximal bottomsets sequence deposited in warm anoxic paleolake (Einsele, 1992), and continuously alimented by high amounts of fine sediment directly produced by intense explosive activity. Downwind of the volcanic centers the drainage basins were often covered by ash fallout deposits, which were immediately reworked and rapidly accumulated in the basin (Smith, 1991; Cuitiño and Scasso, 2013), as testified by the rounded aspect of the shard peaks documented during the microscopic observations.

Facies	Description	Petrography	Interpretation
Sh1b	Massive dark shale with scattered angular, often plurimetric andesite blocks forming. an olistostrome body, up to 20 m thick, in the lower part of Lonco Trapial Formation. This body wedges out to the ESE.	Not observed	Rockfall events triggered by slope instability and water erosion generate chaotic deposits (McPhie et al., 1993 Volcanic Texture book; McGuire, 1996). In Lonco Trapial Formation they occurred when water level rose and the lake approached the unstable slopes of the andesite volcanoes. An alternative interpretation takes into account the proximity of an andesite dome, undergoing endogenous intrusion of new magma which may have caused local bulge and generated rock falls (Ui et al., 1999), directly discharged into the lake.
Sh2	Gray to pale green tabular bed 10 cm thick, with violet, pervasive, tubular inclined to vertical structures (8cm max). This facies is present in the lower part of Las Leoneras Formation.	Not observed	Fr lithofacies of Miall (1996), representing paleosoil horizons A and B, in which vertical oxidized root traces indicate dense vegetation.
Sh3	Dark yellow to gray shales interbedded with sandstones, preserve fossils plants, pieces of wood and trunks, often lying parallet to the weak stratification. Both, reverse and normal grading was recognized in some centimeter thick beds. Scattered, centimetric to pluricentimetric soft clasts as well as wavy lamination have been observed under the microscope. The intermediate volcaniclastic composition of the detritus indicates the Lonco Trapial volcanic centers as the dominant source area.	The silty fraction of the shales is characterized by angular to sub-angular particles composed of abundant plagioclase, with minor quartz and amphibole, whereas plagioclase+amphibole andesite porphyroids, andesite lathworks and minor tuffs are observed in the coarse-silt fraction.	Facies C and Fl lithofacies of Miall (1996), which represent fine sedimentation in vegetated swamp environment together with overbank or waning flood deposits. The recognition of both normal and inverse grading, as well as the alignment of particles and plant remainings, points out to discrete flow events interrupting the normal settling processes in the swamp (Einsele, 1992). The presence of soft pelitic clasts indicates syn-sedimentary reworking of semiconsolidated swamp muds after sub-aerial exposure. Although volcaniclastic detritus largely dominated the sediment supply, the silty sedimentation refers to a low energy environment formed during inter-eruptive times, when sediment production and transport were no more controlled by instantaneous volcanogenic forces, but by long-term allogenic ones

Facies	Description	Petrography	Interpretation
			(Smith, 1991). Vegetation growth is consequence of the absence of active volcanism. In turn, vegetation rapidly stabilizes volcanic/volcaniclastic terrains preserving them from both normal and dramatic erosional processes (Smith, 1991; Alexander et al., 2010) and decreasing the volume and grainsize of sediment input to the basins.
L1	20 to 30 cm-thick, gray, massive beds of packstone (Dunham, 1962), interbedded with thinner dark shales. Normal grading of peloids has been occasionally observed. Small fragments of quartz are found in the micrite matrix, which is in partially silicified.	The packstones are formed by micritic calcite, with peloids and intraclasts.	Central lake deposits in a carbonate-dominated lacustrine depositional system (Einsele, 1992) during times of maximum expansion of the lake.This singular carbonate event defines a period characterized by rapid rise of the lake level and volcanic quiescence. The base level rising together with low sediment production strongly limited the sediment supply (Smith, 1991). As testified by micrite intraclasts and normal grading, carbonate deposition was not derived from primary precipitation processes, but more probably driven by thin turbidite events that remobilized littoral carbonates. These turbidites were settled between the fine-grained, terrigenous sediments typical of suspended sedimentation in the deeper part of the lake. These mechanisms seem to be consistent with the cyclical alternation of carbonate/shale sedimentation, seen as the result of short term climatic variations by Einsele (1992).
Bas1	Bas 1 consists of a plurimetric tabular body of basalt along the contact between the granitic basement and the lowermost beds of Las Leoneras Formation, as well as interdigitated in its basal part. The sandstones of Las Leoneras Formation are strongly altered at the basalt/sandstone contact. Plume structures have been recognized pervasively on the surface of the subvertical joints oriented 110°. A	It is constituted of dark blue massive basalt, characterized by acicular pyroxene phenocrysts in a cryptocrystalline groundmass. Microscopically, the subophitic texture hosts both small acicular plagioclase grains and phenocrystals of	Sill concordantly intruded between the granitic basement and the basal sandstones of Las Leoneras Formation. The varibale attitude of the basalt as well as the skarn-like surface recognized at the basalt/sandstone contact holds the intrusive

Facies	Description	Petrography	Interpretation
	narrow band within the sill shows marked mineralogical foliation along subvertical planes oriented 200°. This consistent with the AMS foliation as defined by the plane containing the maximun and minimum axes.	strongly altered, rarely zoned, pyroxene and olivine. An accidental sub-rounded clast of the basement has been recognized in the groundmass.	character of the basalt. Vertical primary layering and anisotropy directions are consistent with the development of an elongated feeding vent.
Vb1	Vonogenetic volcanic breccia, frequently confined by carapace folded surfaces, composed of a principal body, 10 m thick that pinches out laterally to thinner beds (6-2 m thick), observed in the palochannel. The occurrence of accidental lithics (mean dimension of 0.7 cm) increases in this thinner part. “Onion-skin’’ foliation is occasionally observed in isolated outcrops. Preserved paleoflow direction, pointing to W60N, has been measured perpendicular to the fold axes of the carapace surface. It is consistent with W50N AMS foliation determined in the carapace breccia.	Microscopically, a primary volcanic fraction, formed by andesite fragments and groundmass, and accidental lithics, have been documented. The primary volcanic fraction is represented by porphyritic andesites, with phenocrysts of plagioclase (50%), highly altered horneblende (20%), augite (15%), opaque (15%), in a groundmass of granular, intergrown feldspars and opaques. The accidental fraction is represented by rounded tuff fragments, sometimes containing phenocrystals of quartz and rare biotite, and volcanic lithics. The massive groundmass of the breccia is composed of minute fragments with a composition similar to the primary volcanic fraction.	Lava front structures on a growing lava dome. Fold structures, in fact, are corrugations on lava flows during the exogenous growth and expansion of the dome (Fink and Anderson, 2000). The breccia deposits are interpreted as recurrent Merapi-type block and ash flows developed from lava flows, subjected to incipient mechanisms of front collapse and triggered by excess pore pressure and gravitational force (Sato et al., 1992; Ui et al., 1999; Fink and Anderson, 2000; Platz et al. 2012). The evolution of the front collapse and the associated block and ash flows are subjected to substrate, paleotopography and paleoenvironment. Lateral, thinner beds are the distal tails of the deposits. Their enrichment in accidental lithics from older volcanic rocks of the dome substrate testifies the locally increase in erosive ability, probably due to the flow channelization (Calder et al., 2000; Michol et al., 2008; Brand et al., 2014).
Vb2	Andesite plurimetric (up to 11 m) breccia, in lenticular bodies, that crop out where facies Vb1 is absent or confined to thinner beds. Angular block dimensions reach 43 cm, with a mean about 30 cm. The lower, 1 m-thick interval is composed of welded monogenic volcanic breccia. Its angular, monolithologic fragments, can reach 4 cm and show oxidation rims. The larger fragments show a primary magmatic layering whereas the smaller fragments are massive. Secondary quartz veins are quite diffuse. Laterally equivalent to the Vb2 breccia deposits, a lens-shaped pumice and ash deposit is formed by two coarsening upward sequences of pluricentimeter-sized, flattened white pumices in violet matrix.	Microscopically, the breccia appears altered and is characterized by pervasive secondary silicification. The spatial orientation of the small fragments (up to 5 mm in length) of plagioclase+pyroxene andesite seems to be controlled by primary flow direction.	Complex processes of effusive/explosive andesite dome eruptions (Platz et al., 2007), strongly controlled by the paleotopography generated by the previous emplacement of facies Vb1. The singular occurrence of a basal 1m-thick monogenetic breccia, highly affected by silicification and oxidation, reminds mechanisms of hydraulic fragmentation, typical of hydrothermal processes in magmatic contexts (Karaoğlu & Helvacı, 2012). These were favored by

Facies	Description	Petrography	Interpretation
			andesitic lava emplacement in the shallow braided river paleochannel. Through magma/water mixing extremely high fluid pressures are developed, and the sharp hydraulic gradients result in phreatomagmatic explosions and rock fragmentation (Chi and Xue, 2011). The result was the onset of a violent BAF event (Ui et al., 1999; Scheu et al., 2006). As also documented by Platz et al. (2007), this explosive activity can often generate pumice pyroclastic flows, with highly variable vesicularities and colour, emplaced laterally to the block and ash deposit.
Vb3	Tabular, crudely stratified, heterogenetic, volcanic breccia, reversely to normally graded. Very angular and sub-rounded blocks average 10 cm in size, and four lithotypes have been recognized. Most coarser, very angular blocks are composed of fresh, dark green andesite, in which acicular plagioclase defines a fluidal texture. Other lithologies are present in sensibly smaller, less abundant, more rounded and sometimes hydrothermally altered blocks, and comprise porphyritic andesite, welded tuff and rare plutonic basement. They also constitute the matrix together with loose crystals of quartz, plagioclase, altered K-felspar, pyroxene, amphibole and fine vitric fragments.	Microscopically, it is composed of different large amounts of fresh, dark green andesite, with acicular plagioclase, and less abundant porphyritic andesite, welded tuff and rare plutonic basement. They also constitute the matrix together with loose crystals of quartz, plagioclase, altered K-felspar, pyroxene, amphibole and fine vitric fragments.	Lahar-related hyperpycnite (Mulder et al., 2003). Fresh and angular-shaped andesite blocks, similar to the Vb2 blocks, indicate they suffered minimal transport and weathering before deposition. The rounded shape and advanced weathering of the other detritus, instead, reveal prolonged transport and hydrothermal alteration. Its varied petrography is consistent with a wider provenance area. We infer that the sudden increase in sediment supply, due to the Vb2 BAF event running along the paleovalley of the braided river, triggered a channelized, collapse-induced lahar (Scott, 1988; Ui et al., 1999). Its highly erosive behavior (Vallance, 2000) allowed the incorporation of fluvial bed load sediments, enriching the flow in accidental detritus. Once reached the lake, the lahar proceeded down through the lake bottom, evolving to a lahar-related hyperpycnite.
Vb4	Matrix-supported chaotic breccia exposed 19 m above facies Vb3, constituted of plurimetric (up to 3 m of diameter), dark, volcaniclastic angular blocks, chaotically distributed in an ocher to	In thin section, groundmass appears to be composed only of diaggregated particles of andesite blocks.	Directly comparable with those described by Trofimovs et al. (2008) for a sub-aqueous pyroclastic flow triggered by an

Facies	Description	Petrography	Interpretation
	gray matrix. The lens-shaped body pinches out to WSW. The angular blocks are all from porphyritic intermediate lavas, subsequently enriched in centimeter-sized accidental clasts of purple rhyolites and white scoria. The sandy matrix show similar petrography. Grain size of the matrix decreases eastward, with a scaly texture, changing to parallel near the breccia block borders.		andesite lava dome collapse at the Soufiére Hills volcano. The Facies 1 described by them is constituted of metric blocks buried in a fine-poor matrix (<1 wt% silt-sized particles) equivalent to our facies Vb4. In both cases, the lack of fines is the result of steam explosions developed when a hot PDC reached the water, favoring processes of elutriation and fragmentation (Cole and DeCelles, 1991; White and McPhie, 1997; Cassidy et al., 2013). The few accidental blocks may have been incorporated during the growth of the lava dome. Their low percentage in the matrix indicates the limited erosional behavior of the collapsing PDC (Calder et al., 2000; Michol et al., 2008; Brand et al., 2014) consistent with a dome located close to a lake.
Vb5	Facies Vb5 is represented by a 10 m thick, lens-shaped bed formed by a matrix-supported, monogenetic breccia, with massive to crudely planar stratification. It is composed of angular to sub-angular andesite blocks (maximum dimension 50 cm), in a dark green sandy to silty matrix.	Not observed	The monogenetic composition and angular to sub-angular shape of the clasts suggest Facies Vb5 were accumulated at the distal part of a small fan, dominated by debris-flow processes (Miall, 1996). The fan probably grew up directly on the flank of an andesitic dome. Differently from facies Sh1b, the variable grain-size of the matrix, together with the crudely stratification, indicate that sediment discharge was not controlled by dry rockfalls, but by dense mixtures of silt, sand and water that supported the large blocks during transport .
Ign1	Reddish, 0.05 to 1 m thick, inverse-graded beds, organized in plurimetric, coarsening upward packages up to 14 m thick. Grain size increases with bed thickness. Cross- to parallel-stratification has been often observed. Red color shade spotted the deposits. Lower levels are characterized by frequent centimeter-sized (up to 5 cm) pelitic intraclasts. Single beds are characterized by a tabular geometry, but the entire package is lenticular, pinching out to the E.	Microscopic analyses highlighted a strong internal layering and the crystal-rich nature of the deposit, in a microcrystalline, partially devitrified groundmass. Single crystals of quartz, k-feldspar and chloritized biotite (<2 mm) are the most abundant minerals, followed by rare	Ign1 corresponds to xs to //sLT(cr) non-genetic lithofacies of Branney and Kokelaar (2001) and represents a crystal-rich ignimbrite deposit emplaced in a paleolake. Similar deposits are not rare in the stratigraphic record. The Korean Cretaceous Kusandong Tuff, for example, is

Facies	Description	Petrography	Interpretation
	Paleocurrents in wavy flow structures, point to 220°.	plagioclase, amphibole and olivine. Subordinately, pumices fragments, vitric shards and accidental lithic fragments (rounded porphyritic andesites) are present.	a laterally extensive, crystal-rich, and pumice-free ignimbrite, generated from shallow-level fragmentation of magma followed by highly expanded and turbulent flows, able to transport coarse crystals and lithics over wide areas and to elutriate much of the fine vitric ash (Sohn et al., 2005, 2009).
Ign2	Reddish to pink, centimetric to decimetric pyroclastic beds, grouped in up to 20 m thick packages. Particle size reaches 1 mm. Light green fiamme pumices, flattered along primary layering, have been preserved in the lower part. The middle part is characterized by a spotted oxidized matrix and primary lamination defined by the horizontal arrangement of planar particles. A felty, pink groundmass, in which minerals (quartz, plagiocase and biotite), lithics (scoria and andesite fragments) and red vitric shards are present. Commonly, all particles show a thin rim. Vitric shards are characterized by oxidized core and preserved vescicles. Single beds are characterized by tabular geometry, but the sedimentary body as a whole has a lens-shaped geometry as occurs with Facies 1.	Microscopically, Facies Ign2 is a strongly laminated ignimbrite, characterized by high content of flame pumices (up to 1,5 mm in length), and minor amount of small, elongated, oxidized shards and angular individuals of quartz. Shards are abundant and show oxidation rims and devitrification to fine, elongated zeolite crystals.	bLT(p) to bLT non-genetic lithofacies of Branney and Kokelaar (2001). As suggested by strong grain fabric and basal fiamme pumices, the PDC was characterized by high shear rate, typical features of a granular-dominated flow-boundary zone (Branney and Kokelaar, 2002).
T1	Tabular, pluridecimetric bodies of light ocher ash, in which black acicular shards define a crudely parallel layering.	Microscopically, the deposits are constituted of glass shards, and minor crystals of quartz, biotite and amphibole.	Ash fallout events recorded in the Cañadón Asfalto basin (e.g. Hardardóttir et al., 2001)

Table 1: Facies recognized in the Lower Cañadón Asfalto basin (Las Leoneras Formation and Lonco Trapial Formation)

The lower part of the Cañadon Asfalto basin is characterized by environment instability owing to the complex geodynamic evolution of the SW margin of Godwana (Page and Page, 1993). In Paso del Sapo area, we appreciated such instability that promoted abrupt changes in sedimentation mechanisms and source-to-sink architectures, here below discussed evolutionary stages of the enviroment.

4.2.1 Tectonically-driven erosion and fluvial sedimentation

With the progressive lithospheric thinning and the activation of normal faults (Silva Nieto et al., 2002), a shallow sand-bed braided river developed in the transtentional semi-graben system, unconformably on the plutonic/metamorpic basement, controlling the main processes of transport and deposition. In this phase, tectonic sediment supply resulted dominant, as shown by the point counts on sands (Fig.4). However, the minor volcanic supply, represented by rounded tuff fragments, suggests a far, scattered and syn-sedimentary active volcanism whose fallout events

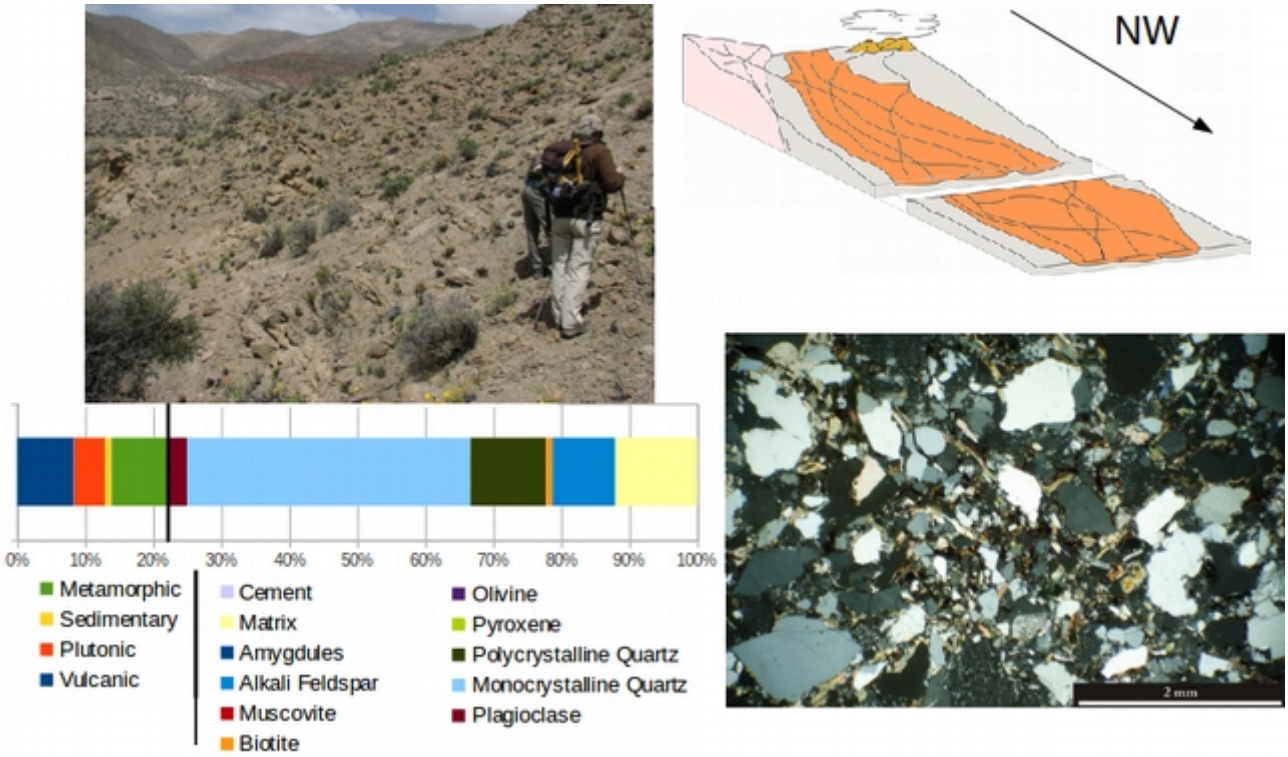

Figure 4: depositional environment and composition of facies San1

periodically fed the sedimentary system. On top, the paleosoil horizon (facies Sh2) indicates the braided channel abandonment.

4.2.2 The first base level rise and the onset of volcanism

When water level started rapidly to increase, driven by the strong basin subsidence (Silva Nieto et al., 2002), the generally wet and warm paleoclimate conditions (Volkheimer et al., 2008) favored

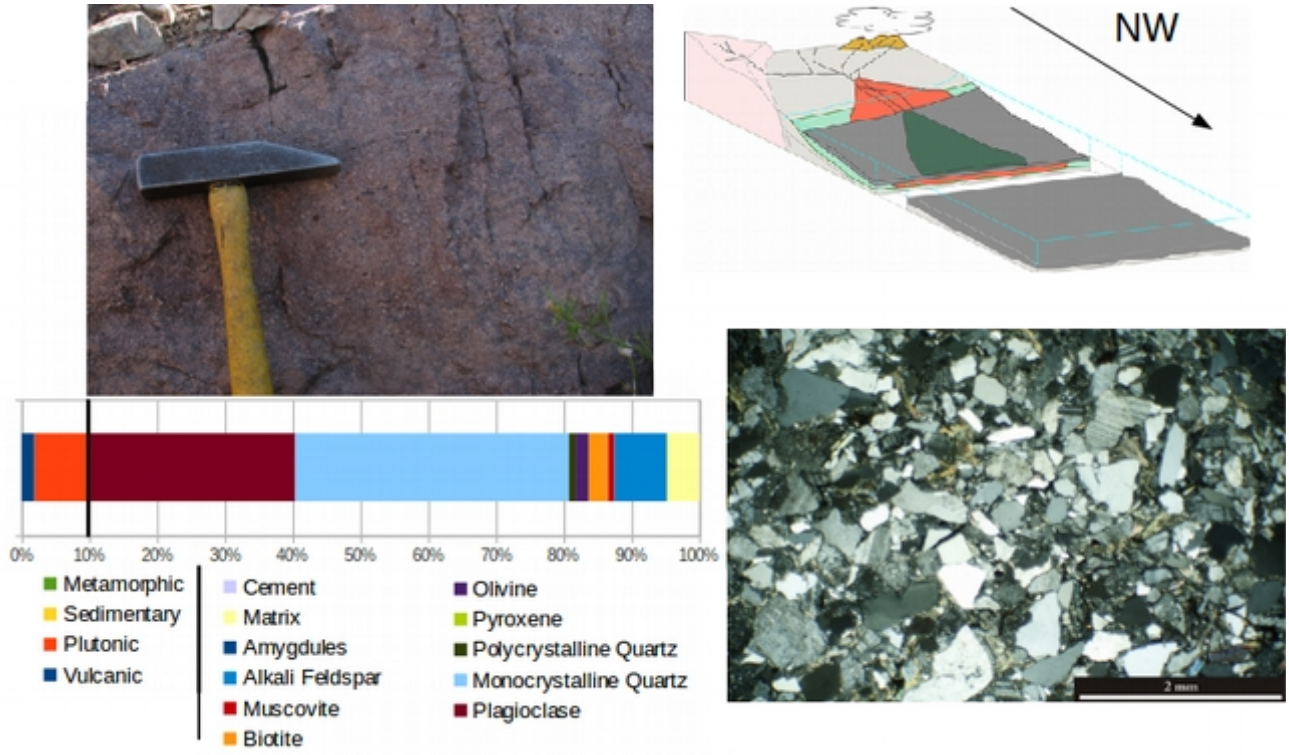

Figure 5: depositional environment and composition of facies San2

the initial production of littoral carbonate facies, whose syn-sedimentary remobilization directly fed small, distal, varve-type turbidites down to the lake bottom, cyclically alternated with black shale beds (e.g. Einsele, 1992). An episodic contraction of the lake triggered the progradation of a small, sub-aerial, basement-fed deltaic system (facies San1d), subsequently flooded, as underlined by its

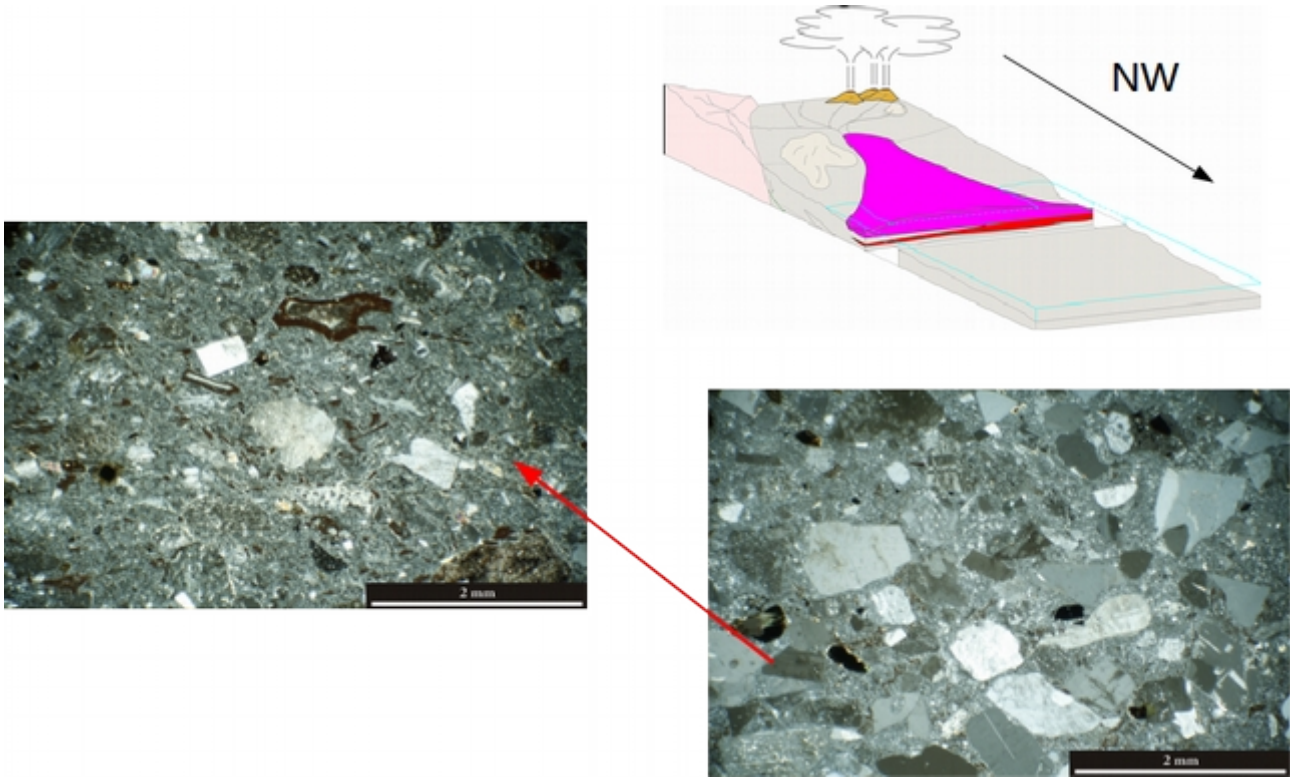

Figure 6: depositional environment of facies Ign1 (lower) and Ign2 (upper). Facies Ign1 may corresponds to crystal-rich ignimbrite facies of Cas et al. (2011).

upper green, reducing horizon. In the monotonous fine lacustrine sedimentation, interrupted by basement detritus-rich turbidite events (facies San2), reworked tuff layers (facies Sh1t) point out the increasing supply of fine, syn-volcanic particles to the sedimentary system (Fig.5). This was consistent with an increase in frequency of ash fallout events, whose loosely to unconsolidated material dispersed were easily subject to rapid erosion and transport by fluvial processes, even at far-distant areas (e.g. Cuitiño and Scasso, 2013). The first peak in volcanic activity was reached with the deposition of the two ignimbrite flows (facies Ign1 and Ign2), for which the reduce accommodation space, owing to the end of the transgressive phase, played a major role on their different depositional mechanisms. The stratigraphic evidences, in fact, show that facies Ign1 was deposited in a relative deep lacustrine basin, where its strong erosion behavior allowed the incorporation of soft pelitic clasts and thin layers from the bottom. Its hot body, rapidly sinking into the water, favored also the violent water/flow mix, that resulted in the high fragmentation processes and crystal enrichment of the deposit. The second event, instead, was definitively thicker than the remanent accommodation space of the lacustrine basin, and rapidly filled it, limiting the water/flow mix, which resulted only in the general oxidation features observed (Fig.6).

4.2.3 Paleo-valley

The paleo-valley incision (Fig.7) represents the first important temporal gap in the volcanic activity, defining the end of an aggradation-degradation sedimentation cycle (Smith, 1991). The drastic decrease in syn-volcanic sediment production and the base level fall determined the re-establishment of the pre-eruption fluvial conditions, during which the volcanic facies were easily eroded. Fluvial sedimentation largely favored the transport of gravelly polylithologic detritus (facies C1), resulting in the development of a shallow gravel-bed braided river (Fig.8). Again, compositional analyses highlighted the strongly volcanic detritus provenance, which quasi-totally cloaked the basement one. In it, the high amounts of andesite material was probably supplied by gravitational rock falls induced by processes of dome endogenic growth and/or slope instability.

4.2.4 Second volcanic cycle and paleo-valley filling

Immediately above the fluvial gravel-beds, the onset of a second volcanic cycle, whose eruptive activity was strongly influenced by the paleo-valley morphology, took place. The weak equilibrium between eruptive and fluvial processes resulted in the deposition of a complex sequence, in which alternatively primary and secondary volcaniclastic events are exposed. When eruptive processes prevailed, facies Ign2 ignimbrite bodies were channelized into the valley and run along it. When

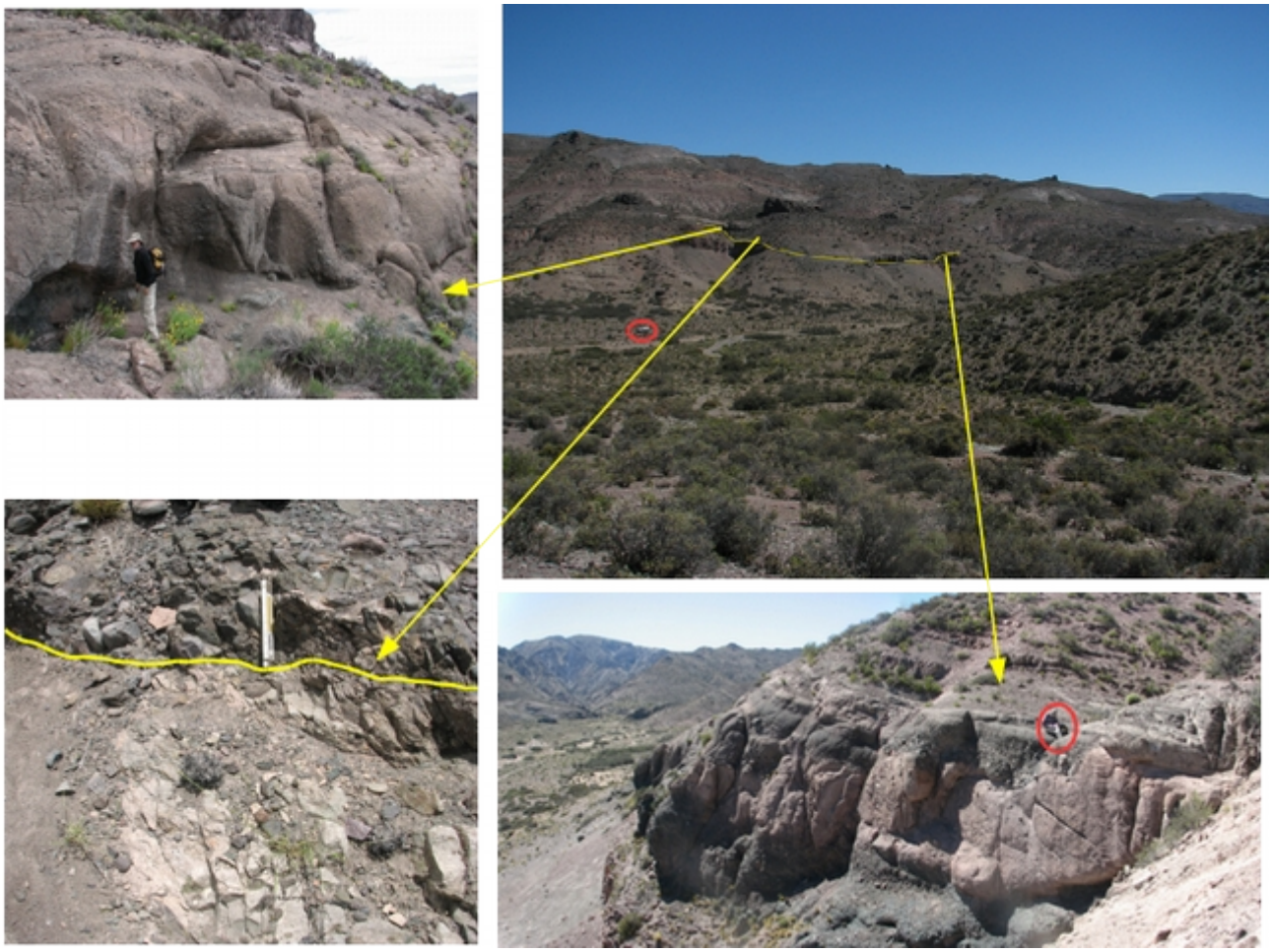

Figure 7: palaeovalley cut into ignimbrite deposits during an inter-eruptive period (according to Smith, 1991).

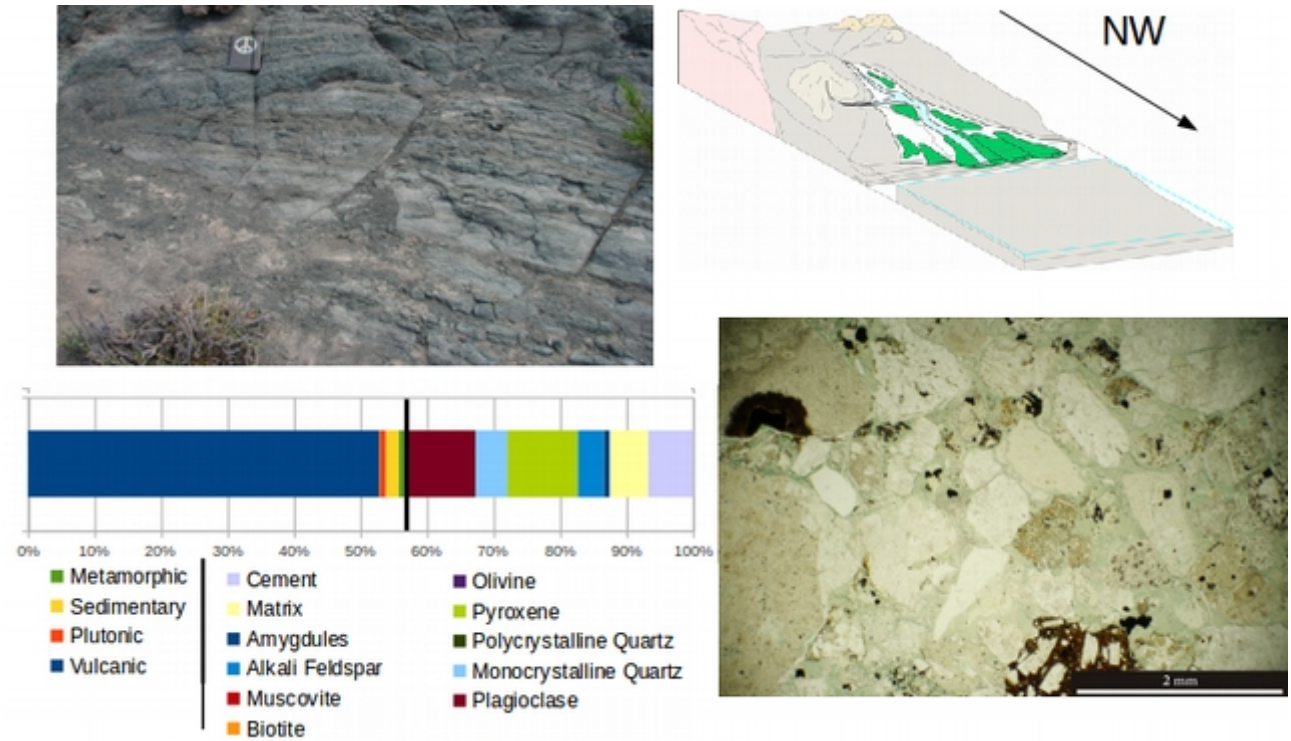

Figure 8: facies C1 and matrix composition, reflecting fluvial deposition during inter-eruptive periods.

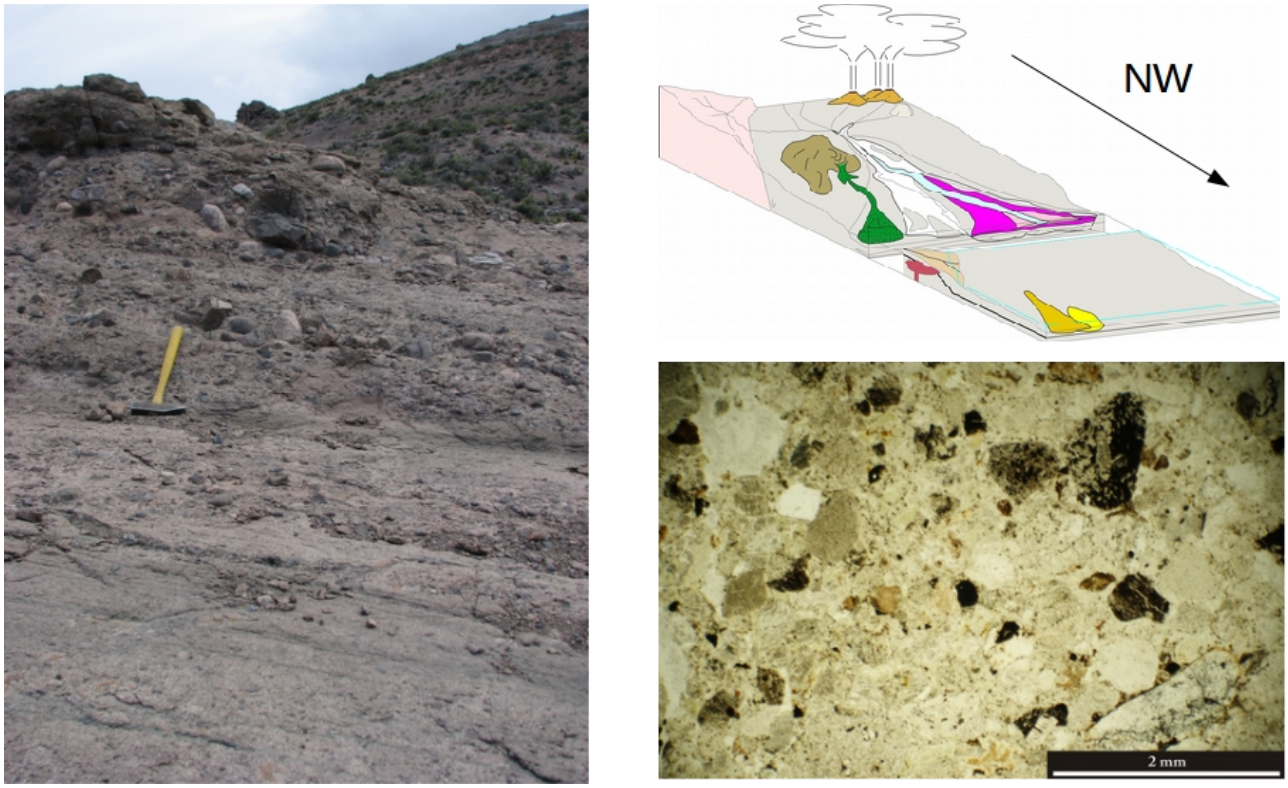

Figure 9: depositional environment of Ign2 and related lahars.

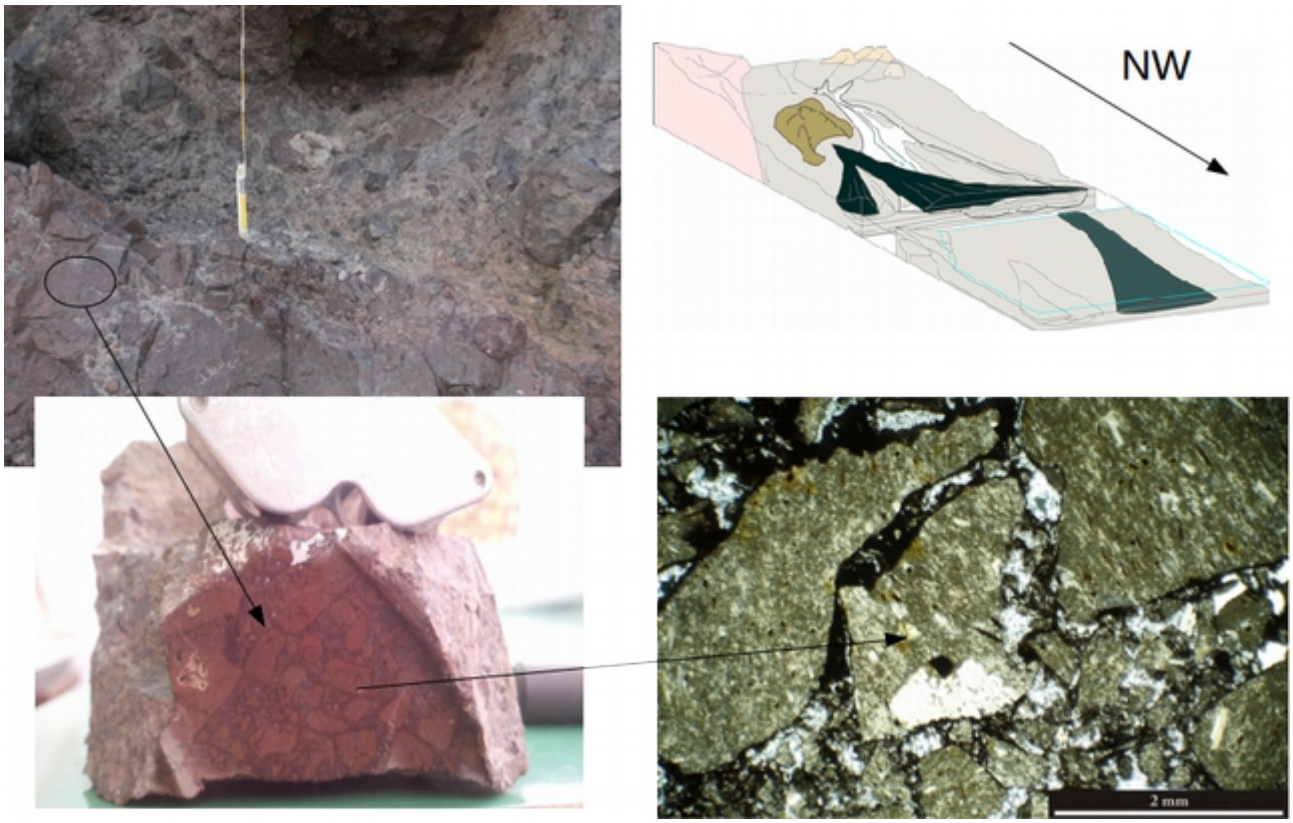

Figure 10: depositional environment of facies Vb1 resulting from dome collapse. Flow generated continued across the fluvial valley into the lacustrin basin furthen NW

fluvial processes prevailed, instead, pyroclastic flows were immediately transformed in large lahar events (Fig.9), able to incorporated the river sediments, or determined the rapid rework of instable PDC deposits. In both cases, however, the rapid aggradation of huge volumes of material

cannibalized the sediment supply and confined the fluvial facies C1 in small, thin interdigitations. On top, the paleo-valley was definitively filled by the exogenous dome activity and collapse (Fig.10). This activity started along the ESE channel bank with through lava lobes propagation, whose small, localized BAF were generated and partially discharged into the valley (facies Vb1). The eruptive climax, instead, was reached following a probably net increase of magma ascent rate, as testified by the larger extension of Vb2 facies. Dome fronts propagated from the bank to the valley, where water/magma mix favored the rapidly transformation from effusive to explosive activity, which results in the extended dome collapse. With the dome collapse event, the second volcanic cycle ended and an another long inter-eruptive period, marked by a second lacustrine transgression, set on.

4.2.5 Lonco Trapial paleo-lake

To the NW, lacustrine sedimentation environment dominated the stratigraphic record above the Las Leoneras Formation fluvial member. Despite to the long period, the sedimentary sequences recorded only a single transgressive-regression cycle, that culminated with the terrestrial sedimentation of the upper Lonco Trapial sub-aerial member. In this area, the absence of carbonate deposits (like facies L1) points out that, during the water rise, lake depth and shoreline distance did not favor carbonate precipitation or resedimentation. The lower deposit observed, represented by

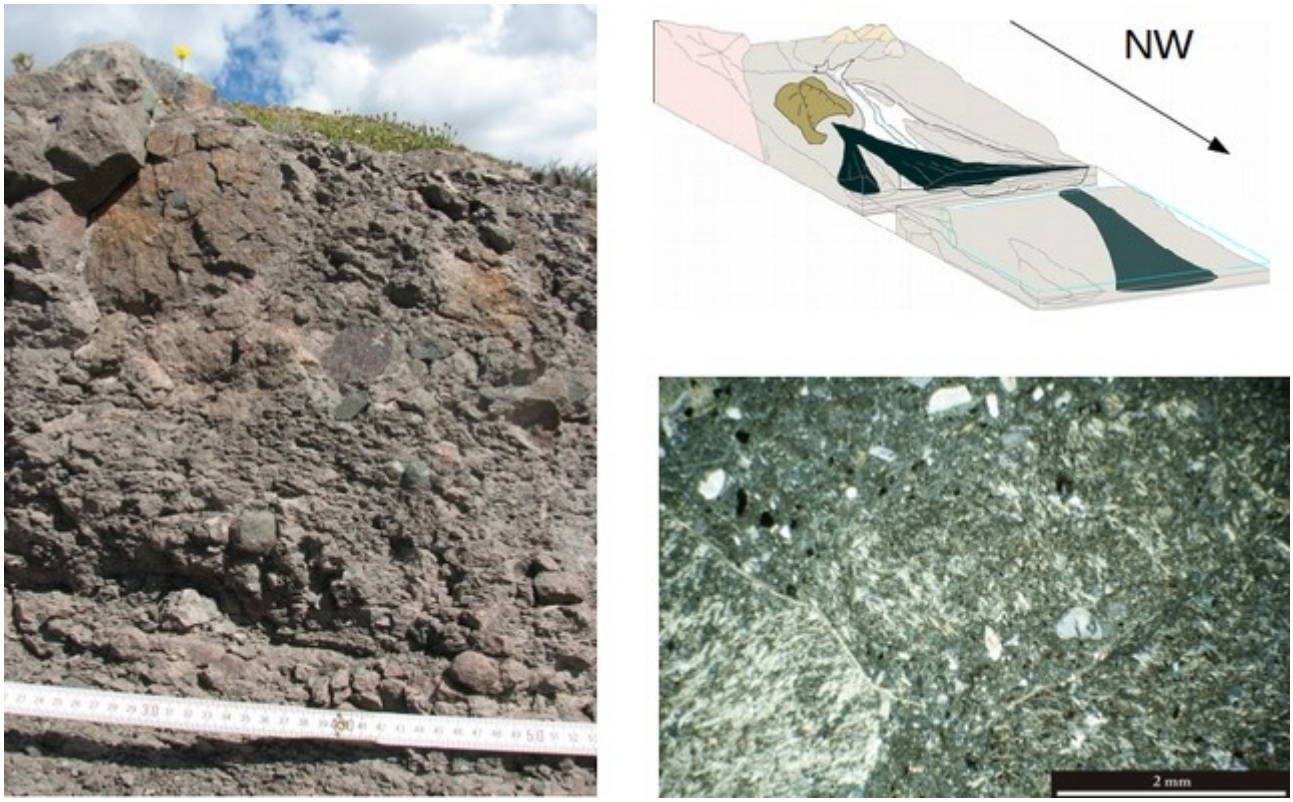

Figure 11: turbidite deposits constituting facies Vb2

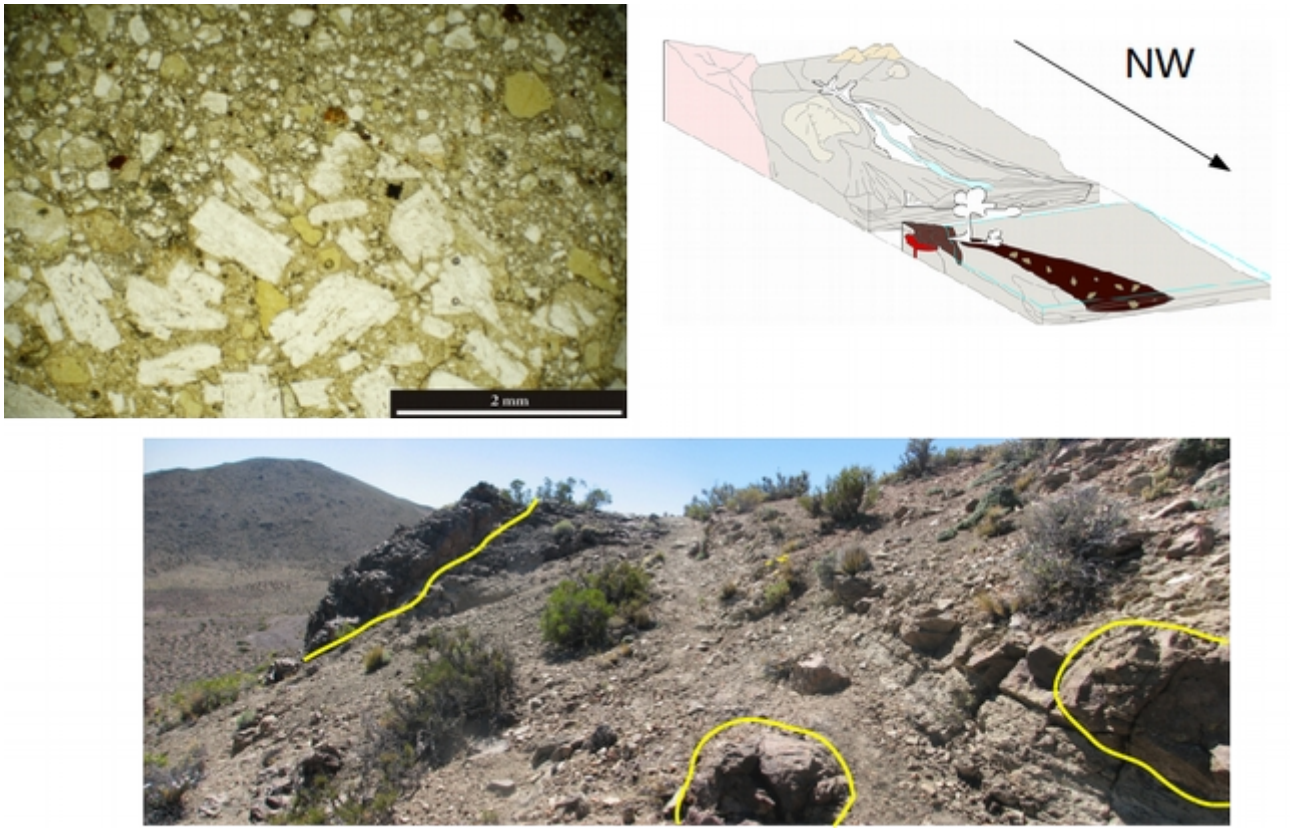

Figure 12: subaqueous block and ash deposit in the Lonco Trapial paleolake. Sediment compositions are comparable to that of turbidites from block and ash flows in front of Montserrat Island (Trofimovs et al., 2008)

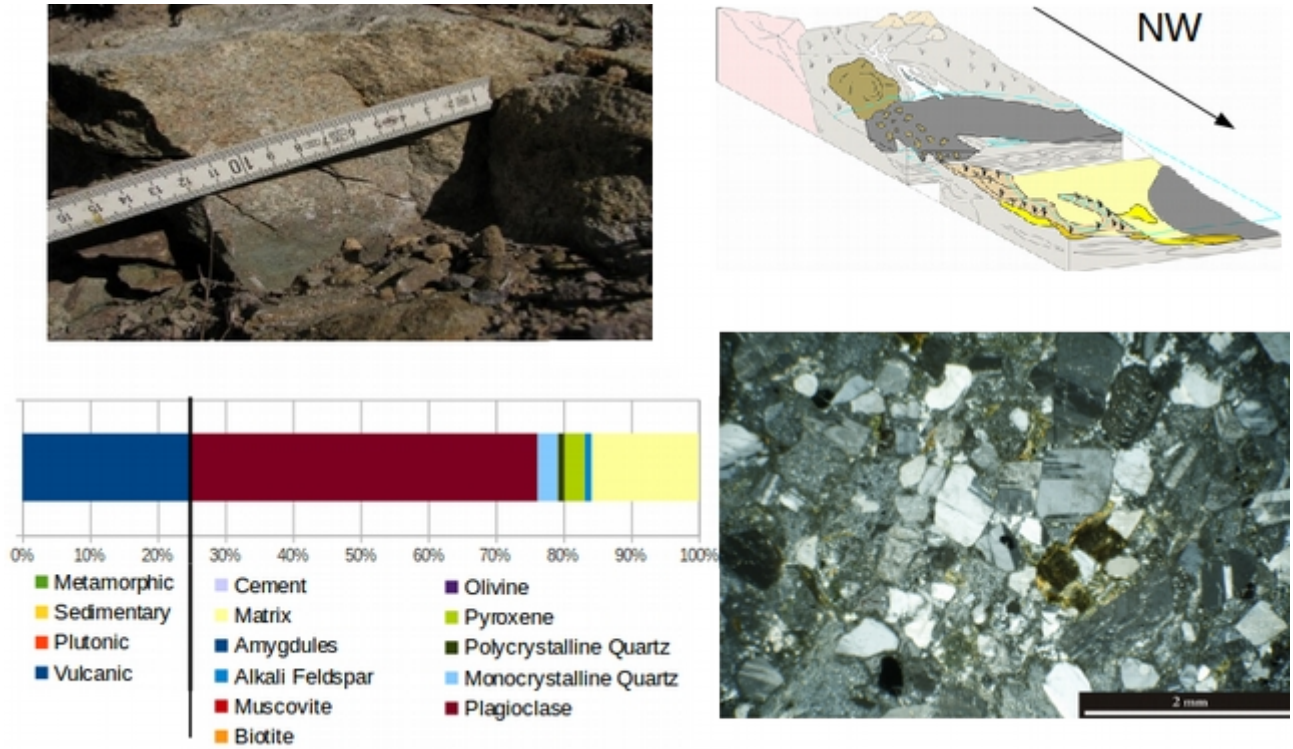

Figure 13: inter-eruptive turbidites. Detritus composition reflects the erosion of volcanic covers and basement at the same time.

facies Vb3, indicates that during the early lacustrine phase, the basin was principally fed by the SE fluvial valley, and recorded its most violent volcano-sedimentary episodes (Fi.11). Above, instead, the geometrical characteristic of the sedimentary bodies (facies C4, San2 and Vb4), rapidly disappearing to the WNW, suggested the onset of a later sediment supply from the ESE part of the lacustrine basin. Also grain size decreasing trend observed in facies Vb4, follows the same westward direction: the eastern part of its deposit, in fact, is characterized by a sandy matrix, rapidly passing to silt-sized one to the W. So, during the later lacustrine phase, fluvial drainage resulted in a more complex path, probably also in response to the channel infilling episode, owing to the dome collapse (Fig.12). Other catchments developed from the main SE area, laterally to the filled one, and shifted the sediment discharge to the E, triggering the progradation of a small turbidite system (Fig.13). With the slowly base level regression and the increase of sedimentation, sediments filled the basin, lake environment passed gradually to a swamp, and vegetation rapidly grew up, consequently also to the onset of a long quiescence volcanic period.

4.2.6 The last transgressive phase and the third volcanic cycle

Above the dome collapse deposits, the last transgressive-regressive cycle set on. A thick pelitic sequence marked the new base level rise, probably up to the dome edifice, and rockfall events usually discharged andesite angular blocks directly into the basin (facies Sh1b). When sediment

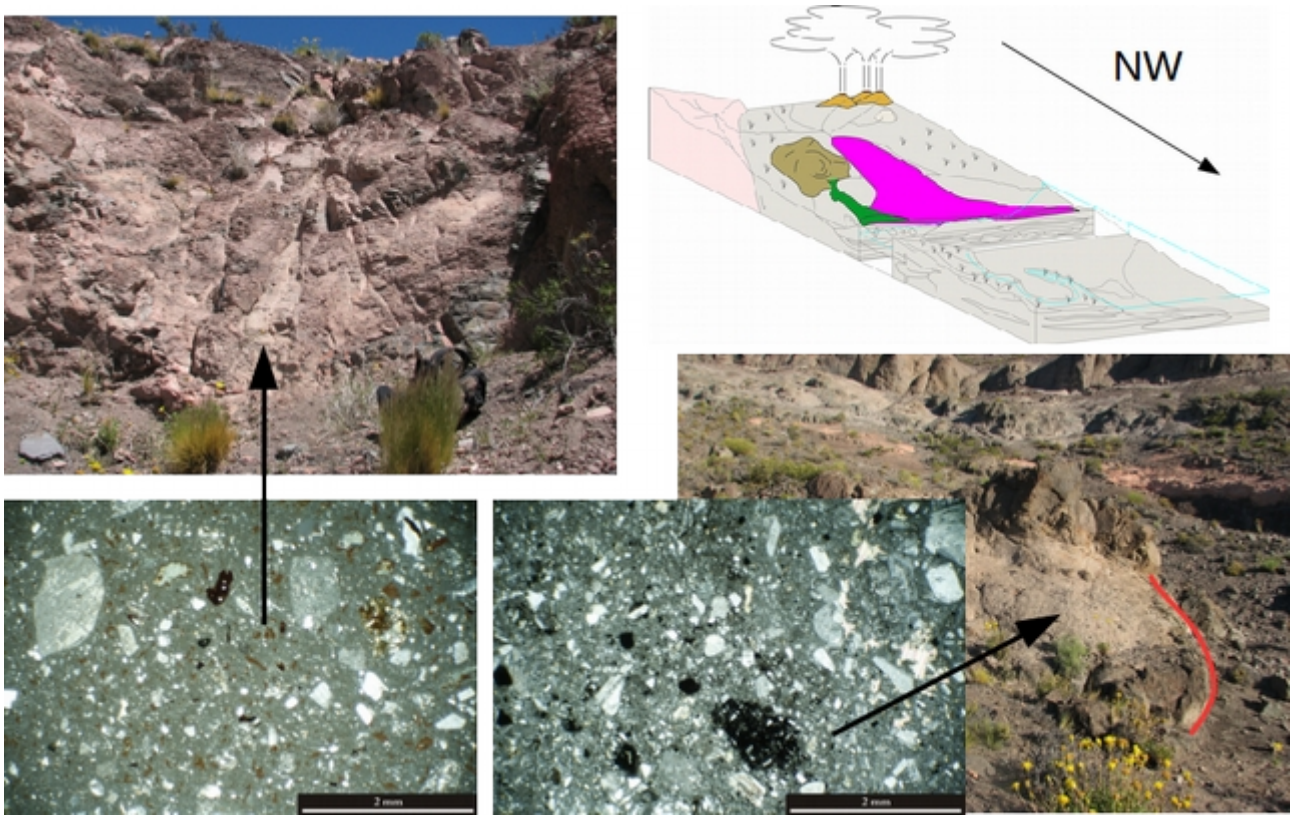

Figure 14: propagation of volcanic activity in a terrestrial environment.

supply and water variation reached the equilibrium, a small debris flow dominated fan (Miall, 1996) started to trap andesite detritus directly from the slope of the dome edifice (facies Vb5). This is the last lacustrine event recorded in the Lonco Trapial Formation sequence. On top, in fact, the incoming of a new, thick ignimbrite event, filling the shallow lake, definitively opened to the terrestrial sedimentation, as well as to the third volcanic cycle (Fig.14). So, new magma injections favored the dome resurgence and the onset of a new, effusive/explosive activity (upper facies Vb1).

5. Final Remarks

In Paso del Sapo area, thick exposure of volcano-sedimentary rocks of Las Leoneras Formation and Lonco Trapial Formation constitutes a natural laboratory to study the great impact of explosive volcanism on the stratigraphic record of an extensional basin, like the Cañadon Asfalto basin. Cyclical base level changes (tectonically controlled?) had the fundamental role to shape the source-to-sink where large amounts of volcanogenic detritus were periodically discharged, resulting in a complex patterns of facies architectures. We recognized that:

- background sedimentation is constituted by basement-supplied detritus, which is constantly deposited in the basin both during pre-, inter- and syn-eruptive periods. It tends to be cannibalized during syn-eruptive periods, and increases when source-to-sink system approaches pre-eruptive conditions.
- during syn-eruptive periods, fluvial system is deeply altered due to the rapid increase of sediments provided by volcanogenic processes. Such processes become the most rapid and efficient way to transfer sediments across the source-to-sink. The same behavior has been recognized in the lacustrine deposits in the NW area.
- preservation of volcanogenic structures are depending to eruptive styles, rather than environmental conditions. This may also influence sediment composition of reworked deposits.

Post-volcanic sedimentation: from tectonically controlled melting to tectonically driven erosion
(Late Oligocene Southalpine Foredeep, Northern Italy – published paper)

Clastic sedimentation in the Late Oligocene Southalpine Foredeep: from tectonically controlled melting to tectonically driven erosion
(DOI: 10.1002/gj.2632)

Abstract
The Villa Olmo Conglomerate (lower member of the Como Conglomerate Formation, Gonfolite Lombarda Group, Southern Alps, Italy) represents the first coarse clastic inputs into the Oligocene Southalpine Foredeep. A number of techniques including sedimentary lithofacies analyses, clast counts on turbidite conglomerate bodies, sandstone petrography through Gazzi-Dickinson point-count method and XRF analyses, and optical and minero-chemical analyses on single clasts have been performed in order to better define the sediment source area and geodynamic conditions which promoted sedimentation in the Southalpine Foredeep at the end of the Oligocene. The Villa Olmo Conglomerate interdigitates with the upper part of the Chiasso Formation, and gradually passes upward into the overlying Como Conglomerate Formation. Provenance analyses (conglomerate clast counts and sandstone petrography) reveals a strong metamorphic provenance signal, likely sourced from eroded Southalpine basement. An increase in igneous plutonic clasts reflects sediment supply from the Southern Steep Belt and a decrease of volcano-sedimentary Mesozoic cover sequences. Optical and minero-chemical analyses on volcanic detritus detect the presence of intrusive to effusive, andesite to rhyolite products, ascribable to the Varese-Lugano Permian volcanoclastic suite, as well as Oligocene andesite products. Plutonic clasts document the presence of tonalites, granites (with two micas), brittle deformed granodiorites, being likely sourced from the tonalite tail of the Bergell Pluton and the plutonic units of the Bellinzona-Dascio Zone. The identification of this provenance suite implies palaeo-drainage from the region between Varese (Southern Alps) and the Bellinzona-Dascio Zone (Central Alps).
The Villa Olmo Conglomerate is the first depositional record of the onset of tectonically driven erosion in the Alpine belt. We infer that the previous low sediment budget regime (Eocene – Middle Oligocene) was a consequence of a tectonically controlled melting phase, during which tectonic events promoted magmatic production in the middle crust of the Central Alps at rates higher than those of crustal deformation, so inhibiting sediment production. We conclude that changes in the deep structures of the Alpine Orogenic chain have controlled the main geodynamic processes during Oligocene-Neogene times, and have controlled sediment composition and supply into the Southalpine Foredeep.

Keywords: Villa Olmo Conglomerate, Alpine tectonics, Periadriatic magmatism

1. Introduction

Sediments within foreland and foredeep basins are fundamental to understand the processes affecting the growth of a collisional orogenic belt (De Celles, 1988; Wandres *et al*., 2004). Progradation of coarse-grained deposits in the most proximal area of an orogen reflect syn-sedimentary tectonics (Burbank *et al*., 1988 and references therein), and are useful to reconstruct source-to-sink systems and migration of thrust fronts (Heller *et al*., 1986; Wandres *et al*., 2004; Grosjean *et al*., 2012). Due to its proximal palaeogeographic position, coarse-grained sedimentary Oligo-Miocene synorogenic sequences comprising the Tertiary Southalpine Foredeep along the southern border of the Alpine Orogen (Fig. 1A) have attracted much attention in the characterization of its early development (Bersezio *et al*. 1993; Valdisturlo *et al*. 1998; Carrapa and Di Giulio 2001; Di Giulio *et al*. 2001; Kulhemann, 2007; Garzanti and Malusà, 2008; Malusà *et al*. 2011). In this work, we focus on the initial coarse clastic inputs into the Southalpine Foredeep Basin, the Late Oligocene Villa Olmo Conglomerate (a lower member of the Como Conglomerate Formation, which is the first clastic Formation of the Gonfolite Lombarda Group that crops out in NW Italy (Tremolada *et al.*, 2010; Bini *et al.*, in press; Fig. 1A-B). The aims of the work are to reconstruct the Late Oligocene source-to-sink system of the Central Alps, to unravel climate versus tectonic controls on sedimentation and to investigate how temporal changes in the deep structure of

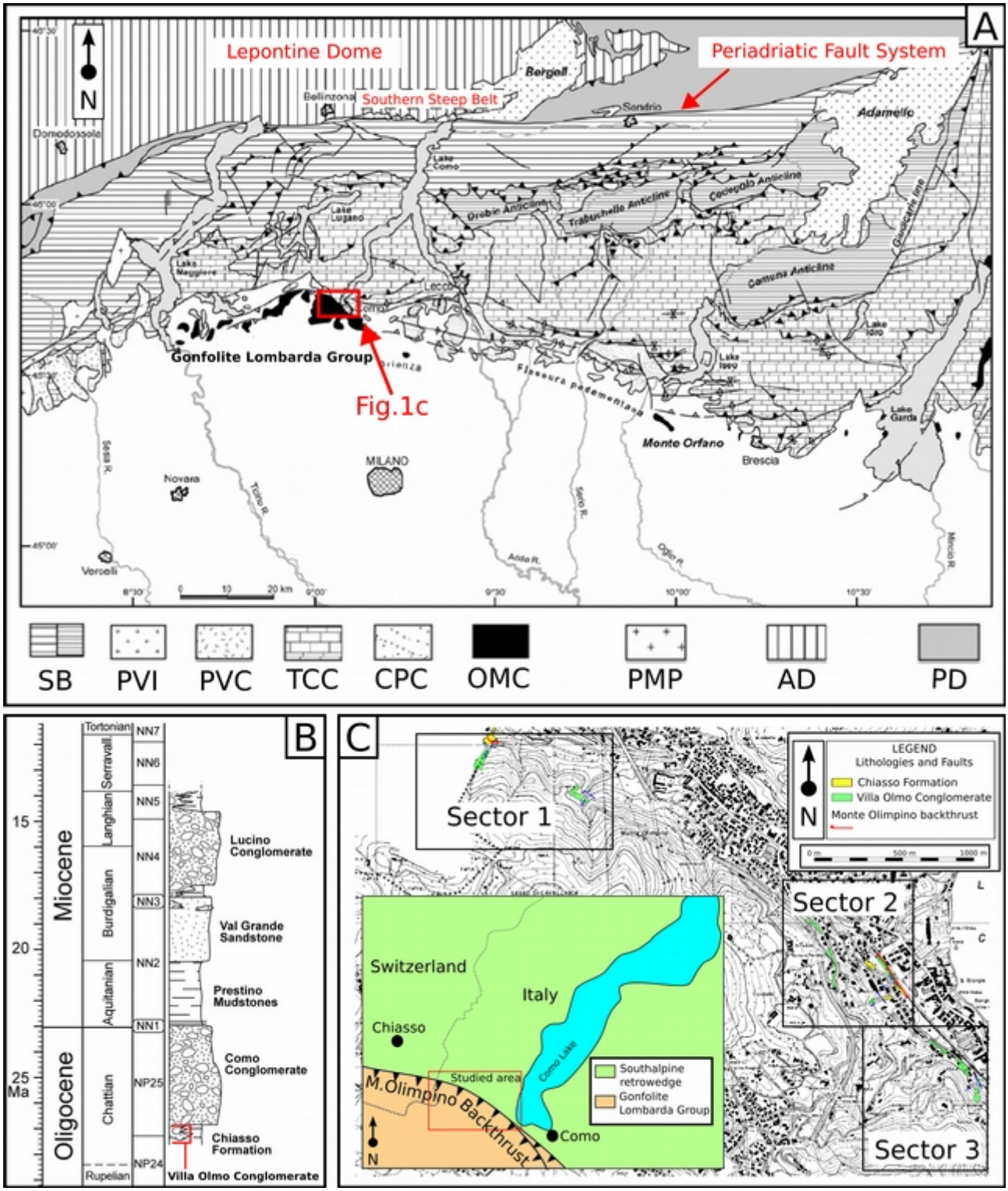

Figure 1: A) Geological sketch of the Southern Alps modified after Sciunnach et al., 2010. Southalpine retro-wedge: SB (Southalpine basement), PVI (Post-Varisican intrusions), PVC (Post-Varisican volcanic covers), TCC (Triassic to Early Cretaceous carbonate rocks), CPC (Late Cretaceous to Paleogene clastics), OMC (Oligo-Miocene clastics); Prowedge: PMP (Periadriatic Magmatism Plutons), AD (Australpine Domain), PD (Penninic Domain). "Southalpine retro-wedge" and "prowedge" from Rosenberg and Berger, 2009. B) stratigraphy of the Gonfolite Lombarda Group (modified after Tremolada et al., 2010); C) field survey map of the studied area.
the Orogen might have affected sediment liberation.

2. Geodynamic setting

2.1 The Starved Stage of the Southalpine Foredeep and the Periadriatic Magmatism

The Starved Stage of the Southalpine Foredeep represents a period during which the Foredeep Basin was characterized by conditions of rapid subsidence and extremely low sediment supply (Middle Eocene – Middle Oligocene, Garzanti and Malusà, 2008). Sedimentation was restricted to local re-sedimented shallow-water carbonate sequences, in which low percentages of Southalpine metamorphic and sedimentary material have been documented (Travedona-Ternate Formation - Middle Eocene to Early Oligocene, Mancin *et al*., 2001); volcaniclastic sequences (Cibrone Formation - Middle Eocene, Gavazzi *et al*., 2003; Di Giulio *et al*., 2005), and marly sequences (Gallare Marls - Middle Eocene, Di Giulio *et al*., 2001). In the Starved Stage, there were three main geodynamic processes acting during the ongoing Alpine collision deformation: 1) the Periadriatic Magmatism event (40 – 28 Ma - Rosenberg, 2004), 2) the re-activation of the main Southalpine lineaments (Middle Eocene - Castellarin *et al*., 2006; D'Adda *et al*., 2010; Zanchetta *et al*., 2011; Zanchetta *et al*., 2012) and, 3) the activation of the Periadriatic Fault System (PFS), at ca. 35 Ma

Figure 2: Typical conglomerate facies of the Villa Olmo Conglomerate in Como area; A) thick clast-supported bed (facies F3of Mutti et al., 2003a); B) rounded to well rounded pebble association; C) orthoconglomerate (facies F3of Mutti et al., 2003a) with clasts up to 23 cm in diameter.

(Handy *et al*., 2005).

2.2 The first clastic inputs into the Southalpine Foredeep (Villa Olmo Conglomerate)

The Villa Olmo Conglomerate represents the first important clastic inputs into the Southalpine Foredeep. It is a member that was first documented by Gunzenhauser (1985), Gelati *et al*. (1988) and Bernoulli *et al*. (1993), as thin-bedded turbidites and deep water conglomerates, intercalated with the silt- and mudstone rich succession of the Chiasso Formation (Bernoulli *et al*., 1993). Initially, the Villa Ormo Conglomerate had an inferred Late Rupelian age (32.1 – 31.1 Ma ca., Gelati *et al*., 1988), with an interpreted Southalpine provenance. Previous work has identified minor inputs of Oligocene andesite and tonalite material (Giger and Hurford, 1989; Giger, 1990; Valdisturlo *et al*., 1998; Carrapa and Di Giulio, 2001; Di Giulio *et al*., 2001; Livio *et al*., 2011; Malusà *et al*., 2011). Recent stratigraphic field observation and biostratigraphic analysis (Tremolada *et al*., 2010; Bini *et al*., in press), has led to base of the Villa Olmo Conglomerate being dated at ca. 27.3 Ma, being considered as the lower member of the Como Conglomerate Formation (Late Oligocene, 27.3 – 23 Ma), which represents the first clastic Formation above the marly Chiasso Formation (31.2 – 26.8 Ma) of the Gonfolite Lombarda Group (31.2 – 13.5 Ma, Fig. 1B).

The Villa Olmo Conglomerate contains an association consisting of reworked Mesozoic cover and also contains a Paleozoic metamorphic unit clast association (Carrapa and Di Giulio, 2001),

reflecting a local Southalpine supply, due to inferred Oligocene climate/eustasy (high frequency) changes, together with the long-term Alpine isostasy (Valdisturlo *et al*., 1998; Di Giulio *et al*., 2001). In contrast, the Como Conglomerate includes metamorphic (50–80%), volcanic (3–6%), and granitoid pebbles (20–50%; Carrapa and Di Giulio, 2001; Di Giulio *et al*. 2001), the presence of which infers the onset of tectonic exhumation and unroofing of the Teriary Bergell Pluton (Giger and Hurford, 1989; Carrapa and Di Giulio, 2001; Di Giulio *et al*., 2001) (Fig. 1A), and the surrounding Central Alpine metamorphic units that comprise the Lepontine Dome (cf. Penninic Domain of the pro-wedge in Fig. 1A; Garzanti and Malusà, 2008).

3. Methods

In order to better characterize sediment provenance of the Oligocene turbidite system of the Villa Olmo Conglomerate, detailed stratigraphic (lithofacies, grain size, sorting, roundness) and petrographic work has been carried out in Como area (Fig. 1C). Fieldbased clast counts have been performed on each of the 11 turbidite beds recognized, in each case comprising a dataset of more than 100 clasts in an area of 1 m² for each bed to detect variations in clast lithology both in space and time. Lithologies were classified into the following groups: orthoderivates, paraderivates, carbonates, marls, terrigenous (sandstone and conglomerate clasts), andesites, rhyolites, and plutonics. Three sandstone lenses in two distinct conglomerate bodies and an additional sandstone bed have been sampled, and subsequently impregnated with araldite, cut into standard thin sections and analyzed by counting 400 points under the microscope (Gazzi-Dickinson method; Gazzi, 1966; Dickinson, 1985, 1988; Ingersoll *et al*., 1984). A total of 22 single clast samples (16 volcanics, 1 sedimentary and 5 plutonics) and the four sandstone samples were selected for optical investigation, using polarized light optical microscopy (PLOM, Leica DME 13595microscope). These samples were also analsysed for mineralogical determination by powder diffraction (XRPD, PANalytical X'Pert PRO PW 3040/60 diffractometer in θ-θ Bragg-Brentano parafocusing geometry with Ni-filtered Cu Kα radiation at 40 kV and 40 mA, in the 4-80° 2θ range). The limit of detection (LOD) of XRPD depends on the mineral phase, and is generally between 0.1 wt % for highly crystalline phases and 5 wt %; qualitative XRPD analyses were performed running the PANalytical X'Pert High-Score software, using the ICSD PDF2 database. Only the 22 single pebbles were considered for major element geochemistry using energy-dispersive X-ray fluorescence (EDXRF, Panalytical Epsilon 3).

4. Results

4.1 Sedimentary lithofacies

The Villa Olmo Conglomerate is composed of unsorted, clast-supported conglomerate beds, up to 10m thick, corresponding to facies F3 (clast-supported, boulder- to coarse pebble-sized conglomerates) of Mutti *et al*. (2003a) (Fig. 2A). Clasts are most commonly rounded to well rounded, and rarely angular (Fig. 2B), reaching up to 330 cm in diameter, with an average of ~8 cm (Fig. 2C). Thin sandstone lenses (up to 30 cm thick) are interbedded with the conglomerates. Locally, matrix-supported, normally-graded conglomerates, corresponding to facies F2 (matrix-supported, boulder- to coarse pebble-sized conglomerates) of Mutti *et al*., (2003a), are observed up to 11 m thick. Massive sandstones corresponding to facies F8 (fine-grained sand without tractional features) of Mutti *et al*., (2003a), up to 3m in thickness have been observed. Facies F2 and F3 are gravelly density flow deposits (Mutti *et al*., 2003a), in which frictional freezing of particles dominated depositional mechanisms (Mulder and Alexander, 2001; Mulder *et al*., 2003). Facies F8 is interpreted as being deposited from liquefied flows dominated by tractional currents (Mulder and Alexander, 2001; Mutti *et al*., 2003a; Breien *et al*., 2010). The observed field relationships of detected lithofacies between three sectors of the study area (Fig 1C) are portrayed in Figure 3. In general, the Villa Olmo Conglomerate is not less than 40 m thick (Fig. 4-6), reaching 100 m in thickness in sector 2 (Fig. 5). Here, the Chiasso Formation is interdigitated in the Villa Olmo Conglomerate (Fig. 3 and Fig. 5), as documented also by Valdisturlo *et al*. (1998) and Tremolada *et*

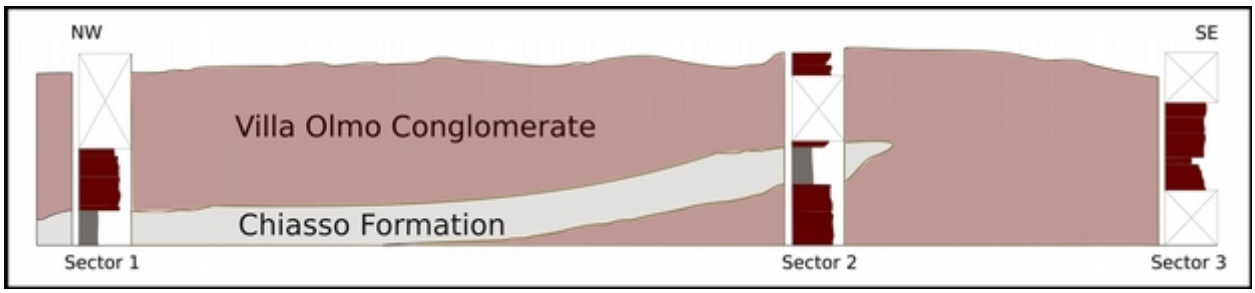

Figure 3: Lithostratigraphic log correlation and lateral geometry interpreted from field observations (Villa Olmo Conglomerate in brown; Chiasso Formation in gray). The horizontal distance between sector 1 and sector 3 is about 2,8 km.

al. (2010). The passage from the Villa Olmo Conglomerate into the upper Como Conglomerate

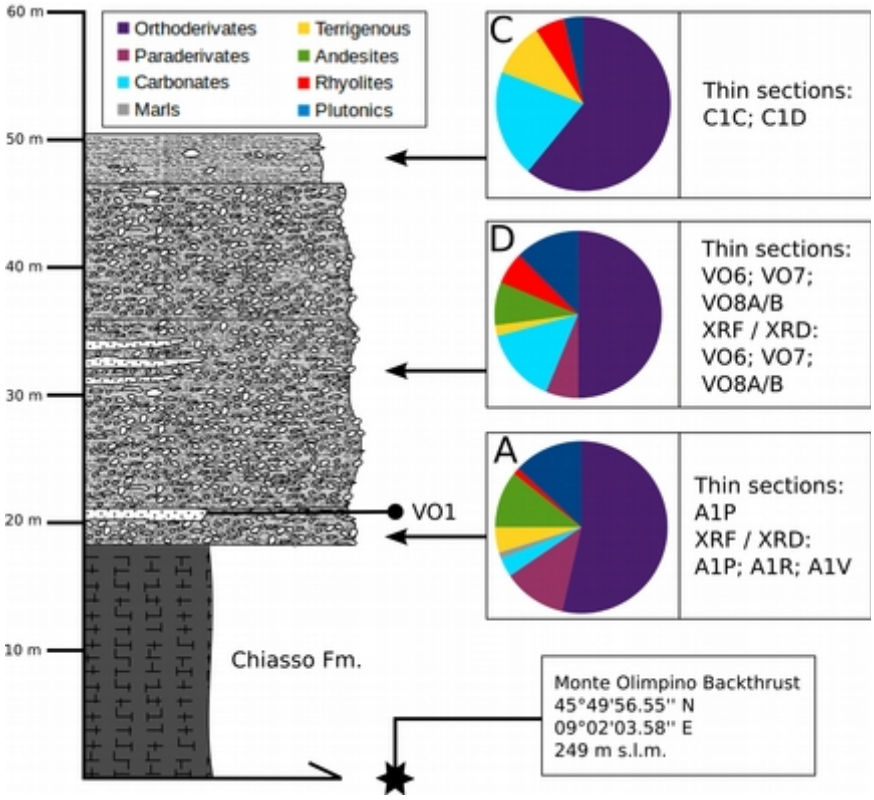

Figure 4: Stratigraphic log, clast counts (in pie charts), names of the samples collected and analyses performed (in frame) of sector 1.

Formation appears to be continuous and conformable (Tremolada *et al*., 2010).

4.1.1 Clast Lithology

In sector 1 (Fig. 1C and Fig. 4), the Villa Olmo Conglomerate contains pebbles and cobbles up to 25 cm in length. Quantitative clast counts (Fig. 4) show abundant presence of orthoderivative/quartzite clasts, a low but constant presence of terrigenous clasts, an upward increase of rhyolites and carbonates, an upward decrease of plutonics, and the disappearance of andesites. Carbonate clasts are mainly limestones. Terrigenous clasts are usually represented by dark gray sandstones and purple conglomerate clasts.

In sector 2 (Fig. 1C and Fig. 5), the Formation is characterized by pebbles and cobbles up to 30 cm in length, decreasing to 10 cm in upper beds. Clast counts (Fig. 5) show a dominance of metamorphic clasts (orthoderivatives/quartzites), with less common carbonate, terrigenous and plutonic clasts with subordinate volcanic (both rhyolite and andesite). Upwards through the sequence, terrigenous and carbonate clasts disappear, rhyolites decrease in abundance whereas plutonic clasts increase in abundance.

In sector 3 (Fig. 1C and Fig. 6), clast counts (Fig. 6) indicate that clast lithotypes are represented by rhyolite, andesite, carbonate and terrigenous clasts, whereas plutonic clasts are absent. Rhyolites predominate over andesites. In Fig. 7, all clast count data is represented in stratigraphic succession. Figure 7A highlights the prevalence of metamorphic lithotypes over all the other lithologies, the upward increase of plutonic clasts and decrease of volcano-sedimentary cover clasts (the Mesozoic cover of Figure 7B). Figure 7C shows that sedimentary cover clats are the most representative lithological association in the central part of the Villa Olmo Conglomerate, and disappear upwards, whereas Mesozoic cover clast are only represented by volcanic lithotypes. This evolution reflects a provenance supply progressive shifting from external to internal parts of the Alpine Belt. The uppermost clast count (Count I, Fig. 5) has a lithological association similar to that documented by sample SP17 of Carrapa and Di Giulio (2001) for the Como Conglomerate Formation. This may reflect a gradual stratigraphic transition between the two formations.

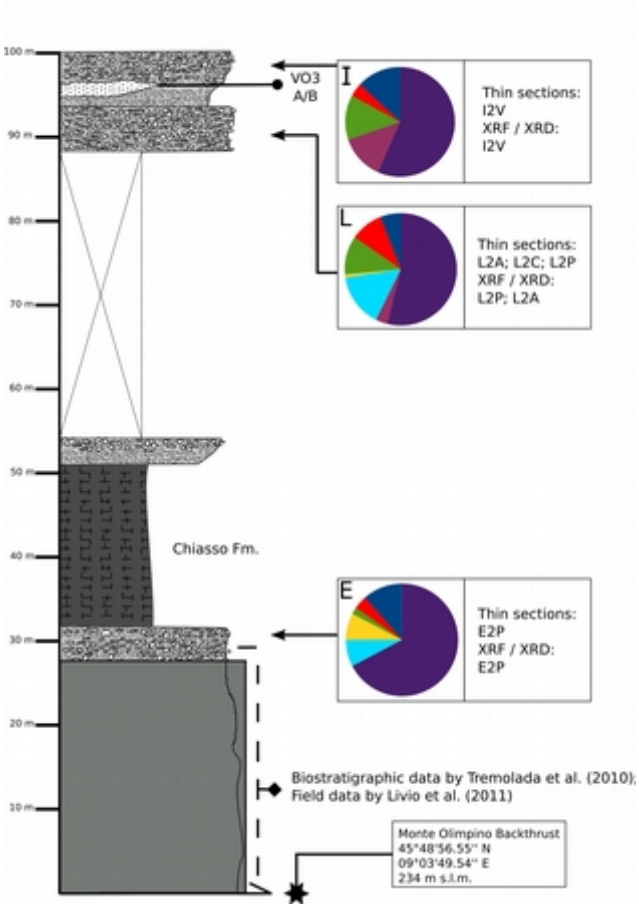

Figure 5: Stratigraphic log, clast counts (in pie charts), names of the samples collected and analyses performed (in frame) of sector 2. The gray rectangle indicates the sequence of Villa Olmo Conglomerate studied by Tremolada et al. (2010), and Livio et al. (2011), which subsequently has been covered by the construction of a wall.

4.1.2 Sandstone Petrography

Quantitative sandstone clast petrography is a powerful tool for interpreting provenance of modern and ancient terrigenous wedges, and it provides fundamental insights for reconstructing the tectonic evolution of mountain belts and associated sedimentary basins (Dickinson, 1988). The evolution of sediment composition and texture within a sediment-dispersal system also reflects a wide range of subsequently modifications to the initial grain population (Johnsson, 1993; Weltje and von Eynatten, 2004). Here, the classical point-counting method (Gazzi-Dickinson method - Gazzi, 1966;

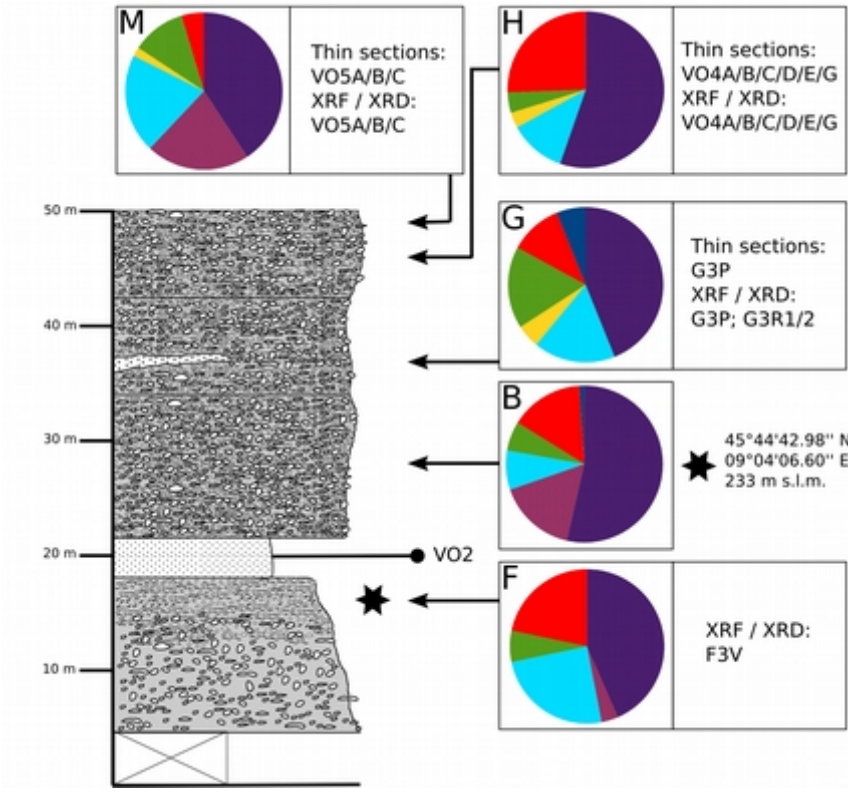

Figure 6: Stratigraphic log, clast counts (in pie charts), names of the samples collected and analyses performed (in frame) of sector 3.

Dickinson, 1985, 1988; Ingersoll *et al*., 1984), as shown in Figure 8, has been combined with XRD analyses (Table 1), in order to obtain a better resolution of sand detrital compositions and trends along the Villa Olmo Conglomerate. In general, Villa Olmo Conglomerate sandstones are poorly sorted, with angular clasts containing under 5% clay (Fig. 8; submature stage of Folk, 1980). They do not show signs of hydraulic sorting (Garzanti *et al*., 2008). Quartz and feldspars represent more than 80% of the sample bulks (Figs. 8B-D and Table 1), and grain counts highlight the prevalence of single crystals (quartz, feldspars and micas) as opposed to composite grains (comprising granite/granodiorite plutonic igneous grains), volcanic (microliths), metamorphic grains (gneiss and metapsammite), and other rock fragments (Figs. 8B and 8D). Minor amounts of calcite and dolomite (Table 1) reflects a negligible influx of limestone/dolomite fragments (Fig. 8D), and both minerals were absent in samples VO3a and VO3b (located at the top of the Formation – Fig. 5). In all samples, heavy-mineral assemblages are strongly depleted because of diagenetic dissolution (Garzanti and Andò, 2007; Andò et al., 2012), and dominated by relatively resistant minerals such as garnet (Garzanti and Malusà, 2008).

Sandstone clast mineralogy correlate with the clast trends identified from conglomerate clast counts, and reflect a mainly metamorphic provenance, with a progressive upward decreasing input of volcano-sedimentary cover sequences (Figs. 8C-D).

4.2 Petrography and geochemistry of clasts

4.2.1 Plutonic rocks

Five plutonic clasts (two in Sector 1, two in Sector 2 and one in Sector 3, Figs. 4-6) were studied in detail (Table 1; Figs. 9A-B, empty triangles). In general, the clasts preserve their original magmatic, granular and phaneritic texture (Figs. 9C-E), with the exception of sample L2P which is characterized by pervasive cataclastic deformation (Fig. 9F). Samples G3P and E2P are diorite to tonalite clasts composed of zoned plagioclase, green hornblende (often altered to chlorite), pyroxene and epidote (sample E2P - Fig. 9C), interstitial quartz and K feldspar (sample G3P). Samples A1P and VO7 are granite clasts, in which quartz is the most abundant component. Sample VO7 exhibits myrmekitic contacts between orthoclase and plagioclase individuals, green to brown

Sample	Lithotype	Mineralogical composition
A1P	Plutonic	Quartz (++), albite (++), K-feldspar (++), muscovite (O), clinochlore (O)
A1R	Volcanic	Anortite (++), quartz (++), sanidine (++), biotite (+), clinochlore (O), calcite (O), iron oxides (O)
A1V	Volcanic	Anortite (++), quartz (++), clinochlore (++), orthoclase (++), calcite (+)
E2P	Plutonic	Anortite (++), quartz (++), orthoclase (+), muscovite (O), clinochlore (O), calcite (O)
F3V	Volcanic	Quartz (++), sericite (++), albite (++), orthoclase (+), clinochlore (O), dolomite (O)
G3P	Plutonic	Quartz (++), K-feldspar (++), albite (++), muscovite (O), clinochlore (O), calcite (O)
G3R1	Volcanic	Quartz (++), albite(++), sericite (O), titanite (O), iron oxides (O)
G3R2	Volcanic	Albite (++), quartz (++), sericite (++), dolomite (+), calcite (O)
I2V	Volcanic	Quartz (++), albite (++), K-feldspar (++), clinochlore (++), biotite (+)
L2A	Sandstone	Quartz (++), albite (++), microcline (++), antigorite (+), calcite (O)
L2P	Plutonic	Muscovite (++), quartz (++), biotite (++), albite (++)
L2R1	Volcanic	Quartz (++), albite (++), microcline (++), sericite (+), calcite (O), iron oxide (O)
L2R2	Volcanic	Quartz (++), albite (++), K-feldspar (++), sericite (+), calcite (O), clinochlore (O), iron oxides (O)
L2R3	Volcanic	K-feldspar (++), quartz (++), sericite (++), orthoclase (++), clinochlore (O), calcite (O)
VO1	Sandstone	Quartz (++), albite (++), muscovite (+), microcline (+), calcite (O), clinochlore (O), dolomite (O)
VO2	Sandstone	Quartz (++) , albite (++), orthoclase (++), muscovite (+), calcite (O), clinochlore (O), dolomite (O)
VO3A	Sandstone	Quartz (++), muscovite (++), k-feldspar (++), albite (++), clinochlore (O)
VO3B	Sandstone	Quartz (++), muscovite (++), k-feldspar (++), albite (++), clinochlore (+)
VO4d	Lava flow	Quartz (++), albite (++), K-feldspar (++), sericite (++), clinochlore (O)
VO4e	Intrusive/dyke	Albite (++), quartz (++), sericite (++), microcline (+), clinochlore (O), calcite (O)
VO5a-b	Pyroclastic flow	Quartz (++), sericite (++), orthoclase (+), albite (+), clinochlore (O), calcite (O)
VO5c	Epiclastic flow	Sericite (++), albite (++), quartz (++), K-feldspar (+), clinochlore (+), iron oxides (O), calcite (O)
VO6	Intrusive/dyke	Albite (++), quartz (++), K-feldspar (++), clinochlore (+), biotite (O)
VO7	Plutonic	Quartz (++), K-feldspar (++), albite (++), clinochlore (+), calcite (O)
VO8a	Intrusive/dyke	Albite (++), quartz (++), K-feldspar (++), clinochlore (++), calcite (O)
VO8b	Intrusive/dyke	Quartz (++), albite (++), microcline (++), sericite (+)

Table 1: XRD analyses results. Clast lithotypes have been defined throughout optical sample observations. Calcite and dolomite traces represent secondary pore filling, sericite represents feldspar and/or volcanic glass alteration, and clinochlore represents biotite alteration. (++) major phase (>10 wt %); (+) minor phase (<10 wt %); (O) trace amounts (5-1 wt %); (-) <LOD.

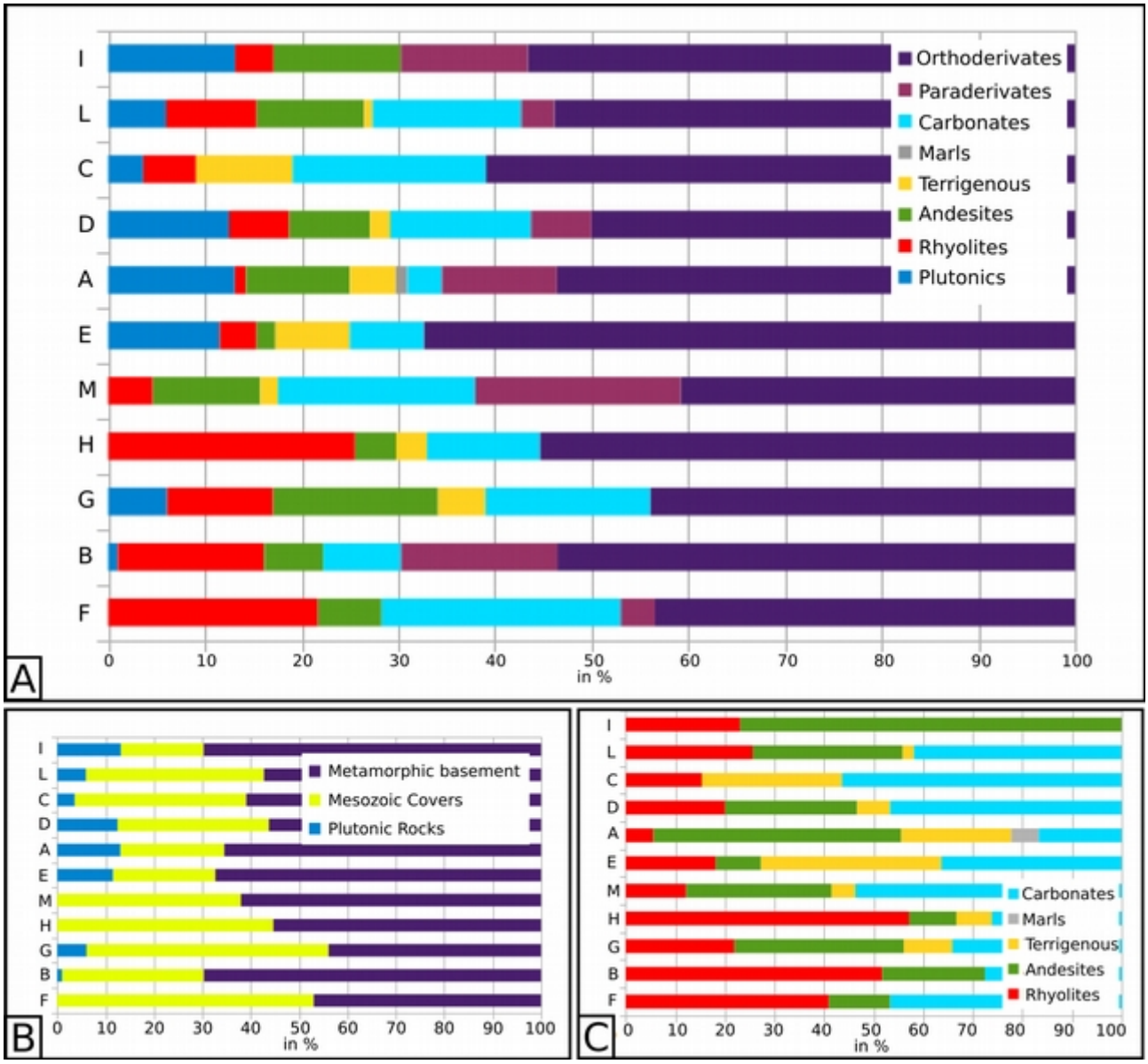

Figure 7: A) Fieldwork clast count results in stratigraphic order; B)clast count results subdivided into lithological general classes; C) clast count results of Permian- Mesozoic volcanic and sedimentary covers only.

amphibole, biotite and relict pyroxene (Fig. 9D). Sample A1P is characterized by megacrystals of orthoclase, zoned plagioclase, biotite and accessory minerals (apatite and zircon) (Fig. 9E). Sample L2P is a two-mica granodiorite, characterized by plagioclase, muscovite, biotite and brittle deformed quartz (Fig. 9F).

4.2.2 Volcanic/volcanoclastic rocks

Two groups of volcanic pebbles have been detected: dark-green andesites and red-purple rhyolites (Table 1; Fig. 9A-B, filled dots). The andesites are characterized by a porphyritic texture with phenocrysts of plagioclase in a dark matrix, whereas the rhyolites show a variety of textures, ranging from aphanitic to porphyritic. Different volcanic lithologies have been identified through texture and porphyric index qualitative evaluation. They range from dykes or sub-intrusives (high porphyritic index, I2V; VO4E; VO6; VO8A, Fig. 9G; VO8B), to possibly lava flows, usually showing porphyritic and/or trachytic textures (VO4D; VO5C, Fig. 9H) and pyroclastic/epiclastic rocks (VO4A; VO5A, Fig. 9I, and VO5B; see Figs. 4-6 for sample stratigraphic position). The absence of chilled margins as contact surfaces among the volcanic clasts and the hosting sandstones matrix in samples VO4B and VO4C excludes a syn-magmatic origin. Siltite sample L2A (Fig. 9L),

found as single pebble in clast count L (Fig. 5), is

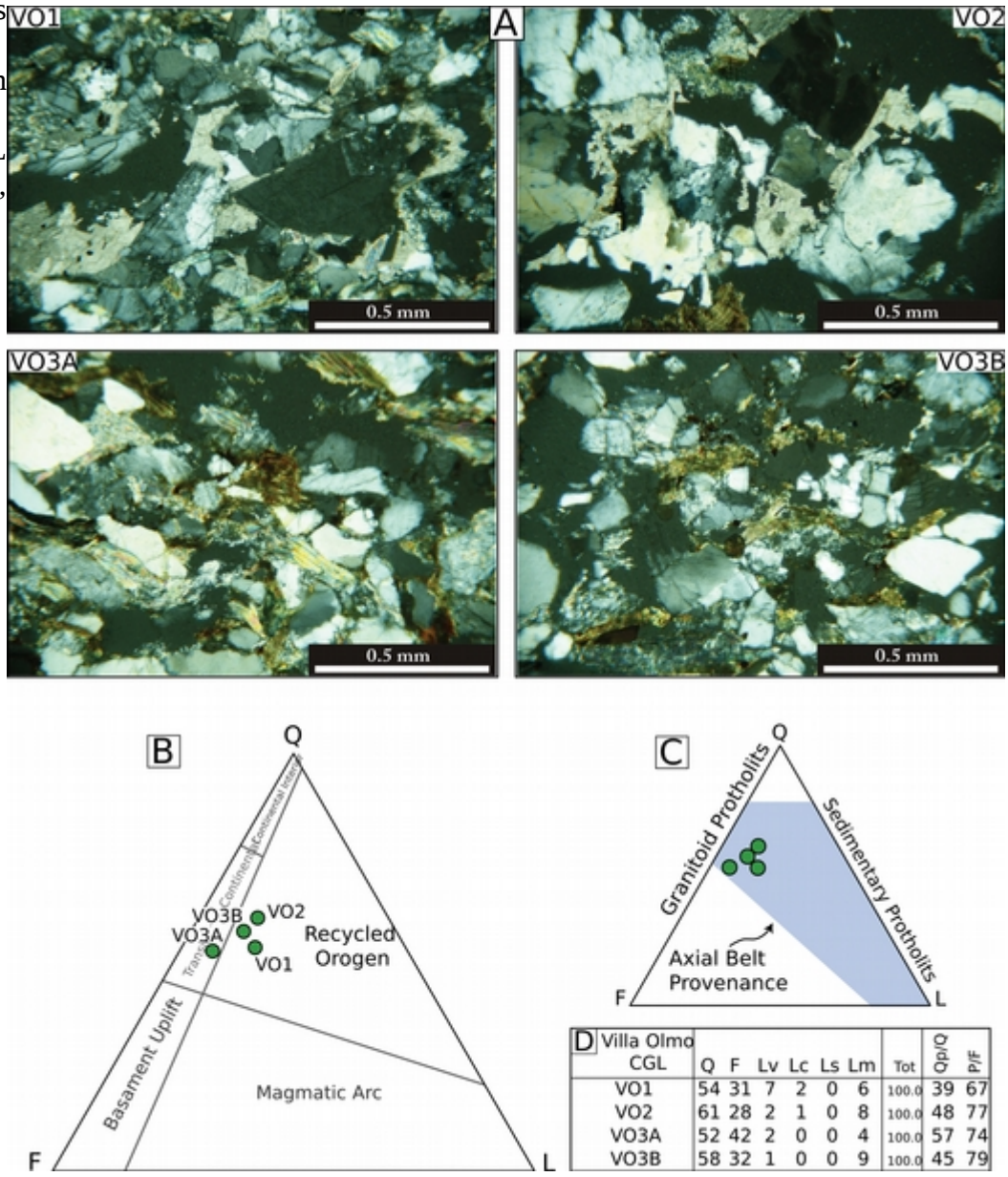

Figure 8: A) representative photomicrographs of the petrographic characteristics of Villa Olmo samples (all images with crossed polars); B) Sandstone sample petrology classified using the QFL-diagram of Dickinson (1985). C) Fingerprints of Axial Belt provenance by Garzanti et al., 2010; Detrital modes depend on protolith type, structural level, and thermal gradients during exhumation (note that the Axial Belt field roughly corresponds to the "Recycled Orogen" field of Dickinson,1985); D) modal composition of analyzed samples: Q, Quartz (Qp=polycrystalline); F, Feldspars (P=plagioclase); L, Lithic grains (Lv=volcanic and subvolcanic; Lc=carbonate; Ls=shale to siltstone; Lm=metamorphic).

characterized by an alteration halo (2mm thick) and a dark green core in hand-sample, has been interpreted as being eroded from an old volcanoclastic sandstone facies, due to its mineralogical association (fresh, idiomorphic grains of quartz and plagioclase, with secondary K-feldspar, antigorite from the alteration of pyroxene, and calcite) (confirmed by XRD analysis, Table 1). The XRF results of the volcanic material sampled (Figs. 9A-9B, filled dots), indicate a volcanic source characterized by a high-K calc-alkaline to shoshonite series association.

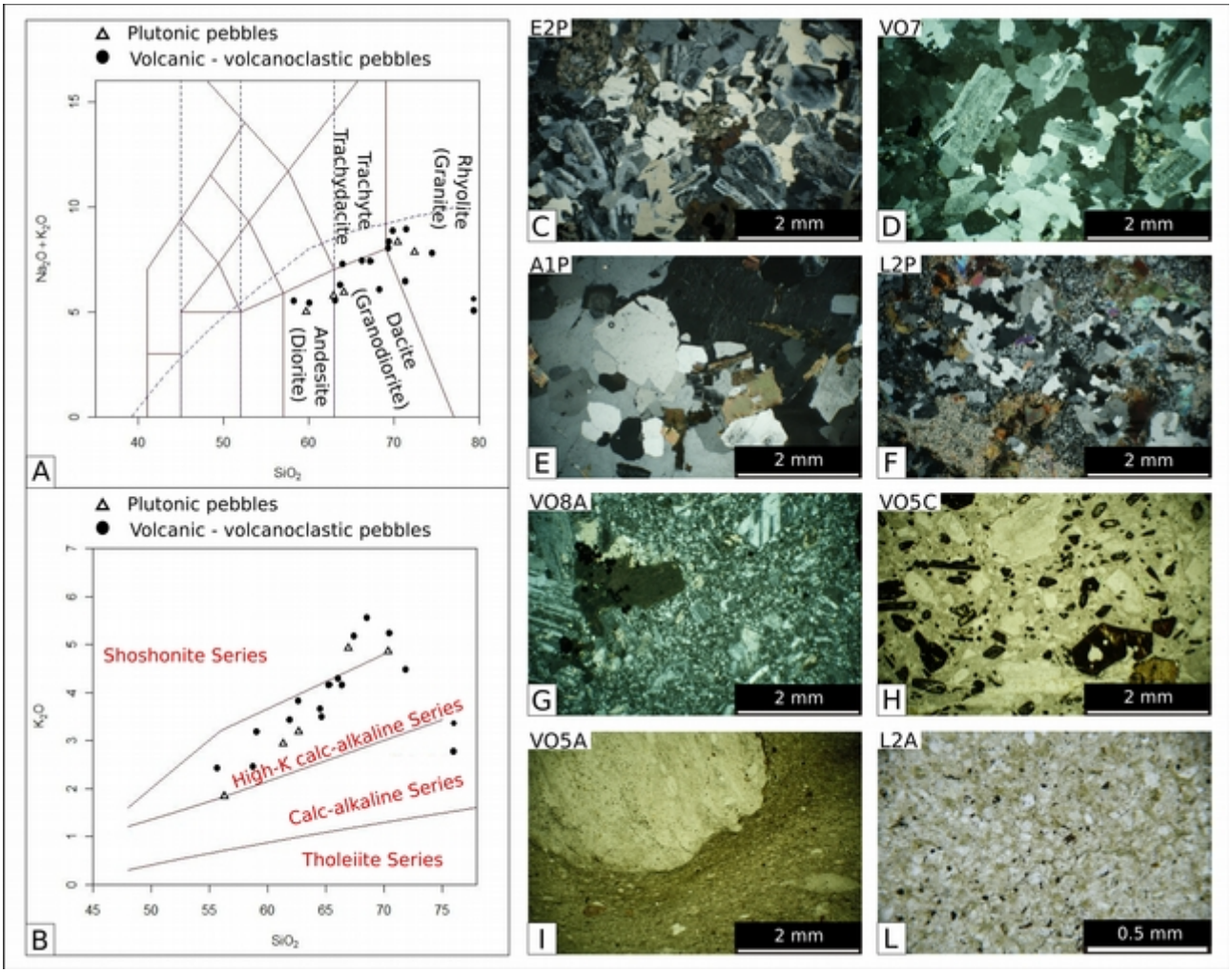

Figure 9: A) TAS diagram (Le Bas et al., 1986) on chemical composition of plutonic (triangles) and volcanic (circles) clasts; B) Peccerillo and Taylor diagram (Peccerillo and Taylor, 1976) on chemical composition of plutonic (triangles) and volcanic (circles) clasts; C) sample E2P (diorite to tonalite) at 2 nicols; D) sample VO7 (granite) at 2 nicols; E) sample A1P (granite) at 2 nicols; F) sample L2P (two micas granodiorite with cataclastic deformation) at 2 nicols; G) sample VO8A (dyke) at 2 nicols; H) sample VO5C (andesite lava) at 1 nicol; I) sample VO5A (epiclastic) at 1 nicol; L) sample L2A (volcaniclastic sandstone pebble) at 1 nicol.

4.2.3 Carbonates

Three carbonate samples were collected at the base (C1C and C1D) and the top of the Formation (L2C). Samples C1C (Fig. 10A) and L2C (Fig. 10B) preserve a similar fossil association content, represented by red algae and foraminifera (Nummulites and Discocyclina). Sample C1D is a dolostone interpreted as being of Triassic age.

5. Discussions

5.1 Implications for sediment provenance

A Southalpine provenance for the Villa Olmo Conglomerate detritus has already been documented by previous authors (e.g. Valdisturlo *et al*., 1998; Carrapa and Di Giulio, 2001; Di Giulio *et al*., 2001; Malusà *et al*., 2011). However, in this work the mineralogical, chemical and petrologic analyses have allowed us to develop an accurate palaeo-drainage reconstruction (Fig. 11), which is consistent with the SW palaeocurrent directions of Fiorentini Potenza (1957) and Napolitano (1985). Our data has enabled specific provenance areas to be identified in the Southalpine region along the NE to SW palaeo-drainage transect. These areas will be discussed sequentially from proximal to distal reaches along the transect.

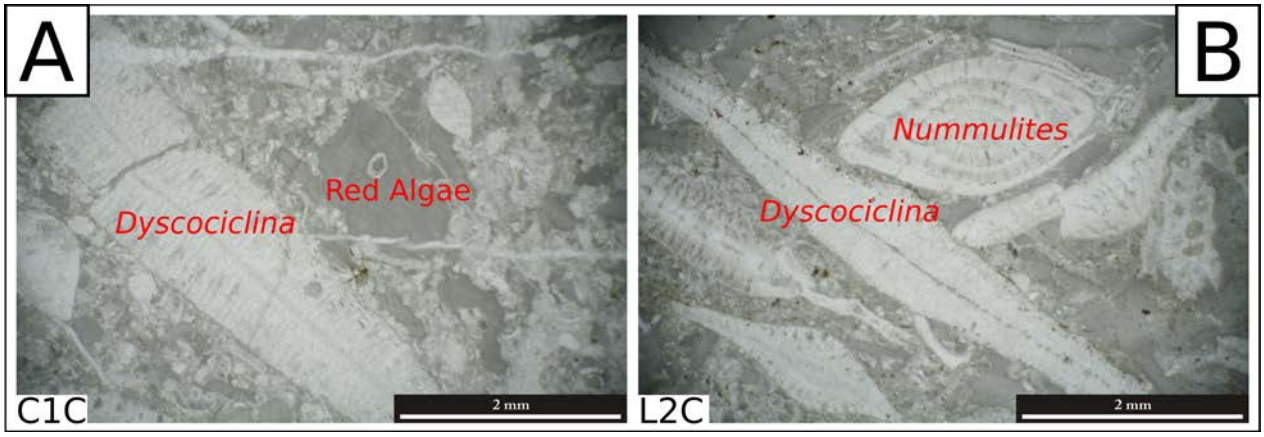

Figure 10: Photomicrograph of samples C1C (A) and L2C (B). Both samples show a micropalaeontological association (red algae, Nummulites and Discocyclina) comparable with that of the Ternate-Travedona Formation (Mancin et al., 2001).

The most proximal source is identified by the re-sedimented shallow-water carbonates of the Ternate-Travedona Formation (samples C1C and L2C), or possibly from liberation of clasts directly from the Tertiary shallow shelf which had fed the Ternate-Travedona Formation (Braghieri and Montanari, 1976; Mancin *et al*., 2001; Cavazza *et al*., 2007; Brandano and Ronca, 2013). In both cases, the source area has subsequently hidden below the N-eastward movement of the Gonfolite Lombarda Group backthrust, locally named the Mt. Olimpino Backthrust (Fig. 1C) (Pieri and Groppi, 1981; Bernoulli *et al*., 1989; Bersezio *et al*., 1993; Cardinetti *et al*., 2005). The sample C1D is comparable to dolomitic limestones common in the platform carbonate sequences that are well-documented in the Southalpine region (Carrapa and Di Giulio, 2001). The occurrence of andesite-rhyolite volcanic material suggests a provenance from the Varese-Lugano Permian volcanoclastic rocks (Carrapa and Di Giulio, 2001), represented by a sequence (up to 1500 m thick) composed of, from bottom to top, (1) rhyodacites and rhyolites, (2) pyroxene-, biotite-bearing andesites and dacites, and finally (3) rhyolites and rhyodacites (Cortesogno *et al*., 1998). The preponderance of metamorphic detritus, in particular gneiss and quarzite clasts, with rare serpentinite (Livio *et al*., 2011) indicates deep erosion of the Southalpine basement, focused near the Periadriatic Fault System (cfr. Zurbriggen *et al*., 1997; Giobbi Mancini *et al*., 2003). Samples L2P, VO7and A1P might have been sourced from the Tectonic Accretionary Channel (TAC), located in the Southern Steep Belt (Lepontine Dome) of the Central Alps (Berger *et al*., 2005 and ref. therein). Sample L2P (muscovite-biotite cataclastic granodiorite) is likely to represent the brittle-deformed units now exposed around Bellinzona (Switzerland), into the Bellinzona-Dascio Zone. Here, granodiorite rocks, containing the sillimanite+K-feldspar association, reflect anatectic and migmatitic processes at 0.6-0.8 GPa and 700 ± 50°C, from muscovite dehydration melting that took place approximately 30 Ma ago (Burri *et al*., 2005). Unfortunately, the comparison here is made only through observations of a similar mineralogical association, as no geochemical data is available in published sources. Samples VO7 and A1P (underformed granites), have the same mineralogical associations of migmatitic and granitic bodies, and aplitic to pegmatitic dykes included in the undeformed crystalline units of the Bellinzona-Dascio zone of Berger *et al*. (2005) and Burri *et al*. (2005). Similar migmatitic to pegmatitic rocks were already documented in the Villa Olmo Conglomerate by Carrapa and Di Giulio (2001), but no consistent discussions on their source area were presented. Dioritic to tonalitic pebbles (G3P and E2P), have been attributed to the tonalitic Bergell body (Berger *et al*., 2008; Alagna *et al*., 2010), cropping out in the Bellinzona-Dascio Zone (Giger and Hurford, 1989; Carrapa and Di Giulio, 2001). Finally, some of the andesite clasts have yielded an Oligocene K-Ar biotite age (Giger, 1990), and are here considered to result from the erosion of either a hypothetical volcanic edifice (Malusà *et al*., 2011) or intrusive dykes along the PFS during magma ascent (Rosenberg, 2004; Berger *et al*., 2008- see section 5.3 for more details). In both cases provenance from the Central Alps is inferred.

5.2 Tectonic versus climate fingerprint

Gravel progradation in the most proximal area (tens to hundreds of kilometers, Wandres *et al*., 2004) of an orogenic belt can be considered as the sedimentological indicator of syn-sedimentary thrust activity (Burbank *et al*., 1988 and ref. therein). The transition from a period of climate stability to a time of frequent and abrupt changes in temperature, precipitation and vegetation may prevent fluvial systems from establishing equilibrium states, resulting in an increase in sedimentation rates and grain sizes (Peizhen *et al*., 2001). Both tectonic and climatic influence may be inferred in the Oligocene Alpine belt. The Oligocene–Neogene contractional evolution the Southalpine retrowedge (Fig.1A - Castellarin *et al*., 2006; Rosenberg and Berger, 2009; Sciunnach *et al*., 2010), and the progressive exhumation of the Lepontine Dome in the prowedge along the Southern Steep Belts (Fig. 1A), is documented by the cooling paths of Rosenberg and Berger (2009). Unstable climate conditions occurred at the Eocene-Oligocene boundary, and continued through the Oligocene period (Haq *et al*., 1987; Miller *et al*., 1987, 1991, 2005, 2008, 2011; Zachos *et al*., 2001; Wade and Pälike, 2004; Pälike *et al*., 2006; Francis *et al*., 2008; Kominz *et al*., 2008; Cramer *et al*., 2009), also affected the Alpine area (Di Giulio *et al*., 2001; Kuhlemann *et al*., 2002; Di Capua *et al*., 2014). The diachronous influx of Southalpine clastic sedimentation of the Southalpine Foredeep (Mellere *et al*., 2000; Stefani *et al*., 2007; Schiunnach *et al*., 2010), seems to corroborate a primary tectonic control on sediment production, rather than a climatic one. The relative small extension of the basin and the emergence of an embryonic relief-drainage system (Mancin *et al*., 2001; Castellarin *et al*., 2006; Garzanti and Malusà, 2008; Zanchetta *et al*., 2012), might reflect a synchronous sedimentary response to a globally recognized sea-level drop. In this study, we recognize a strong Southalpine source signal (Palaeozoic basement and Mesozoic volcano-sedimentary covers) at the beginning of the Oligocene–Neogene contraction and basin evolution (Castellarin *et al*., 2006; Rosenberg and Berger, 2009; Sciunnach *et al*., 2010). It is also feasible to infer that the upward increase in plutonic detritus (Fig. 7A-B and Fig. 8D) reveals the progressive onset of prowedge exhumation in Lepontine Dome, along the Southern Steep Belts, in the Bellizona-Dascio Zone through the activation of thin-skinned tectonics. Nevertheless, the climatic influences must have had an important role in sediment transport to the basin (Peizhen *et al*., 2001). As inferred by Mutti *et al*. (2003b), high frequency depositional sequences result mainly from climatic and small-scale eustatic variations. Flood and flood-triggered turbidites, which dramatically increase sediment supply to submarine basins, possibly reflect typical climatic-controlled events (e.g. hard rainfall - Lavigne and Suwa, 2004). Direct inference of a climatic influence on the source to sink processes responsible for deposition of the Villa Olmo Conglomerate, however are not recognized in this study.

5.3 From "tectonically controlled melting" to "tectonically driven erosion"

Along the PFS segment of Central Alps (Fig. 1A), the first stage of tectonic activity corresponds to: 1). tectonically controlled melting, which triggered the generation and ascent of magma feeding the Bergell Pluton (33-28 Ma, von Blackenburg and Davies, 1995; Rosenberg, 2004) directly through dehydration of the metapelites of the Southern Alps basement (Berger *et al*., 2008), and 2). water-assisted partial melting processes, triggered by the episodic injection of hydrous fluids during the in-situ migmatization and intrusion of aplitic and pegmatitic bodies (Burri *et al*., 2005). Intrusion took place along the steeply oriented crustal-scale shear zone, and rates of magma ascent and fluid injection were higher than the rates of deformation, as inferred by Rosenberg (2004). These magmatic/migmatitic crustal P-T conditions initially prevented the development of the deformation fronts into the Southalpine Alps, thus the Foredeep was dominated by ephemeral inputs during early Oligocene times. The progressive collisional deformation and the Adria indentation, coupled withchanges in the deep structure of the Orogen (Garzanti and Malusà, 2008; Rosenberg and Berger, 2009) ended pressure-temperature conditions in the Orogen which had favored the magmatic/migmatitic processes (Garzanti and Malusà, 2008). The consequent increase of the tectonic deformation along the PFS crustal-scale shear zone was directly transmitted to the crustal

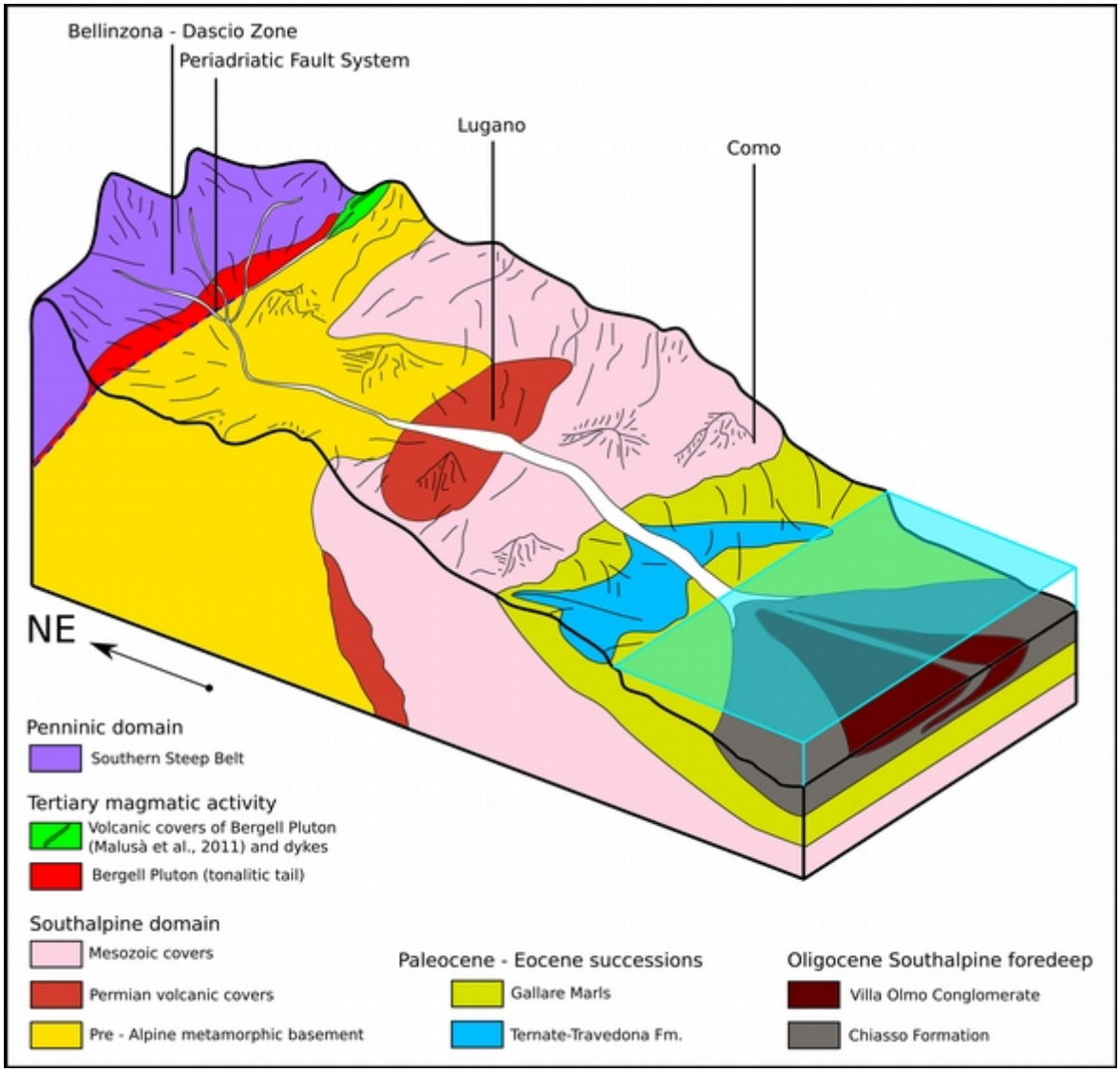

Figure 11: Palaeogeographic reconstruction of source-to-sink system of the Villa Olmo Conglomerate.

levels juxtaposed, and resulted in the intracrustal decoupling model proposed by Handy *et al*. (2005), with: 1). the exhumation of the rocks of the Southern Steep Belt and, subsequently, the entire Lepontine Dome (also according to the cooling paths by Rosenberg and Berger, 2009), and 2). the activation and progressive southward migration of the deformation fronts.

5.4 Exhumation/deformation causes

There is difficulty in correlating the migration of the deformation fronts and specific changes in sediment discharge from source to sink in the Southalpine region. This study, and that of Rosenberg and Berger (2009) demonstrates that: 1). the Villa Olmo Conglomerate, is a temporal marker of the deformation onset and subsequent liberation of sediment into the basin; 2). there is a progressive eastward migration of the Southalpine sediment transport that correlates to the eastward migration of the deformation front along the retrowedge (Mellere *et al*., 2000; Stefani *et al*., 2007; Schiunnach *et al*., 2010); 3). in association with the westward migration of the deformation front deep into the prowedge, there is an upward increase in the presence of clasts sourced from the Lepontine Dome in the upper Como Conglomerate (Di Giulio *et al*., 2001; Garzanti and Malusà, 2008; Malusà *et al*., 2011).

Analysis of likely tectonic processes that have driven sediment supply have highlighted the fundamental role of the PFS during ongoing continental collision. This study implies that changes in the deep structure of the Orogen had a prime control on the lateral migration of the

deformation/exhumation fronts as indicated earlier by Rosenberg and Berger (2009).

6. Conclusion

Sedimentological lithofacies, clast petrography, X-ray powder diffraction and X-ray fluorescence analyses have been carried out on the Villa Olmo Conglomerate. It comprises unsorted, clast-supported conglomerate beds, up to 10 m thick, (corresponding to facies F3 and F2), with minor sandstone beds (corresponding to facies F8 of Mutti *et al*., 2003a). It is interdigitated with the upper part of the Chiasso Formation, and gradually passes into the Como Gonglomerate Formation. Optical and minero-chemical analyses on single clasts highlight that the volcanic detritus is composed of intrusive to effusive, andesite to rhyolite products, ascribable to the Varese-Lugano Permian volcanoclastic suite, which "dilutes" the previously documented Oligocene andesite signal (Giger, 1990; Malusà *et al*., 2011). Analysis of plutonic igneous pebbles has identified the presence of two micas, and brittle deformed granodiorite interpreted as being sourced from deformed granodiorite cropping out in the Bellinzona-Dascio Zone (Burri *et al*., 2005). Provenance analyses on conglomerate clasts and sandstones reveal a persistent metamorphic signal linked to the erosion of the Southalpine basement, an increase of plutonic supply from the Southern Steep Belt and a decrease of clasts sourced from volcano-sedimentary Mesozoic cover sequences. This data, in combination with secondary source data on the Oligo-Miocene Southalpine Foredeep clastic sediments, has allowed us to:

1) redefine the Villa Olmo Conglomerate detritus provenance area across the Southalpine/Penninic area, compred between the Varese area (Southalpine domain) and the Bellinzona-Dascio Zone (Southern Steep Belt);

2) identify the importance of the PFS in the onset and trend evolution of gravel progradation into the Southalpine Foredeep. In particular, low sediment budgets during the Eocene – Middle Oligocene (Garzanti and Malusà, 2008) were a consequence of a tectonically controlled melting phase, (Burri *et al*., 2005; Berger *et al*., 2008), during which the tectonic events that promoted magmatic production in the middle crust of the Central Alps rather than crustal deformation, and associated sediment production was inhibited. The end of the tectonically controlled melting along the PFS (Berger *et al*., 2008) has been triggered by the onset of the thick-skinned tectonic in the Southern Alps and exhumation of the Lepontine Dome in the Central Alps, which promote large amounts of sediments to reach the Southalpine Foredeep;

3) unravel the correlation between the onset and migration of the deformation fronts in the Alpine chain (eastward in the Southalpine domain and westward into the Lepontine Dome), with the onset and compositional changes of the sediment discharges in the Southalpine Foredeep.

ACKNOWLEDGEMENTS

The article benefited from the critical review of R. Hiller, J. Cuitiño and two anonymous reviewers, and from fieldwork support and discussion with F. Livio, A. Berlusconi, A. Vernej, F. Riva, F. Lucini and J. A. Andiloro. We also thank A. Crippa for laboratory support. Further discussion with G. Muttoni (climatic vs tectonic signal), A. Tunesi, A. Resentini, M. Padoan, G. Coletti (palaeontological associations), M. Locatelli (Periadriatic dyke persistence), D. Sciunnach (Gonfolite Lombarda Group stratigraphy) and G. Scardia are gratefully acknowledged. An earlier version of the manuscript greatly benefited by suggestions of A. Di Giulio, R. Scasso and S. Andò. Financial grant assistance from the "Fratelli Confalonieri" Fellowship (A.D.C.) is acknowledged.

Conclusion and final remarks

Conclusion and final remarks

This PhD thesis includes 6 works that have been carried out on three sedimentary basins between the Alps/Apennines system (southern France/Switzerland and northern Italy) and the Cañadón Asfalto basin (Chubut Province, Argentina). Syn-volcanic sedimentation and post-volcanic, tectonically driven sedimentation have been compared, in order to discriminate the possibility of recognizing syn-sedimentary volcanism in ancient sedimentary records. The following remarks have been highlighted:

- Recognition of PDC deposits represents the most convincing proof of the presence of a syn-sedimentary volcano active in an ancient source-to-sink system when volcanic centers were completely eroded (e.g. Val d'Aveto Formation). On the contrary, presence of volcanoclastic detritus may result ambiguous (e.g. Val d'Aveto Formation and Villa Olmo Conglomerate).
- Preservation of pyroclastic density currents entering the water is function of the flow behavior (Las Leoneras Formation and Val d'Aveto Formation). Water/flow mixing rapidly produces vapor, that can trigger phreatomagmatic explosions and PDC disaggregation, if not reabsorbed. As resorption is inhibited by fluid escape mechanisms (Branney and Kokelaar, 2002), i.e. in fluidized flow, we suggest that granular flows are supposed to usually enter the water and follow downslope without being disaggregated by violent water/flow mixing.
- Recognition of disaggregated PDCs is still a belief matter, as Trofimovs et al., (2006, 2008) have demonstrated that when a PDC is disaggregated by entering the water it is rapidly reworked as cold, water-supported turbidite currents. However, some characteristics in ancient settings may suggest the volcanogenic origins (Las Leoneras Formation, Lonco Trapial Formation, Taveyanne Sandstones). Generally monolithologic composition and large amounts of volcanic rock fragments, immaturity of the volcanic detritus, sand-structures (bedforms of Douillet et al., 2013) have been used to identify all the facies supposed to be generated by phreatomagmatic explosion triggered when PDCs encounter the water.
- According to previous authors (e.g. Smith 1988, 1991; Manville et al., 2009; Alexander et al., 2010; Sisavath et al., 2011, 2012; Di Capua and Groppelli, 2014) volcanism has a great impact on the environment, not only by inundating it with large amounts of detritus produced and instantaneously moved across whatever fluvial system, but also by increasing the transport energy available in the system, i.e. delivering sediments to more distal depositional areas. It appears that syn-eruptive sedimentation is not controlled by classical sedimentary processes (weathering, hydraulic/aeolian transportation mechanisms across the source-to-sink), resulting thus in a general increase in detritus grain size (Val d'Aveto Formation, Taveyanne Sandstones). However, the volcanogenic signature is much greater in the sandy-sized fraction, than in the gravel-sized fraction (Val d'Aveto Formation; Smith, 1991; Di Capua et al., 2014).
- Persistence of environmental modifications due to main volcanic eruptions is recognizable in sequences, because main events are often followed by minor events in which volcanic detritus tends to progressively decrease upward (Taveyanne Sandstones). This reflects the “washing” process acting on the environment by fluvial system approaching pre-eruptive conditions.
- Tectonics acts as background sedimentation, episodically obliterated by volcanogenic sediments discharged in the environment (Las Leoneras Formation, Lonco Trapial Formation, Val d'Aveto Formation, Taveyanne Sandstones). In successions where PDCs are not preserved (Taveyanne Sandstones), it is particularly useful to recognize inter-eruptive phases, when volcanogenic signature becomes more and more diluted in the detritus.
- Tectonics and climate shape the environments, whilst volcanism more commonly modifies it for short (tens to hundreds of years) periods. This behavior has been observed both in subaereal and submarine environments. In Las Leoneras and Lonco Trapial Formations, environments change consequently to cyclical modifications of the base level. In Taveyanne

Sandstones, the monotonous turbidite system architecture is controlled by sudden deliveries of large amounts of volcanogenic material. Tectonics mainly shaped the basin geometries, providing only very few amounts of sediments (e.g. Sinclair, 1992). The well-developed turbidite system architecture of the Val d'Aveto Formation has been controlled by sea level drops and volcanism represents only one of the surface processes that were producing, transporting and discharging detritus in the basin. In contrast, gravel progradation recorded in Villa Olmo Conglomerate detects the long-term tectonic impact affecting the Southalpine foredeep basin in response to the beginning of the Alps growth.

- Tectonics signature in the sediments represents a definite tool for provenance analysis (Val d'Aveto Formation, Villa Olmo Conglomerate), as tectonics controls focused sediment production, but environmental response to tectonics, or tectono-climate may be ambiguous. Even thrust propagation toward the basin has been documented by different authors (e.g. Sinclair and Tomasso, 2002; Dumont et al., 2008), in Taveyanne Sandstones ephemeral is the sediment amounts deriving from the growing Alpine Belt. On the other side, in Villa Olmo Formation, the strong modifications which underwent the Alpine Belt during the Oligocene (e.g. Garzanti and Malusà, 2008) rapidly favor gravel-sized detritus propagation in the Southalpine Foredeep basin (Di Capua et al., 2015).
- Tectonics can influence grain size patterns of sediments (Villa Olmo Formation), but may need suitable climate conditions to promote sedimentation in distal basins (Val d'Aveto Formation).

References

References

- Alagna, K. E., Peccerillo, A., Martin, S., Donati, C. 2010. Tertiary to Present Evolution of Orogenic Magmatism in Italy. Journal of the Virtual Explorer, 36, 1-63. DOI:10.3809/jvirtex.2010.00233
- Alexander, J., Barclay, J., Susnik, J., Loughlin, S.C., Herd, R.A., Darnell, A., Crosweller, S. 2010. Sediment-charged flash floods on Montserrat: The influence of synchronous tephra fall and varying extent of vegetation damage. Journal of Volcanology and Geothermal Research, vol. 194, pp. 127–138.
- Allen, P.A. 2008. From landscapes into geological history. Nature, vol. 451, pp. 274-276.
- Allen, P.A., Burgess, P.M., Galewsky, J., Sinclair, H.D. 2001. Flexural-eustatic numerical model for drowning of the Eocene perialpine carbonate ramp and implications for Alpine geodynamics. GSA Bulletin, vol.113, pp.1052-1066.
- Allen, S.R., Freundt, A. 2006. Resedimentation of cold pumiceous ignimbrite into water: facies transformations simulated in flume experiments. Sedimentology, vol. 53, pp.717-734.
- Amy, L.A., Peakall, J., Talling, P.J. 2005. Density- and viscosity-stratified gravity currents: Insight from laboratory experiments and implications for submarine flow deposits. Sedimentary Geology, vol.179, pp. 5-29.
- Amy, L.A., Kneller, B.C., McCaffrey, W.D. 2007. Facies architecture of the Grès de Peïra Cava, SE France: landward stacking patterns in ponded turbiditic basins. Journal of the Geological Society, vol. 164, pp.143-162.
- Amy, L.A., Peakall, J., Talling, P.J., 2005. Density- and viscosity-stratified gravity currents: Insight from laboratory experiments and implications for submarine flow deposits. Sedimentary Geology, vol.179, pp.5-29.
- Andò, S., Garzanti, E., Padoan, M., Limonta, M. 2012. Corrosion of heavy minerals during weathering and diagenesis: a catalog for optical analysis. Sedimentary Geology, 280, pp. 165-178.
- Bellot, J.P., Bronner, G., Laverne, C. 2000. Analyse de la déformation finie et signification des lentilles ultrabasiques des Maures occidentales (Var, France). Implications géodynamiques. C. R. Acad. Sci. Paris, Sciences de la Terre et des planètes, pp. 803-809.
- Berger, A., Burri, T., Alt-Epping, P., Engi, M. 2008. Tectonically controlled fluid flow and water-assisted melting in the middle crust: An example from the Central Alps. Lithos, 102, 598-615. DOI:10.1016/j.lithos.2007.07.027
- Berger, A., Mercolli, I., Engi, M. 2005. The central Lepontine Alps: Notes accompanying the tectonic and petographic map sheet Sopra Ceneri (1:100’000). Schweizerische

Mineralogische und Petrographische Mitteilungen, 85, 109-146.

- Bergomi, M.A., Zanchetta, S., Tunesi, A. 2014. The Tertiary dyke magmatism in the Southern Alps: greochronological data and geodynamic significance. International Journal of Earth Science. DOI 10.1007/s00531-014-1087-5.
- Bernoulli, D., Bertotti, G., Zingg, A. 1989. Northward thrusting of the Gonfolite Lombarda ("South-Alpine Molasse) onto the Mesozoic sequence of the Lombardian Alps: Implications for the deformation history of the Southern Alps. Eclogae geol. Helv., 82, 841-856.
- Bernoulli, D., Giger, M., Muller, D.W., Ziegler, U.R.F. 1993. Sr-isotope stratigraphy of the Gonfolite Lombarda Group ("South - Alpine Molasse", Northern Italy) and radiometric constraints of its age of deposition. Eclogae Geologicae Helvetiae, 86, 751 –767.
- Bersezio, R., Fornaciari, M., Gelati, R., Napolitano, A., Valdisturlo, A. 1993. The significance of the Upper Cretaceous to Miocene clastic wedges in the deformation history of the Lombardian southern Alps. Gèologie Alpine, 69, 3-20.
- Bini, A., Sciunnach, D., Bersezio, Scardia, G., Tomasi, F. in press. Note illustrative della Carta Geologica D'Italia alla scala 1:50.000, Foglio CARG 96 "Seregno". pp.58-59.
- Boni, A., Braga, G., Conti, S., Gelati, R., Marchetti, G., Passeri, L.D. 1969. Note illustrative della Carta Geologica d'Italia, foglio Rapallo, foglio Chiavari.
- Borradaile, G. J., and Jackson, M. (2004). Anisotropy of magnetic susceptibility (AMS): magnetic petrofabrics of deformed rocks. Geological Society, London, Special Publications, 238(1), 299–360. doi:10.1144/GSL.SP.2004.238.01.18
- Borradaile, G., and Alford, C. (1987). Relationship between magnetic susceptibility and strain in laboratory experiments. Tectonophysics, 133(1-2), 121–135. doi:10.1016/0040-1951(87)90285-X
- Borradaile, G.J., and Henry, B. (1997). Tectonic applications of magnetic susceptibility and its anisotropy. Earth-Science Reviews, 42(1-2), 49–93. doi:10.1016/S0012-8252(96)00044-X
- Borradaile, Graham J., and Hamilton, T. D. (2009). Re-computing palaeopoles for the effects of tectonic finite strain. Tectonophysics, 467(1-4), 131–144. doi:10.1016/j.tecto.2008.12.020
- Borradaile, Graham J., and Jackson, M. (2010). Structural geology, petrofabrics and magnetic fabrics (AMS, AARM, AIRM). Journal of Structural Geology, 32(10), 1519–1551. doi:10.1016/j.jsg.2009.09.006
- Borradaile, Graham John, and Dehls, J. F. (1993). Regional kinematics inferred from magnetic subfabrics in Archean rocks of Northern Ontario, Canada. Journal of Structural Geology, 15(7), 887-894.

- Borradaile, Graham John. (1991). Correlation of Strain with Anisotropy of Magneti Susceptibility (AMS). Pageoph, 135(1).
- Boyet, M., Henriette, L., Tardy, M., Bosch, D., and Maury, R. (2001). Nature des sources des composants andésitiques des Grès du Champsaur et des Grès de Taveyannaz. Implications dans l'évolution des Alpes occidentales au Paléogène. Bull. Soc. géol. France, 172(4), 487-501.
- Braghieri, R., Montanari, L. 1976. Calcari Nummulitico-Algali di Travedona e Ternate (VA). Att. Soc. It. Sc. Nat. Mus. Civ. Milano, 117(1-2), 69-76.
- Brand, B.D., Mackaman-Lofland, C., Pollock, N.M., Bendana, S, Dawson, B., Wichgers, P. 2014. Dynamics of pyroclastic density currents: Conditions that promote substrate erosion and self channelization — Mount St Helens, Washington (USA). Journal of Volcanology and Geothermal Research, vol.276, pp. 189–214.
- Brandano, M., Ronca, S. 2014. Depositional processes of the mixed carobate-siliciclastic rhodolith beds of the Miocene Saint-Florent basin, Northern Corsica. Facies, 60, 73-90.
- Branney, M.J., Kokelaar, P. 1992. A reappraisal of ignimbrite emplacement: progressive aggradation and changes from particulate to non-particulate flow during emplacement of high-grade ignimbrite. Bulletin of Volcanology, vol.54, pp. 504-520.
- Branney, M.J., Kokelaar, P. 2002. Pyroclastic density currents and the sedimentation of ignimbrites. Geological Society, London, Memoirs, 27.
- Breien, H., De Blasio, F.V., Elverhøi, A., Nystuen, J.P., Harbitz, C.B. 2010. Transport mechanisms of sand in deep-marine environments – Insights based on laboratory experiments. Journal of Sedimentary Research, 80, 975–990.
- Bromley, R.G., Ekdale, A.A. 1984. Chondrites: A Trace Fossil Indicator of Anoxia in Sediments. Science, vol. 224, pp.872-874.
- Burbank, D.W., Beck R.A., Raynolds R.G.H., Hobbs R., Tahirkheli R.A.K. 1988. Thrusting and gravel progradation in foreland basins: A test of post-thrusting gravel dispersal. Geology 16, 1143-1146.
- Burri, T., Berger, A., Engi, M. 2005. Tertiary migmatites in the Central Alps: Regional distribution, field relations, conditions of formation, and tectonic implications. Schweizerische Mineralogische und Petrographische Mitteilungen, 85, 215-232.
- Cabaleri, N., Volkheimer, W., Armella, C., Gallego, O., Silva Nieto, D., Páez, M., Cagnoni, M., Ramos, A., Panarello, H., Koukharsky, M., 2010a. Estratigrafía, análisis de facies y paleoambientes de la Formación Cañadón Asfalto en el depocentro jurásico Cerro Cóndor, provincia del Chubut. Revista de la Asociación Geológica Argentina 66, 349-367.
- Cabaleri, N., Volkheimer, W., Silva Nieto, D., Armella, C., Cagnoni, M., Hauser, N.,

Matteini, M., Pimentel, M., 2010b. U-Pb ages in zircons from Las Chacritas and Puesto Almada members of the Jurassic Cañadón Asfalto Formation, Chubut province, Argentina. VII South American Symposium on Isotope Geology, Brasilia, 190-193.

- Calder, E.S., Sparks, R.S.J, Gardeweg, M.C. 2000. Erosion, transport and segregation of pumice and lithic clasts in pyroclastic flows inferred from ignimbrite at Lascar Volcano, Chile. Journal of Volcanology and Geothermal Research, vol. 104, pp. 201-235.
- Capponi, G., Crispini, L. 2008. Note illustrative della Carta Geologica d'Italia, foglio Genova.
- Cardinetti, L., Viganò, A., Martin, S., Zattin, M., Malusà, M.G. 2005. Late Alpine deformation in the Como region (central Southern Alps, Northern Italy). Geophysical Research Abstracts, 7, 09940.
- Carrapa, B., Di Giulio, A. 2001. The sedimentary record of the exhumation of a granitic intrusion into a collisional setting: the lower Gonfolite Group, Southern Alps, Italy. Sedimentary Geology, 139, 217–228.
- Cas, R.A.F., Wright, J.V. 1991. Subaqueous pyroclastic flows and ignimbrites: an assessment. Bull Volcanol, vol. 53, pp. 357-380
- Cas, R.A.F., Wright, H.M.N., Folkes, C.B, Lesti, C., Porreca, M., Giordano, G., Viramonte, J.G. 2011. The flow dynamics of an extremely large volume pyroclastic flow, the 2.08-Ma Cerro Galàn Ignimbrite, NW Argentina, and comparison with other flow types. Bulletin of Volcanology, vol. 73, pp. 1583-1609.
- Cassidy, M., Trofimovs, J., Palmer, M.R., Talling, P.J., Watt, S.F.L., Moreton, S.G., Taylor, R.N. 2013. Timing and emplacement dynamics of newly recognised mass flow deposits at ~ 8–12 ka offshore Soufrière Hills volcano, Montserrat: How submarine stratigraphy can complement subaerial eruption histories. Journal of Volcanology and Geothermal Research vol. 253, pp. 1–14.
- Cassidy, M., Watt, S.F.L., Palmer, M.L., Trofimovs, J., Symons, W., Maclachlan, S.E., Stinton, A.J. 2014. Construction of volcanic records from marine sediment cores: A review and case study (Montserrat, West Indies). Earth-Science Reviews, vol. 138, pp. 137–155.
- Castellarin A., Vai G.B. Cantelli L. 2006. The Alpine evolution of the Southern Alps around the Giudicarie faults: A Late Cretaceous to Early Eocene transfert zone. Tectonophysics, 414, 203-223.
- Catanzariti, R., Cerrina Feroni, A., Ottria, G., Levi, N. 2009. The Contribution Of Calcareous Nannofossil Biostratigraphy In Solving Geological Problems: The Example Of The Oligocene–Miocene Foredeep Of The Northern Apennines (Italy). In: Geologic Problem Solving with Microfossils: A Volume in Honor of Garry D. Jones, SEPM Special Publication No. 93, pp. 309-321.

- Catuneanu, O., Galloway, W.E., Kendall, C.G.S.C., Miall, A.D., Posamentier, H.W., Strasser, A., Tucker, M.E. 2011. Sequence stratigraphy: Methodology and Nomenclature. Newsletters on Stratigraphy, vol.44/3, pp. 173-245.
- Cavazza, W., De Celles, P.G., Fellin, M.G., Paganelli, L. 2007. The Miocene Saint-Florent Basin in northern Corsica: stratigraphy, sedimentology, and tectonic implications. Basin Research, 19, 507-527.
- Chandra, A.P., Gerson, A.R. 2010. The mechanisms of pyrite oxidation and leaching: A fundamental perspective. Surface Science Reports, vol. 65, pp. 293–315
- Cibin, U., Spadafora, E., Zuffa, G.G., Castellarin, A. 2001. Continental collision history from arenites of episutural basins in the Northern Apennines, Italy. Geological Society of America Bulletin, vol. 113, pp. 4-19.
- Codignotto, J., Nullo, F., Panza, J., Proserpio, C., 1978. Estratigrafía del Grupo Chubut, entre Paso de Indios y Las Plumas, Chubut. Congreso Geológico Argentino, No. 7, Actas 1,
- Cognè, J., Chen, Y., Courtillot, V., Rocher, F., Wang, G., Bai, M., and You, H. (1995). A paleomagnetic study of Mesozoic sediments from the Junggar and Turfan basins, northwestern China. Earth and Planetary Science Letters, 133, 353–366.
- Cole, P.D. 1991. Migration direction of sand-wave structures in pyroclastic-surge deposits: Implications for depositional processes. Geology, vol.19, 1108-1111.
- Cole, R.B., DeCelles, P.G. 1991. Subaerial to submarine transitions in early Miocene pyroclastic flow deposits, southern San Joaquin basin, California. Geological Society of America Bulletin, vol. 103, pp. 221-235.
- Coletti, G., Basso, D. 2014. Paleontological applications of resedimented skeletal materials. Rendiconti della Società Geological Italiana, suppl.1 to vol.31, p. 128.
- Corsini, M., Rolland, Y. 2009. Late evolution of the southern European Variscan belt: Exhumation of the lower crust in a context of oblique convergence. C. R. Geoscience, vol.341, pp.214–223
- Cortesogno, L., Cassinis, G., Dallagiovanna, G., Gaggero, L., Oggiani, G., Ronchi, A., Seno, S., Vanossi, M. 1998. The Variscan post-collisional volcanism in Late Carboniferous-Permian sequences of Ligurian Alps, Southern Alps and Sardinia (Italy): a synthesis. Lithos, 45, 305-328.
- Cortiñas, J.S., 1996. La cuenca de Somuncurá-Cañadón Asfalto; sus límites, ciclos evolutivos del relleno sedimentario y posibilidades exploratorias. The Somuncura-Cañadon Asfalto Basin; its boundaries, cycles of sedimentary evolution and exploration possibilities. Actas del Congreso Geológico Argentino XIII 1, 147-163.
- Cramer, B. S., Toggweiler, J. R., Wright, J. D., Katz, M. E., Miller, K. G. 2009. Ocean

overturning since the Late Cretaceous: Inferences from a new benthic foraminiferal isotope compilation. Paleoceanography, 24(4), 1-24. DOI:10.1029/2008PA001683

- Cuitiño, J.I., Scasso, R.A. 2013. Reworked pyroclastic beds in the early Miocene of Patagonia: Reaction in response to high sediment supply during explosive volcanic events. Sedimentary Geology, vol. 289, pp.194–209.
- Cúneo, R.A, Ramezani, J., Scasso, R.A., Pol,D., Escapa, I., Zavattieri, A.M., Bowring, S., 2013. High-precision U-Pb geochronology and a new chronostratigraphy for the Cañadón Asfalto Basin, Chubut, cent ral Patagonia: implications for terrestrial faunal and floral evolution in Jurassic. Gondwana Reseach, in press.
- D'Adda, P., Zanchi, A., Bergomi, M., Berra, F., Malusà, M. G., Tunesi, A., Zanchetta, S. 2010. Polyphase thrusting and dyke emplacement in the central Southern Alps (Northern Italy). International Journal of Earth Sciences, 100(5), 1095–1113. DOI:10.1007/s00531-010-0586-2
- Dal Piaz, G. V., and Venturelli, G. (1983). Brevi riflessioni sul magmatismo post - ofiolitico nel quadro dell'evoluzione spazio - temporale delle Alpi. Mem. Soc. Geol. It., 26(1), 5-19.
- Dall'Olio, E., Felletti, F., and Muttoni, G. (2013). Magnetic-Fabric Analysis As A Tool To Constrain Mechanisms of Deep-Water Mudstone Deposition In the Marnoso Arenacea Formation (Miocene, Italy). Journal of Sedimentary Research, 83(2), 170–182. doi:10.2110/jsr.2013.12
- De Blasio, F., Engvik, L., Harbitz, C.B., Elverhøi, A. 2004. Hydroplaning and submarine debris flows. Journal of Geophysical Research, vol.109, pp.1-15.
- De Celles, P.G. 1988. Lithologic provenance modeling applied to the Late Cretaceous synorogenic Echo Canyon Conglomerate, Utah: A case of multiple source areas. Geology, 16, 1039-1043.
- Dellino, P., Isaia, R., Veneruso, M. 2004. Turbulent boundary layer shear £ows as an approximation of base surges at Campi Flegrei (Southern Italy). Journal of Volcanology and Geothermal Research, vol.133, pp. 211-228.
- Di Capua, A., Groppelli, G., Vezzoli, G. 2012. Stratigraphic trend evolution of the sedimentary pulses of Val d'Aveto Formation. Rendiconti della Società Geological Italiana, vol. 20, pp. 35-37.
- Di Capua, A., Groppelli, G., Vezzoli, G. 2014. Volcanism, Relative Sea-Level Change, and the Stratigraphic Record: An Oligocene Example. In: STRATI 2013. At the Cutting Edge of Stratigraphy. (Eds.) Rocha, R., Pais, J., Kullberg, J.C., Finney, S. Springer International Publishing Switzerland. DOI: 10.1007/978-3-319-04364-7_91
- Di Capua, A., Vezzoli, G., Cavallo, A., Groppelli, G. 2015. The clastic sedimentation of the Late Oligocene Southalpine foredeep: from tectonically controlled melting to tectonically

driven erosion in the Central Alps. Geological Journal.

- Di Giulio, A., Carrapa, B., Fantoni, R., Gorla, L., Valdisturlo, A. 2001. Middle Eocene to Early Miocene sedimentary evolution of the western Lombardian segment of the South Alpine Foredeep (Italy). International Journal of Earth Sciences, 90(3), 534–548. DOI:10.1007/s005310000186
- Di Giulio, A., Dunkl, I., Falletti, P., and Sciunnach, D. 2005. Plagioclase-arenites from the Northern Appennines and Southern Alps: Record of a palaeogene Island Arc Related to Alpine Subduction. 7th Alpine Workshop, Opatijia, Abstracts book, 21-22.
- Dickinson, W.R., 1985. Interpreting provenance relation from detrital modes of sandstones. In: Provenance of Arenites, Zuffa, G.G. (ed.). NATO ASI Series: Dordrecht, 333–363.
- Dickinson, W.R., 1988. Provenance and sediment dispersal in relation to paleotectonics and paleogeography of sedimentary basins. In: New Perspectives in Basin Analysis. Kleinspehn, K.L., Paola, C. (Eds.), Springer-Verlag, New York, pp. 3–25.
- Doronzo, D.M. 2012. Two new end members of pyroclastic density currents: Forced convection-dominated
- and inertia-dominated. Journal of Volcanology and Geothermal Research, vol.219–220, pp. 87–91
- Doudoux, B., Chaplet, M., and Tardy, M. (1987). Les series marines Paleogenes post - Lutetiennes du massif subalpin des Bornes (Alpes Occidentales). Gèologie Alpine, 13(299 - 312).
- Douillet, G.A., Pacheco, D.A., Kueppers, U., Letort, J., Tsang-Hin-Sun, E., Bustillos, J., Hall, M., Ramòn, P., Dingwell, D.B. 2013. Dune bedforms produced by dilute pyroclastic density currents from the August 2006 eruption of Tungurahua volcano, Ecuador. Bulletin of Volcanology, vol.72,pp.1-20.
- Dumont, T., Simon-Labric, T., Authemayou, C., Heymes, T. 2011. Lateral termination of the north-directed Alpine orogeny and onset of westward escape in the Western Alpine arc: Structural and sedimentary evidence from external zone. Tectonics, vol. 30, pp. 1-31.
- Dumont, T., Simon-Labric, T., Authemayou, C., Heymes, T. 2011. Lateral termination of the north-directed Alpine orogeny and onset of westward escape in the Western Alpine arc: Structural and sedimentary evidence from the external zone. Tectonics, vol.30, pp.1-31.
- Edmonds, M., Herd, R.A. 2005. Inland-directed base surge generated by the explosive interaction of pyroclastic flows and seawater at Soufrière Hills volcano, Montserrat. Geology, vol. 33, pp- 245-248. DOI: 10.1130/G21166.1
- Elter, P., Catanzariti, R, Ghiselli,F., Marroni, M., Molli, G., Ottria, G., Pandolfi L. 1999. L'Unità Aveto (Appennino Settentrionale): caratteristiche litostratigrafiche, biografia, petrografia, delle areniti ed assetto strutturale. Bollettino della Società Geologica Italiana,

vol.118, pp.41-63.

- Elter, P., Ghiselli, F., Marroni, M., Ottria, G. 1999. Note illustrative della Carta Geologica d'Italia, foglio Bobbio.
- Elter, P., Lasagna, S., Marroni, M., Pandolfi, L., Vescovi, P., Zanzucchi, G. 2005. Note illustrative della Carta Geologica d'Italia, foglio Bedonia.
- Elter, P., Marroni, M., Pandolfi, L. 2006. Note illustrative della Carta Geologica d'Italia, foglio Bargagli.
- Encarnación, J., Fleming, T.H., Elliot, D.H., Eales, H.V., 1996. Synchronous emplacement of Ferrar and Karoo dolerites and the early breakup of Gondwana. Geology 24, 535-538.
- Einsele, G. 1991. Sedimentary Basins. Evolution, facies and sedimentary budget. Springer-Verlag (Berlin Heidelberg).
- Escapa, I., Cúneo, R., Cladera, G., 2008. New evidence for the age of the Jurassic flora from Cañadón del Zaino, Sierra de Taquetrén, Chubut. Ameghiniana 45, 633-637. Ph.D. dissertation. Universidad Nacional del Comahue, Bariloche, Argentina.
- Escapa, I.H., Cúneo, N.R., Rothwell, G.W., Stockey, R.A., in press. Pararaucaria delfueyoi from the late Jurassic Cañadón Calcáreo Formation, Chubut, Argentina: insights into the evolution of Cheirolepidiaceae. International Journal of Plant Sciences.
- Etienne, S., Mulder, T., Razin, P., Bez., M., Désaubliaux, G., Joussiaume, R., Tournadour, E. 2013. Proximal to distal turbiditic sheet-sand heterogeneities: Characteristics of associated internal channels. Examples from the Trois Evêchés area, Eocene-Oligocene Annot Sandstones (Grès d'Annot), SE France. Marine and Petroleum Geology, vol. 41, pp. 117-133.
- Evans, M.J, Mange-Rajetzky, M.A. 1991. The provenance of sediments in the Barrême thrust-top basin, Haute-Provence, France. In: Morton, A.C., Todd, S.P., Haughton, P.D.W. (eds), Developments in sedimentary provenance studies, Geological Society Special Publication No.57, pp.323-342.
- Feruglio, E., 1949. Descripción geológica de la Patagonia, I. Dirección General Yacimientos Petroliferos Fiscales, Buenos Aires, p. 334.
- Figari, E.G., 2005. Evolución tectónica de la cuenca de Cañadón Asfalto (zona del Valle Medio del Río Chubut). Universidad de Buenos Aires, Ph.D. dissertation, Buenos Aires.
- Fígari, E.G., Courtade, S.F., 1993. Evolución tectosedimentaria de la cuenca de Cañadón Asfalto, Chubut, Argentina. Tectono-sedimentary evolution of the Cañadón Asfalto Basin, Chubut, Argentina. Actas del Congreso Geológico Argentino 12, Vol. 1, 66-77.
- Figari, E.G., Courtade, S.F., Constantini, L.A., 1996. Stratigraphy and tectonics of Cañadón Asfalto Basin, Lows of Gastre and Gan Gan, North of Chubut Province, Argentina.

GeoResearch Forum 1-2, 359-368.

- Fiorentini Potenza, M. 1957. Ricerche stratigrafico-petrografiche sulla molassa subalpina terziaria comasca (Gonfolite). Rend. Ist. Lomb. Sc. Lett., 92(1), 10-22.
- Folk, R.L., 1980. Petrology of Sedimentary Rocks. Hemphill Publ. Co., Austin. 182pp.
- Ford, M., Lickorish, H. 2004. Foreland basin evolution around the western Alpine Arc. Geological Society, London, Special Publications, vol.221, pp. 39-63.
- Francis, J.E., Marenssi, S., Levy, R., Hambrey, M., Thron, V.C., Mohr, B., Brinkhius, H., Warnaar, J., Zachos, J., Bohaty, S., DeConto, R. 2009. From Greenhouse to Icehouse – The Eocene/Oligocene in Antarctica. In: Antarctic Climate Evolution. Developments in Earth & Environmental Sciences. (eds.) Florindo, F., Siegert, M., The Netherlands: Elsevier, 8, 309-368.
- Frenguelli, J., 1949. Los estratos con "Estheria" en el Chubut (Patagonia). Revista de la Asociación Geológica Argentina 4, 11-24.
- Gallego, O.F., Cabaleri, N.G., Armella, C., Volkheimer, W., Ballent, S.C., Martínez, S., Monferran, M.D., Silva Nieto, D.G., Páez, M.A., 2011. Paleontology, sedimentology and paleoenvironment of a new fossiliferous locality of the Jurassic Cañadón Asfalto Formation, Chubut Province, Argentina. Journal of South American Earth Sciences 31, 54-68.
- Garzanti, E., Andò, S. 2007. Heavy mineral concentration in modern sands: implication for provenance interpretation. Developments in Sedimentology, 68, pp. 507-545.
- Garzanti, E., Malusà, M. G. 2008. The Oligocene Alps: Domal unroofing and drainage development during early orogenic growth. Earth and Planetary Science Letters, 268(3-4), 487–500. DOI:10.1016/j.epsl.2008.01.039
- Garzanti, E., Resentini, A., Vezzoli, G., Andò, S., Malusà, M., Padoan, M., Paparella, P. 2010. Detrital Fingerprints of Fossil Continental-Subduction Zones (Axial Belt Provenance, European Alps). The Journal of Geology, 118, 341–362.
- Gavazzi, A., Miletta, S., Sciunnach, D., and Tremolada, F. 2003. Eocene plagioclase-arenites from the Southern Alps: record of a “meso-Alpine” volcanic arc. Annales Universitatis Scientiarum Budapestinensis, Sectio Geologica 35, 102-103.
- Gazzi, P., 1966. Le Arenarie del Flysch Sopracretaceo dell'Appennino Modenese: Correlazioni con il Flysch di Monghidoro. Mineralogica e Petrografica Acta, 12, 69-97.
- Gelati, R., Napolitano, A., Valdisturlo, A., 1988. La “Gonfolite Lombarda”: stratigrafia e significato nell'evoluzione del margine sudalpino. Riv. It. Paleont. Strat., 94, 285–332.
- Giger, M. 1990. Geologische und Petrographische Studien an Geröllen und Sedimenten der Gonfolite Lombarda Gruppe (Südschweiz und Norditalien) und ihr Vergleich mit dem Alpinen Hinterland. PhD Thesis, University of Bern.

- Giger, M., Hurford, A.J. 1989. Tertiary intrusives of the Central Alps: their tertiary uplift, eriosion, redeposition and burial in the South-Alpine foreland. Eclogae Geologicae Helvetiae, 82(3), 857–866.
- Giobbi Mancini, E., Boriani, A., Villa, I.M. 2003. Pre-Alpine ophiolites in the basement of Southern Alps: the presence of a bimodal association (LAG- Leptyno-Amphibolitic Group) in the Serie dei Laghi (N-Italy, Ticino-CH). Rend. Fis. Acc. Lincei, 14, 79-99.
- Gladstone, C., Ritchie, L.J., Sparks, R.S.J., Woods, A.W. 2004. An experimental investigation of density-stratified inertial gravity currents. Sedimentology, vol. 51, pp. 767-789.
- Graham, U.M., Ohmoto H. 1994. Experimental study of formation mechanisms of hydrothermal pyrite. Geochimica et Cosmochimica Acta, vol. 58, pp. 2 187-2202.
- Grosjean, A.S., Pittet, B., Ferry, S., Mahéo, G., Gardien, V. 2012. Reconstruction of Tertiary palaeovalleys in the South Alpine Foreland Basin of France (Eocene-Oligocene of the Castellane arc). Sedimentary Geology, 275-276, 1-21.
- Gunzenhauser, B.A. 1985. Zur Sedimentologie und Palaogeographie der oligo-miocaenen Gonfolite Lombarda zwischen Lago Maggiore und der Brianza (Sudtessin, Lombardei). Beitr. Geol. Karte Schweiz N.F. 159, 114pp.
- Handy, M.R., Babist, J., Wagner, R., Rosenberg, C., Konrad, M. 2005. Decoupling and its relation to strain partitioning in continental lithosphere: insight from the Periadriatic fault system (European Alps). Geological Society, London, Special Publications, 243(1), 249–276. DOI:10.1144/GSL.SP.2005.243.01.17
- Haq, B. U., Hardenbol, J., and Vail, P. R. 1987. Chronology of fluctuating sea levels since the Triassic. Science (New York, N.Y.), 235(4793), 1156–67. DOI:10.1126/science.235.4793.1156
- Haughton, P., Davis, C., McCaffrey, W., Barker, S. 2009. Hybrid sediment gravity flow deposits – Classification, origin and significance. Marine and Petroleum Geology, vol. 26, pp.1900-1918.
- Heller, P.L., Bowdler, S.S., Chambers, H.P., Coogan, J.C., Hagen, E.S., Shuster, M.W., Winslow, N.S., Lawton, T.F. 1986. Time of Thrusting in the Sevier orogenic belt, Idaho-Wyoming and Utah. Geology, 14, 388-391.
- Hrouda, F. (1978). The magnetic fabric in some folds. Physics of the Earth and Planetary Interiors, 17, 89–97.
- Jutzeler, M., McPhie, J., Allen, R.S. 2014. Facies architecture of a continental, below-the-wave volcaniclastic basin: The Ohanapecosh Formation, Ancestral Cascades arc (Washington, USA). GSA Bulletin, vol.126, pp.352-376.

- Ingersoll, R.V., Bullard, T.F., Ford, R.L., Grimm, J.P., Pickle, J.D., Sares, S.W. 1984. The effect of grain size on detrital modes: a test of the Gazzi-Dickinson point-counting method. Journal of Sedimentary Petrology, 54, 103–116.
- Jelinek, V. I. T. (1981). Characterization of the magnetic fabric of rocks. Tectonophysics, 79, 63–67.
- Johnsson, M. J. 1993. The system controlling the composition of clastic sediments. In: Processes Controlling the Composition of Clastic Sediments. Johnsson, M.J., Basu, A. (Eds.), Geological Society of America, Special Paper, 284, pp. 1–19.
- Joseph, P., Lomas, S.A. 2004. Deep-water sedimentation in the Alpine Foreland Basin of SE France: New perspectives on the Grès d'Annot and related systems - an introduction. Geological Society, London, Special Publications 2004, vol.221, pp.1-16.
- Kataoka, K.S. 2011. Geomorphic and sedimentary evidence of a gigantic outburst flood from Towada caldera after the 15 ka Towada–Hachinohe ignimbrite eruption, northeast Japan. Geomorphology, vol. 125, pp.11-26.
- Kataoka, K.S., Manville, V., Nakjo, T., Urabe, A. 2009. Impacts of explosive volcanism on distal alluvial sedimentation: Examples from the Pliocene–Holocene volcaniclastic successions of Japan. Sedimentary Geology, vol. 220, pp.306-317.
- Komitz, M.A., Browning, J.V., Miller, K.G., Sugarman, P.J., Mizintseva, S., Scotese, C.R. 2008. Late Cretaceous to Miocene sea-level estimates from the New Jersey and Delaware coastal plain coreholes: an error analysis. Basin Research, 20, 211-226.
- Kuhlemann, J. 2007. Palaeogeographic and palaeotopographic evolution of the Swiss and Eastern Alps since the Oligocene. Global and Planetary Change, 58, 224–236.
- Kuhlemann, J., Frisch, W., Székely, B., Dunkl, I., Kázmér, M. 2002. Post-collisional sediment budget history of the Alps: tectonic versus climatic control. Int. J. Earth Sci., 91, 818-837.
- Lateltin, O. (1988). Les dépois torbiditiques oligocènes d'avant-pays entre Annency (Haute-Savoie) et le Sanetsch (Suisse). Grès de Taveyanne et du Val d'Illiez. Thèse Fribourg, 127 pp.
- Lavigne, F., Suwa, H. 2004. Contrasts between debris flows, hyperconcentrated flows and stream flows at a channel of Mount Semeru, East Java, Indonesia. Geomorphology, 61, 41-58.
- Le Bas, M. J., Le Maitre, R. W., Streckeisen, A. Zanettin, B. 1986. A chemical classification of volcanic rocks based on the total alkali–silica diagram. Journal of Petrology, 27, 745–750.
- Le Friant, A., Deplus, C., Boudon, G, Sparks, R.S.J., Trofimovs, J., Talling, P.J. 2009. Submarine deposition of volcaniclastic material from the 1995–2005 eruptions of Soufriére

Hills volcano, Montserrat. Journal of the Geological Society, London, vol. 166, pp. 171–182. DOI: 10.1144/0016-76492008-047.

- Le Friant, A., Lebas, E., Clément, V., Boudon, G., Deplus, C., de Voogd, B., Bachèlery, P. 2011. A new model for the evolution of La Réunion volcanic complex from complete marine geophysical surveys. Geophysical Research Letters, vol.38, pp.1-6.
- Legros, F., Druitt, T.H. 2000. On the emplacement of ignimbrite in shallow-marine environments. Journal of Volcanology and Geothermal Research, vol.95, pp. 9–22.
- Livio, F., Berlusconi, A., Chunga, K., Michetti, A., Sileo, G. 2011. New stratigraphic and structural evidence for Late Pleistocene surface faulting along the Monte Olimpino Backthrust (Lombardia , N Italy). Rendiconti online della Società Geologica italiana, 14, 17–25. DOI:10.3301/ROL.2011.03
- Lowe, D.R. 1976. Subaqueous liquified and fluidized sediment flows and their deposits. Sedimentology, vol. 23, pp. 285-308.
- Lowe, D.R. 1982. Sediment gravity flows: II. Depositional models with special reference to the deposits of high-density turbidity currents. Journal of Sedimentary Petrology, vol.52, pp. 0279-0297.
- Lowrie, W. (1990). Identification of ferromagnetic minerals in a rock by coercivity and unblocking temperature properties. Geophysical Research Letters, 17(2), 159–162.
- Lube, G., Cronin, J.S., Manville, V., Procter, J.N, Cole, S.E., Freundt, A. 2012. Energy growth in laharic mass flows. Geology, vol.40, pp.475-478.
- Maeno, F., Taniguchi, H. 2009. Sedimentation and welding processes of dilute pyroclastic density currents and fallout during a large-scale silicic eruption, Kikai caldera, Japan. Sedimentagy Geology, vol. 220, pp. 227-242.
- Malusà, M. G., Villa, I. M., Vezzoli, G., Garzanti, E. 2011. Detrital geochronology of unroofing magmatic complexes and the slow erosion of Oligocene volcanoes in the Alps. Earth and Planetary Science Letters, 301(1-2), 324–336. DOI:10.1016/j.epsl.2010.11.019
- Mancin, N., Ceriani, A., Tagni, F., Brambilla, G. 2001. La Formazione di Ternate (Italia settentrionale): contenuto micropalaeontologico e caratterizzazione petrografica. Atti Ticinesi di Scienze della Terra, 42, 37-46.
- Mandeville, C.W., Carey, S., Sigurdsson, H., King, J. Paleomagnetic evidence for high-temperature emplacement of the 1883 subaqueous pyroclastic flows from Krakatau Volcano, Indonesia. Journal of Geophysical Research, vol. 99, pp.9487-9504.
- Manville, V., Nemeth, K., Kano, K. 2009. Source to sink: A review of three decades of progress in the understanding of volcaniclastic processes, deposits, and hazards. Sedimentary Geology, vol.220, pp.136-161.

- Manville, V., Newton, E.H., White, J.D.L. 2005. Fluvial responses to volcanism: resedimentation of the 1800a Taupo ignimbrite eruption in the Rangitaiki River catchment, North Island, New Zealand. Geomorphology, vol.65, pp-49-70.
- Marroni, M., Ottria, G., Pandolfi, L. 2006. Note illustrative della Carta Geologica d'Italia, foglio Cabella Ligure.
- Mattei, M., Cipollari, P., Cosentino, D., Argentieri, a., Rossetti, F., Speranza, F., and Di Bella, L. (2002). The Miocene tectono-sedimentary evolution of the southern Tyrrhenian Sea: stratigraphy, structural and palaeomagnetic data from the on-shore Amantea basin (Calabrian Arc, Italy). Basin Research, 14(2), 147–168. doi:10.1046/j.1365-2117.2002.00173.x
- Mattioli, M., Di Battistini, G., Zanzucchi, G. 2002. Petrology, geochemistry and age of the volcanic clasts from the Canetolo Unit (Northern Apennines, Italy). Boll. Soc. Geol. It., vol. 1, pp. 399-416.
- Mattioli, M., Lustrino, M., Ronca, S., Bianchini, G. 2012. Alpine subduction imprint in Apennine volcaniclastic rocks. Geochemical–petrographic constraints and geodynamic implications from Early Oligocene Aveto-Petrignacola Formation (N Italy). Lithos, vol.134-135, pp.201-220.
- Mellere, D., Stefani, C., Angevine, C. 2000. Polyphase tectonics through subsidence analysis: the Oligo-Miocene Venetian and Friuli Basin, north-east Italy. Basin Research, 12, 159-182.
- Miall, A.D. 1996. The geology of fluvial deposits. Springer-Verlag (Berlin Heidelberg)
- Miller, K.G, Mountain, G. S., Browning, J. V. 2011. A 180-Million-Year record of Sea Level and Ice Volume Variation from Continental Margin and Deep - Sea Isotopic Records. Oceanography, 24, 40-53. DOI:10.5670/oceanog.2011.26.
- Miller, K.G, Wright, J.D., Fairbanks, R.G. 1991. Unlocking the Ice House: Oligocene - Miocene Oxygen Isotopes, Eustasy, and Margin Erosion. Journal of Geophysical Research, 96(B4), 6829-6848.
- Miller, K.G., Browning, J.V., Aubry, M.P., Wade, B.S., Katz, M.E., Kulpecz, A.A., Wright, J.D. 2008. Eocene-Oligocene global climate and sea-level changes: St. Stephens Quarry, Alabama. Geological Society of America Bulletin, 120(1-2), 34–53. DOI:10.1130/B26105.1
- Miller, K.G., Fairbanks, R.G., Mountain, G.S. 1987. Tertiary oxigen isotope synthesis, sea level history, and continental margin erosion. Paleoceanography, 2(1), 1-19.
- Miller, K.G., Kominz, M.A., Browning, J.V, Wright, J.D., Mountain, G.S., Katz, M.E., Sugarman, P.J., Cramer, B.S., Christie-Blick, N., Pekar, S.F. 2005. The Phanerozoic record of global sea-level change. Science (New York, N.Y.), 310(5752), 1293–1298. DOI:10.1126/science.1116412

- Milliman, J.D., Syvitski, J.P 1992. Geomorphic/Tectonic Control of Sediment Discharge to the Ocean: The Importance of Small Mountainous Rivers. The Journal of Geology, vol.100, pp. 525-544.
- Montenat, C., Leyrit, H., Gillot, P.Y., Janin, M.C., Barrier, P. 1999. Extension du vulcanisme oligocène dans l'arc de Castellane (chaine subalpines de Haute-Provence). Géologie de la France, vol.1, pp.43-48.
- Mulder, T., Alexander, J. 2001. The physical character of subaqueous sedimentary density flows and their deposits. Sedimentology, 48, 269-299.
- Mulder, T., Cochonat, P. 1996. Classification of offshore mass movements. Journal of Sedimentary Research, vol.66, pp.43-57.
- Mulder, T., Syvitski, J.P.M., Migeon, S., Faugères, J.-C., Savoye, B. 2003. Marine hyperpycnal flows: initiation, behavior and related deposits. A review. Marine and Petroleum Geology, 20(6-8), 861–882. DOI:10.1016/j.marpetgeo.2003.01.003
- Musacchio, E., 1995. Estratigrafia y micropaleontología del Jurásico y el Cretácico en la comarca del valle medio del río Chubut, Argentina, Actas 6° Congreso de Paleontología y Bioestratigrafía, Trelew, pp. 179-187.
- Musacchio, E.A., Beros, C., Pujana, I., 1990. Microfósiles continentales del Jurásico y el Cretácico en Chubut y su contribución a la bioestratigrafia de la Cuenca del Golfo de San Jorge, Argentina, In: Volkheimer, W. (Ed.), Bioestratigrafía de los sistemas regionales del Jurásico y Cretácico de América del Sur, 2. Comité Sudamericano del Jurásico y Cretácico, Mendoza.
- Mutti, E., Ricci Lucchi, F. 1972. Le torbiditi dell'Appennino Settentrionale: introduzione all'analisi di facies. Memorie della Società Geologica Italiana, vol. 31, pp. 161-199.
- Mutti, E., Papani, L., Di Biase, D., Davoli, G., Mora, S., Segadelli, S., Tinterri, R. 1995. Il Bacino Tertiario Epimesoalpino e le sue implicazioni sui rapporti tra Alpi ed Apennini. Memorie della Società geological Italiana, vol.47, pp. 217-244.
- Mutti, E., Tinterri, R., Benevelli, G., di Biase, D., Cavanna, G. 2003b. Deltaic, mixed and turbidite sedimentation af ancient foreland basins. Marine and Petroleum Geology, 20, 733-755.
- Mutti, E., Tinterri, R., Remacha, E., Mavilla, N., Angella, S., Fava, L. 2003a. An introduction to the analysis of ancient turbidite basins from an outcrop prospective. American Association of Petroleum Geologists, continuing education course note series 39. pp.92
- Nakayama, C., 1973. Sedimentitas pre-Bayocianas en el extremo austral de la Sierra de Taquetrén, Chubut (Argentina). Pre-Bajocian sedimentary rocks in the southern extreme of Sierra de Taquetrón, Chubut, Argentina. Actas de las Jornadas Geológicas Argentinas, 269-

277.

- Napolitano, A. 1985. Stratigrafia e sedimentologia della "Gonfolite" nel settore di Como. Rend. Soc. Geol. It., 8, 69-72.
- Nullo, F., Proserpio, C., 1975. La Formación Taquetrén en Cañadón del Zaino (Chubut) y sus relaciones estratigráficas en el ámbito de la Patagonia, de acuerdo a la flora, República Argentina. The Taquetrén Formation in Cañadón del Zaino, Chubut, and its biostratigraphic (floral) relationship in the limits of Patagonia, Argentina. Revista de la Asociación Geológica Argentina 30, 133-150.
- Nullo, F.E., 1983. Descripción geológica de la Hoja 45c, Pampa de Agnia, provincia del Chubut., Nacional Bol. 199, 94 pp. Servicio Geológico, Buenos Aires.
- Oliva-Urcia, B., Rahl, J. M., Schleicher, A. M., and Parés, J. M. (2010). Correlation between the anisotropy of the magnetic susceptibility, strain and X-ray Texture Goniometry in phyllites from Crete, Greece. Tectonophysics, 486(1-4), 120–131. doi:10.1016/j.tecto.2010.02.013
- Olivera, D.E., Zavattieri, A.M., Quattrocchio, M., Escapa, I.H., Cúneo, R., 2012. Paleoambiente y potencial generador de hidrocarburos de dos secciones jurásicas en el Depocentro Cerro Cóndor, Cuenca de Cañadón Asfalto, Provincia de Chubut, XV Simposio Argentino de Paleobotánica y Palinología, Resúmenes, Corrientes, p. 99.
- Onézime, J., Faure, M., Crévola, G. 1998. Etudie pétro-structurale du complexe granitique Rouet – Plan-d-la-tour (massif des Maureset du Tanneron occidental, Var). C. R. Acad. Sci. Paris, Sciences de la Terre et des planètes, vol.328 pp. 773-779.
- Page, R., Page, S. 1993. Petrologìa y significado tectònico del Juràsico volcànico del Chubut central. Revista de la Asociaciòn Geològica Argentina, vol.48, pp.41-58.
- Pälike, H., Norris, R. D., Herrle, J. O., Wilson, P., Coxall, H. K., Lear, C. H., Shackleton, N. J., Tripati, A.K., Wade, S.W. 2006. The heartbeat of the Oligocene climate system. Science, 314 (5807), 1894–1908. DOI:10.1126/science.1133822
- Pankhurst, R.J., Leat, P.T., Sruoga, P., Rapela, C.W., Márquez, M., Storey, B.C., Riley, T.R., 1998. The Chon Aike province of Patagonia and related rocks in West Antarctica: A silicic large igneous province. Journal of Volcanology and Geothermal Research 81, 113-136.
- Parés, J. M., Van der Pluijm, B. A., and Dinarès - Turell, J. (1999). Evolution of magnetic fabrics during incipient deformation of mudrocks (Pyrenees , northern Spain). Tectonophysics, 307, 1–14.
- Peccerillo, A., Taylor, S.R. 1976. Geochemistry of eocene calc-alkaline volcanic rocks from the Kastamonu area, northern Turkey. Contributions to Mineralogy and Petrology, 58, p. 63-81.
- Peizhen, Z., Molnar, P., Downs, W.R. 2001. Increased sedimentation rates and grain sizes 2-

4Myr ago due to the influence of climate change on erosion rates. Nature, 410, 891-897.

- Piatnitzky, A., 1936. Estudio geológico de la región del río Chubut y del río Genua. Boletín de Informaciones Petroliferas (1924) 137, 83-118.
- Pieri, M., Groppi, G. 1981. Subsurface geological structure of the Po plain, Italy. Prog. Finalizzato Geodinamica C.N.R., 414.
- Pirkenseer, C., Spezzaferri, S., Berger, J.P. 2011. Reworked microfossils as a paleogeographic tool. Geology, vol. 39, pp. 843-846.
- Poitrasson, F., Pin, C. 1998. Extreme Nd isotope homogeneity in a large rhyolitic province: the Estérel massif, southeast France. Bulletin of Volcanology, vol.60, pp.213-233.
- Proserpio, C.A., 1987. Descripción geológica de la Hoja 44e, Valle General Racedo, Provincia del Chubut; Carta geologico-economica de la Republica Argentina, escala 1:200.000. Geologic description of Sheet 44e, General Racedo Valley, Chubut; economic-geologic map of Argentina, 1:200,000 scale, Boletín 201 - Servicio Geologico Nacional, Buenos Aires, p. 102.
- Ranalli, J.N., Peroni, G.O., Boggetti, D.A., Manoni, R., 2011, Cuenca Cañadón Asfalto, modelo tectosedimentario. VIII Congreso de Exploración y Desarrollo de Hidrocarburos, Simposio Cuencas Argentinas: visión actual. pp. 185-215.
- Rauhut, O.W.M., 2006. A brachiosaurid sauropod from the Late Jurassic Cañadón Calcáreo Formation of Chubut, Argentina. Fossil Record - Mitteilungen aus dem Museum fuer Naturkunde in Berlin 9, 226-237.
- Réhault, J.P., Honthass, C., Guennoc, P., Bellon, H., Ruffet, G., Cotten, J., Sosson, M., Maury, R.C. 2012. Offshore Oligo-Miocene volcanic fields within the Corsica-Liguria Basin: Magmatic diversity and slab evolution in the western Mediterranean Sea. Journal of Geodynamics, vol.58, pp.73-95.
- Ricci Lucchi, F. 2003. Turbidites and foreland basins: an Apenninic perspective. Marine and Petroleum Geology, vol. 20, pp. 727-732.
- Rivano Garcia, S. (1978). Contribution a l'etude geologique du se du massif des Bornes: la partie meridionale de la chaine des Aravis entre le Col des Aravi et la cluse de Faverges - Ugine (Haute - Savoie, France). PhD Thesis
- Roche O., Druitt, T.H., Cas, R.A.F. 2001. Experimental aqueous fluidization of ignimbrite. Journal of Volcanology and Geothermal Research, vol. 112, pp. 267-280
- Rochette, P., Jackson, M., and Aubourg, C. (1992). Rock magnetism and the interpretation of anisotropy of magnetic susceptibility. Reviews of Geophysics, (92), 209–226.
- Rollet, N., Déverchére, J., Beslier, M.O., Guennoc, P., Réhault, J.P., Sosson, M., Truffet, C. 2002. Back arc extension, tectonic inheritance, and volcanism in the Ligurian Sea, Western

Mediterranean. Tectonics, vol.21, pp.1-17.

- Rosenberg, C.L. 2004. Shear zones and magma ascent: A model based on a review of the Tertiary magmatism in the Alps. Tectonics, 23(3), 1-21. DOI:10.1029/2003TC001526
- Rosenberg, C.L., Berger, A. 2009. On the causes and modes of exhumation and lateral growth of the Alps. Tectonics, 28, 1-16.
- Rougier, G.W., Garrido, A., Gaetano, L., Puerta, P.F., Corbitt, C., Novacek, M.J., 2007a. First Jurassic triconodont from South America. American Museum Novitates 3580, 17.
- Rougier, G.W., Martinelli, A.G., Forasiepi, A.M., Novacek, M.J., 2007b. New Jurassic mammals from Patagonia, Argentina; a reappraisal of australosphenidan morphology and interrelationships. American Museum Novitates 3566, 54.
- Ruffini, R. (1995). Evidenze di attività vulcanica terziaria nelle Alpi Occidentali: problemi ed ipotesi. PhD Thesis, pp 147.
- Ruffini, R., Polino, R., Callegari, E., Hunziker, J. C., and Pfeifer, H. R. (1997). Volcanic clast-rich turbidites of the Taveyanne sandstones from Thônes syncline (Savoie, France): records for a Tertiary postcollisional volcanism. Schweizerische Mineralogische und Petrographische Mitteilungen, 77, 161-174.
- Saint-Ange, F., Bachelery, P., Babonneau, N., Muchon, L., Jorry, S.J. 2013. Volcaniclastic sedimentation on the submarine slopes of a basaltic hotspot volcano: Piton de la Fournaise volcano (La Réunion Island, Indian Ocean). Marine Geology, vol.337, pp.35-52.
- Saint-Ange, F., Savoye, B., Michon, L., Bachelery, P., Deplus, C., De Voogd, B., Dyment, J., Le Drezen, E., Voisset, M., Le Friant, A., Boudon, G. 2011. A volcaniclastic deep-sea fan off La Réunion Island (Indian Ocean): Gradualism versus catastrophism. Geology, vol.39, pp.271-274.
- Saint-Bezar, B., Hebert, R. L., Aubourg, C., Robion, P., Swennen, R., and Frizon de Lamotte, D. (2002). Magnetic fabric and petrographic investigation of hematite-bearing sandstones within ramp-related folds: examples from the South Atlas Front (Morocco). Journal of Structural Geology, 24(9), 1507–1520. doi:10.1016/S0191-8141(01)00140-7
- Salani, F.M., 2007. Aporte a la edad de la Formación Cañadón Asfalto, Chubut, Argentina. 30 Simposio Argentino del Jurásico, 71.
- Schmidt, D., Livi, K. J. T., and Frey, M. (1999). Reaction progress in chloritic material: an electron microbeam study of the Taveyanne graywacke, Switzerland. J. metamorphic Geol., 17, 229–241.
- Schmidt, D., Schmidt, S. T., Mullis, J., Mahlmann, R. F., and Frey, M. (1997). Very low grade metamorphism of the Taveyanne formation of western Switzerland. Contrib. Mineral. Petrol., 129, 385–403.

- Sciunnach D., Scardia G., Tremolada F., Premoli Silva E. 2010. The Monte Orfano Conglomerate revisited: stratigraphic constraints on Cenozoic tectonic uplift of the Southern Alps (Lombardy, northern Italy). Int. J. Earth Sci. (Geol Rundsch), 99, 1335–1355.
- Scott, K.M. 1988. Lahars and lahar-runout flows in the Toutle-Cowlitz River system, Mount St. Helens, Washington. Geological Survey professional paper. pp.1-83.
- Shanmugam, G. 1997. The Bouma sequence and the turbidite mind set. Earth-Science Review, vol.42, pp. 201-229.
- Shanmugam, G. 2000. 50 years of the turbidite paradigm (1950s-1990s): deep-water processes and facies models – a critical prospective. Marine and Petroleum Geology, vol.17, pp.285-342.
- Shanmugam, G. 2002. Ten turbidite myths. Earth-Science Review, vol.58, pp.311-341.
- Shanmugam, G., Damuth, J.E., Moiola, R.J. 1985. Is the turbidite facies association scheme valid for interpreting ancient submarine fan environment? Geology, vol.13, pp.234-237.
- Shanmugam, G., Moiola, R.J. 1988. Submarine fans: characteristics, models, classification, and reservoir potential. Earth-Science Review, vol.24, pp.383-428.
- Shanmugam, G., Moiola, R.J., McPherson, J.G., O'Connell, S. 1988. Comparison of turbidite facies associations in modern passive-margin Mississippi fan with ancient active-margin fans. Sedimentary Geology, vol.58, pp. 63-77.
- Silva Nieto, D., Cabaleri, N., Salani, F., Coluccia, A., 2002. Cañadón Asfalto, una cuenca de tipo “pull-apart” en el área de Cerro Cóndor, provincia del Chubut. 15° Congreso Geológico Argentino, Calafate, 238-243.
- Silva Nieto, D., Cabaleri, N.G., Armella, C., Volkheimer, W., Gallego, O.F., Zavattieri, A.M., Giambiagi, L.B., Moschetti, M.A., Mancuso, A., 2007. Hipótesis sobre la evolución tecto-sedimentaria de los depocentros de la cuenca de Cañadón Asfalto (Jurásico-Cretácico), provincia del Chubut. Ameghiniana 44 (Suppl.), 67R.
- Sinclair, H. D. (1992). Turbidite sedimentation during Alpine thrusting: the Taveyannaz sandstones of eastern Switzerland. Sedimentology, 39(5), 837–856. doi:10.1111/j.1365-3091.1992.tb02156.x
- Sinclair, H.D., 2000. Delta-Fed Turbidites Infilling Topographically Complex Basins: A New Depositional Model For The Annot Sandstones, Se France. Journal Of Sedimentary Research, vol. 70,pp. 504–519.
- Sinclair, H.D., Cowie, P.A. 2003. Basin-Floor Topography and the Scaling of Turbidites. The Journal Of Geology, vol.111, pp.277-299.
- Sinclair, H.D., Tomasso, M. Depositional Evolution of Confined Turbidite Basins. Journal of Sedimentary Research, vol.72, pp.451-456.

- Sisavath, E., Babonneau, N., Saint-Ange, F., Bachelery, P., Jorry, S.J., Deplus, C., De Voogd, B., Savoye, B. 2011. Morphology and sedimentary architecture of a modern volcaniclastic turbidite system: The Cilaos fan, offshore La Réunion Island. Marine Geology, vol. 288, pp.1-17.
- Sisavath, E., Mazuel, A., Jorry, S.J., Babonneau, N., Bachelery, P.,Deplus, C., De Voogd, B., Salpin, M., Emmanuel, L., Beaufort, L. Toucanne, S. 2012. Processes controlling a volcaniclastic turbiditic system during the last climatic cycle: Example of the Cilaos deep-sea fan, offshore La Réunion Island. Sedimentary Geology, vol. 281, pp.180-193.
- Smith, G.A. 1988. Sedimentology of proximal to distal volcanoclastics dispersed across an active foldbelt: Ellensburg Formation (late Miocene), central Washington. Sedimentology, vol. 35, pp.953-977.
- Smith, G.A. 1991. Facies Sequences and Geometries in Continental Volcaniclastic Sediments. In: Sedimentation in Volcanic Settings, SEMP Special Publication no. 5.
- Sohn, K.Y., Park, K.H., Yoon, S.H. 2008. Primary versus secondary and subaerial versus submarine hydrovolcanic deposits in the subsurface of Jeju Island, Korea. Sedimentology, vol.55, pp.899-924.
- Sohn, Y.K., Leong, J.O., Son, M. 2005. Long-runout pyroclastic surge on a Cretaceous alluvial plain, Republic of Korea. Terranova, vol. 17, pp. 13-24.
- Sohn, Y.K., Son, M., Jeong, J.O., Jeon, Y.M. 2009. Eruption and emplacement of a laterally extensive, crystal-rich, and pumice-free ignimbrite (the Cretaceous Kusandong Tuff, Korea). Sedimentary Geology, vol.220, pp.190-203.
- Soto, R., Mattei, M., and Casas, A. M. (2003). Relationship between AMS and folding in an area of superimposed folding (Cotiella-Bóixols nappe, Southern Pyrenees). Geodinamica Acta, 16(2-6), 171–185. doi:10.1016/j.geoact.2003.08.001
- Sparks, R.S.J, Young, S.R. 2002. The eruption of Soufri6re Hills Volcano, Montserrat (1995-1999): overview of scientific results. In: Druitt, T.H. and Kokelaar, B.P. (eds) 2002. The Eruption of Soufriére Hills Volcano, Montserrat, from 1995 to 1999. Geological Society, London, Memoirs, 21, 45-69. 0435-4052/02/$15 9 The Geological Society of London 2002.
- Sparks, R.S.J., Gardeweg, M.C., Calder, E.S., Matthews, S.J. 1997. Erosion by pyroclastic flows on Lascar Volcano, Chile. Bull Volcanolcanology, vol. 58, pp. 557–565.
- Sparks, R.S.J., Sigursdsson, H., Carey, S.N. 1980. The Entrance Of Pyroclastic Flows Into The Sea, II. Theoretical Considerations On Subaqueous Emplacement And Weldins. Journal of Volcanology and Geothermal Research, vol. 7, pp. 87-96.
- Stanley, D.J. 1980. The Saint-Antonin Conglomerate in the Maritime Alps: A Model for Coarse Sedimentation on a Submarine Slope. Smithionian contribution to the Marine Sciences, vol. 5, pp.1-25.

- Stefani, C., Fellin, M.G., Zattin, M., Zuffa, G.G., Dalmonte, C., Mancin, N., Zanferrari, A. 2007. Provenance and paleogeographic evolution in a multi-source foreland: the Cenozoic Venetian-Friulian basin (NE Italy). Journal of sedimentary research, 77, 867-887.
- Stipanicic, P., Rodrigo, F., Baulíes, O.L., Martínez, C.G., 1968. Las formaciones presenonianas en el denominado Macizo Nordpatagónico y regiones adyacentes. The pre-Senonian formations in the north Patagonian shield and adjacent areas. Revista de la Asociación Geológica Argentina 23, 67-98.
- Stow, D.A.V., Mayall, M. 2000. Deep-water sedimentary systems: New models for the 21st century. Marine and Petroleum Geology, vol.17, pp.125-135.
- Strachan, L.J. 2008. Flow transformations in slumps: a case study from the Waitemata Basin, New Zealand. Sedimentology, vol. 55, pp.1311-1332.
- Sulpizio, R., Bonasia, R., Dellino, P., Mele, D., Di Vito, M.A., La Volpe, L. 2010. The Pomici di Avellino eruption of Somma–Vesuvius (3.9 ka BP). Part II: sedimentology and physical volcanology of pyroclastic density current deposits. Bull Volcanol, vol. 72, pp.559–577.
- Sulpizio, R., Dellino, P., Doronzo, D.M., Sarocchi, D. 2014. Pyroclastic density currents: state of the art and perspectives. Journal of Volcanology and Geothermal Research, vol. 283, pp. 36–65.
- Sulpizio, R., Mele, D., Dellino, P., La Volpe, L. 2005. A complex, Subplinian-type eruption from low-viscosity, phonolitic to tephri-phonolitic magma: the AD 472 (Pollena) eruption of Somma-Vesuvius, Italy. Bull Volcanol, vol. 67, pp.743–767
- Sulpizio, R., Mele, D., Dellino, P., La Volpe, L. 2007. Deposits and physical properties of pyroclastic density currents during complex Subplinian eruptions: the AD 472 (Pollena) eruption of Somma-Vesuvius, Italy. Sedimentology, vol.54, pp.607-635.
- Talling, P.J., Douglas, G.M., Sumner, E., Malgesini, G. 2012. Subaqueous sediment density flows: Depositional processes and deposit types. Sedimentology, vol.59, pp.1937-2003.
- Talling, P.J., Malgesini, G, Felletti, F. 2013. Can liquefied debris flows deposit clean sand over large areas of sea floor? Field evidence from the Marnoso-arenacea Formation, Italian Apennines. Sedimentology, vol.60, pp.720-762.
- Tremolada, F., Guasti, E., Scardia, G., Carcano, C., Rogledi, S., Sciunnach, D. 2010. Reassessing the biostratigraphy and the palaeobathymetry of the Gonfolite Lombarda Group on the Como area (Northern Italy). Rivista Italiana di palaeontologia e Stratigrafia, 116(1), 35-49.
- Trofimovs, J., Amy, L., Boudon, G., Deplus, C., Doyle, E., Fournier, N., Hart, M.B., Komorowski, J.C., Le Friant, A., Lock, E.J., Pudsey, C., Ryan, G., Sparks, R.S.J., Talling, P.J. 2006. Submarine pyroclastic deposits formed at the Soufrière Hills volcano, Montserrat

(1995 − 2003): What happens when pyroclastic flows enter the ocean? Geology, vol.34, pp.549-552.

- Trofimovs, J., Fisher, J.K., MacDonald, H.A., Talling, P.J., Sparks, R.S.J, Hart, M.B., Smart, C.W., Boudon, G., Deplus, C., Komorowski, J.C., Le Friant, A., Moreton, S.G., Leng, M.J. 2010. Evidence for carbonate platform failure during rapid sea-level rise; ca 14 000 year old bioclastic flow deposits in the Lesser Antilles. Sedimentology, 57, pp. 735-759.
- Trofimovs, J., Foster, C., Sparks, R.S.J., Loughlin, S., Le Friant, A., Deplus, C., Porrit, L., Christopher, T., Luckett, R., Talling, P.J., Palmer, M.R., Le Bas, T. 2012. Submarine pyroclastic deposits formed during the 20th May 2006 dome collapse of the Soufrière Hills Volcano, Montserrat. Bulletin of Volcanology, vol. 74, pp. 391-405.
- Trofimovs, J., Sparks, R.S.J., Talling, P.J. 2008. Anatomy of a submarine pyroclastic flow and associated turbidity current: July 2003 dome collapse, Soufrière Hills volcano, Montserrat, West Indies. Sedimentology, vol.55, pp.617-634.
- Uchman, A. 2007. Deep-sea trace fossils from the mixed carbonate-siliciclastic flysch of the Monte Antola Formation (Late Campanian-Maastrichtian), North Apennines, Italy. Cretaceous Research, vol.28, pp., 980-1004
- Ui, T., Takarada, S., Yoshimoto, M. 2001. Debris Avalanches. In: Encyclopedia of Volcanoes, Sirgudsson, H., Houghton, B.F., McNutt, S.R., Rymer, H., Stix., J. (eds) Academic Press.
- Valdisturlo, A., Castradori, D., Fantoni, R., Pessina, C., Torricelli, S. 1998. Livelli clastici grossolani pre - Gonfolite (Oligocene inferiore) e loro significato nell'evoluzione del settore lombardo dell'avanfossa sudalpina. Riunione Gruppo Informale di sedimentologia.
- Van Gorp, W., Veldkamp, A., Temme, A.J.A.M., Maddy, D., Demir, T., van der Schriek, T., Reimann, T., Wallinga, J., Wijbrans, J., Schoorl, J.M. 2013. Fluvial response to Holocene volcanic damming and breaching in the Gediz and Geren rivers, western Turkey. Geomorphology, vol.201, pp.430-448.
- Vescovi, P. 1998. Le Unità Subliguri della alta Val Parma. Atti Ticinesi delle Scienze della Terra, vol.40, pp. 215-231.
- Volkheimer, W., Gallego, O.F., Cabaleri, N.G., Armella, C., Narvaez, P.L., Silva Nieto, D.G., Paez, M.A., 2009. Stratigraphy, palynology, and conchostracans of a Lower Cretaceous sequence at the Canadon Calcareo locality, extra-Andean central Patagonia; age and palaeoenvironmental significance. Cretaceous Research 30, 270-282.
- Volkheimer, W., Quattrocchio, M., Cabaleri, N., García, V., 2008. Palynology and paleoenvironment of the Jurassic lacustrine Cañadón Asfalto Formation at Cañadón Lahuincó locality, Chubut Province, Central Patagonia, Argentina. Revista Española de Micropaleontología 40, 77-96.

- Von Blanckenburg, F., Davies, J.H. 1995. Slab breakoff: a model of syncollisional magmatism and tectonics in the Alps. Tectonics, 14, 120-131.
- Vuagnat, M. (1983). Le Grès de Taveyanne et roches similaires: vestiges d'une activitè magmatique tardi - alpine. Mem. Soc. Geol. It., 26, 39-53.
- Wade, B. S., Pälike, H. 2004. Oligocene climate dynamics. Paleoceanography, vol. 19(4), 1-16. DOI:10.1029/2004PA001042
- Wandres, A. M., Bradshaw, J. D., Weaver, S., Maas, R., Ireland, T., Eby, N. 2004. Provenance analysis using conglomerate clast lithologies: a case study from the Pahau terrane of New Zeland. Sedimentary Geology, 167, 57-89.
- Weltje, G.J., von Eynatten, H., 2004. Quantitative provenance analysis of sediments: review and outlook. Sedimentary Geology, 171, 1–11.
- White, M.J., McPhie, J. 1997. A submarine welded ignimbrite-crystal-rich sandstone facies association in the Cambrian Tyndall Group, western Tasmania, Australia. Journal of Volcanology and Geothermal Research, vol. 76, pp. 277-295.
- Whitman, A.G. 1989. The Behaviour Of Subaerially Produced Pyroclastic Flows In A Subaqueous Environment: Evidence From The Roseau Eruption, Dominica, West Indies. Marine Geology, vol.86, pp.27-40.
- Wynn, R.B., Masson, D.G., Stow, D.A.V., Weaver, P.P.E. 2000. Turbidity current sediment waves on the submarine slopes of the western Canary Islands. Marine Geology, vol. 113, pp.185-198.
- Zachos, J., Pagani, M., Sloan, L., Thomas, E., Billups, K. 2001. Trends, rhythms, and aberrations in global climate 65Ma to present. Science (New York, N.Y.), 292, 686-93. DOI:10.1126/science.1059412
- Zanchetta, S., D'Adda, P., Zanchi, A., Barberini, V., Villa, I.M. 2011. Cretaceous-Eocene compression in the central Southern Alps (N Italy) inferred from 40Ar/39Ar dating of pseudotachylytes along regional thrust faults. Journal of geodynamics, 51(4), 245-263. DOI:10.1016/j.jog.2010.09.004
- Zanchetta, S., Garzanti, E., Doglioni, C., Zanchi, A. 2012. The Alps in the Cretaceous: a doubly vergent pre-collisional orogen. Terra Nova, 00, 1-6. DOI:10.1111/j.1365-3121-2012.01071.x
- Zurbriggen, R., Franz, L., Handy, M.R. 1997. Pre-Varisican deformation, metamorphism and magnetism in the Strona-Ceneri Zone (southern Alps of the northern Italy and southern Switzerland). Schweiz. Mineral. Petrogr. Mitt., 77, 361-380.